BPIFA1 INTERACTIONS WITH BACTERIA AND THEIR IMPORTANCE FOR AIRWAY HOST DEFENCE

RENATA CAIKAUSKAITE

A thesis submitted for the degree of

Doctor of Philosophy (Ph.D.)

September 2018

University of Sheffield

Faculty of Medicine, Dentistry and Health

Department of Infection, Immunity and Cardiovascular Disease

Supervisors: Prof Colin Bingle

Dr Lynne Bingle

Dedicated to my family

To the people who believe, support, and encourage me to strive for excellence and follow my dreams

ABSTRACT

Bactericidal/permeability-increasing protein fold-containing family member A1 (BPIFA1) is abundantly secreted protein of the upper airways that plays a pleiotropic role in airway defence, including antimicrobial and bacteriostatic functions. The mechanisms by which BPIFA1 exhibits these diverse functions is not fully resolved.

I investigated the regions of BPIFA1 predicted to be functionally important by using BPIFA1-tagged proteins to visualise their ability to bind to bacteria. The ability of mouse and human BPIFA1 to bind to bacteria were compared. I also used *in vitro* differentiated mouse tracheal epithelial cells (mTECs) from wild-type (WT) and *Bpifa1*$^{-/-}$ mouse tracheas to investigate if BPIFA1 plays a role in host response to nontypeable *Haemophilus influenzae* (NTHi).

Human full-length and disulphide-bond mutant BPIFA1 proteins bound to both Gram-negative and Gram-positive bacteria. However, human BPIFA1 lacking residues 22-42 was not able to bind to bacteria, implying that this region may be important for BPIFA1's binding. Mouse BPIFA1 also bound to both Gram-negative and Gram-positive bacteria. No apparent differences in the bacterial binding of human and mouse BPIFA1 proteins were observed. *In vitro* studies with WT and *Bpifa1*$^{-/-}$ mTECs showed the trend towards an increased NTHi colonisation in *Bpifa1*$^{-/-}$ mTEC cultures compared to WT. NTHi caused patchy infection of mTECs, suggesting that they exhibit resistance to NTHi. No clear differential infection between WT and *Bpifa1*$^{-/-}$ cells was detected. NTHi was capable of associating with the multiple cell types of tracheal epithelium, but not with BPIFA1-positive cells. NTHi infection disrupted cellular tight-junctions, suggesting that epithelial barrier function was impaired. This, in turn, allowed NTHi to cross through the mTECs. Differences in the BPIFA1 secretion by NTHi-exposed WT mTECs was observed compared to WT MOCK-exposed mTECs but no clear difference between WT and *Bpifa1*$^{-/-}$ mTECs inflammatory responses was detected.

Overall, the data from this study suggest that human and mouse BPIFA1 proteins play a role in airway defence by binding to Gram-negative and Gram-positive bacteria. The S18 region (G22-L42) of human BPIFA1, but not the disulphide bond, appears to be important for the binding activity of protein but further research is required to determine the true biological functions of this region. Mouse BPIFA1 binds to NTHi and appears to initially protect BPIFA1-positive cells from NTHi invasion, however BPIFA1 deficiency does not lead to significantly increased NTHi infection in mTECs. These findings imply that BPIFA1 is mucosal defence molecule that functions to modulate bacterial infection of the airways.

ACKNOWLEDGEMENTS

The successful outcome of this project required a lot of work, guidance, and assistance. I am thankful for being selected to work on this fascinating project as it helped me to broaden my knowledge, learn new experimental techniques, and develop professionally. The kindness and assistance from many people helped me to complete this project and I am largely grateful to all of them.

I would like to say first huge thank you to my project supervisor and mentor Prof Colin Bingle whose guidance throughout all these four years of my PhD was invaluable. I am hugely grateful for the opportunity to work with you as your knowledge and assistance enabled me to learn a lot and acquire new skill set which will be highly beneficial for my future career. Thank you for your patience and providing me with opportunity to work on this project. I wish to every PhD student to have such mentor like you! I would also like to say a special thank you to Dr Lynne Bingle whose support, advice, and lessons helped to plan my experiments and achieve the best results possible in four years of my studies. I am thankful for the opportunity to work under such special supervision of Prof Colin Bingle and Dr Lynne Bingle as they both created friendly and driven work environment.

I would not forget Dr Khondoker Akram of his advice and timely support throughout my PhD. Thank you, I learnt a lot about being a successful researcher from you. I would also like to say a huge thank you to lab technical support at the University of Sheffield: Brenka McCabe, Jason Heath, Kirsty Franklin, Vanessa Singleton, Lynne Williams, Jessica Willis, Benjamin Durham, Catherine Cooke, Jonathan Kilby, and John Finner. Work without all of you would be so much more difficult!

I would like to express my gratitude to our collaborating researchers Dr Helen Marriott from the University of Sheffield for providing wild-type mice and Prof James Stewart from the University of Liverpool for providing BPIFA1-VR1255 constructs and *Bpifa1*$^{-/-}$ mice for this project. I would like to thank Prof James Stewart for always making sure that I had a

safe trip from Liverpool to Sheffield while transporting mice and the staff of the University of Liverpool: Dr Nathifa Moyo, Sarah Roper, and Lynn McLaughlin for preparing *Bpifa1*$^{-/-}$ mice for transportation to the University of Sheffield.

A huge thank you to all members of Bingle's group and PhD friends who made every day of my PhD studies enjoyable and meaningful experience. Thank you to Lucy, Furaha, Sayali, Jess, Chloe, Emily, Grace, Hannah, Daniela, Mehul, Jake, Ernesto, and Bezaleel for being wonderful friends and PhD colleagues! A heartfelt thank you to Priyanka for helping me when I was struggling with my work and for motivational talks. A massive thank you to Apoorva for guidance, support, and for gifting me the computer monitor which definitely reduced the strain on my eyes and back while writing up my thesis.

I am also extremely grateful to my family: parents Rasa and Romualdas for unconditional love, support, motivation, and opportunity to live my dreams; grandparents Ona and Mikas for encouragement to achieve my goals; and my fiancé Milgintas for being always here for me through difficult times and giving me love and support. I would never be able to complete this journey without any of you!

Finally, I would like to express my appreciation to the University of Sheffield for funding this project and enabling me to attend a number of different conferences and meetings during my PhD studies.

CONFERENCE PRESENTATIONS

- Poster presentation: Host defence functions of SPLUNC1/BPIFA1. **Medical School Research Day**, Sheffield, UK, June 2015.
- Podium presentation: Functional analysis of SPLUNC1/BPIFA1. **COST WG2 integration meeting**, Malta, April 2016.
- Poster presentation: Role of BPIFA1 in Nontypeable *Haemophilus influenzae* infection. **Medical School Research Day**, Sheffield, UK, June 2016.
- Poster presentation: Functional analysis of BPIFA1/SPLUNC1. **British Association of Lung Research (BALR)**, Sheffield, UK, July 2016.
- Poster presentation: Host defence functions of BPIFA1 against Nontypeable *Haemophilus influenzae*. **European Respiratory Society (ERS)**, Paris, France, September 2018.

ABBREVIATIONS

Aa	Amino acid
ALI	Air liquid interface
ANOVA	Analysis of variance
ASL	Airway surface liquid
B. abortus	*Brucella abortus*
BAL	Bronchoalveolar lavage fluid
B. cepacia	*Burkholderia cepacia*
BHI	Brain-Heart Infusion
BPI	Bactericidal/permeability-increasing protein
BPIF	Bactericidal/permeability-increasing fold-containing
BPIFA	Bactericidal/permeability-increasing protein fold-containing family member A
BPIFB	Bactericidal/permeability-increasing protein fold-containing family member B
CCL-	C-C motif ligand
CCR-	C-C chemokine receptor
CCSP	Clara cell secretory protein
CD14	Cluster of differentiation-14
CD54	Cluster of differentiation-54
cDNA	Complementary DNA
CETP	Cholesteryl ester-transfer protein
CF	Cystic fibrosis
CFTR	Cystic fibrosis transmembrane conductance regulator
CHO	Chinese Hamster Ovary cell line
COPD	Chronic obstructive pulmonary disease
CXCL	C-X-C motif chemokine
DAPI	4',6-diamidino-2-phenylindole
DMEM	Dulbecco's Modified Eagle's Medium
DNA	Deoxyribonucleic acid
DPPC	Dipalmitoylphosphatidylcholine
EBV	Epstein-Barr virus
ECL	Enhanced chemiluminescence
E. coli	*Escherichia coli*
ENaC	Epithelial sodium channel
ET	Eustachian tube
F/R	Forward/Reverse
FBS	Foetal bovine serum
G-CSF	Granulocyte colony-stimulating factor
GFP	Green fluorescent protein
GM-CSF	Granulocyte-macrophage colony-stimulating factor
H_2O	Water
HBEC	Human bronchial epithelial cells
HEK293T	Human embryonic kidney 293 SV40 large T antigen expressing cells
Hpi	Hours post infection
HRV	Human rhinovirus
IAV	Influenza A virus
IF	Immunofluorescence
IFC	Immunofluorescence confocal
IFN-γ	Interferon gamma
IL-	Interleukin
IMS	Industrial Methylated Spirit

IPF	Idiopathic pulmonary fibrosis
kDa	Kilodalton
K. pneumoniae	*Klebsiella pneumoniae*
LB	Lysogeny broth
LBP	Lipopolysaccharide-binding protein
LMP1	latent membrane protein 1
LOS	Lipooligosaccharide
LPLUNC	Long palate lung and nasal epithelium clone
LPS	Lipopolysaccharide
MOI	Multiplicity of infection
M. pneumonia	*Mycoplasma pneumoniae*
mRNA	Messenger ribonucleic aid
MRSA	Methicillin-resistant *S. aureus*
MSCRAMM	Microbial surface components recognizing adhesive matrix molecules
mTECs	Mouse tracheal epithelial cells
NAD	Nicotinamide adenine dinucleotide
NCI-H292	Human mucoepidermoid pulmonary carcinoma cell line
NF-κB	Nuclear factor kappa-light-chain enhancer of activated B cells
NOD	Nucleotide-binding oligomerization domain
NTHi	Nontypeable *Haemophilus influenzae*
Oaz1	Ornithine Decarboxylase Antizyme 1
OD	Optical density
Orai1	Calcium release-activated calcium channel protein 1
OVA	Ovalbumin
P. aeruginosa	*Pseudomonas aeruginosa*
PAMPs	Pathogen-associated molecular patterns
PBLs	Peripheral blood lymphocytes
PBS	Phosphate-buffered saline
PCR	Polymerase Chain Reaction
PET	Polyethylene Terephthalate
PLTP	Phospholipid transfer protein
PLUNC	Palate lung and nasal epithelium clone
PVDF	Polyvinylidene difluoride
RPMI-1640	Roswell Park Memorial Institute-1640 growth medium
RSV	Respiratory syncytial virus
RT	Room temperature
S. aureus	*Staphylococcus aureus*
SDS-PAGE	Sodium dodecyl sulphate polyacrylamide gel electrophoresis
SEM	Standard error of the mean
SLPI	Secretory leukocyte peptidase inhibitor
SPLUNC	Short palate lung and nasal epithelium clone
S. pneumoniae	*Streptococcus pneumoniae*
TBS	Tris buffered saline
Tekt1	Tektin 1
TGF-β	Transforming growth factor beta
T_H2	T helper type 2
TIMP1	Tissue inhibitor 1 of metalloproteinases
TLR-	Toll-like receptor
TNF-α	Tumour necrosis factor alpha
UV	Ultraviolet
WT	Wild-type

CONTENTS

LIST OF FIGURES

LIST OF TABLES

CHAPTER 1: INTRODUCTION

The airway epithelium plays an essential role in innate host defence as it forms a barrier between the host and environmental hazards. Maintenance of normal airway epithelial function is crucial as airway mucosa is the first line of host defence against respiratory pathogens and irritants (Akira et al., 2006, Tam et al., 2011). Upon the recognition of pathogens, airway epithelial cells secrete various mediators into the airways, which immediately act against invading foreign particles. These mediators include cytokines, mucins, antimicrobial peptides such as defensins and cathelicidins, and antimicrobial proteins such as lysozyme and **B**actericidal/**P**ermeability-**I**ncreasing **F**old-containing protein (BPIF) A1 (BPIFA1) (Bals and Hiemstra, 2004, Guaní-Guerra et al., 2010, Steinstraesser et al., 2011). BPIFA1 is an abundantly secreted protein found in epithelial lining fluids and much data supports its role in airway defence (Britto et al., 2013, Gakhar et al., 2010, Jiang et al., 2013b, Leeming et al., 2015, Liu et al., 2013b, Sayeed et al., 2013). A better understanding of the contribution of BPIFA1 to airway defence may enable the development of drug targets for the treatment of respiratory diseases and bacterial infections (Ahmad et al., 2016, Garland et al., 2013, Walton et al., 2016).

1.1 Respiratory tract infections

Infections of the respiratory tract affect people worldwide and are mainly caused by bacterial and viral pathogens. Infectious airway diseases are divided into upper and lower respiratory tract infections. Epiglottitis, rhinosinusitis, and pharyngitis are examples of upper respiratory tract infectious diseases (Jain et al., 2001, Melio and Berge, 2014), whereas pneumonia and acute bronchitis are examples of lower respiratory tract infections (Finegold and Johnson, 1985, Priftis et al., 2013, Worrall, 2008). These infections are associated with bacterial pathogens such as *Staphylococcus aureus*, *Streptococcus pneumoniae*, and NTHi. These are also frequently linked to the exacerbations of pre-existing lung diseases such as chronic obstructive pulmonary disease (COPD) (Qureshi et al., 2014, Sethi, 2010), cystic fibrosis (CF) (Ciofu et al., 2013, Lyczak et al., 2002), asthma (Toews, 2005), and bronchiectasis (Goeminne et al.,

2014, Whitters and Stockley, 2012). However, *S. aureus*, *S. pneumoniae*, and NTHi are also often defined as commensal bacteria of the upper respiratory tract, which together with other types of commensal microorganisms form the airway microbiome. In a balanced state, these microorganisms colonise the upper respiratory tract without causing any infections, but imbalances caused by environmental insults can lead to the spread of these microbes from their normal environmental niche into sites of the respiratory tract where they cause invasive infections (Bosch et al., 2013, Pettigrew et al., 2008, Siegel and Weiser, 2015, de Steenhuijsen Piters et al., 2015).

1.1.1 *Staphylococcus aureus* and respiratory tract

Staphylococcus aureus is a Gram-positive coccus which can exist aerobically and anaerobically. The ability of *S. aureus* to tolerate anaerobic conditions allows the bacterium to invade host cells and cause tissue infection. In the balanced state, *S. aureus* is commensal microbe of the nasopharynx, but under environmental insults it may switch into a pathogen causing an invasive infection (Feng et al., 2008, Parker and Prince, 2012). This switch of *S. aureus* to a pathogenic state is triggered after a movement from the normal environmental niche to a different environment within the lower airways where the bacterium encounters more potent host defence mechanisms. The ability of *S. aureus* to bind the nasal epithelium is mediated through expression of clumping factor B which enables a binding to cytokeratins on the surface of epithelial cells. After a successful adherence to epithelial tissue, *S. aureus* multiples and initiates colonisation (Liu, 2009, Parker and Prince, 2012). Additionally, *S. aureus* must persist in the face of the host defence system and become a successful coloniser and to do so it uses microbial surface components recognising adhesive matrix molecules (MSCRAMM). MSCRAMMs (e.g. surface proteins and secreted toxins) also enable the bacterium to invade host cells. Expression of surface proteins and secreted toxins is controlled by the accessory gene regulator (*agr*), which plays an important role in the invasive airway infection. For example, one of the secreted toxins α-hemolysin

contributes to development of tissue infection through induction of pro-inflammatory responses, impairs ciliary function, calcium fluxes, and increases permeability of the airway epithelium (Liu, 2009, Parker and Prince, 2012). Moreover, *S. aureus* has evolved to persist in the lower respiratory tract during infection by avoiding host bacterial clearance mechanisms. Expression of factors such as the bacterial capsule, protein A, clumping factor A, and complement inhibitors, preventing *S. aureus* from being phagocytosed by specialised host immune cells such as macrophages and neutrophils (Lin and Peterson, 2010, Parker and Prince, 2012). It is also evident that *S. aureus* can survive within macrophages and is less resistant to neutrophil killing (Liu, 2009, Parker and Prince, 2012). Consequently, *S. aureus* secretes a number of molecules such as Panton-Valentine leukocidin and chemotaxis inhibitory protein to escape from neutrophil killing (Guerra et al., 2017, Liu, 2009, Parker and Prince, 2012, Waness, 2010).

S. aureus infections are associated with pre-existing respiratory diseases such as CF and linked to the worsening of symptoms (Ahlgren et al., 2015, Chmiel et al., 2014, Sanders et al., 2010). *S. aureus* infection in CF lungs causes damage to the epithelial surfaces, leading to the adherence of other bacterial pathogens such as *Pseudomonas aeruginosa*, which is highly associated with mortality of patients (Goss and Muhlebach, 2011, Lyczak et al., 2002). Respiratory infections caused by *S. aureus* are usually treated with antibiotics, but the emergence of antibiotic resistant strains (e.g. penicillin-, oxacillin-, and methicillin-resistant strains) has complicated treatment (Foster, 2017). For example, only a limited number of antibiotics work against methicillin-resistant *S. aureus* (MRSA) infection and there is a significant concern of the bacteria becoming resistant even to last resort antibiotics. The ability of MRSA to colonise healthy individuals possesses additional threats as these individuals usually become asymptomatic carriers of the bacterium and increase its spread (Goss and Muhlebach, 2011, Parker and Prince, 2012, Waness, 2010). Therefore, there is an urgent need for developing new antimicrobials to treat respiratory infections caused by *S. aureus*.

1.1.2 *Streptococcus pneumoniae* and respiratory tract

Streptococcus pneumoniae is extracellular Gram-positive spherical bacterium. The peptidoglycan structure of *S. pneumoniae* is unique as it contains a ribitol phosphate backbone and phosphorylcholine, meaning that the bacterium requires choline uptake (Henriques-Normark and Tuomanen, 2013). *S. pneumoniae* is commonly described as a commensal organism of the upper respiratory tract where it is usually found within nasal passages. Children under 5 years of age are the main asymptomatic carriers of *S. pneumoniae* with less than 10% of adults being carriers (Henriques-Normark and Tuomanen, 2013). *S. pneumoniae* is also a common cause of invasive airway infection. *S. pneumoniae* exists in two states: transparent and opaque colony types, with transparent colonies being dominant colonisers of the nasopharynx and opaque colonies being dominant in causing pulmonary infection (Bogaert et al., 2004, Henriques-Normark and Tuomanen, 2013). Adherence of *S. pneumoniae* to the surface of epithelial cells within nasal passages is mediated through the number of different bacterial proteins such as choline-binding protein A, pneumococcal surface adhesin A, neuraminidase, IgA protease and pilus proteins (Bogaert et al., 2004, Henriques-Normark and Tuomanen, 2013). After successful attachment to the epithelial cells, *S. pneumoniae* initiates multiplication and colonisation of the tissue. Colonisation of nasal passages with *S. pneumoniae* does not induce disease and is usually asymptomatic. However, *S. pneumoniae* transforms into a pathogenic bacterium after environmental insult and causes invasive tissue infection (Bogaert et al., 2004, Henriques-Normark and Tuomanen, 2013). After translocation into the lower respiratory tract, *S. pneumoniae* enhances expression of its virulence factors to escape from the hosts' defence mechanisms. Increased expression of neuraminidase enables the bacterium to cross through the mucus avoiding mucosal defence mechanisms and loosely adhere to the epithelial surfaces. Firm attachment to the cells is achieved through enhanced production of surface proteins and the release of pneumolysin, which impairs ciliary

function, induces release of pro-inflammatory cytokines, and increases epithelial permeability by disrupting cellular tight-junctions (Bogaert et al., 2004, Henriques-Normark and Tuomanen, 2013). After epithelial insult, *S. pneumoniae* replicates and causes further damage to the alveolar epithelium which leads to the development of pneumonia. *S. pneumoniae* also employs its polysaccharide capsule and pneumolysin to escape from host defence mechanisms. The polysaccharide capsule exhibits antiphagocytic activity which prevents the bacterium from being phagocytosed by immune cells and pneumolysin is known for impairing the function of immune cells and inducing apoptosis (Henriques-Normark and Tuomanen, 2013, Kadioglu et al., 2002, Zysk et al., 2000). If pulmonary infection with *S. pneumoniae* is not treated in time, it can progress into bacteremia and cause sepsis (Henriques-Normark and Tuomanen, 2013). Airway infections caused by *S. pneumoniae* are also associated with pre-existing respiratory diseases such as COPD (Qureshi et al., 2014, Sethi, 2010) and asthma (Toews, 2005). *S. pneumoniae* infection in the lungs of COPD and asthmatic patients causes exacerbations of disease and significant mortality. The treatment of patients with *S. pneumoniae* infection is usually based on antibiotics. However, the emergence of antibiotic resistant *S. pneumoniae* strains complicates treatment of infection because these bacterial strains exhibit resistance to most antibiotics. Vancomycin is the last resort antibiotic which still can successfully eliminate *S. pneumoniae* infection (Henriques-Normark and Tuomanen, 2013). The ability of *S. pneumoniae* to exhibit resistance to the most antibiotics creates a need for development of new antimicrobial therapies to fight the infection.

1.1.3 Nontypeable *Haemophilus influenzae* and respiratory tract

NTHi is a Gram-negative coccobacillus lacking a polysaccharide capsule. It can grow aerobically and anaerobically. However, the aerobic growth of NTHi requires hemin and nicotinamide adenine dinucleotide (NAD) (King, 2012, Van Eldere et al., 2014). NTHi is recognised as a part of the normal nasopharyngeal microbiome of healthy individuals,

but it can also spread down to the lower airways and cause inflammation and disease. NTHi is an extracellular microorganism, but some published studies observed this bacterium within or between airway epithelial cells (Clementi and Murphy, 2011). NTHi is able to adhere to cell secretions to initiate colonisation and infection of tissue. Fimbriated NTHi strains bind the mucus more efficiently than non-fimbriated NTHi strains. It multiples in the mucus and then binds to the airway epithelium which is structurally damaged and lacks functioning cilia (Read et al., 1991). Binding of NTHi to the injured but not healthy epithelium may depend on the specific receptors expressed by damaged epithelial cells. Expression of these receptors on the surface of cells may lead to the interactions of bacterial adhesins with epithelial cells. This may be a strategy used by NTHi to attach to the areas of damaged epithelium (Ahearn et al., 2017, Read et al., 1991). The first-line of host defence against bacterial airway infection is mucociliary clearance which enables the removal of pathogens from the respiratory tract. The function of mucociliary clearance is usually impaired in the lungs of patients with chronic respiratory disease (Livraghi and Randell, 2007, McIlwaine et al., 2017). This impairment of mucociliary apparatus may enable NTHi remain bound to the mucus longer, allowing bacterium to multiple and firmly adhere to the injured epithelial cells (Read et al., 1991). Furthermore, NTHi has evolved a range of strategies to disrupt the function of mucociliary apparatus (King, 2012). For example, lipooligosaccharide (LOS) present in the wall of NTHi acts as a ciliostatic substance and affects the function of ciliated cells (Denny, 1974, King and Sharma, 2015).

NTHi is associated with a variety of respiratory diseases such as CF, COPD, and pneumonia (King, 2012, King and Sharma, 2015). The ability of NTHi to colonise and infect the lower respiratory tract tissue is dependent on the presence of the underlying airway disease (Foxwell et al., 1998). NTHi is prevalent in the lungs of CF patients and its presence predisposes patients to the development of pneumonia (King and Sharma, 2015). NTHi may also induce the inflammatory responses which allow colonisation of CF lungs with *P. aeruginosa*, which is also well known for causing pneumonia (Van Eldere et

al., 2014). NTHi is a dominant cause of bacterial infection in the lungs of COPD patients and its prevalence is associated with exacerbations of the disease (King and Sharma, 2015, Van Eldere et al., 2014). Pulmonary infections caused by NTHi are usually treated with standard antibiotics and full recovery of the patients is often observed. However, treatment of NTHi-infected patients with pre-existing respiratory disease is more complicated as NTHi usually establishes a niche within the airways which protects it from antibiotics. In such case, antibiotic treatment only partially clears bacteria from the lungs. Consequently, re-occurrence of NTHi infections is common among the patients with pre-existing respiratory disease (King, 2012, Van Eldere et al., 2014).

1.2 Airway epithelium and its importance in host defence

1.2.1 Structure of respiratory tract and airway epithelium

The respiratory tract is divided in the conducting airways (also known as conditioning zone) and respiratory region (Figure 1.1). The conditioning zone comprises of the nasal cavity, pharynx, larynx, trachea, bronchi, and up to terminal bronchioles. The respiratory portion of airways consists of respiratory bronchioles, alveolar ducts and alveoli. The conducting airways are responsible for transporting cleaned and moistened air to the distal portion of the airways, whereas the function of respiratory zone is to carry out gas exchange (Soleas et al., 2012).

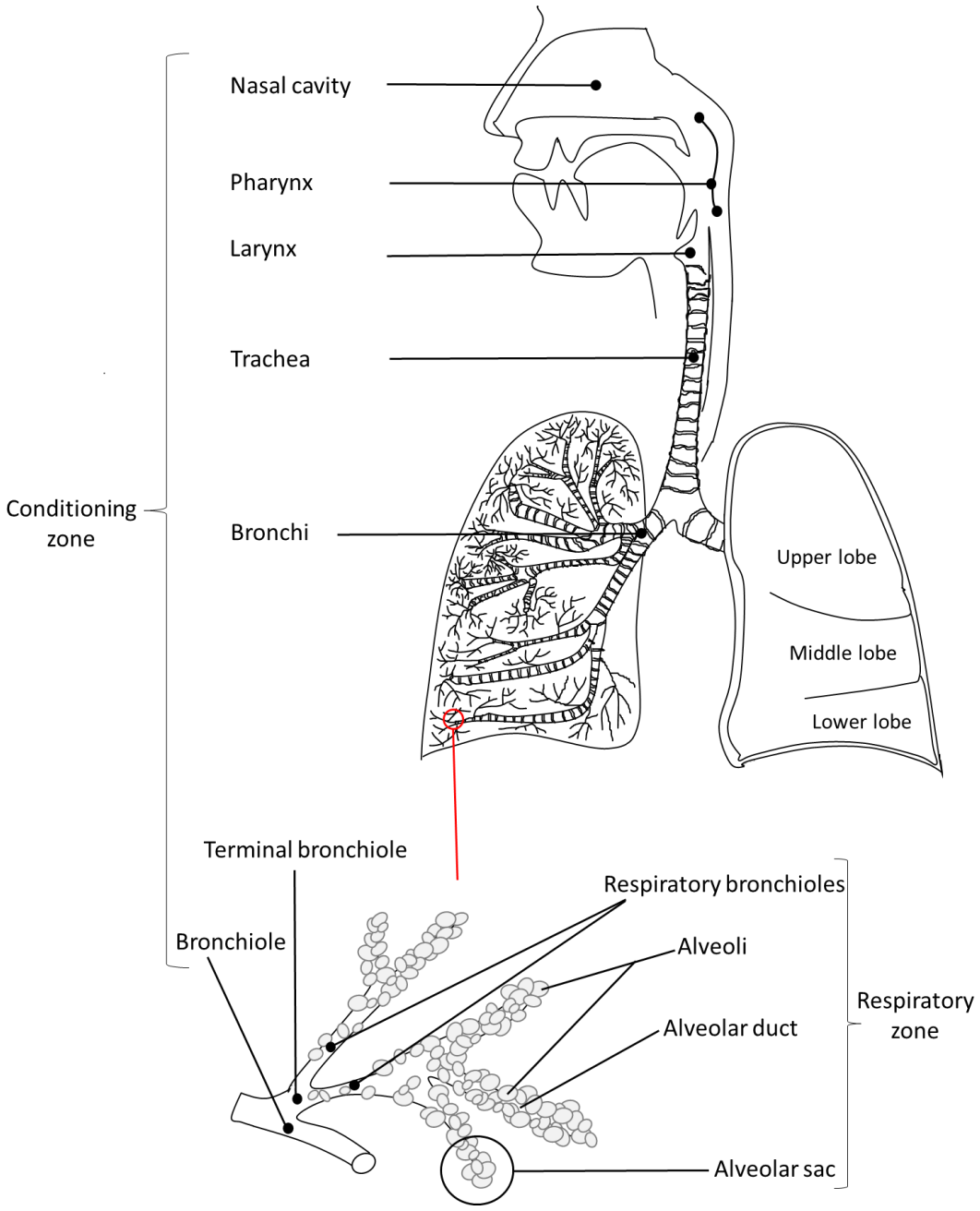

Figure 1.1: Human respiratory tract.
The human respiratory tract is divided into the conditioning zone and the respiratory zone. Conditioning zone includes the nasal cavity, pharynx, larynx, trachea, bronchi, and up to terminal bronchioles. The respiratory zone comprises of respiratory bronchioles, alveolar ducts and alveoli.

The interior of the respiratory tract is lined with a layer of epithelium, which is pseudostratified in the large airways and simple cuboidal in the small airways (Figure 1.2). Simple cuboidal epithelium changes to simple squamous epithelium in the alveolar ducts and alveoli (Crystal et al., 2008, Soleas et al., 2012). The major types of airway

epithelial cells include: ciliated, undifferentiated columnar, secretory (goblet, serous, and club cells) and basal cells. All major types of airway epithelial cells are found in the pseudostratified epithelium. The number of ciliated, goblet, and basal cells is reduced, and number of club cells is increased in the simple cuboidal epithelium. The squamous epithelium which lines the alveolar ducts and alveoli consists of specialised type 1 and type 2 alveolar cells (Crystal et al., 2008, Soleas et al., 2012).

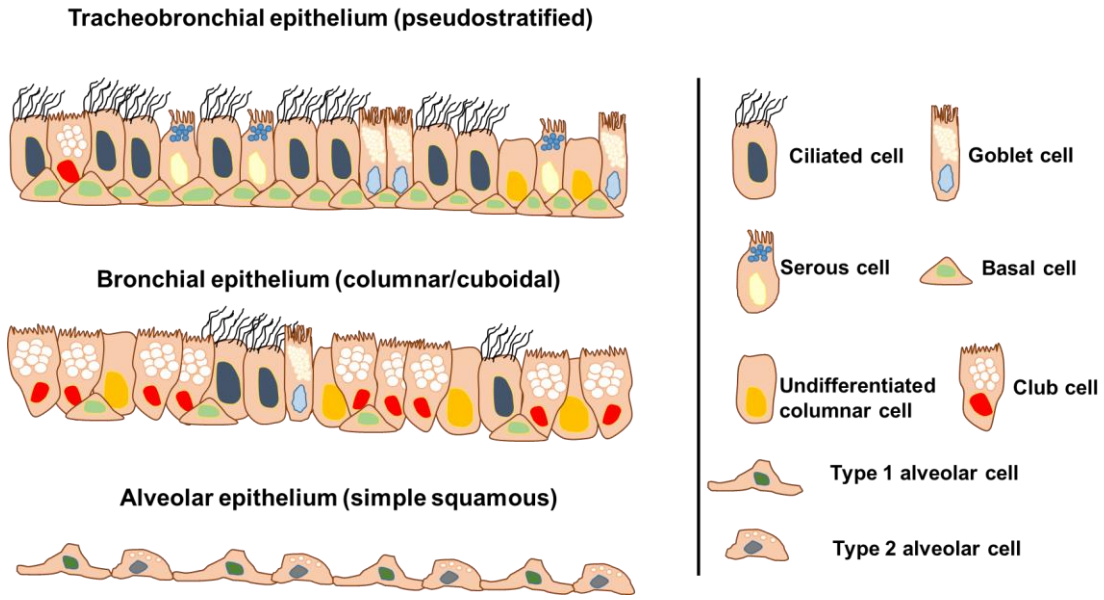

Figure 1.2: Airway epithelium and major types of epithelial cells.
Large airways are lined with pseudostratified epithelium, which later changes in to columnar-cuboidal epithelium in the small airways. Alveoli are lined with simple squamous epithelium.

1.2.2 Functions of airway epithelial cells

Major cell types of airway epithelial cells are ciliated, secretory and basal cells. Each cell plays a different role in the respiratory tract.

1.2.2.1 Ciliated cells

Ciliated cells possess motile cilia on their apical surfaces and one ciliated cell can have up to 300 cilia. The cilia have motor proteins which enable them to beat in coordinated waves, allowing the transport of mucus from the lungs. Removal of the mucus from the lungs through mucociliary apparatus is important as foreign particles and

microorganisms get trapped within mucus after invading respiratory tract. Impairment in ciliary function may result in the build-up of mucus, foreign particles, and potentially pathogenic microorganisms within the respiratory tract, which eventually may contribute to the development of respiratory disease (Knight and Holgate, 2003, Soleas et al., 2012).

1.2.2.2 Secretory cells

There are three types of secretory cells present within airway epithelium: goblet, serous, and club cells. Goblet cells also known as mucous cells, secrete mucus into the airway lumen which moistens the inhaled air. Balanced secretion and viscoelasticity of mucus are important as mucus traps harmful respiratory pathogens and particles which are removed from the respiratory tract through mucociliary apparatus (Knight and Holgate, 2003, Soleas et al., 2012). Serous cells morphologically resemble goblet cells and provide a host defence for airway mucosa by secreting bactericidal compounds such as lysozyme, lactoferrin, and peroxidase. In addition, serous cells play a role in the renewal of airway epithelium as they are able to convert into goblet cells (Crystal et al., 2008, Basbaum et al., 1990, Widdicombe and Wine, 2015). Functions of club cells involve production of bronchial surfactants and secretion of antimicrobial peptides. Club cells also play an important role as progenitor cells in the repopulation of goblet and ciliated cells in the smaller airways (Knight and Holgate, 2003, Soleas et al., 2012).

1.2.2.3 Basal cells

Basal cells are abundant in the epithelium of the conducting airways, but their numbers are significantly reduced, or they are absent in the respiratory zone (Ganesan et al., 2013, Knight and Holgate, 2003, Rackley and Stripp, 2012). Basal cells play an important role in tissue renewal after airway injury as they give a rise to secretory and ciliated cells and maintain homeostasis of normal epithelium. In addition, they express hemidesmosomes which enable them to firmly attach to the basement membrane. Basal

cells also play a role in the attachment of columnar cells (i.e. ciliated and secretory cells) to the basement membrane, as they are able to form desmosomal attachments with adjacent columnar cells (Knight and Holgate, 2003, Soleas et al., 2012).

1.2.3 Airway epithelium as the first-line host defence barrier

The airway epithelium forms a physical barrier between the body and environmental hazards. The main component of this barrier are the airway epithelial cells, which attach to each other by cell-cell junctions. These junctions include tight junctions, adherens junctions, gap junctions, and desmosomes. Cell-cell junctions form a barrier to respiratory pathogen entry and spreading into the airway submucosa (Vareille et al., 2011).

The mucus layer lining the airway epithelium protects the airway mucosa as mucus forms a semipermeable barrier. This barrier allows the exchange of gases, water, and nutrients but it is impermeable to most lung pathogens and irritants (Vareille et al., 2011). Airborne particles and respiratory pathogens are trapped within the mucus layer, where they are inactivated by the innate mucosal defence system and removed from the respiratory tract through the mucociliary apparatus (Joo et al., 2004). Mucus is continuously secreted by epithelial goblet cells and mucous cells of the submucosal glands. The main components of mucus include mucins, antimicrobial substances, cytokines, and antioxidant proteins. Balanced secretion of mucus is important as an increased secretion of mucus in lung infection causes airway obstruction which leads to impaired respiratory function. Mucus hypersecretion is associated with the pathogenesis of severe airway obstruction in infection-induced exacerbations of CF, COPD, and asthma (Vareille et al., 2011).

1.2.4 Antimicrobial products of the airway epithelium

Airway epithelial cells produce antimicrobial products which play a host defence role in the airway mucosa. Production of many of these is induced upon recognition of airborne particles, including pathogens (Bals, 2000, Parker and Prince, 2011). Major antimicrobial products of airway epithelium include β-defensins, cathelicidin LL37, C-C motif chemokine ligand 20 (CCL20, also known as MIP-3α), lactoferrin, and lysozyme.

1.2.4.1 β-defensins

There are six different β-defensin peptides found in the human body, but only β-defensins 1-4 are expressed in the airway epithelium (Parker and Prince, 2011). β-defensins have a great range of activity against enveloped viruses, fungi, and as well as bacteria (Bals, 2000). For example, β-defensin-1 and -2 exhibit bactericidal activity against *Escherichia coli* and *P. aeruginosa* (Harder et al., 2000, Singh et al., 1998). β-defensins are normally not found in healthy bronchoalveolar lavage fluid (BAL), but their levels are increased in airway fluid from the patients with respiratory disease (Singh et al., 1998).

1.2.4.2 Cathelicidin (LL37)

LL37 is a cationic peptide that has a broad-spectrum of antimicrobial activity (Bals, 2000, Parker and Prince, 2011). LL37 possesses bactericidal activity and has been shown to kill Gram-negative bacteria *in vitro* (Singh et al., 2000). In addition to its killing ability, LL37 exhibits anti-inflammatory functions. LL37 was shown to play a role in the blocking of Gram-negative bacterial signalling pathways through toll-like receptor 4 (TLR4) (Kahlenberg and Kaplan, 2013) and reduce levels of pro-inflammatory cytokines in the airways of influenza virus-infected mice (Barlow et al., 2011).

1.2.4.3 Motif chemokine ligand 20 (CCL20)

CCL20 is another airway protein that exhibits antimicrobial and chemotactic functions. Production and secretion of CCL20 is induced by a variety of microorganisms (Parker

and Prince, 2011). It was shown to be secreted in response to *Brucella abortus* infection and pro-inflammatory cytokines produced by *B. abortus*-infected monocytes. It does not exhibit direct antimicrobial properties and acts by stimulating the recruitment of adaptive immune cells to the site of infection (Hielpos et al., 2015). Interaction of CCL20 with C-C chemokine receptor type 6 (CCR6) was shown to induce migration of immune cells such as immature dendritic cells and T-cells to the site of infection (Starner et al., 2003).

1.2.4.4 Lactoferrin

Lactoferrin is an iron-binding protein found in the serum and mucosal secretions. It can produce an iron deficient environment which limits the growth of microorganisms. Lactoferrin is directly bactericidal to microorganisms and can increase the activity of immunoglobulin A (Actor et al., 2009, Ellison et al., 1988, Lee et al., 2016, Orsi, 2004). Lactoferrin causes release of lipopolysaccharide (LPS) from the outer membrane of *E. coli* and *Salmonella typhimurium* (Ellison et al., 1988). This results in increased permeability of the bacterial outer membrane, making bacteria more susceptible to other host defence mechanisms. It has also been demonstrated that the bactericidal activity of lactoferrin against Gram-negative and Gram-positive bacteria increased synergistically when in combination with lysozyme (André et al., 2015, Singh et al., 2000).

1.2.4.5 Lysozyme

Lysozyme is secreted by epithelial cells and submucosal glands of the respiratory tract (Dajani et al., 2005). Levels of lysozyme in the lungs are directly associated with the ability of airways to clear bacterial infection (Dajani et al., 2005). In addition, lysozyme in combination with human secretory leukocyte peptidase inhibitor (SLPI) was shown to have an increased bacterial killing activity, meaning that these proteins functioned synergistically (Singh et al., 2000). It has been suggested that lysozyme cannot easily penetrate the outer membrane of Gram-negative bacteria, suggesting that it performs a secondary function in host defence against these microorganisms (Liu et al., 2015,

Martinez and Carroll, 1980, Ragland and Criss, 2017, Ragland et al., 2018). In contrast, Gram-positive bacterial strains are highly sensitive to lysozyme activity as it can degrade β-(1→4)-glycosidic linkage of the N-acetylglucosaminyl-N-acetylmuramic acid polymer in the bacterial peptidoglycan (Liu et al., 2015, Ragland and Criss, 2017, Wadström and Hisatsune, 1970).

1.2.4.6 Antimicrobial products of airway epithelium for the treatment of pulmonary infections

Interest in the role of airway epithelium derived peptides and proteins in host defence has become of more significance with the emergence of antibiotic resistant bacterial strains. Respiratory epithelium derived products have the potential to become new antimicrobial agents as they can kill a wide range of microorganisms and are largely non-immunogenic (Hancock and Lehrer, 1998). Understanding the mechanisms employed by antimicrobial peptides and proteins in the killing of microbes may contribute to the development of novel treatment for microbial infections (Bals, 2000, Czaplewski et al., 2016, Prat and Lacoma, 2016, Hancock and Lehrer, 1998). BPIFA1, as a multifunctional, antimicrobial protein of the respiratory tract, is a potential candidate which could be used as antimicrobial agent for the treatment of respiratory tract infections in the future. However, the mechanisms by which BPIFA1 performs its biological functions are not fully determined and require further investigations. Consequently, the main focus of this thesis is to gain a better understanding of the mechanisms used by BPIFA1 to perform its antimicrobial functions and the role of BPIFA1 in host defence against respiratory bacterial pathogens.

1.3 PLUNC/BPIF protein family

The **P**alate **L**ung and **N**asal **E**pithelium **C**lone (PLUNC) proteins belong to, and form a separate branch of, the BPI/LBP protein superfamily, and consequently, were recently renamed as BPIF proteins (Bingle and Craven, 2002, Bingle et al., 2011b). BPIF proteins

share sequence and structure similarity with four other members of BPI/LBP protein superfamily, namely: bactericidal/permeability-increasing protein (BPI), lipopolysaccharide (LPS)-binding protein (LBP), phospholipid transfer protein (PLTP), and cholesteryl ester-transfer protein (CETP) (Bingle and Craven, 2002). BPI proteins are composed of C-terminal and N-terminal domains. The cationic, antibacterial and endotoxin-neutralising functions of BPI is conferred by its N-terminal region, whereas anionic/hydrophobic and opsonic functions of BPI is conferred by its C-terminal region (Levy, 2000). BPI has anti-inflammatory activity as it inhibits LPS signalling and prevents LPS transfer to Cluster of differentiation-14 (CD14) (Elsbach and Weiss, 1998, Levy, 2000, Tobias et al., 1997). This, in turn, stops activation of toll-like receptors (TLRs) and production of pro-inflammatory cytokines. In comparison to BPI, LBP has a pro-inflammatory activity as it binds to LPS to transfer it to CD14 (Elsbach and Weiss, 1998). BPIF family proteins share between 13% to 22% pairwise amino acid identity with proteins of the wider BPI/LBP family (Bingle and Craven, 2002). The structural similarity of BPIF proteins to LBP and BPI initially led to the suggestion that BPIF proteins may have a role in host defence against bacteria (Bingle and Craven, 2002, Bingle et al., 2004). This hypothesis is further supported by the rapid evolution of BPIF proteins and their low levels of sequence identity (Bingle and Craven, 2002, Bingle et al., 2011a). The BPIF family is subdivided into two groups: BPIFA (previously short PLUNC (SPLUNC)) proteins, and BPIFB (previously long PLUNC (LPLUNC)) proteins (Bingle and Craven, 2002, Bingle et al., 2011b). This subdivision is based on the size of BPIF proteins and the two-domain structure of the BPI fold. BPIFA proteins contain one domain structurally similar to N-terminal domain of BPI, whereas BPIFB proteins contain two domains structurally similar to both N-terminal and C-terminal domains of BPI (Bingle and Craven, 2002, Bingle et al., 2004). Human BPIFA proteins (BPIFA1, BPIFA2, and BPIFA3) consist of approximately 250 amino acids whereas human BPIFB proteins (BPIFB1, BPIFB2, BPIFB3, BPIFB4 and BPIFB6) consist of approximately 450 amino acids (Bingle and Craven, 2002, Bingle et al., 2011a). BPIF proteins are encoded by genes

found in a single locus on human chromosome 20 and on mouse chromosome 2 (Figure 1.3) (Bingle and Craven, 2002, Bingle et al., 2011a). Fourteen *Bpif* genes (of which one *Bpifa2f-ps* is a pseudogene) have been identified in the mouse locus, whereas eleven *BPIF* genes (of which three *BPIFA4P, BPIFB5P*, and *BPIFB9P* are pseudogenes) have been identified in the human locus (Bingle et al., 2011a). It is important to note that the number of *BPIF* genes present varies across mammalian species and that the full repertoire of *BPIF* genes are only found in mammals (Bingle et al., 2004, Bingle et al., 2011a).

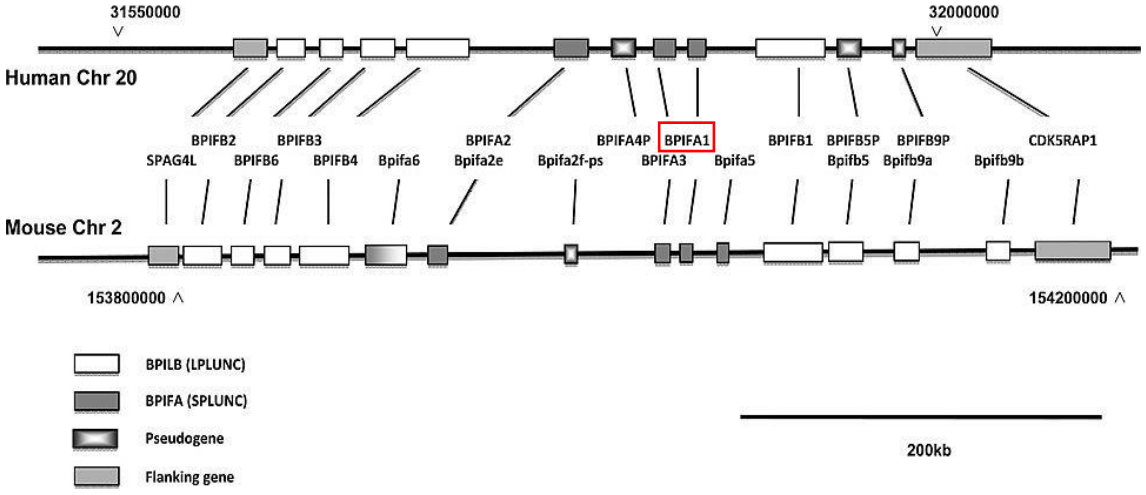

Figure 1.3: Chromosomal positions of human and mouse *BPIF* genes.
Human *BPIF* genes are located on the chromosome 20 and mouse *BPIF* genes are located on the chromosome 2. Orthologs of individual genes are demonstrated by arrows. Chromosomal positions of human and mouse *BPIF* genes on the chromosomes are indicated by arrowheads. Grey boxes represent *BPIFA* genes, white boxes – *BPIFB* genes, and shaded boxes – *BPIF* pseudogenes. *SPA4L* and *CDK5RAP1* are unrelated genes flanking the loci of mouse and human *BPIF* genes. *BPIFA1* is highlighted in red rectangle. Scale bar: 200kb. Image re-used with permission from (Bingle et al., 2011a), copyright 2011 Portland Press.

1.4 Expression and distribution of BPIFA1

1.4.1 Mouse BPIFA1

BPIFA1 was first described in 1999. The gene was localised to the epithelium of nasal structures of the embryonic mouse. BPIFA1 was also detected in the epithelium of the trachea and upper bronchi of adult mice (Weston et al., 1999). Following this, a study from our laboratory confirmed that nasal passages and upper respiratory tract of mice

are the main sites of *Bpifa1* expression (Musa et al., 2012). Further analysis of mouse BPIFA1 localisation sites revealed that BPIFA1 is also found in Bowman's glands of the nasal passages and serous glands in the posterior region of tongue (Musa et al., 2012). The presence of BPIFA1 was also confirmed in Bowman's gland ducts. In addition, epithelium of larynx at the opening of trachea was shown to be positive for BPIFA1. It was also reported that BPIFA1 is localised within non-ciliated epithelial cells of respiratory tract (Musa et al., 2012). Recently, mouse BPIFA1 has also been shown to be present in the epithelium of middle ear (Mulay et al., 2016).

1.4.2 Human BPIFA1

Expression of *BPIFA1* is also found in the major airways of humans (Campos et al., 2004, Bingle and Bingle, 2000, Bingle et al., 2005). BPIFA1 has been localised to the serous cells of submucosal ducts and glands and non-ciliated cells of the surface bronchial epithelium have been shown to be positive for *BPIFA1* expression. In the distal airways, BPIFA1 has been detected in luminal secretions and along the ciliary border of the epithelium (Campos et al., 2004, Bingle et al., 2005). Furthermore, Bingle et al. showed that BPIFA1 is present in the minor glands of the nasal cavity, sinuses and the posterior part of the tongue (Bingle et al., 2005). The presence of BPIFA1 in nasal lavage fluid has been reported (Ghafouri et al., 2004). BPIFA1 has been localised to the normal submandibular gland of human, where it is found within the ducts and the mucous cells of acini (Vargas et al., 2008). The highest expression of *BPIFA1* is found in the trachea and lungs (Figure 1.4). More recently, expression of *BPIFA1* was also shown within the epithelium of middle ear (Hadzhiev et al., 2017). BPIFA1 is not found in the normal epithelium of the smaller airways (peripheral lung). However, the levels of BPIFA1 are highly increased in the smaller airways in respiratory diseases such as CF, where BPIFA1 is seen in the inflammatory plugs within the airway lumen, suggesting that it is secreted (Bingle et al., 2007).

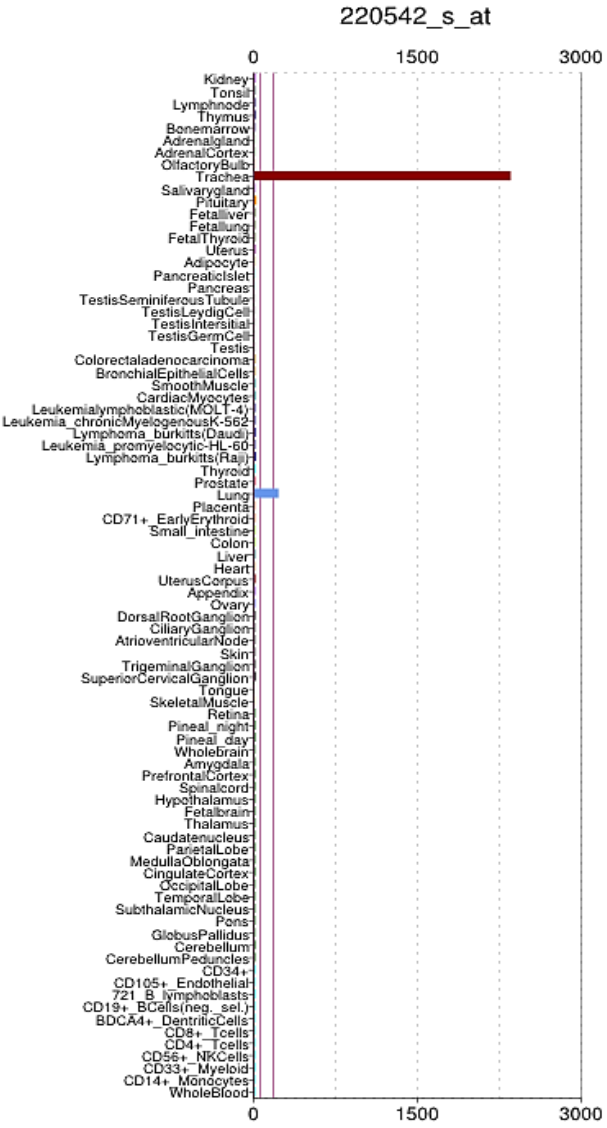

Figure 1.4: *BPIFA1* is expressed in limited tissues.
Human tissue microarray data, showing a restricted expression of *BPIFA1*. The highest expression found in trachea and lungs. Data was recovered from BioGPS portal and is based on the study by Su et al. (Su et al., 2004).

1.5 Structure of BPIFA1

The structures of human and mouse BPIFA1 proteins have been recently defined. Availability of BPIFA1 secondary structures may facilitate determination of the mechanisms used by BPIFA1 to perform its biological functions.

1.5.1 Human BPIFA1

Bingle et al. were first to predict the secondary structure of BPIFA1 and suggest its similarity to the secondary structure of BPI proteins (Bingle and Craven, 2002). BPIFA1 was also determined as glycine-leucine-rich protein that may confer BPIFA1 with a high degree of conformational flexibility. Furthermore, the glycine-leucine-rich region was suggested to be associated with a hydrophobic core of protein, potentially allowing it to bind to hydrophobic lipids (Bingle and Craven, 2002). More recently the crystal structure of BPIFA1 has been determined (Figure 1.5). Two studies defined similar structures, with exception of two helices and a short helix fragment (located in the region between residues 193 and 203), which were absent in one study (Garland et al., 2013, Ning et al., 2014). BPIFA1 was described as a monomer comprising of six antiparallel β-sheets orientated centrally within the structure and flanked by six α-helices (Garland et al., 2013). The S18 region (G22-A39) of BPIFA1 was not present in the crystal structure, with the first residue identified being amino acid 43 (Garland et al., 2013). Residue 43 was shown to be located in the close proximity to a cluster of charged residues (D112, K138, R152 and D193), forming the salt bridge within the structure. This was reported to be associated with pH-dependant functioning of protein and its removal was shown to render BPIFA1 activity pH-insensitive (Garland et al., 2013). The cluster of charged residues and S18 region of human BPIFA1 were shown to differ from mouse and rat BPIFA1 proteins, suggesting that function and pH-sensitivity may vary among species (Garland et al., 2013). Moreover, Ning et al. reported that α3 helix and β5 sheet of BPIFA1 are connected by disulphide bridge, which provides the whole protein structure with stability (Ning et al., 2014). However, the disulphide bridge was later determined to be present between α5 helix and β5 sheet (Walton et al., 2016). These discrepancies were associated with the different methods of protein crystallisation used in the studies, because Ning et al. reported that BPIFA1 consists of 4 helices (Ning et al., 2014) whereas it actually consists of 6 helices. Position of α3-helix determined by Ning et al.

was actually a position of α5-helix as shown in other studies (Ahmad et al., 2016, Garland et al., 2013, Walton et al., 2016).

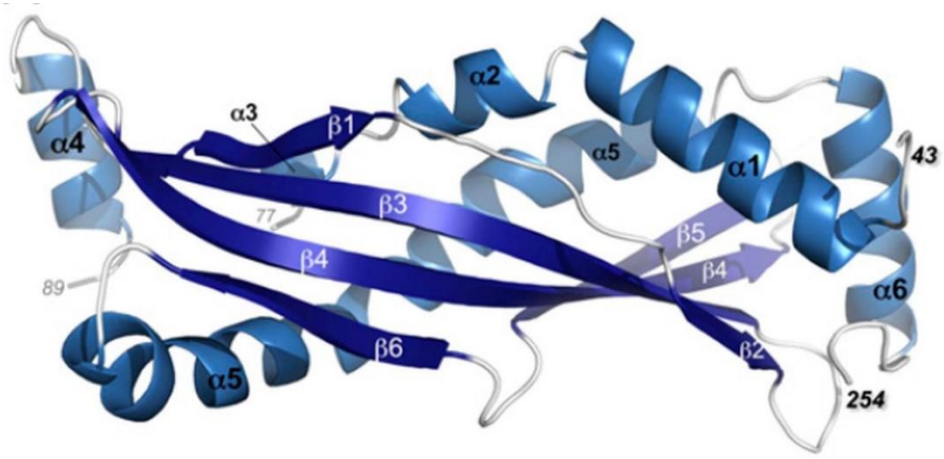

Figure 1.5: Structure of human BPIFA1.
The protein consists of six α-helices and six β-sheets. Residues 43, 77, 89, and 254 are labelled for clarity. Image re-used with permission from (Garland et al., 2013), copyright PNAS.

1.5.2 Mouse BPIFA1

Differences between mouse and human BPIFA1 were first identified by Bingle et al. (Bingle and Bingle, 2000). Weston et al. demonstrated that extreme N-terminal region of mouse BPIFA1 contains a PLPL repeat region, which was later shown to be missing from the sequence of human BPIFA1 (Bingle and Bingle, 2000, Weston et al., 1999). This region exhibits high variability among different species (Bingle and Bingle, 2000, Garland et al., 2013). Mouse BPIFA1 consists of 278 amino acids, while human BPIFA1 consists of 256 amino acids, meaning that mouse BPIFA1 (28.6kDa) is a slightly larger protein compared to human BPIFA1 (26.6kDa). Human and mouse BPIFA1 proteins share 66% sequence identity, suggesting that some mechanisms by which these both BPIFA1 proteins perform biological functions may differ (Britto and Cohn, 2015, Little and Redinbo, 2018). For example, it was reported that proline-rich region of mouse BPIFA1 is longer compared to human BPIFA1 and a salt bridge present in the structure of human BPIFA1 is missing from mouse BPIFA1 (Little and Redinbo, 2018). The salt bridge of

human BPIFA1 (charged residues D112, K138, R152 and D193) is not conserved in mouse BPIFA1, meaning that electrostatic charge of human and mouse BPIFA1 proteins are different. Human BPIFA1 exhibits a positive surface electrostatic charge within this region of protein (Garland et al., 2013), whereas mouse BPIFA1 shows a negative charge in this region (Little and Redinbo, 2018). The overall fold of mouse BPIFA1 was determined to be similar to the fold of human BPIFA1, with the greatest structural variability detected within the regions of the connecting loops: β3-β4, β4-β5, β6-α5 (Little and Redinbo, 2018). In addition, α4-helices were shown to differ between human and mouse BPIFA1 proteins (Figure 1.6). The α4-helix of mouse BPIFA1 folds in two distinct helices (α-4a and α-4b), whereas in human BPIFA1 α4 is present as single helix (Little and Redinbo, 2018).

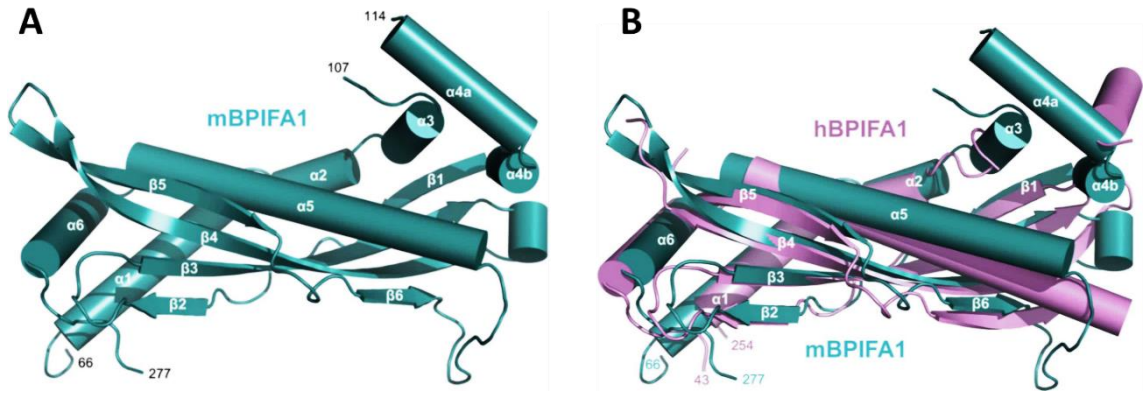

Figure 1.6: Structure of mouse BPIFA1.
Structure of mouse BPIFA1, revealing residues 66-277 and lacking residues 108-113. Mouse BPIFA1 consists of six β-sheets orientated centrally within the structure and flanked by six α-helices (α4-helix folds in two distinct helices: α-4a and α-4b. Residues 66, 107, 114 and 277 are labelled for clarity (**A**). Superposition of mouse and human BPIFA1 proteins, showing structure similarity between two proteins (**B**). Images re-used with permission from (Little and Redinbo, 2018), copyright International Union of Crystallography.

1.6 Biological functions of BPIFA1

Studies have shown that BPIFA1 exhibits a variety of functions, including: antimicrobial, immunodulatory, chemotactic, and surfactant. BPIFA1 was also reported to be involved in the mucociliary clearance and regulation of airway surface liquid (ASL).

1.6.1 Antibacterial properties of BPIFA1

The structural similarity of BPIFA1 to BPI/LBP protein superfamily led to the prediction of an involvement in host defence (Bingle and Craven, 2002). Many different studies have been published on the antimicrobial activity of human and mouse BPIFA1 proteins against bacterial pathogens with the main focus on Gram-negative bacteria.

1.6.1.1 Antibacterial functions of human BPIFA1

In vitro studies with recombinant human BPIFA1 showed that the protein exhibits bacteriostatic activity against *P. aeruginosa*, *Mycoplasma pneumoniae*, and *Klebsiella pneumoniae*. The ability of human BPIFA1 to inhibit the growth of bacterium was determined to be dose-dependent (Chu et al., 2010, Sayeed et al., 2013, Zhou et al., 2008). It was also reported that BPIFA1 maintained its bacteriostatic activity against Gram-negative bacteria for 24hrs (Sayeed et al., 2013). Activity of BPIFA1 against *P. aeruginosa* was shown to be associated with its ability to form small pores in the bacterial outer membrane, suggesting that BPIFA1 increases permeability of the bacterial cell wall (Sayeed et al., 2013). The antibacterial role of BPIFA1 was studied in *M. pneumoniae* infection model *in vivo* using human BPIFA1 transgenic mice. Bacterial load was three-fold lower and bacterial clearance was increased in the lungs of BPIFA1 transgenic mice compared to controls. Bacteriostatic activity of BPIFA1 against *M. pneumoniae* was linked to its ability to inhibit P1 adhesin expression, which plays an important role in the adherence process of *M. pneumoniae* to the host epithelial cells (Gally et al., 2011). Human BPIFA1 is also capable of interfering with formation of Gram-negative bacterial biofilm *in vitro* (Gakhar et al., 2010). These studies demonstrated the antibacterial properties of human BPIFA1 but neither the regions of protein important for these functions nor mechanisms by which BPIFA1 performs its biological activity were fully defined. Recently Walton et al. and Ahmad et al. undertook studies to determine the regions of human BPIFA1 important for protein's antibacterial functions. In these studies, it was further confirmed that human BPIFA1 acts as bacteriostatic and anti-biofilm agent

against Gram-negative bacteria, including *P. aeruginosa* and *Burkholderia cepacia* (Ahmad et al., 2016, Walton et al., 2016). The antibacterial activity of human BPIFA1 was strain dependent for *B. cepacia* strains (Ahmad et al., 2016). Both studies reported that antimicrobial activity of human BPIFA1 against Gram-negative pathogens was dependent on the α4-helix (76-105 residues) and that deletion of this region resulted in the loss of antibacterial properties (Ahmad et al., 2016, Walton et al., 2016).

BPIFA1 does not exhibit anti-growth and anti-biofilm properties against *S. aureus*, suggesting that BPIFA1 exerts antibacterial activity only against Gram-negative bacteria (Ahmad et al., 2016, Walton et al., 2016). However human BPIFA1 was able to inhibit the formation of *S. aureus* biofilm after the electrostatic charge of GL-rich region between residues 58 and 88 was altered (Walton et al., 2016). This suggests that the neutral electrostatic charge of human BPIFA1 surface within GL-rich region may be linked to BPIFA1's inability to exhibit anti-biofilm activity against Gram-positive bacteria (Walton et al., 2016). However, it is important to mention that this study analysed anti-biofilm activity of human BPIFA1 against only one Gram-positive bacterium, *S. aureus*. Therefore, antibacterial activity of BPIFA1 against Gram-positive bacteria requires further investigations to enable a full determination of its role against Gram-positive pathogens.

1.6.1.2 Antibacterial functions of mouse BPIFA1

Antibacterial properties of mouse BPIFA1 have also been studied and it has been shown that it is also able to act as bacteriostatic and anti-biofilm agent. The role of mouse BPIFA1 was investigated in respiratory bacterial infection models with NTHi, *P. aeruginosa*, *M. pneumoniae*, *K. pneumoniae*, and *S. aureus*. *In vivo* studies with WT and *Bpifa1*$^{-/-}$ mice intranasally challenged with *P. aeruginosa* and intratracheally challenged with *K. pneumoniae* showed that bacterial load was significantly higher in *Bpifa1*$^{-/-}$ mice compared to control littermate mice. It was also demonstrated that mouse BPIFA1 was able to inhibit the formation of *P. aeruginosa* and *K. pneumoniae* biofilms *in vitro* and that bacterial biofilm biomass was reduced in the dose-dependent pattern (Liu et al., 2013a,

Liu et al., 2013b). Deficiency of BPIFA1 was also shown to be associated with increased bacterial burden and inflammation in the lungs of *Bpifa1*$^{-/-}$ mice challenged with NTHi and *M. pneumoniae* (Gally et al., 2011, Jiang et al., 2013b). In addition, recombinant mouse BPIFA1 was shown to exhibit bacteriostatic activity against *M. pneumoniae* in a dose-dependent manner (Chu et al., 2007). Therefore, existing data shows anti-growth and anti-biofilm functions of mouse BPIFA1 against Gram-negative bacteria, but there is no data available on the direct antibacterial activity of mouse BPIFA1 against Gram-positive bacteria. Mouse BPIFA1 has been shown to be able to bind *S. aureus in vivo* (Ventura et al., 2008) but no other antibacterial properties of protein against this Gram-positive pathogen have been investigated.

Overall, ability of the mouse protein to act as a bacteriostatic and anti-biofilm agent in the host defence against Gram-negative bacteria is currently well reported. However, none of the studies investigated the mechanisms by which mouse BPIFA1 performs its antibacterial activity. The regions of protein important for antibacterial functions of mouse BPIFA1 also remain to be determined.

1.6.2 Antiviral activity of BPIFA1

Antimicrobial activity of BPIFA1 is not unique for bacterial pathogens as BPIFA1 also plays a role in the host defence against viral infections. Antiviral activity of BPIFA1 was first reported in the study by Zhou et al., which showed that addition of BPIFA1 to the primary cultures of peripheral blood lymphocytes (PBLs) infected with Epstein-Barr virus (EBV) increased apoptosis of virus-infected PBLs and reduced the expression of EBV latent membrane protein 1 (LMP1). These findings suggested a role for BPIFA1 in host defence against EBV-induced nasopharyngeal carcinoma (Zhou et al., 2008). Subsequently, it was revealed that BPIFA1 exhibits antiviral activity against respiratory syncytial virus (RSV), human rhinovirus (HRV) and influenza A virus (IAV) (Akram et al., 2018, Fornander et al., 2011, Wu et al., 2014). Decreased levels of BPIFA1 were shown to be associated with worse outcome of RSV-infected infants, suggesting that lower

levels of BPIFA1 are linked to the development of severe pneumonia (Fornander et al., 2011). Furthermore, BPIFA1 deficient mice were shown to have increased IAV and HRV viral replication and cell death compared to their littermate controls (Akram et al., 2018, Wu et al., 2014).

Overall, the findings suggest an important role of BPIFA1 in host defence against viral infections and reduced levels or loss of BPIFA1 may be a contributing factor to the increase of viral replication and worsening of infection.

1.6.3 Chemotactic properties of BPIFA1

Chemotactic properties of BPIFA1 were examined in the presence of bacterial infections caused by *P. aeruginosa*, *M. pneumoniae*, and *K. pneumoniae*. *In vivo* and *in vitro* studies were used to determine the effect of mouse and human BPIFA1 on migratory immune cells. Results from *in vitro* cell migration assay showed that recombinant human BPIFA1 stimulates migration of neutrophils and macrophages, suggesting that human BPIFA1 acts as a chemotactic agent (Sayeed et al., 2013). In agreement with these findings it was also shown that migration of neutrophils and macrophages was induced after human BPIFA1 transgenic mice were challenged with *P. aeruginosa* (Lukinskiene et al., 2011). This study also reported that human BPIFA1 transgenic mice demonstrated a reduced recruitment of neutrophils compared to control WT mice, suggesting that over-expression of *BPIFA1* may reduce tissue inflammation (Lukinskiene et al., 2011). The ability of BPIFA1 to act as anti-inflammatory factor was also shown by Chu et al., demonstrating that *in vivo* blockade of BPIFA1 in mice before intranasal challenge with *M. pneumoniae* resulted in increased neutrophil recruitment into the lungs. The number of neutrophils detected in the BAL fluid from anti-BPIFA1 pre-treated mice after bacterial exposure was significantly higher compared to WT mice (Chu et al., 2007). These findings are similar to those of Lukinskiene et al. and suggest that up-regulation of *Bpifa1* in respiratory bacterial infection may reduce tissue inflammation and enhance bacterial clearance (Chu et al., 2007, Lukinskiene et al., 2011). Other studies also demonstrated

significantly increased neutrophil counts in the BAL fluid from *Bpifa1*$^{-/-}$ mice after bacterial exposure compared to WT mice (Gally et al., 2011, Liu et al., 2013a, Liu et al., 2013b). Despite increased neutrophil numbers in the lungs of *Bpifa1*$^{-/-}$ mice, it was reported that the activity of neutrophil elastase was significantly diminished compared to WT mice. These findings suggested that reduced neutrophil elastase activity may contribute to the impairment of host defence against bacterial infection in *Bpifa1*$^{-/-}$ mice (Gally et al., 2011). It was also shown that macrophage infiltration to the lungs of WT mice challenged with *P. aeruginosa* was greater compared to *Bpifa1*$^{-/-}$ mice, suggesting that the killing of bacteria in WT mice is more efficient (Liu et al., 2013b).

Overall, these studies suggest that BPIFA1 may act as anti-inflammatory agent and its loss in the case of respiratory bacterial infection may be linked to the increased severity of tissue inflammation due to the recruitment of elevated numbers of inflammatory cells to the site of infection.

1.6.4 Immunomodulatory properties of BPIFA1

A number of studies have investigated the immunodulatory properties of BPIFA1 in the inflammation caused by bacterial infections. BPIFA1 appears to suppress the release of pro-inflammatory cytokines in the response to Gram-negative bacterial challenge. *In vivo* and *in vitro* studies showed that the release of pro-inflammatory cytokines such as IL-8, IL-6, TNF-α, IL-1α and IL-1β was significantly elevated in the absence of BPIFA1 (Chu et al., 2007, Liu et al., 2013a, Liu et al., 2013b, Lukinskiene et al., 2011). Considerably increased production of pro-inflammatory chemokines such as CXCL1, CXCL2, CCL3, CCL5 and CCL20 was also detected in the absence of BPIFA1 (Liu et al., 2013a, Liu et al., 2013b, Lukinskiene et al., 2011). Increased release of pro-inflammatory molecules in the absence of BPIFA1 is also directly linked to the elevated infiltration of inflammatory cells to the site of infection, and these both events are directly associated with increased severity of tissue inflammation. These studies also showed that the profile of pro-inflammatory cytokines and chemokines generated by the host defence system in the

response to bacterial challenge was bacterial strain dependent. BPIFA1 may also control airway inflammation by influencing production of other antimicrobial molecules. It was reported that *Bpifa1*$^{-/-}$ mice show significantly decreased expression of *LL37*, *Lysozyme*, and *Lactoferrin* after bacterial challenge compared to WT mice (Liu et al., 2013b). Reduced expression of *LL37*, *Lysozyme*, and *Lactoferrin* could contribute to a decrease in bacterial clearance from the lungs of mice.

An immunodulatory role of BPIFA1 was also investigated in an allergic airway inflammation study, where BPIFA1 deficiency caused an increased production of T_H2 cytokines and was associated with elevated numbers of eosinophils. This allergic host defence response was rescued by transgenic expression of *Bpifa1* (Wright et al., 2010). In agreement with this this study, Thaikoottathil et al. showed that ovalbumin-challenge significantly increased levels of eotaxin-2 in the lungs of *Bpifa1*$^{-/-}$ mice compared to WT. Elevated levels of eotaxin-2 were directly associated with increased number of eosinophils in the lungs, causing allergic airway inflammation (Thaikoottathil et al., 2012). In contrast to the findings of above studies, Di et al. showed that BPIFA1 is capable of acting as both a pro-inflammatory and anti-inflammatory factor (Di et al., 2013). The immunodulatory role of BPIFA1 was investigated in a model of respiratory inflammation caused by inhalation of carbon nanotubules. Overexpression of human *BPIFA1* in mice was associated with significantly increased leukocyte infiltration and release of pro-inflammatory cytokines in the lungs during acute inflammation caused by inhalation of the nanotubules. These findings suggest that BPIFA1 functions as pro-inflammatory agent. However, an anti-inflammatory activity of BPIFA1 was observed during the chronic phase of inflammation. BPIFA1 was shown to reduce levels of TNF-α secretion and inhibit processes causing pulmonary fibrosis.

1.6.5 Role of BPIFA1 in mucociliary clearance

Another proposed function of BPIFA1 is its ability to influence mucociliary clearance. BPIFA1 loss in the airways of mice causes a reduction in the expression of major airway

mucin genes (*Muc5ac* and *Muc5b)* and the gene for Clara cell secretory protein (CCSP), which contribute to the formation of extracellular lining fluid and are involved in mucociliary clearance (Liu et al., 2013b). Ablation of BPIFA1 also decreased expression of *Foxj1*, a gene involved in ciliogenesis and a marker of ciliated cells. Consequently, it was suggested that BPIFA1 deficiency is associated with impaired mucociliary clearance and causes an increased bacterial burden in the lungs during the airway infection (Liu et al., 2013b). A study on chinchillas reported that BPIFA1 exhibits surfactant properties, which are essential for a normal function of Eustachian tube (ET) in NTHi-induced Otitis media (McGillivary and Bakaletz, 2010). Silencing expression of chinchilla *Bpifa1* was shown to result in the impaired mucociliary clearance in the ET, which is associated with defective functioning of the tympanum. In contrast to this, Mulay et al. reported no phenotypic alterations and inflammation signs in the middle ear of NTHi-challenged BPIFA1 deficient mice, suggesting that the absence of BPIFA1 alone does not cause development of Otitis media (Mulay et al., 2018). Discrepancies in these results may be associated with the usage of different animal models, different techniques of BPIFA1 deletion, size of NTHi inoculum and usage of different NTHi strains.

1.6.6 Surfactant properties of BPIFA1

The possibility that BPIFA1 may exhibit surfactant activity was predicted after BPIFA1 and latherin were shown to share sequence similarity. Bingle et al. demonstrated that latherin, which is a known surfactant protein, shares sequence similarity with BPIFA1 (Bingle et al., 2004). Afterwards, protein sequence similarity between BPIFA1 and latherin was reported in other two studies (Gakhar et al., 2010, McDonald et al., 2009), but Gakhar et al. was first to reveal surfactant properties of BPIFA1. It was shown that BPIFA1 reduced surface tension and inhibited *P. aeruginosa* biofilm formation at the air-liquid interface in aqueous solutions (Gakhar et al., 2010). Following this, it was demonstrated that the ability of BPIFA1 to modulate surface tension reduced *K. pneumoniae* biofilm biomass and inhibited of *P. aeruginosa* biofilm formation on the

apical surface of mouse airway epithelial cells (Liu et al., 2013a, Liu et al., 2013b). In addition, BPIFA1 was reported to act as a surfactant in the middle ear and the loss of BPIFA1 was shown to be associated with impaired function of the ET. BPIFA1 deficiency may weaken the ability of the ET to block the entry of microorganisms into the middle ear and contribute to the development of Otitis media (McGillivary and Bakaletz, 2010). Recently, leucine residues present in the α4-helix of BPIFA1 were defined to be crucial for the surfactant properties (Walton et al., 2016). However, Ning et al. demonstrated the capacity of BPIFA1 to bind airway surfactant molecules such as dipalmitoylphosphatidylcholine (DPPC), suggesting that BPIFA1 does not function directly as surfactant itself but stimulates function of other surfactant molecules in the ASL (Ning et al., 2014).

1.6.7 BPIFA1 regulates the height of ASL and ion transport

The respiratory epithelium is covered by ASL, which prevents mucus from adhering to epithelial surfaces and enables efficient mucus clearance from the airways. Maintenance of normal ASL volume (~7μm) homeostasis in the airways is crucial for defence against respiratory pathogens. Airway epithelial ASL volume is influenced by the levels of sodium (Na^+) and chloride (Cl^-) ions and the precise balance of these ions is regulated by absorption of Na^+ via epithelial sodium channel (ENaC) and secretion of Cl^- via cystic fibrosis transmembrane conductance regulator (CFTR) (Gaillard et al., 2010, Tarran, 2004). The activity of ENaC has been shown to be influenced by BPIFA1 in the ASL (Garcia-Caballero et al., 2009, Garland et al., 2013, Hobbs et al., 2013, Kim et al., 2018, Rollins et al., 2010). BPIFA1 binds to ENaC and protects it from proteolytic cleavage and activation (Garcia-Caballero et al., 2009). It was also demonstrated that BPIFA1 deficiency in human bronchial epithelial cells (HBECs) caused an increase in ASL absorption and addition of BPIFA1 to HBECs rescued this effect and restored normal ASL height (Garcia-Caballero et al., 2009). It was also suggested that BPIFA1 regulates ENaC activity by reducing expression of ENaC molecules in the plasma membrane of

the airway epithelial cells (Rollins et al., 2010). The protein specifically binds to the β-subunit of ENaC but not α- and γ- subunits (Hobbs et al., 2013). This BPIFA1 binding was reported to be highly dependent on the glycosylation state of ENaC β-subunit. Furthermore, the S18 peptide consisting of 18 amino acids corresponding to residues G22-A39 of BPIFA1 was shown to control ENaC function in the similar manner to full-length BPIFA1 and BPIFA1 lacking this region was demonstrated to have no effect on the ENaC activity. These findings suggested that the S18 region of BPIFA1 is important for inhibition of ENaC proteolytic cleavage and activation. The S18 peptide was also shown to retain its functionality in the presence of high proteolytic activity, which is common in CF airways (Hobbs et al., 2013). ASL height is not affected by the absence of BPIFA1 nor addition of recombinant BPIFA1 in CF airway cultures (Garland et al., 2013). However, addition of both BPIFA1 and bicarbonate to CF airway cultures restored a normal height of ASL, suggesting that the ability of BPIFA1 to control ENaC activity is pH-dependent. Consequently, it was suggested that an acidic pH of CF ASL causes an impairment in BPIFA1 function, that blocks binding to ENaC and blocks Na^+ hyperabsorption. Subsequently, it was shown that the S18 peptide was able to control ENaC activity in pH-insensitive manner (Garland et al., 2013). More recently, Kim et al. determined the mechanism by which BPIFA1 regulates ENaC activity (Kim et al., 2018). It was shown that BPIFA1 acts as allosteric regulator of ENaC that causes dissociation of αβγ-ENaC, leading to the internalisation of αγ-ENaC and allowing the formation of BPIFA1 and β-ENaC complex within the plasma membrane of cells (Kim et al., 2018).

Overall, it appears that BPIFA1 controls ENaC function. Maintenance of the ASL height homeostasis is crucial for healthy functioning of airways. In the case of respiratory disease such as CF, ASL height is reduced, mucus is thickened, and the function of BPIFA1 is impaired.

1.6.8 Other proposed functions of BPIFA1

Two other proposed functions of BPIFA1 are the ability to maintain airway homeostasis and to regulate airway smooth muscle contractions.

Existing literature suggests that BPIFA1 plays a role in the maintenance of airway mucosal homeostasis, but this function is impaired under epithelial insult. McGillivary et al. was first to propose that BPIFA1 functions as homeostatic factor (McGillivary and Bakaletz, 2010). BPIFA1 deficiency caused abnormal middle ear pressure and diminished mucociliary clearance by the ET, suggesting that loss of BPIFA1 impairs host defence against bacterial pathogens and contributes to the development of Otitis media (McGillivary and Bakaletz, 2010). A homeostatic function of BPIFA1 in the middle ear mucosa was later confirmed in another study which showed that BPIFA1 deficiency in a murine model of chronic Otitis media caused worsening of disease (Mulay et al., 2018). The ability of BPIFA1 to maintain mucosal homeostasis of upper respiratory tract was also proposed by Liu et al. and Chu et al., who showed that the absence of BPIFA1 was linked to diminished mucociliary clearance and increased bacterial burden (Chu et al., 2007, Liu et al., 2013b). A homeostatic role of BPIFA1 has not been well studied yet, but existing evidence does support this function for BPIFA1.

Recently, it was reported that BPIFA1 is also involved in the regulation of airway smooth muscle contractions by inhibiting activity of Ca^{2+} influx channel Orai1. The structural region responsible for this function was defined as α6-helix of BPIFA1. The absence of BPIFA1 was shown to be associated with the increased airway smooth muscle contractility which may contribute to the development of airway hyperresponsiveness (Wu et al., 2017).

1.7 Regulation of BPIFA1 by respiratory pathogens and inflammation

Expression and secretion of BPIFA1 by airway epithelial cells are influenced by respiratory pathogens and tissue inflammation.

Mice infected with viral pathogens such as IAV and gammaherpesvirus were shown to have considerably reduced BPIFA1 expression and secretion after 7 days post-infection compared to mock-infected controls but increased or not significantly different after 14 days post-infection. These fluctuations in the expression and secretion of BPIFA1 during viral infections were suggested to indicate a role for BPIFA1 in host defence against viral pathogens (Akram et al., 2018, Britto et al., 2013, Leeming et al., 2015, LeMessurier et al., 2016). Reduction in the levels of BPIFA1 during early infection may trigger an activation of more specific host defence mechanisms against viral pathogens and increased or normalised levels of BPIFA1 during later stages of infection may contribute towards to the recovery of airway epithelium and resolution of inflammation.

Infections caused by bacteria have also been shown to influence the expression and secretion of BPIFA1. *S. pneumoniae* and *P. aeruginosa* significantly reduced BPIFA1 in the lungs of infected mice (Britto et al., 2013). In contrast, levels of BPIFA1 were reported to be significantly up-regulated upon infection with *M. pneumoniae* and *K. pneumoniae* (Chu et al., 2007, Chu et al., 2010, Liu et al., 2013a). These findings suggest that activation of innate immune responses by pathogen-associated molecular patterns (PAMPs) causes alterations in BPIFA1 levels and direction of change is bacterial strain dependent. Moreover, stimulation of cells with pro-inflammatory cytokines such as IFN-γ, IL-1α, IL-6, IL-17A, and TGF-β were shown to cause a significant reduction in BPIFA1 amounts (Wei et al., 2014), whereas stimulation with IL-1β and TNF-α did not cause a decrease of *Bpifa1* (Bingle and Bingle, 2000). These results suggest that BPIFA1 is regulated by pro-inflammatory mediators and that such alterations are stimulus-specific.

Allergic inflammation driven by T_H2 cytokines was reported to modulate BPIFA1 levels. Airway epithelial cells stimulated with T_H2 cytokines such as IL-13 and IL-4 were shown to significantly decrease expression and secretion of BPIFA1 (Chu et al., 2007, Wei et al., 2014). In contrast, Britto et al. showed that IL-13 stimulation of human and mouse airway epithelial cells caused an increase in BPIFA1 levels (Britto et al., 2013). However,

T_H2 stimulation-induced allergic inflammation in mice was demonstrated to reduce amounts of BPIFA1 (Britto et al., 2013). Discrepancies seen in the *in vitro* data may be caused by differences in the cell culture techniques and treatment conditions. Although existing *in vitro* data is contradictory, it may be suggested that T_H2 driven inflammation causes a down-regulation of BPIFA1.

1.8 Role of BPIFA1 in pulmonary diseases

Multiple studies have investigated BPIFA1 in respiratory diseases such as CF, COPD, asthma, and idiopathic pulmonary fibrosis (IPF). BPIFA1 is predominantly expressed and produced by upper airway epithelial cells, however its expression and production profiles are altered in the airways of patients with pulmonary disease.

1.8.1 BPIFA1 and CF

The role of BPIFA1 in CF lung disease is not clear, but it has been shown that levels of *BPIFA1* mRNA and protein are increased in the respiratory tract of CF patients compared to non-CF subjects (Roxo-Rosa et al., 2006, Scheetz et al., 2004). BPIFA1 staining was significantly increased in the epithelium of CF small airways compared to non-CF small airways (Bingle et al., 2007). Strong staining of BPIFA1 was also seen in the inflammatory plugs within the airway lumen of CF patients, suggesting secretion of BPIFA1. Increase in the levels of BPIFA1 within the epithelium of CF small airways is probably a consequence of phenotypic alterations of the airway epithelium (Bingle et al., 2007). Subsequently, βENaC-transgenic mice, a model for CF-like lung disease, were shown to have increased levels of BPIFA1 in the peripheral lung compared to their littermate controls (Bingle et al., 2012). More recently, Saferali et al. reported that a single nucleotide polymorphism in the G allele of rs1078761 located in the exon 3 of the *BPIFB1* gene is associated with the reduced mRNA and protein levels of BPIFA1 and BPIFB1 in the lungs of CF patients. Decreased levels of BPIFA1 and BPIFB1 in CF lungs were correlated with the greater severity of CF disease. This suggests that the G

allele of rs1078761 is a non-CFTR genetic factor influencing the severity of CF disease (Saferali et al., 2015).

Dysregulation of ENaC is a factor contributing to the development of CF lung disease, as it is known to be associated with a significantly reduced volume of ASL and increased mucus dehydration (Garland et al., 2013). This impaired regulation of ENaC has been suggested to be the result of the reduced ASL pH and impaired function of BPIFA1 in the airways of CF patients (Garland et al., 2013). Since BPIFA1 is involved in the regulation of ENaC cleavage and activity, therapy directed towards raising the pH of CF airways may restore the function of BPIFA1. In addition, antibacterial properties of BPIFA1 were suggested to be hindered by decreased pH and elevated levels of neutrophil elastase in CF, resulting in the increased bacterial burden in the airways of CF patients (Garland et al., 2013, Jiang et al., 2013a, Jiang et al., 2013b, Nichols et al., 2015).

1.8.2 BPIFA1 and COPD

The main risk factor contributing to the development of COPD is tobacco smoking (Turato et al., 2001). Cigarette smoke has been shown to be associated with BPIFA1 reduction in the airways. Diminished amounts of BPIFA1 protein were reported in the upper respiratory tract of smokers compared to never smokers (Steiling et al., 2009). Subsequently, levels of BPIFA1 in the BAL of COPD smokers and non-COPD smokers were shown to be significantly reduced compared to the healthy non-smokers (Jiang et al., 2013b). *In vitro* exposure of human airway epithelial cells to the electronic cigarette liquid with or without nicotine was also shown to inhibit BPIFA1 expression (Wu et al., 2014). However, levels of BPIFA1 seem to be highly variable in the airways of smokers and COPD patients. Ghafouri et al. reported that amounts of BPIFA1 were considerably increased in the nasal lavage fluid from smokers compared to non-smokers (Ghafouri et al., 2002). In addition, Di et al. showed a significantly elevated BPIFA1 expression in the serous cells and ducts of submucosal gland, airway epithelial surface, and sputum of COPD patients compared to healthy controls (Di et al., 2003). It was suggested that this

was a consequence of the recurrent respiratory infections observed in COPD patients (Di et al., 2003). The reasons for these discrepancies are unclear, but it may be explained by the type of samples used for analysis, small number of samples, degrees of COPD severity, and smoking pack-years. More recently, De Smet et al. used the large number of samples to investigate the expression of BPIFA1 in COPD (De Smet et al., 2018). It was demonstrated that *BPIFA1* expression was significantly increased in stage 3 and 4 COPD patients compared to patients with stage 2 COPD and healthy controls. Moreover, COPD patients were shown to have significantly increased levels of BPIFA1 protein compared to control subjects and these elevated BPIFA1 levels were associated with worsening of COPD (De Smet et al., 2018). Although this study did not measure the levels of secreted BPIFA1 in the sputum and BAL fluid of COPD patients, the increased levels of secreted BPIFA1 were suggested based on the findings from the previous studies (Di et al., 2003, Ghafouri et al., 2002). It was also suggested that increased levels of BPIFA1 in COPD lungs are required to resolve inflammation and restore airway homeostasis (De Smet et al., 2018). However, the attempt of host defence system to resolve inflammation and restore airway homeostasis in COPD lungs by increasing expression and secretion of BPIFA1 seems to be not efficient and the reason for this might have been provided by Moore et al. (Moore et al., 2018). Exposure of BPIFA1 to the cigarette smoke triggered a disulphide bond modification, causing a significant alteration in the protein structure. This disulphide bond modification was shown to inhibit BPIFA1 ability to bind and control ENaC activity, resulting into ASL hyperabsorption and impaired airway homeostasis (Moore et al., 2018).

1.8.3 BPIFA1 and IPF

IPF is characterised by chronic inflammation and progressive lung tissue fibrosis, with approximate survival of patients for 2.5-5 years after disease diagnosis (Fujimoto et al., 2015, Richeldi et al., 2017). The role of BPIFA1 in IPF airways has not been widely studied yet and remains unclear. In the study by Boon et al., levels of *BPIFA1* were

reported to differ between IPF patients and healthy controls. Approximately 9-fold increase in *BPIFA1* mRNA was detected in the lungs of patients with rapidly progressive IPF compared to the patients with relatively stable IPF (Boon et al., 2009). In addition, investigation of BPIFA1 cellular distribution in the IPF and normal lung tissue showed BPIFA1 in the bronchial columnar cells, bronchial and bronchiolar epithelia, and mucus in IPF patients, whereas it was absent from these regions in the healthy subjects (Boon et al., 2009). The expression of another BPIF family member *BPIFB1* was also shown to be increased in the lungs of IPF patients. This increase in *BPIFB1* is greater than the increase in *BPIFA1* expression (Bingle et al., 2013). Therefore, current findings suggest that alterations in BPIFA1 may play a role in IPF, but there is no data available on the association of BPIFA1 and IPF pathogenesis.

1.8.4 BPIFA1 and asthma

Asthma is an obstructive airway disease, causing the chronic airway inflammation which leads to the airway hyperresponsiveness and reversible airflow limitation in the most of asthmatic patients (Saetta and Turato, 2001). The most common clinical symptoms of asthma such as wheezing, chest tightness, breathlessness and coughing occur due to the airway hyperresponsiveness (Buist, 2003). Follettie et al. showed markedly reduced *Bpifa1* mRNA in the lungs of mice with an asthmatic phenotype produced after antigen challenge (ovalbumin; OVA), either alone or treated with IL-13 antagonist compared to the mice challenged with PBS control buffer (Follettie et al., 2006). These findings were confirmed by Chu et al. by showing that *Bpifa1* was significantly diminished in the lungs of mice with allergic airway inflammation after exposure to OVA (Chu et al., 2007). Intranasal administration of IL-13 and IL-4 neutralising antibodies caused an increase in *Bpifa1* in the lungs of OVA challenged-mice, suggesting that IL-13 and IL-4 contribute to BPIFA1 reduction in the allergic situation (Chu et al., 2007). Subsequently, Thaikoottathil et al. showed that airway inflammation was significantly increased in the lungs of *Bpifa1*$^{-/-}$ mice after OVA-challenge compared to WT mice (Thaikoottathil et al., 2012). This

inflammation was characterised by elevated numbers of leukocytes and increased *Muc5ac* expression. It was also suggested that BPIFA1 deficiency promotes eotaxin-2 production by alveolar macrophages which caused an increased eosinophil infiltration. These findings suggested that restoring levels of BPIFA1 in the lungs of patients with allergic airway inflammation may reduce eosinophilic inflammation and improve symptoms of disease (Thaikoottathil et al., 2012). More recently, Fang et al. and Wu et al. reported significantly reduced BPIFA1 levels in samples from asthmatic patients (Fang et al., 2017, Wu et al., 2017). Reduced BPIFA1 levels were also shown to be associated with increased airway smooth muscle contractility which causes airway hyperresponsiveness. Consequently, it was suggested that the therapy aiming to restore natural BPIFA1 levels in the lungs of asthmatic patients should help to treat this disease (Wu et al., 2017).

In summary, the discovery of antimicrobial properties of BPIFA1 led to further investigations of BPIFA1's role in host defence. Studies have demonstrated that the levels of BPIFA1 expression differ in the airways of CF, COPD, IPF, and asthmatic patients compared to healthy controls. Expression of BPIFA1 was shown to be increased in the airways of CF and COPD patients, whereas it was found to be decreased in the airways of asthmatic patients. Reduced levels of BPIFA1 in the lungs of asthmatic patients were reported to be associated with disease severity. In the case of IPF, *BPIFA1* expression was shown to be significantly elevated in the patients with rapidly progressive IPF compared to the patients with relatively stable IPF. Currently, the reasons for BPIFA1 level differences in the diseased airways are not fully clear and require further investigations. Existing data also supports the role of BPIFA1 in airway defence but the exact mechanisms by which BPIFA1 performs its functions remain to be determined. Therefore, further studies are required to elucidate how BPIFA1 protects the airways from infections and injury.

1.9 Hypotheses and aims

This project consists of two parts and hypotheses of this project are:

1. BPIFA1 protein plays a role in the host defence by binding to respiratory pathogens.
2. The loss of BPIFA1 results in the enhanced susceptibility of mouse airway epithelial cells to NTHi infection.

This project consisted of three major aims:

1. To determine the regions of human BPIFA1 enabling it to bind to respiratory pathogens: *S. aureus*, *S. pneumoniae*, and NTHi.
2. To compare the bacterial binding abilities of mouse BPIFA1 with human BPIFA1.
3. To determine whether the BPIFA1 loss in mTECs causes an enhanced susceptibility of the cells to NTHi infection.

CHAPTER 2: MATERIALS AND METHODS

General methods

2.1 Cloning and transformation

2.1.1 Cloning and ligation reactions

VR1255 and pcDNA5/FRT/V5-His-TOPO (pcDNA5/FRT) were used for generation of BPIFA1-plasmid constructs. For BPIFA1 DNA cloning into pcDNA5/FRT (Invitrogen), DNA was diluted in relation to the amount of vector used and cloned into vector according to the established protocol. For ligation of digested BPIFA1 DNA into VR1255, DNA was diluted and T4 DNA ligase with ligase 10x buffer (Promega) was used in ligation reactions according to "T4 DNA Ligase, Blue/White Cloning Qualified" protocol. Ligation reactions were performed at 15ºC for 18 hours.

2.1.2 Transformation of *Escherichia coli*

TOP10 *E. coli* and One Shot® Mach1TM1 Phage-Resistant Chemically Competent *E. coli* (Invitrogen) were transformed with DNA of BPIFA1-plasmid constructs according to the Invitrogen protocols. Transformed *E. coli* cells were grown on LB-agar plates containing ampicillin (100µg/mL) or kanamycin (100µg/mL) overnight at 37ºC. Positive transformants were grown in LB-broth containing ampicillin (100µg/mL) or kanamycin (100µg/mL) overnight at 37ºC on the orbital shaker (200 RPM).

2.2 Extraction of plasmid DNA and verification of DNA

2.2.1 Minipreparation and maxipreparation

Transformed *E. coli* cells were miniprepped or maxiprepped to extract and purify plasmid DNA. Minipreps were performed using Thermo Scientific GeneJET Plasmid Miniprep Kit and protocol. Maxipreps were performed using Qiagen Plasmid Maxiprep kit and protocol. Concentration of minipreps and maxipreps was determined using NanoDrop ND-1000 (ThermoScientific). Quality of extracted DNA was verified by restriction digestion and Sanger sequencing.

2.2.2 Agarose gel electrophoresis of DNA

DNA products were run alongside 1kb or 100bp DNA ladder (New England BioLabs Inc.) on 1% or 2% agarose gels containing ethidium bromide (Fisher Scientific) at 70V. Gels were prepared using 1g or 2g of agarose powder (Geneflow) in 100ml of 1x Tris Acetate EDTA (TAE) buffer and 0.5µg/ml of ethidium bromide (Fisher Scientific). Fragments of DNA were visualised using Biorad ChemiDoc^{TM} XRS+.

2.2.3 DNA extraction from agarose gel

DNA samples were run on an agarose gel and visualised using UV transilluminator. DNA fragments of interest were cut from the agarose gel and recovered using GeneJET Gel Extraction and DNA Cleanup Micro Kit (Thermo Scientific). Concentration of recovered DNA was determined using NanoDrop ND-1000 (Thermo Scientific). DNA was stored at -20ºC.

2.2.4 Restriction digestion

Plasmid DNA was digested with restriction endonucleases (Promega). In all cases, 1µL of restriction endonuclease, 1µL of 10x buffer (Promega) and 5µL of plasmid-DNA were used, and the total volume was made up to 10µl with nuclease free H_2O. Digests were incubated overnight at 37ºC prior to analysis. HyPlus loading buffer green (1µl; Bioline) was added to digested plasmid DNA (10µl) and sample was run alongside 1kb or 100bp DNA ladder (New England BioLabs Inc.) on 1% or 2% agarose gels containing ethidium bromide.

2.2.5 Sanger sequencing

Verification of DNA was performed using Sanger sequencing. DNA (10µl) was sequenced to validate the orientation of insert and scan for any possible mutations. DNA sequencing was performed at the Core Genomics Facility, Faculty of Medicine, Dentistry and Health, University of Sheffield. Primers used for sequencing are provided in Table 2.1:

Table 2.1: Primer pairs used in Sanger sequencing.

Primer name	Primer type	Sequence (5'-3')
T7	Forward	TAATACGACTCACTATAGGG
BGH	Reverse	TAGAAGGCACAGTCGAGG
pVR1255	Forward	AATAGCTGACAGACTAACAGACTG
	Reverse	GAGTGAGCTGATACCGCTC
GFP	Reverse	GCTGATCAGCGGGTTTAATTC

2.3 Gene expression studies

2.3.1 RNA extraction

Cells were lysed in 250µl Trizol reagent (Sigma-Aldrich) and RNA was extracted according to the manufacturer's protocol. Briefly, 50µl of chloroform (Fisher Scientific) was added to cell lysate, vortexed for approximately 30 seconds, and incubated for 15 minutes at room temperature (RT). Samples were centrifuged at 13,000 RPM for 15 minutes at 8˚C. Subsequently, the aqueous phase containing RNA was transferred to a new eppendorf tube and 125µl of isopropanol (Fisher Scientific), and 1µl of GlycoBlue™ dye (Ambion) were added. Samples were vortexed, incubated for 10 minutes at RT, and then centrifuged at 13,000 RPM for 10 minutes at 8˚C. The isopropanol was removed, and the RNA pellet was washed with 250µl of 75% ethanol (Fisher Scientific) and centrifuged as described previously. The ethanol was discarded, the RNA pellet was air-dried, and resuspended in 20µl of nuclease free H_2O. Concentration of RNA was measured using NanoDrop ND-1000 (Thermo Scientific). RNA samples were stored at -20ºC.

2.3.2 Agarose gel electrophoresis of RNA

RNA samples were prepared for analysis as follows: 2µl of total RNA was added into 4µl of RNA sample loading buffer containing ethidium bromide (Sigma) and gently mixed. Samples were heated at 65ºC to denature the RNA. Samples were loaded onto the denaturing formaldehyde (37-41% solution; Fisher Chemical) 1% agarose (Thermo

Scientific) gel and electrophoresed in 1X MOPS buffer (Fisher Scientific) at 70V to visualise RNA and determine its integrity. All equipment used in the assay was RNase free. Gel visualisation was performed using Biorad ChemiDoc™ XRS+.

2.3.3 DNase treatment

DNase I treatment (Promega) was used to remove a residual genomic DNA contamination from 200ng of extracted RNA. Briefly, RQ1 RNase free 10x reaction buffer (1µl) and RQ1 RNase free DNase (1µl) were added to RNA sample, and the total volume was made up to 10µl with nuclease free H_2O. The components were mixed, and the sample incubated for 30 minutes at 37ºC in the thermocycler (MJ Research PTC-200). Afterwards, 1µl of RQ1 DNase STOP solution was added and sample was incubated for 10 minutes at 65ºC in the thermocycler to terminate DNase activity. DNase treated RNA was used in cDNA synthesis.

2.3.4 Complementary DNA (cDNA) synthesis

DNase treated RNA was reverse transcribed into cDNA using AMV Reverse Transcriptase kit (Promega). Briefly, 0.5µl of OligoDT (Sigma) was added to RNA solution and the total reaction volume was made up to 19µl with nuclease free H_2O. The sample was heated at 70˚C for 5 minutes in the thermocycler. Afterwards, 6µl of reverse transcription master mix, consisting of AMV RT 5x buffer (5µl), AMV RT enzyme (0.25µl), RNasin ribonuclease inhibitor (0.25µl), and dNTPs (100µM) was added to the sample and cDNA was synthesised for 42˚C for 1 hour and denatured at 95˚C for 5 minutes. cDNA samples were stored at -20ºC.

2.3.5 Polymerase Chain Reaction (PCR)

Polymerase chain reaction was used to analyse genes of interest. All PCR reactions were performed using Maxima Hot Start Green PCR Master Mix (Thermo Scientific) according to the manufacturer's protocol. Briefly, cDNA sample was diluted in the nuclease free water at the ratio of 1:4 and 1µl of it was added into the tube, containing

12.5µl of Maxima Hot Start Green PCR Master Mix, 4.5µl of nuclease free water, and 1µM of forward and reverse primers. The list of primer pairs used in PCR reactions is provided in Table 2.2. PCR reaction samples were vortexed, and PCR was performed at the following cycling conditions in the thermocycler: 1) Initial denaturation/enzyme activation 95ºC for 4 minutes; 2) Denaturation at 95ºC for 1 minute; 3) Annealing at 60ºC for 1 minute; 4) Elongation at 72ºC for 1 minute; and 5) Final elongation at 72ºC for 7 minutes. PCR reactions were run for 35 cycles for all genes (steps from 2 to 4 repeated), except for *Bpifa1* for which 30 cycles were used. The endogenous control for all PCR reactions was *Oaz1* gene. PCR products were run on the agarose gel and visualised using Biorad ChemiDoc™ XRS+.

Table 2.2: Primer pairs used in PCR reactions.

Gene	Primer type	Sequence (5'-3')	Product size (bp)
Oaz1	Forward	ACAGAGGAGCCGACGTCTAA	274
	Reverse	CCAAGAAAGCTGAAGGTTC	
Tekt1	Forward	CAGTGCGAAGTGGTAGACG	373
	Reverse	TTCACCTGGATTTCCTCCTG	
Ltf	Forward	TCTGTCCCTGTGTATTGGT	237
	Reverse	GTTTCCGGGTGTCATCAAGG	
Bpifa1	Forward	GGTGCACAACATTGCTGAAT	127
	Reverse	CAAGAGGCAGGAGACTGAG	

2.4 Cell line culture and transfections

2.4.1 Cell line cultures

Three cell lines were used for transfections: NCI-H292 (human mucoepidermoid pulmonary carcinoma 292), Flp-In-CHO (Chinese hamster ovary), and HEK293T (human embryonic kidney 293 SV40 large T antigen expressing). Growth medium was changed

twice a week for all cell lines. Dulbecco's Modified Eagle's Medium (DMEM; Sigma-Aldrich) growth medium was used for the maintenance of NCI-H292 and HEK293T cell lines. Roswell Park Memorial Institute-1640 growth medium (RPMI-1640; Sigma-Aldrich) was used for the maintenance of Flp-In-CHO cells. Both types of growth media were supplemented with foetal bovine serum (10%) (FBS; Sigma), penicillin (100U/ml), streptomycin (100mg/ml) (Sigma) and L-glutamine (2mM; Sigma). Cell line cultures were split upon reaching the confluence using 1x Trypsin-EDTA solution (Sigma). Cell line cultures were grown in the incubator at 37ºC, 5% CO_2.

2.4.2 Optimisation of G418 killing assay

A killing assay was performed to determine the lowest concentration of G418 (Melford) required to kill 100% of NCI-H292 cells within 7 days from the start of selection. NCI-H292 cells were seeded ($8x10^4$ cells/well) onto 24-well culture plate one day prior to introducing G418 antibiotic selection. The following day, DMEM growth medium (Sigma-Aldrich) was removed and medium containing G418 was added to the cells. Different concentrations (µg/mL: 200, 400, 600, 800, and 1000) of antibiotic were used. G418 untreated cells were used as the control.

2.4.3 Transfections of cell lines

Two types of transfection methods were used: stable transfections and transient transfections. NCI-H292 and Flp-In-CHO cells were used for stable transfections, whereas HEK293T cells were used for transient transfections. NCI-H292 cells were transfected using FuGENE® HD (Promega) according to "Promega FuGENE® HD Transfection Reagent" protocol. Flp-In-CHO cells were transfected using Lipofectamine™ LTX transfection reagent (Invitrogen) according to "Flp-In System" protocol. After transfections, G418 (1000µg/mL) was used to select positively transfected NCI-H292 cells and establish a stable cell line expressing *BPIFA1*. Hygromycin B (450µg/ml; Invitrogen) was used for selection of positively transfected Flp-In-CHO cells

and establishment for a stable cell line expressing *BPIFA1*. Transient transfections of HEK293T cells were carried out using a standard calcium phosphate protocol.

2.5 Immunoblotting

2.5.1 Sodium Dodecyl Sulphate Polyacrylamide Gel Electrophoresis (SDS-PAGE)

Samples prepared in 2x SDS lysis buffer were heated at 95°C for 10 minutes to denature proteins. Afterwards, samples were loaded onto 10% or 12% SDS-PAGE gel and run alongside 10µl of marker (Geneflow wide range 10-245kDa ladder or New England BioLabs® Inc. broad range 11-245kDa standard) at 100V through the stacking gel, and at 150V through the resolving gel till the dye reached the bottom of the gel. Subsequently, the stacking gel was discarded, and the resolving gel was placed in 1x transfer buffer. Transfer of proteins from the resolving gel onto PVDF membrane (Milipore) was performed using semi-dry blotter system (Biorad Trans-bot turbo). Transfer of proteins was prepared in the following order from the anode to the cathode direction: three layers of Whatman paper, methanol activated PVDF membrane, resolving gel, and three layers of Whatman paper. All components were soaked in 1x transfer buffer before assembly and buffer excess was removed before the semi-dry transfer. Proteins were transferred onto PVDF membrane at 25V for 25 minutes. PVDF membranes were blocked in 5% milk in 1x Tris buffered saline-Tween (TBS-Tween) buffer for 1 hour on the orbital shaker. Membranes were washed for 5 minutes 1x TBS and probed with primary antibody (Table 2.3) overnight at 4ºC on a rolling platform. Primary antibodies were diluted in 5% milk in TBS-Tween buffer. The following day, membranes were washed three times for 10 minutes in 1x TBS-Tween. The primary antibody was detected using a secondary antibody (Table 2.3) diluted in 5% milk in TBS-Tween. Membranes were incubated for 1 hour on the rolling platform at RT. Afterwards, membranes were washed three times in 1x TBS-Tween and enhanced chemiluminescence (ECL) detection solution (Biorad) was added onto the membranes

for detection of the secondary antibody. Membranes were placed in a plastic sleeve and 1ml of ECL solution (0.5ml solution A (luminol) and 0.5ml solution B (H_2O_2)) was added onto the membrane. Excess ECL was removed and plastic sleeve with membrane was placed in a light-proof cassette. Two methods were used for visualisation:

1. Photographic X-ray film (GE Healthcare) was exposed to membrane for an appropriate period of time in the dark room. Subsequently, the film was developed, rinsed in water and fixed.
2. The membranes were exposed for an appropriate period of time using Biorad ChemiDoc™ XRS+ and the bands were developed.

Please see Appendix I (Table I) for detailed preparation of all stock solutions used in SDS-PAGE. Densitometry was used for analysis of SDS-PAGE results. Quantification was performed using ImageJ-win32 program.

Table 2.3: Primary and secondary antibodies used for SDS-PAGE.

Primary antibodies			
Antibody	**Type**	**Dilution**	**Manufacturer**
Anti-GFP tag	Mouse monoclonal	1:3000	ThermoFisher Scientific
Anti-FLAG tag M2, Clone2	Mouse monoclonal	1:1000	Sigma -Aldrich
Anti-human BPIFA1	Rabbit polyclonal	1:200	Prepared in lab (De Smet et al., 2018)
Anti-mouse BPIFA1	Rabbit polyclonal	1:200	Prepared in lab (Musa et al., 2012)
Secondary antibodies			
Antibody	**Type**	**Dilution**	**Manufacturer**
Anti-mouse HRP	Goat polyclonal	1:2000	Dako
Anti-rabbit HRP	Goat polyclonal	1:2000	Dako

2.5.2 Dot blotting

Samples of apical cell secretions (10µl) were dotted on the PVDF membrane (Milipore) and air-dried. The membrane was blocked in 5% milk in 1x TBS-Tween buffer for 1 hour on the orbital shaker. Subsequent steps were performed as per the SDS-PAGE method using polyclonal rabbit anti-mouse BPIFA1 primary and polyclonal goat anti-rabbit secondary antibodies (Table 2.3). Results were visualised using Biorad ChemiDoc™ XRS+. Densitometry was used for analysis of results. Quantification was performed using ImageJ-win32 program. Data was analysed, and statistical tests were performed.

2.6 Cell fixation and DAPI staining

Cells, grown onto glass chamber slides, were fixed in 10% buffered formalin for 30 minutes at RT. Subsequently, formalin was removed, and cells were washed with 1x PBS (Gibco). The frame of glass chamber slide was removed from the glass slide and a drop of Vectashield mounting medium for fluorescence with DAPI (Vector Laboratories, Inc.) was added. A coverslip was applied on the cell samples and DAPI excess was drained from the slide. The coverslip was sealed onto the glass slide with nail polish. Slides were stored in a light-proof box at -4ºC.

Methods for the study of BPIFA1 interactions with bacterial pathogens

2.7 Bioinformatic analysis of human and mouse BPIFA1

2.7.1 Structure and sequence similarity of human BPIFA1 protein to BPI, LBP, PLTP, and CETP proteins

Multiple sequences analysis of human BPIFA1, BPI, LBP, PLTP, and CETP proteins was performed using Kalign (EMBL-EBI, 2018) and BoxShade (Hofmann and Baron, 2018). Protein sequences of all proteins were gained from NCBI protein data base (NCBI, 2017). Information about protein sequences is provided in the Table 2.4. Investigation of

structure similarity between BPIFA1 and BPI was performed using Protein Homology/analogY Recognition Engine V 2.0 (Phyre2) (Kelley et al., 2015). 3D models of proteins were built using Phyre2 and PyMOL was used for visualisation and construction of protein superpositions (Schrodinger, 2015). The aim was to highlight the position of cysteine residues which form the disulphide bond in BPIFA1 and BPI proteins and to show that disulphide bond is present at the same position in all proteins analysed.

Table 2.4: Information about BPIFA1, BPI, LBP, PLTP, and CETP protein sequences.

Protein (*Homo sapiens*)	Sequence NCBI number
BPIFA1	**NP_001230122.1**
BPI	**CAD99178.1**
LBP	**NP_004130.2**
PLTP	**BAB79630.1**
CETP	**AAA51977.1**

2.7.2 Features of human and mouse BPIFA1 proteins

Predict Protein Open Software was used to predict binding sites and residue composition of mouse and human BPIFA1 proteins (Yachdav et al., 2014). Conserved domains, sites and regions of BPIFA1 were predicted using ExPASy Prosite (Sigrist et al., 2013), EMBL-EBI InterPro (Finn et al., 2017), and Motif Scan-MyHits (Pagni et al., 2004). Multiple sequences alignment of BPIFA1 from a variety of species was constructed using Kalign (EMBL-EBI, 2018) and BoxShade (Hofmann and Baron, 2018). Protein sequences of all proteins were from NCBI protein data base (NCBI, 2017). Information about sequences is provided in the Table 2.5.

Table 2.5: Information about BPIFA1 protein sequences.

Species of BPIFA1 protein	Sequence NCBI number
Human (*Homo sapiens*)	NP_001230122.1
Mouse (*Mus musculus*)	NP_035256.2
Wood mouse (*Apodemus sylvaticus*)	AEA07326.1
Rat (*Rattus norvegicus*)	NP_742028.1
Hamster (*Mesocricetus auratus*)	XP_012979514.1
Chinchilla (*Chinchilla lanigera*)	NP_001269294.1
Kangaroo rat (*Dipodomys ordii*)	XP_012866135.1
Shrew (*Elephantulus edwardii*)	XP_006881757.1
Cow (*Bos taurus*)	NP_776851.1
Camel (*Camelus dromedaries*)	XP_010982659.1
Elephant (*Loxodonta Africana*)	XP_003411552.1
Pig (*Sus scrofa*)	NP_001005727.1
Sheep (*Ovis aries*)	AIG92771.1
Dolphin (*Tursiops truncates*)	XP_004319467.1
Whale (*Delphinapterus leucas*)	XP_022448419.1

2.8 Generation of GFP- and FLAG-tagged BPIFA1 constructs

BPIFA1 proteins were fused either to GFP tag or FLAG tag to generate BPIFA1 constructs for transfection assays. GFP-tagged human full-length (256aa), F/R1 (39aa), and F/R2 (58aa) BPIFA1 constructs were previously generated in the laboratory. FLAG-tagged human full-length and cysteine mutant (cysteine 224 residue replaced by glycine residue) BPIFA1 constructs were previously generated in Prof J. Stewart's group

(University of Liverpool). FLAG-tagged human S18 mutant and mouse full-length BPIFA1 constructs were generated during this study.

2.8.1 Synthesis of human S18 mutant BPIFA1-FLAG gene

Human S18 deletion BPIFA1-FLAG gene was synthesised by Invitrogen GeneArt™ Gene Synthesis service (ThermoFisher Scientific). DNA sequence of human BPIFA1-FLAG gene missing 22-42 amino acids was synthesised and cloned into pMA-T vector (Appendix I: Figure I). DNA sequence of the gene can be found in Appendix I (Figure II). Plasmid DNA was purified from transformed bacteria and concentration was determined by UV spectroscopy. The final construct was verified by sequencing. Sequencing data of the construct can be found in Appendix I (Figure III). Lyophilised plasmid DNA (5µg) containing DNA of human S18 deletion BPIFA1-FLAG was provided.

2.8.2 Generation of mouse full-length BPIFA1-FLAG construct

RNA of mouse endogenous BPIFA1 was isolated from mTECs differentiated at the air liquid interface (ALI) conditions (section 2.14.4). Isolation of RNA was performed, and genomic DNA was removed by DNase treatment as described. DNase digested RNA was reverse transcribed into cDNA which was used in PCR using the primer pair shown in Figure 2.1.

mA1 Not I Forward:

Not I **Kozak**

5’-ATGCGGCCGCCGCCGCCACCATGTTTCTAGTTGGGAGCCT-3’

mA1 Stop Reverse:

BamH I **Stop** **FLAG tag**

5’-GCGGATCCTTACTTGTCATCGTCGTCCTTGTAGTCAACTTTGATGACAAACTGTAG-3’

Figure 2.1: Primer pair used to generate mouse BPIFA1-FLAG construct.
DNA sequences highlighted in the red colour represent sequences of restriction endonucleases – sites which are necessary for cloning reactions in the linear VR1255 vector (digested with NotI and BamHI). DNA sequence highlighted in the yellow colour represents Kozak sequence which plays a role in the initiation of translation process. STOP codon is highlighted in the green colour and nucleotide sequence of FLAG tag in the cyan colour.

2.9 Generation of BPIFA1-plasmid constructs

DNA of human full-length (256aa), F/R1 (39aa), and F/R2 (58aa) BPIFA1-GFP were previously cloned in pcDNA3.1/CT-GFP-TOPO (pcDNA3.1) vector in the laboratory to prepare BPIFA1 constructs for transfection assays. In this study, all human BPIFA1-GFP constructs were re-cloned in pcDNA5/FRT plasmid. DNA of human full-length and cysteine mutant BPIFA1-FLAG were previously cloned in VR1255 expression system in Prof J. Stewart’s group (University of Liverpool). DNA of the human S18 deletion and mouse BPIFA1-FLAG were ligated to VR1255 vector DNA (kindly gifted to our group by Prof J. Stewart) during this study to generate BPIFA1 constructs for transfection assays.

2.9.1 Preparation of BPIFA1-GFP constructs for cloning into pcDNA5/FRT

TOP10 *E. coli* cells were transformed with DNA of human full-length, F/R1, and F/R2 BPIFA1-pcDNA3.1 constructs. Ampicillin (100µg/mL) was used for selection of positive transformants. DNA minipreps were performed and DNA of pcDNA3.1 plasmids containing FL-, F/R1-, and F/R2-BPIFA1-GFP were digested with HindIII and BamHI in

10x buffer E. Miniprep samples (10µL) of all three constructs were sent for Sanger sequencing which was performed using T7 and BGH primers. The coding regions of human pcDNA3.1-BPIFA1-GFP constructs were amplified using PCR and primers (Sigma-Aldrich) flanking the CT-GFP-TOPO restriction sites (F: 5'-GATCCACTAGTCCAGTGTGGT-3'; R: 5'-GCTGATCAGCGGGTTTAATTC-3'). The PCR reaction was run for 35 cycles. PCR products were run on 1% agarose gel to visualise DNA fragments.

2.9.2 Cloning BPIFA1-GFP constructs into pcDNA5/FRT vector system

PCR products of full-length, F/R1-, and F/R2-BPIFA1-GFP were diluted in relation to the amount of vector used (FL-BPIFA1-GFP - 1:15; F/R1-BPIFA1-GFP - 1:20; and F/R2-BPIFA1-GFP - 1:5) and cloned into pcDNA5/FRT. After the cloning reaction, TOP10 *E. coli* cells were transformed with plasmid DNA and ampicillin (100µg/mL) was used for selection of positive transformants. Minipreps were performed and plasmid DNA was digested with NcoI in 10x buffer D. Restriction digests were run on agarose gel to visualise DNA fragments. Minipreps (10µl) of pcDNA5/FRT-BPIFA1-GFP constructs were sent for Sanger sequencing which was performed using T7 and BGH primers.

2.9.3 Transformation of *E. coli* with pOG44 plasmid

Empty pOG44 plasmid, which works in the Flp-In system, was required for co-transfections of Flp-In-CHO cells. TOP10 *E. coli* cells were transformed with DNA of pOG44 plasmid and ampicillin (100µg/mL) was used for selection of positive transformants. Minipreps were digested with EcoRI in 10x buffer H to verify the quality of plasmid DNA.

2.9.4 Preparation of VR1255 for ligation reactions with BPIFA1 DNA

To verify a quality of VR1255, vector DNA was digested with BamHI and NotI in 10x buffer D. To generate a linear plasmid DNA for ligation reactions, VR1255 DNA (1267ng)

was digested with BamHI and NotI and the DNA fragment of interest (4761bp) was visualised using UV transilluminator, cut from the gel and recovered.

2.9.5 Preparation of human S18 mutant BPIFA1-FLAG for ligation with VR1255

Nuclease free water (50µl) was added to 5µg of lyophilised pMA-T plasmid DNA containing S18 mutant BPIFA1-FLAG and incubated for 1 hour at RT. Plasmid DNA was used to transform TOP10 *E. coli* cells and ampicillin (100µg/mL) was used for selection of positive transformants. Six transformed *E. coli* colonies were grown and miniprepped. DNA was digested with NotI and BglII in 10x buffer D. Restriction digests were run on 1% agarose gel and the fragment (773bp) was recovered from the agarose gel. The quality of recovered DNA was verified using agarose gel electrophoresis.

2.9.6 Preparation of mouse BPIFA1-FLAG for ligation with VR1255

PCR product of mouse BPIFA1-FLAG was cloned into pCRII-TOPO vector (Invitrogen) according to the “TOPO TA Cloning® Kit” protocol. DNA minipreps were performed and DNA was digested with NotI and BamHI in 10x buffer D. Restriction digests were run on 1% agarose gel and the DNA fragment (878bp size) was recovered from the agarose gel.

2.9.7 Ligation of human S18 deletion and mouse BPIFA1-FLAG with VR1255

Linear VR1255 vector DNA was ligated using T4 DNA ligase with S18 deletion BPIFA1-FLAG DNA at the ratio of 1:6 and with mouse BPIFA1-FLAG DNA at the ratio of 1:1, 1:3, and 3:1. TOP10 *E. coli* cells were transformed with ligation products and kanamycin (100µg/mL) was used for selection. DNA minipreps were performed and DNA was digested as described:

- VR1255 ligated with S18 deletion BPIFA1-FLAG:

1. EcoRV and KpnI in Multi-Core buffer;
2. BamHI and XbaI in 10x buffer E.

- VR1255 ligated with mouse BPIFA1-FLAG:
  1. EcoRV and KpnI in Multi-Core buffer;
  2. HindIII in 10x buffer E.

Miniprep samples (10µL) were sequenced using pVR1255F and pVR1255R primers.

2.9.8 Transformation of *E. coli* with human full-length and cysteine mutant BPIFA1-FLAG constructs

TOP10 *E. coli* cells were transformed with DNA of FLAG-tagged human full-length and cysteine mutant BPIFA1-VR1255. Kanamycin (100µg/mL) was used for selection of positive transformants. Samples were miniprepped and DNA was digested with NotI and BamHI.

2.10 Transfections

Transfections were performed to obtain secreted BPIFA1 recombinant proteins for the functional analysis of BPIFA1. Three different techniques were used to transfect cells. All transfections were performed using maxiprep samples of BPIFA1 constructs.

2.10.1 Preparation of BPIFA1 constructs and control vectors for transfections

E. coli cells transformed with DNA of pOG44 vector and BPIFA1 expression constructs were used for DNA maxipreps. All DNAs were digested to confirm their identity (sections: 2.9.3, 2.9.7, and 2.9.8).

2.10.2 Stable transfections of NCI-H292 cells

NCI-H292 cells were seeded ($8x10^4$ cells/well) onto 24-well plates and the next day were transfected with pcDNA3.1-BPIFA1-GFP. Empty EGFP-C3 served as a positive control for the transfection assay. Transfection was performed in the duplicates using FuGENE®

HD. Transfection was undertaken using 500ng of DNA and 1µL-2µL-3µL of FuGENE reagent per well at the ratio of transfection reagent to DNA of 1:1, 2:1 and 3:1, respectively. Transfection reagent and DNA was added into 100µL of OptiMEM reduced serum medium (Gibco® by Life technologies) and incubated for 15mins at RT. Growth medium was removed from the cell culture plate, cells were washed with OptiMEM medium, and fresh 400µL of OptiMEM was added to the cells. After 15 minutes, DNA-transfection reagent mixture was added to the cells and the plate was returned to the incubator (37ºC/5% CO_2) for 24 hours incubation. The following day, the transfection mixture was removed, cells were washed with OptiMEM medium, and DMEM growth medium was added into the cell culture plate. Transfection efficiency was determined using fluorescent microscopy. Two days after transfection, DMEM growth medium was removed and medium containing 1000µg/ml of G418 was added. Cells were fed every third day with fresh medium containing G418 (1000µg/ml) to establish a stable cell line expressing *BPIFA1*. Cells transfected with EGFP-C3 were also fed with medium containing G418 and used as the control. After selection for the positive cells, G418 was still used in the cell culture for the maintenance of selected cell line. Subsequently, serial dilution was used for isolation of BPIFA1-GFP positive cells. Cells were collected from 24-well culture plates and seeded onto 96-well culture plates. Serial dilutions were performed to enable the isolation of single cell colonies expressing the protein of interest. BPIFA1-GFP positive single cell colonies were transferred back onto 24-well culture plate when cells reached the confluence. After cells were confluent in 24-well plate, they were moved onto 6-well plates. A sample of transfected cells was collected and lysed in 2x SDS lysis buffer for western blotting analysis. Afterwards, transfected cells were grown in T75 flasks and once they were confluent, $6x10^6$ of cells were taken for cell sorting by flow cytometry to isolate human BPIFA1-GFP positive cells from negative cells. Flow cytometry cell sorting was performed at the University of Sheffield core facility. Sorting of cells was done based on the GFP fluorescence associated with BPIFA1-GFP positive cells. NCI-H292 control cells were used as a negative control

sample. Highly fluorescent cells were selected as BPIFA1-GFP positive ones. Samples of BPIFA1-GFP positive and negative cells were collected. Both types of cells were seeded into different T75 flasks and returned to the incubator (37ºC/5% CO_2). Next, positive and negative cells were seeded into T25 flasks in the serum supplemented and serum-free DMEM medium (2ml). The following day, conditioned medium and cell samples were collected. Cells were lysed in 2x SDS buffer as were conditioned medium samples. Samples were analysed for BPIFA1-GFP protein production and secretion using SDS-PAGE.

2.10.3 Stable transfections of Flp-In-CHO cells

CHO (pFRT/*lacZ-Zeocin*) cells were seeded ($4x10^4$ cells/well) onto 24-well plates the day before transfection. The next day, co-transfection of CHO cells was performed in the duplicates using Lipofectamine™ LTX transfection reagent. Co-transfection components were mixed in the following order: 1) 2µL of Lipofectamine was added into 100µl of OptiMEM medium (Gibco® by Life technologies) (ratio of DNA to Lipofectamine: 1:2); and 2) 100ng of GFP-tagged BPIFA1-pcDNA5/FRT (i.e. full-length, F/R1, and F/R2-BPIFA1-GFP) with 900ng of pOG44 were added into 100µl of OptiMEM medium (ratio of construct DNA to pOG44 – 1:9). The DNA mix and transfection reagent mix were combined and incubated for 30 minutes at RT. During the incubation time, RPMI-1640 growth medium was removed from the cell culture plates, cells were washed with OptiMEM reduced serum medium and fresh 800µl of OptiMEM was added. The mixed DNA and transfection reagent was added to the cells and plates were returned to the incubator (37ºC/5% CO_2) for 4 hours incubation. CHO cells were also co-transfected with empty EGFP-N1 and pOG44 as positive controls. After incubation, the transfection mixture was removed and 1ml of RPMI-1640 growth medium was added. The following day, RPMI-1640 growth medium was removed and RPMI-1640 growth medium containing hygromycin B (450µg/ml; Invitrogen) was added to the cells for selection of positively transfected cells. Cells were fed every third day with RPMI-160 growth medium

containing hygromycin B for two weeks until stable cell lines expressing *BPIFA1* were established. Samples of stably transfected cells were taken for genomic DNA extraction to verify integration of GFP-tagged BPIFA1-pcDNA5/FRT DNA into the genome of CHO cells. DNeasy® Blood & Tissue Kit (Qiagen) was used according to the quick-start protocol. Genomic DNA from GFP-tagged full-length, F/R1, and F/R2-BPIFA1 cells was used for PCR. The coding regions of FL, F/R1-, and F/R2-BPIFA1 were amplified with primers flanking the TOPO cloning site (F: 5'-ACCCACTGCTTACTGGCTTA-3'; R: 5'-GCAACTAGAAGGCACAGTCG-3'). Minipreps of construct DNA were used as positive controls. Samples of stably transfected cells and serum supplemented conditioned medium were collected for detection of BPIFA1-GFP protein. Cells were lysed in 2x SDS lysis buffer as were conditioned medium samples at the ratio of 1:1. Samples were processed for western blotting as described.

2.10.4 Transient transfections of HEK293T cells

Transient co-transfections of HEK293T cells with FLAG-tagged BPIFA1-VR1255 constructs (i.e. human full-length, cysteine mutant, S18 deletion BPIFA1-FLAG and mouse BPIFA1-FLAG) were performed to generate BPIFA1 secreted proteins. Empty pEGFP-N1 was used as a control. The day before transfection, HEK293T cells were seeded onto 24-well plate ($2.5x10^5$ cells/well) for small-scale co-transfection to find out whether proteins of interest would be produced and secreted by transfected cells. Empty pEGFP-N1 was used as a positive control for transfection efficiency. The following day, HEK293T cells were transfected using a standard calcium phosphate protocol. DMEM growth medium was replaced with fresh growth medium 4 hours before transfection. A volume of 3.8µl $CaCl_2$ (2.5M concentration), 1.52µg of BPIFA1-VR1255 construct and 100ng of pEGFP-N1 were mixed together in the eppendorf tube. Subsequently, the DNA/$CaCl_2$ mixture was added dropwise, while mixing gently, to a bijou tube containing 38µl of 2x HEPES-buffered saline and incubated for 20 minutes at RT. Transfection-DNA mixture was added dropwise to HEK293T cells and the plate was returned to incubator

for 18 hours (37ºC/5% CO_2). The next day, the medium containing transfection-DNA mixture was removed, and cells were washed with PBS (without calcium and magnesium chloride; Sigma-Aldrich), followed by addition of the fresh DMEM growth medium (500µl). Cells were then incubated for 30 hours (37ºC/5% CO_2). Afterwards, the conditioned medium and cell samples were collected for SDS-PAGE analysis. Conditioned media samples were centrifuged for 5 minutes at 1000 RPM to remove debris. Subsequently, 25µl of conditioned medium was lysed in 25µl of 2x SDS lysis buffer. Collected samples of transfected cells were lysed in 100µl of 2x SDS lysis buffer. Samples were analysed using western blotting. After verification of BPIFA1 production and secretion, large-scale co-transfections were used to generate large quantities of secreted human and mouse BPIFA1-FLAG proteins. Co-transfections were performed in T75 and T175 flasks. Volumes of transfection reagents and DNA were increased accordingly to the surface area of the flask. Conditioned medium samples were collected every day for four days. After collection of conditioned media containing FBS serum, cells were washed with PBS and fresh serum-free medium was added to the cells. Serum-free conditioned medium samples were collected every day for three days. Cell lysate samples were collected for the western blotting analysis on the last day of the conditioned media collection.

Appendix I (Table II) shows detailed preparation of all stock solutions used in transfections of HEK293T cells.

2.11 Fluorescence microscopy

Fluorescence microscopy was used to visually determine transfection efficiency and observe BPIFA1 recombinant proteins within the cells.

2.11.1 Cells transfected with BPIFA1-GFP constructs

Transfected NCI-H292 and Flp-In-CHO cells were seeded onto the glass chamber slides when the transfection assays were completed. The aim was to determine transfection efficiency. Cells were grown until almost confluent and then fixed with 10% formalin and

stained with DAPI. Images of NCI-H292 cells were taken using Olympus epifluorescence microscope, whereas images of Flp-In-CHO cells were taken using Zeiss Axioplan 2 imaging microscope. Cells were visualised at 20x and 60x magnification. Images were processed using ImageJ-win32 program.

2.11.2 Analysis of FLAG-tagged BPIFA1 proteins within the cells

NCI-H292 cells were transfected with FLAG-tagged BPIFA1-VR1255 constructs for observation of recombinant proteins within the cells. Cells were seeded onto 6-well plate ($4x10^5$ cells/well) the day before calcium phosphate transfection. The day after transfection, cells were seeded onto the glass chamber slides and grown until almost confluent. Cells were fixed by immersion in the ice-cold methanol (100%; Fisher Chemical) for 10 minutes at -20ºC. Methanol was removed, and cells were washed with 1x PBS (Gibco® by Life technologies). Subsequently, the staining of cells was performed. Triton X-100 (Sigma) in PBS (0.5%) was added to the cells for 5 minutes at RT. Afterwards, cells were washed with 1x PBS. For the blocking step, cells were incubated in the goat serum (Sigma) diluted (1:10) in 1x PBS with 0.5% Triton X-100 (blocking buffer) for 1 hour on the orbital shaker (80 RPM) at RT. Subsequently, the blocking buffer was removed, and cells were washed with 1x PBS. Mouse monoclonal ANTI-FLAG® M2 antibody (Sigma-Aldrich) was diluted 1:500 in the blocking buffer and added to the cells for 2 hours on the orbital shaker (80 RPM) at RT. Control cell samples were incubated in the blocking buffer only (without primary antibody). After incubation, the primary antibody mixture was removed, and cells were washed with 1x PBS. The primary antibody was detected with secondary Alexa Flour 488 conjugated goat anti-mouse IgG (H+L) cross-adsorbed antibody (ThermoFisher Scientific) diluted 1:1000 in the blocking buffer and incubated for 1 hour in the dark on the orbital shaker (80 RPM) at RT. The secondary antibody mixture was aspirated, and cells were washed with 1x PBS. The frames of glass chamber slides were removed, and cells were stained with DAPI. Images of the cells were taken at 100x magnification using Zeiss Axioplan 2 imaging

immunofluorescence microscope and processed using ImageJ-win32 program. Fields for imaging were chosen randomly. After images were taken, ten imaged fields of transfected cells were analysed by counting total number of cells per field as well as counting cells positive for BPIFA1. The aim was to determine the ratio of BPIFA1 transfected cells with and without fluorescent granules. Ratio was calculated by using equation:

$$\frac{Average\ \%\ of\ cells\ with\ granules}{Average\ \%\ cells\ without\ granules} = Ratio$$

2.12 Purification of BPIFA1-FLAG recombinant proteins

BPIFA1-FLAG proteins were purified from 15ml of serum-free conditioned media using anti-FLAG® M2 affinity gel (Sigma-Aldrich) according to established protocols. FLAG® peptide (Sigma-Aldrich) instead of 3X FLAG peptide was used for the elution of proteins, because BPIFA1 proteins of interest were fused to the FLAG tag. Purified BPIFA1-FLAG proteins were stored at -20ºC. Samples of purified proteins were collected for SDS-PAGE analysis as were conditioned medium samples before and after purification, and anti-FLAG® M2 affinity gel beads before and after purification.

2.13 Bacterial pull-down assays

Bacterial pull-down assays were used to investigate the ability of BPIFA1 to bind to the respiratory bacteria. Binding of BPIFA1 to *S. aureus*, *S. pneumoniae*, and NTHi were studied. Both FLAG-tagged BPIFA1 recombinant proteins and endogenous BPIFA1 proteins were used. Mouse endogenous BPIFA1 was collected as apical secretion washes from WT mTECs differentiated at the ALI conditions (section 2.14.4). Human endogenous BPIFA1 was collected as the apical secretion washes from normal and asthmatic bronchial epithelial cells differentiated at the ALI conditions (kindly gifted to us by Synairgen (Southampton)). The list of BPIFA1 proteins used in bacterial pull-down assays is provided in the Table 2.6.

Table 2.6: The list of BPIFA1 proteins used in the bacterial pull-down assays.

Protein	Amount
Mouse endogenous BPIFA1	25µl of ALI wash
Mouse recombinant BPIFA1-FLAG	50µl of serum-free conditioned medium
Purified mouse recombinant BPIFA1-FLAG	10µl of purified protein in TBS
Human endogenous BPIFA1 (Synairgen)	10µl of ALI wash
Human recombinant full-length BPIFA1-FLAG	50µl of serum-free conditioned medium
Human recombinant cysteine mutant BPIFA1-FLAG	50µl of serum-free conditioned medium
Human recombinant S18 deletion BPIFA1-FLAG	50µl of serum-free conditioned medium

2.13.1 BPIFA1 binding to *S. aureus*

S. aureus strain SH1000, a laboratory strain derived from *S. aureus* strain NCTC 8325 (Baek et al., 2013, O'Neill, 2010) was used in the pull-down assays. *S. aureus* was grown on LB-agar (Sigma) plate overnight in the incubator (37ºC/5% CO_2). Bacterial colonies were picked up and added into Brain-Heart Infusion (BHI) culture broth (Sigma-Aldrich) for overnight incubation (37ºC/5% CO_2) on the orbital shaker (200 RPM). The optical density (O.D.) of 1ml overnight bacterial culture was measured at a wavelength of 600nm using Jenway 6300 spectrophotometer calibrated against 1ml of uninoculated BHI broth. Bacterial culture amounts equivalent to OD_{600} of 1 (approximately $2x10^8$ of bacteria) were used for each reaction. Bacterial culture amount for an OD_{600} of 1 was calculated using equation:

$$\frac{1}{OD-600\,Value} = Amount\ of\ culture\ (ml)$$

Bacterial samples were centrifuged at 13000 RPM for 5 minutes to collect bacterial pellet. The broth was removed, and bacteria were washed three times in 1ml of PBS and centrifuged (13000 RPM/5mins) to collect a pellet. The pellet was resuspended in the

samples containing BPIFA1 (Table 2.6) and incubated in the incubator (37ºC/5% CO_2) for: 0, 10, 30, and 60 minutes. Samples were centrifuged (13000 RPM/5mins) to collect bacterial-protein pellets which were then washed three times in PBS. Bacterial-protein pellets were lysed in 2x SDS lysis buffer along with the recovered pull-down fluids and analysed using SDS-PAGE.

2.13.2 BPIFA1 binding to *S. pneumoniae*

S. pneumoniae strain D39, a clinical isolate obtained from the patient in 1916 (Lanie et al., 2007), was used in the pull-down assays. *S. pneumoniae* was grown on the blood agar plates overnight in the incubator (37ºC/5% CO_2). Bacterial colonies were picked up and added into 20ml of BHI broth (Sigma-Aldrich) supplemented with 20% heat inactivated FBS (Sigma) for the overnight incubation (no shaking) in the incubator (37ºC/5% CO_2). The optical density of 1ml bacterial culture was measured as described in the section 2.13.1. Bacterial culture amounts equivalent to OD_{600} of 1 (approximately $8.5x10^7$ of bacteria) were used for each reaction with the protein of interest (Table 2.6). Overnight bacterial culture samples which measured below OD_{600} 0.7 were used in the bacterial pull-down assays. *S. pneumoniae* samples were prepared and bacterial pull-downs were performed as described in the section 2.13.1.

2.13.3 BPIFA1 binding to NTHi

Streptomycin resistant NTHi strain 375-SR was used in the bacterial pull-downs. NTHi strain 375 is a clinical isolate obtained from the pneumococcal vaccine study (Cody et al., 2003). NTHi was grown on the BHI agar (Sigma-Aldrich) plates supplemented with 10µg/ml hemin (Sigma-Aldrich), 2µg/ml NAD hydrate (Sigma-Aldrich) and 200µg/ml streptomycin sulphate (Melford Laboratories). Bacteria were streaked onto BHI plates and incubated overnight in the incubator (37ºC/5% CO_2). Bacterial colonies were picked up and added into 4ml of BHI broth (Sigma-Aldrich) supplemented with NAD (2µg/ml) and hemin (10µg/ml) for 3 hours incubation on the orbital shaker at 200 RPM (37ºC/5%

CO_2). The optical density (O.D.) of 1ml overnight bacterial culture was measured at a wavelength of 490nm using Jenway 6300 spectrophotometer calibrated against uninoculated BHI broth. Bacterial culture amounts equivalent to OD_{490} of 1 (approximately $5x10^9$ of bacteria) were used for each reaction with the protein of interest (Table 2.6). Bacterial culture amount for an OD_{490} of 1 was calculated using equation:

$$\frac{1}{OD - 490\ Value} = Amount\ of\ culture\ (ml)$$

NTHi samples were prepared and bacterial pull-downs were performed as described in the section 2.13.1.

Methods for the study of mTEC challenge with NTHi

2.14 mTEC culture

mTECs, isolated from WT and transgenic *Bpifa1*$^{-/-}$ mice, were used in NTHi challenge study. The aim was to investigate whether the loss of BPIFA1 in mTECs results to the enhanced NTHi infection.

2.14.1 WT and transgenic *Bpifa1*$^{-/-}$ mice

Mice deficient in *Bpifa1* were generated by Prof Ralph Shohet at the University of Hawaii as described (Akram et al., 2018). Animal work with *Bpifa1*$^{-/-}$ mice was approved by the University of Liverpool Animal Welfare Committee and performed under UK Home Office Project Licences 40/2083 and 70/8599. Mice lacking *Bpifa1* used in this study were at the age of 13-17 weeks, whereas WT C57BL/6J control mice were at the age of 20-31 weeks. Wild-type C57BL/6J mice were obtained from Charles River. Animal work with WT mice was approved by the University of Sheffield Animal Welfare Committee and performed under Scientific procedures Act 1968 and UK Home Office Project License 40/3726.

2.14.2 Harvesting of mouse tracheas

Terminal intra-peritoneal injection of 100µL pentobarbital (50mg/ml, Henry Schein®) was used to euthanise mice which were then exsanguinated by cutting the inferior vena cava. The dissection method was adapted from the study by You et al. (You et al., 2002). Briefly, mice were kept on the ice and before dissection was started, they were sprayed with 70% Industrial Methylated Spirit (IMS). Dissection was performed in the class 2 safety cabinet. Using sterile technique, a longitudinal, midline incision from the clavicles to the submandibular region was made to expose the trachea (Figure 2.2 B). The muscles overlying trachea were separated and midline incision in the sternum was made to access the trachea within the thoracic cavity (Figure 2.2 C). Trachea was lifted, and the oesophagus was dissected away from the posterior surface of the trachea. Resection of trachea was performed by cutting at the proximal part of trachea distal to the larynx (Figure 2.2 D) and by cutting trachea at the bifurcation of the mainstem bronchi (Figure 2.2 E). Resected tracheas were placed in sterile **'mTEC-basic media'**: DMEM/Ham's F-12 media (containing HEPES and L-glutamine; Life Technology) supplemented with penicillin (100 µg /ml) and streptomycin (100 µg/ml) (Life Technology) and kept on the ice until the dissection of all mice was finished. Subsequently, the remaining adherent tissues were removed from the trachea under Olympus SZX10 dissecting microscope (Figure 2.2 H). Cleaned tracheas were placed in the fresh cold mTEC-basic media and kept on the ice until all tracheas were cleaned. Tracheas were cut open lengthwise and placed in the 15ml falcon tube containing 5ml of freshly made 0.15% pronase solution (Roche Applied Science) in mTEC-basic media for overnight (18-24 hours) incubation at 4ºC. For each batch of mTECs, approximately six harvested tracheas were pooled in the one tube.

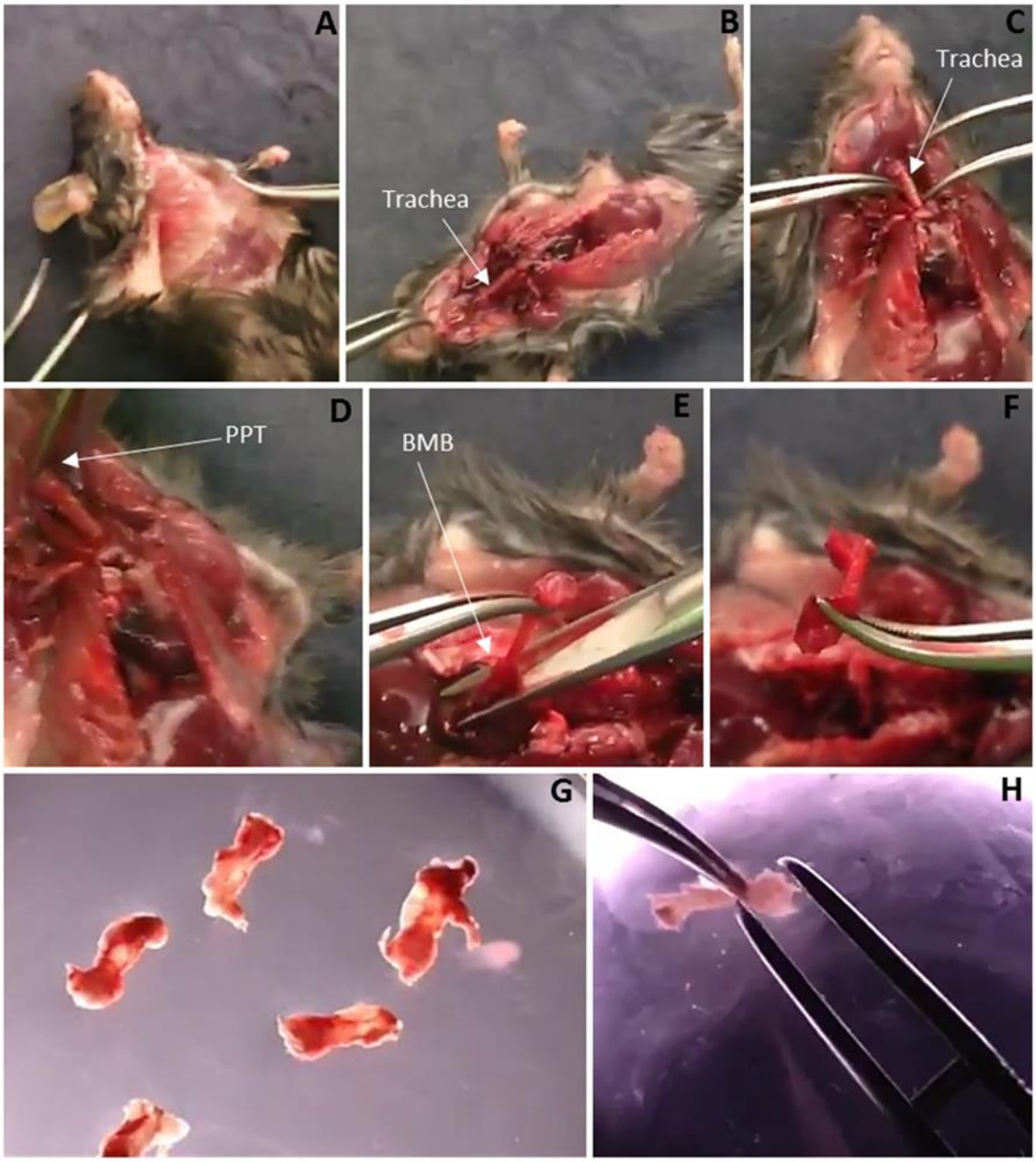

Figure 2.2: Dissection of mouse trachea.
The removal of skin by the longitudinal, midline incision from the distal part of the rib cage to the submandibular region (**A**). Exposure of trachea (**B**). Separation of muscles from the trachea (**C**). Resection of trachea by cutting at the proximal part of trachea (PPT) distal to the larynx (**D**) and by cutting trachea at the bifurcation of the mainstem bronchi (BMB) (**E**). Resected trachea (**F**). Visualisation of tracheas under the dissection microscope (**G**). Removal of remaining adherent tissues from the trachea (**H**).

2.14.3 Isolation and submerged culture of mTECs

The methodology for isolation and culture of mTECs was adapted from the previously described method (You et al., 2002, You and Brody, 2013). After overnight incubation, 10% FBS (Life Technologies) was added in the tube, containing harvested tissues to neutralise the activity of pronase and the tube was gently inverted approximately 20 times to dislodge epithelial cells that were attached to the tracheas. Tracheas were transferred into a new 15ml falcon tube, containing 2ml of warm mTEC-basic medium supplemented with 10% FBS and again inverted gently for approximately 20 times. This process was repeated four times. Harvested tissues were discarded and the contents of all tubes were combined in a new tube. To collect cells, the sample was centrifuged at 1495 RPM for 15 minutes at 10ºC. The supernatant was aspirated, and the cell pellet was resuspended in 1ml of cold DNase solution, containing 0.5mg/ml pancreatic DNase I (Sigma-Aldrich) and 1mg/ml bovine serum albumin (Sigma-Aldrich). The cell suspension (15µl) was loaded on the Neubauer counting chamber for counting of the total number of cells and the rest of the cells were incubated in DNase solution for 5 minutes on the ice. During incubation, cell viability was assessed, and the total number of the cells was determined. Cells were centrifuged at 1495 RPM for 5 minutes at 10ºC and the pellet was resuspended in 5ml of mTEC-basic medium supplemented with 10% FBS. The cells were plated onto 60mm surface treated tissue culture dish (Nunc™ Brand Products) and incubated for 3-4 hours in the incubator (37ºC/5% CO_2) to allow fibroblasts to attach to the surface. After incubation, the tissue culture dish was gently swirled a few times and non-adherent epithelial cells were collected. Cells were centrifuged at 1495 RPM for 5 minutes at 10ºC to collect cell pellet. During this time, 5ml of mTEC-basic medium containing 10% FBS was added to fibroblasts and cells were cultured till confluent. Epithelial cells were resuspended in **'mTEC-plus medium'**: mTEC-basic medium containing 5% FBS, 10µg/ml of insulin (Sigma-Aldrich), 5µg/ml of transferrin (Sigma-Aldrich), 0.1µg/ml of cholera toxin (Sigma-Aldrich), 25ng/ml of mouse epidermal growth

factor (BD Biosciences), 30µg/ml bovine pituitary extract (Gibco® by Life Technologies), 0.01µM of freshly added retinoic acid (Sigma-Aldrich), and 10µM of Rho Kinase inhibitor Y-27632 dihydrochloride (Tocris bioscience). Sample of epithelial cells (original cells) was taken for RNA extraction. The rest of isolated epithelial cells were seeded at the density of 3-3.5x10^4 (cells/transwell) onto 0.4µm pore sized transparent Polyethylene Terephthalate (PET) membranes coated with 50µg/ml of rat-tail collagen type I (BD Biosciences) in 24-well cell culture plates supporting transwell format (Corning Incorporated Costar®). Cells were cultured in the submerged conditions until confluent (mTEC-plus media: 200µl in the top chamber and 700µl in the bottom chamber). Cells were fed with fresh media every second day.

2.14.4 ALI culture of mTECs

mTECs were differentiated into upper airway-like epithelium in ALI conditions using a previously described method (You et al., 2002, You and Brody, 2013). After mTECs became confluent, mTEC-plus media was removed from the top and bottom chambers and 800µl of **'mTEC-ALI media'** was added to the bottom chamber: mTEC-basic media containing 5µg/ml insulin, 5µg/ml transferrin, 0.025µg/ml cholera toxin, 5ng/ml mouse epidermal growth factor, 30µg/ml bovine pituitary extract, 1mg/ml BSA (Sigma-Aldrich) and 0.01µM of freshly made retinoic acid. Sample of Day 0 ALI cells was collected for RNA extraction. Epithelial cells were differentiated in ALI culture for 14 days (Figure 2.3). Cells were fed with fresh mTEC-ALI media and the apical surfaces were washed with 200µl of warm Hank's Balanced Salt Solution (HBSS; Gibco® by Life technologies) every 48 hours and stored at -20ºC. Washes were analysed for BPIFA1 secretion using SDS-PAGE. Samples of differentiated mTECs were collected on Day 14 ALI for RNA extraction and western blotting analysis. Transwells were also fixed on Day14 ALI for immunostaining and confocal microscopy. The rest of the differentiated mTECs were used in NTHi challenge study.

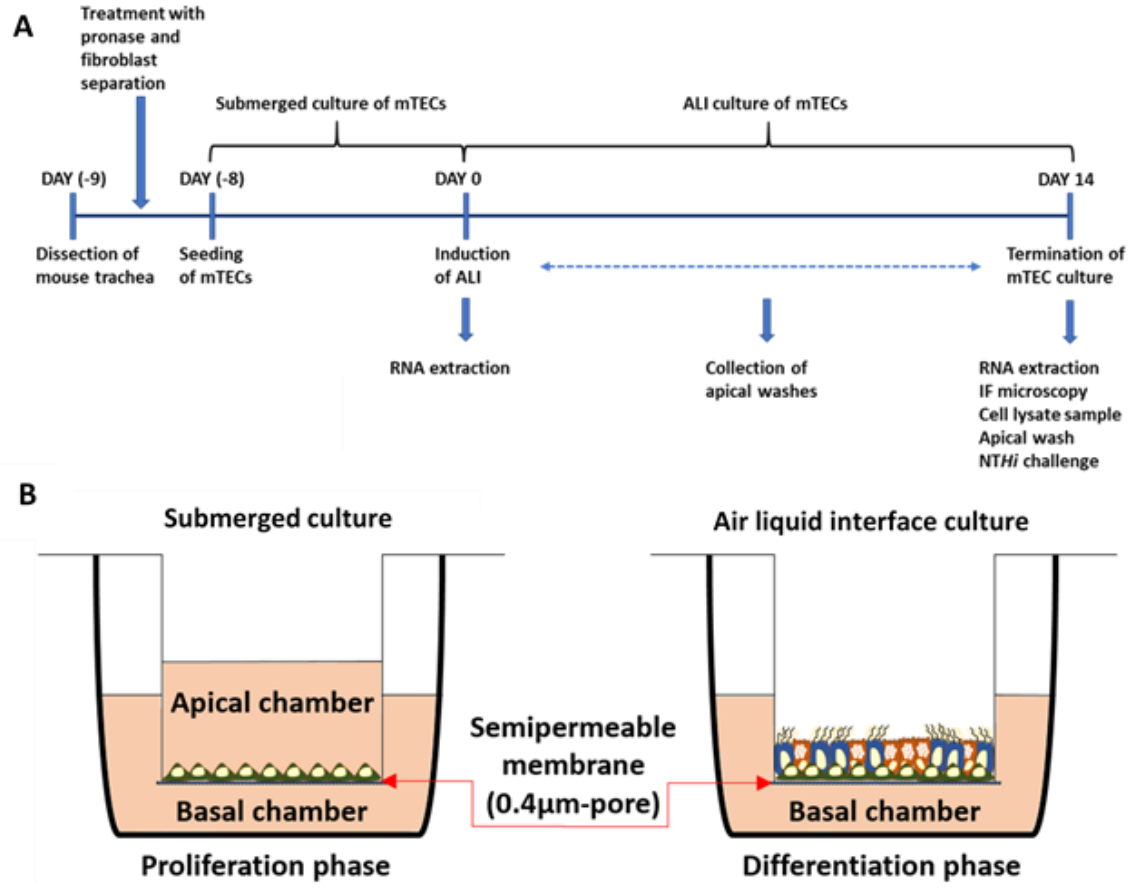

Figure 2.3: Chronology and method for ALI culture of mTECs.
Figure shows chronology of mTEC culture. Mouse tracheas were dissected and subjected to proteolysis in pronase solution. mTECs were separated from fibroblasts and grown in the submerged culture until confluent. ALI conditions were induced upon the confluence. Samples were collected for analysis at the regular time points (**A**). Figure also shows a schematic diagram of submerged culture in which most of the cells present are basal cells (green). ALI conditions were induced when mTECs became confluent, promoting cell differentiation into secretory cells (red) and ciliated cells (blue) (**B**).

2.14.5 Mouse fibroblast culture

Adherent fibroblasts from mouse tracheas were cultured in 60mm surface treated tissue culture dishes (Nunc^{TM} Brand Products) containing mTEC-basic media supplemented with 10% FBS. Once confluent, cells were dissociated by Trypsin-EDTA (Sigma). The cell pellet was resuspended in 5ml of fresh mTEC-basic/10% FBS media and the cells were grown until confluence. Subsequently, fibroblasts were subjected to a second trypsinization and seeded in T25 flasks. Fibroblasts were then lysed in Trizol reagent (250µl/flask) for RNA extraction or in 2x SDS (100µl/flask) lysis buffer for SDS-PAGE.

2.15 NTHi challenge assays

mTECs, isolated from WT and *Bpifa1*$^{-/-}$ mice, were exposed to streptomycin resistant GFP-tagged NTHi-375 aiming to understand the role of BPIFA1 in NTHi infection.

2.15.1 Preparation of GFP-tagged NTHi-375-SR inoculum

GFP-tagged NTHi-375-SR was grown as described in the section 2.13.3. Sample of bacterial culture (1ml) was centrifuged at 13,000 RPM for 5 minutes and resuspended in the required volume of PBS to achieve an inoculum concentration of $1x10^{10}$ bacteria/ml. The following formula was used to determine the volume of PBS required:

$$\frac{OD - 490\ value}{0.4} \times (2 \times 10^9) = Amount\ of\ culture\ (ml)$$

2.15.2 Exposure of mTECs to NTHi

Differentiated mTECs (Day 14 ALI) were washed with warm HBSS and antibiotic free mTEC-ALI media was added to the plate 3 hours before NTHi challenge. The number of mTECs per well at Day 14 ALI was counted using a haemocytometer (n=3) and one well was determined to contain approximately $1.3x10^5$ cells. An appropriate amount of NTHi inoculum was diluted into antibiotic free mTEC-ALI media and added to the transwells in the such way that the apical surfaces of the cells were exposed to bacteria. NTHi challenge assays were performed using a multiplicity of infection (MOI) of 1:200, 1:500, and 1:1000 (mTECs: bacteria). An equal amount of sterile PBS diluted into antibiotic free mTEC-ALI media was used to generate MOCK-challenged controls. mTECs were exposed to NTHi for 1 hour at 37ºC, 5% CO_2. Subsequently, media was removed from the bottom and top chambers and cells were washed three times with warm PBS to remove non-adherent bacteria. Fresh antibiotic free mTEC-ALI media was added to the basal chambers and cells were returned to incubator for 24, 48, and 72 hours. After each incubation time point, immunofluorescence microscopy was used to analyse the cells. Subsequently, the following samples were collected: 1) apical secretion washes in 200µl

of HBSS for western blotting and dot blotting; 2) cell lysate in 250µl Trizol reagent for gene expression studies; and 3) one transwell for cell fixation, immunohistochemical staining and confocal microscopy analysis.

2.16 Immunofluorescence (IF) microscopy

Live mTECs exposed to GFP-tagged NTHi-375-SR were visualised under IF microscope for the determination of NTHi colonisation. Fluorescence immunohistochemical staining was used for the localisation of proteins produced by original, Day 14 ALI and NTHi exposed mTECs. Fixed and stained mTECs were imaged using confocal (IFC) microscope (Olympus Fluoview 1000).

2.16.1 Visualisation of mTECs exposed to GFP-tagged NTHi-375-SR

Live mTECs exposed to NTHi were imaged using Zeiss Axiovert 200M IF microscope at 24, 48, and 72 hours post infection (hpi). Images were taken of six fields on every membrane at 20x magnification to define an area for quantification (Figure 2.4). The aim was to determine the intensity of NTHi colonisation in WT and *Bpifa1*$^{-/-}$ mTEC cultures. The intensity of bacterial colonisation was measured by the mean integrated intensity of the six fields using ImageJ-win32 program. Three individual batches of WT and *Bpifa1*$^{-/-}$ mTECs were analysed for quantification.

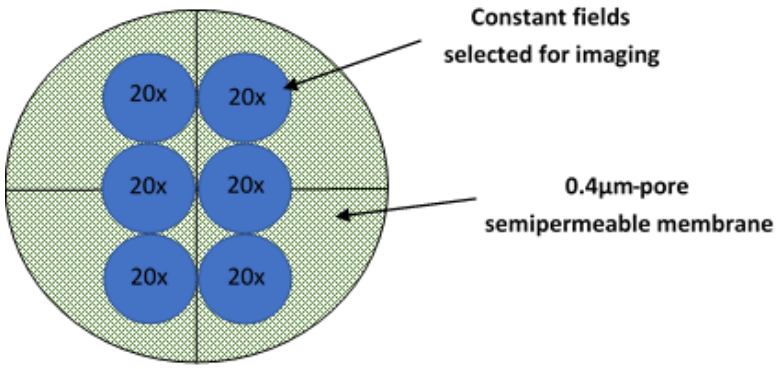

Figure 2.4: Quantification of NTHi colonisation.
Constant six fields were selected on the membrane for imaging at 24, 48, and 72hpi. The mean integrated intensity was measured of all six fields to define bacterial colonisation.

2.16.2 Immunohistochemical staining and confocal imaging

mTECs on transwell membranes were fixed with 10% formalin. Cells were permeabilised by incubation in the goat serum diluted 1:10 in 1x PBS with 0.5% Triton X-100 (blocking buffer) for 1 hour on the orbital shaker (80 RPM) at RT. Afterwards, mTECs were washed with 1x PBS and primary antibody (Table 2.7) diluted in blocking buffer was added to the cells for overnight incubation on the orbital shaker (80 RPM) at 4ºC. Cells were washed three times with 1x PBS and secondary antibody (Table 2.7) diluted in the blocking buffer was added to the cells for 1 hour incubation in the dark on the orbital shaker (80 RPM) at RT. Subsequently, cells were washed three times with 1x PBS and membranes were cut from the transwell frames. The membrane was placed on a glass microscope slide and a drop of Vectashield mounting medium for fluorescence with DAPI (Vector Laboratories, Inc.) was added to stain nuclei. Stained cells were imaged using Olympus Fluoview 1000 IFC microscope. Images were processed using ImageJ-win32 program.

Table 2.7: Primary and secondary antibodies used in immunohistochemical staining.

Primary antibodies			
Antibody	**Dilution**	**Type**	**Manufacturer**
Anti-BPIFA1	1:200	Rabbit polyclonal	Produced in lab (Musa et al., 2012)
Anti-β tubulin	1:100	Mouse monoclonal – Clone TUB2.1	Sigma-Aldrich (Cat. # T5201)
Anti-FOXJ1	1:200	Mouse monoclonal – Clone 2A5	eBioscience (Cat. # 14-9965-82)
Anti-MUC5B	1:100	Rabbit polyclonal – Clone H-300	Santa Cruz (Cat. # sc-20119)
Anti-ZO1	1:100	Rabbit polyclonal	Thermo Fisher Scientific (Cat. # 40-2200)
Secondary antibodies			
Antibody	**Dilution**	**Type**	**Manufacturer**
Alexa Fluor 488	1:200	Goat anti-mouse	Life technology (Cat. # A11011)
Alexa Flour 568	1:200	Goat anti-mouse	Life technology (Cat. # A11004)
Alexa Flour 568	1:200	Goat anti-rabbit	Life technology (Cat. # A11011)
Alexa Flour 633	1:200	Goat anti-mouse	Life technology (Cat. # A21050)

2.17 Analysis of gene expression in mTEC cultures

Gene expression by mTECs exposed to NTHi was analysed at 24, 48, and 72hpi. mTECs were lysed in 250µl Trizol. RNA extraction, RT and RT-PCR were performed as described. Expression of *Oaz1*, *Tekt1*, *Ltf*, and *Bpifa1* was studied.

2.18 Mouse cytokine array

Mouse cytokine array was performed to generate a full profile of cytokines and chemokines produced by WT and *Bpifa1*$^{-/-}$ mTECs exposed to GFP-tagged NTHi-375-SR. This assay was performed using Mouse Cytokine Array Panel A (R&D Systems) according to the manufacturer's protocol. The assay was carried out using 1ml of the apical secretion wash from each WT and *Bpifa1*$^{-/-}$ mTEC cultures exposed to GFP-

tagged NTHi-375-SR at MOI-1000 for 72 hours. Equal volumes of the apical secretion washes were pooled from four different batches of each WT and *Bpifa1*$^{-/-}$ mTEC cultures to produce a total volume of 1ml. Results were analysed using densitometry according to the manufacturer's recommendations. Signal values (pixel density) of each dot were analysed using ImageJ-win32 program. Data was plotted and visualised using GraphPad Prism7 software.

2.19 Dot blotting of mTEC samples

Dot blotting was used to analyse the levels of secreted BPIFA1 in the apical secretions from NTHi exposed and MOCK-challenged mTEC ALI cultures. Apical secretion washes from four different batches of NTHi-exposed and MOCK-challenged WT mTECs were used in the dot blotting analysis. Apical secretion washes were used from WT mTECs exposed to NTHi at MOI-200, MOI-500, and MOI-1000 for 24, 48, and 72 hours. Apical secretion washes from MOCK-challenged WT mTECs collected at 24, 48, and 72hpi were used as controls. Dot blotting was performed as described in the section 2.5.2.

2.20 Statistics

Levene's test was used prior to the statistical analysis to determine parametricity and variance of experimental groups. Levene's test was performed using Microsoft Excel 2016. GraphPad Prism (version 7.0) was used to plot graphs and perform statistical tests. Unpaired non-parametric two-tailed student's t-test with Mann-Whitney test was used to compare two groups of interest. Two-way analysis of variance (ANOVA) with Sidak multiple comparison test was used to compare more than two groups. Significance threshold was set at $p \leq 0.05$. Data was presented as the mean ± standard deviation (SD) or as the mean ± standard error of the mean (SEM). Significance levels represented on graphs are as follows: ns - not significant; *$p \leq 0.05$; **$p \leq 0.01$; ***$p \leq 0.001$; ****$p \leq 0.0001$.

CHAPTER 3: GENERATION OF HUMAN AND MOUSE BPIFA1 EXPRESSION VECTORS

3.1 Introduction

BPIFA1 is an abundantly secreted protein released by airway non-ciliated epithelial cells in the upper respiratory tract and pharynx (Bingle and Craven, 2002). As outlined in the introduction the function of BPIFA1 is not fully understood but available data supports its role in the airway defence. A multitude of defensive functions have been proposed for the protein ranging from roles in the regulation of ion transport, a contribution to the surfactant properties of airway secretions (Garcia-Caballero et al., 2009, Garland et al., 2013, Liu et al., 2013, McGillivary and Bakaletz, 2010, Rollins et al., 2010), antimicrobial activities, including bacterial anti-growth (Chu et al., 2010, Chu et al., 2007, Gally et al., 2011, Sayeed et al., 2013, Zhou et al., 2008) and anti-biofilm functions (Gakhar et al., 2010, Liu et al., 2013), through to chemotactic (Gally et al., 2011, Liu et al., 2013, Lukinskiene et al., 2011, Sayeed et al., 2013) and immunomodulatory properties (Chu et al., 2007, Liu et al., 2013, Lukinskiene et al., 2011). Although data supports the role of BPIFA1 in airway defence some of mechanisms underpinning these functions remain undetermined.

Previous studies aimed to answer this question and investigated the structure of BPIFA1 protein. It was initially reported that BPIFA1 shares sequence and structure similarity with BPI/LBP protein superfamily (Bingle and Craven, 2002). Similarity of BPIFA1 to these proteins led to further investigations of protein structure with two groups having solved the crystal structure of the protein (Garland et al., 2013, Ning et al., 2014). Proceeding this, it was shown that BPIFA1 controls the cleavage and activation of ENaC and the region responsible for this is at the position of amino acids G22-A39, also known as S18 region (Garcia-Caballero et al., 2009, Garland et al., 2013, Rollins et al., 2010). The study by Ahmad et al. demonstrated BPIFA1 bacteriostatic and anti-biofilm functions against several *Burkholderia cenocepacia* complex clinical isolates. Alpha 4-helix (residues I76-I105) was identified as protein region responsible for this effect. It was also

highlighted that α4 peptide of BPIFA1 (residues K77-L101) exhibited antimicrobial activity (Ahmad et al., 2016).

On the basis of what is known about the protein, I propose that BPIFA1 plays a role in the airway host defence by binding to respiratory pathogens and specific regions of protein are responsible for such function.

3.2 Objectives of this chapter

The aim of this chapter was to generate the tools required to begin functional analysis of BPIFA1. Therefore, this chapter has the following objectives:

1. To analyse human and mouse BPIFA1 protein sequences using bioinformatic approach.
2. To generate the series of GFP and FLAG tagged BPIFA1 constructs.
3. To transfect NCI-H292, CHO and HEK293T cells with BPIFA1 constructs and obtain secreted recombinant proteins.
4. To transfect NCI-H292 cells with FLAG-tagged BPIFA1-VR1255 constructs and visualise recombinant proteins in the cells.
5. To purify recombinant BPIFA1 proteins from conditioned medium samples.

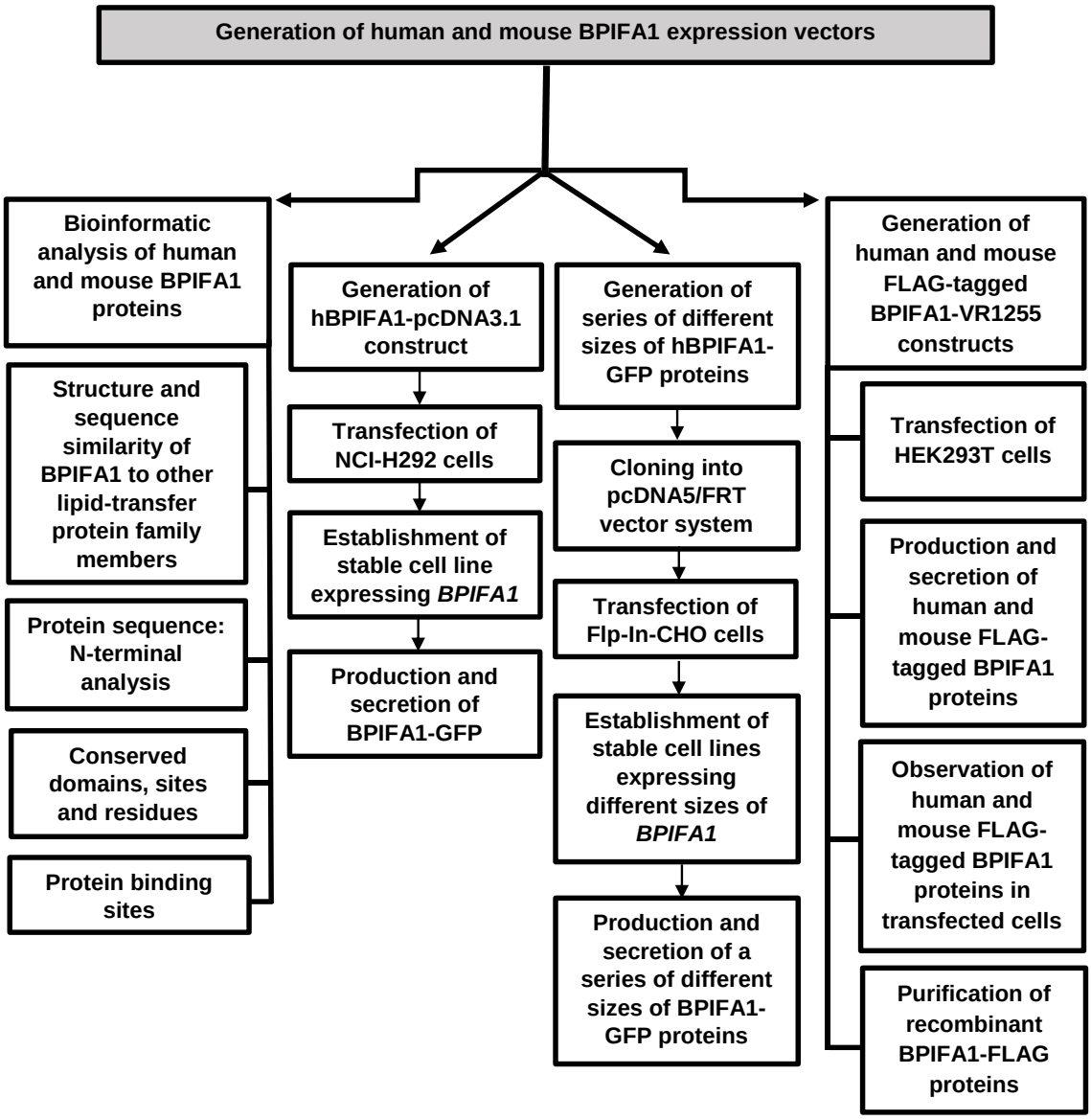

Figure 3.1: Study plan for this chapter.

3.3 Results

3.3.1 Bioinformatic analysis of human BPIFA1 (hBPIFA1) and mouse BPIFA1 (mBPIFA1) proteins

3.3.1.1 Human BPIFA1 and other lipid-transfer protein family members

I used bioinformatic tools to analyse BPIFA1 protein sequence to understand which regions of BPIFA1 may be important for biological functions. Human BPIFA1 shares amino acid sequence similarity with the N-terminal domain of BPI, LBP, PLTP, and CETP (Figure 3.2), these all belong to a larger lipid-transfer protein family. Kalign and BoxShade tools were used to generate multiple sequences alignment to identify conserved residues. Conserved residues can provide clues for functionally important regions of BPIFA1. Cysteine residues forming the disulphide bond are completely conserved and appear at the same position among all proteins analysed, suggesting their importance for biological activity of BPIFA1. It is already known that the disulphide bond of BPI is essential for the secretion of biologically active BPI (Horwitz et al., 1996) and this may also be a case with BPIFA1.

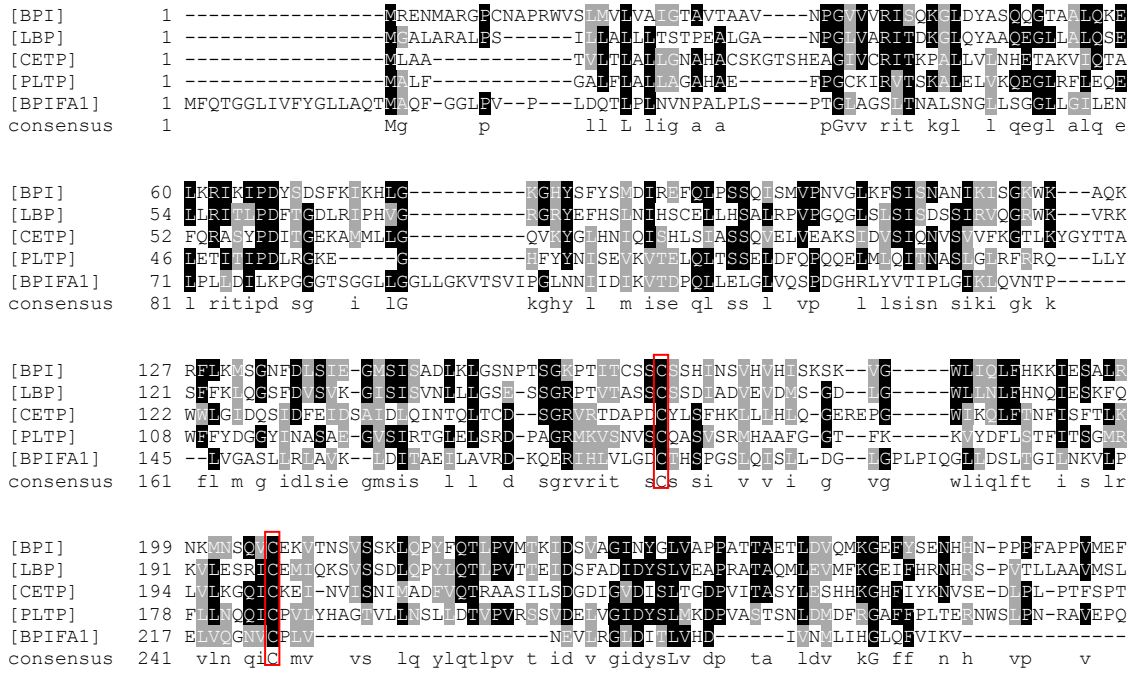

Figure 3.2: Amino acid sequence similarity of human BPIFA1 with BPI, LBP, CETP, and PLTP proteins.

A sequence similarity of hBPIFA1 with N-terminal regions of human BPI, LBP, CETP, and PLTP proteins. Cysteine residues forming disulphide bond of all proteins analysed are highlighted in red. Multiple sequences alignment was produced using Kalign and BoxShade version 3.2, written by K. Hofmann and M. Baron. Capital-case letter means that same amino acid appears in each sequence of that column and is conserved among all proteins analysed. Lower-case letter means that structurally similar amino acid (semi-conserved) is present in each sequence of proteins analysed.

I used protein Homology/analogY Recognition Engine V 2.0 (Phyre2), SWISS-MODEL template library (SMTL version 2018-01-03), and ProMod3 modelling engine to build 3D models of proteins to enable visualisation of disulphide bond position within BPI and hBPIFA1 protein structures (Figure 3.3). PyMOL was used to construct superpositions of proteins. Residues 43-256 of hBPIFA1 were superposed on full-length human BPI. The root mean square distance (RMSD) value over 176 residues was of 5.77. The structure of BPI was obtained from RCSB PDB database with resolution of 1.7Å (DOI: 10.2210/pdb1ewf/pdb). The disulphide bond of hBPIFA1 and BPI proteins was observed at the same position within the model structure (Figure 3.3).

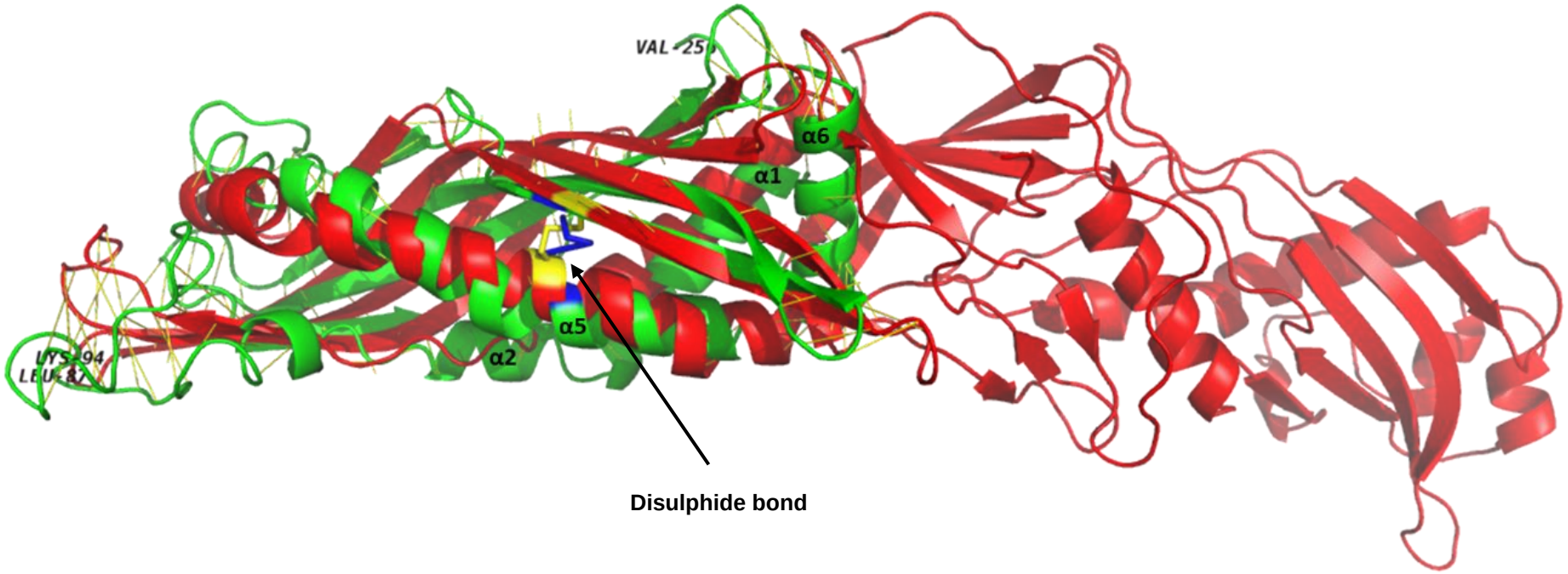

Figure 3.3: Disulphide bond of human BPIFA1 and BPI proteins is at the same position within the structure.

Superposition of hBPIFA1 (green) and BPI (red) proteins. Amino acids 87 94, and 256 of hBPIFA1 are labelled for clarity, as are α helices 1, 2, 5 and 6. Helix α4 of hBPIFA1 is missing, but its predicted position is at residues 76-105. Disulphide bond of hBPIFA1 is shown in blue (residues: C180-C224), whereas disulphide bond of BPI is presented in yellow (residues: C135-C175). PyMOL Molecular Graphics System (version 2.0.6) and Phyre2 (version 2.0) were used for analysis. Similar superposition of human BPIFA1 and BPI proteins was published by Garland et al. (Garland et al., 2013), however the position of disulphide bond was not demonstrated.

3.3.1.2 Analysis of human BPIFA1 protein sequence

hBPIFA1 can be classified as alpha-beta protein as it contains: α-helices > 30% and β-strands > 20%. Data of predicted solvent accessibility composition of hBPIFA1 showed that 55% residues of hBPIFA1 are exposed with more than 16% of their surface. Additionally, residue composition of hBPIFA1 was analysed and showed that the most common amino acids in the protein sequence are leucine (22.7%) and glycine (12.9%). hBPIFA1 can, therefore, be described as leucine-glycine rich protein. To understand which regions of protein may be involved in the binding processes, the sequence was analysed through Predict Protein Open software to predict protein-protein and protein-polynucleotide binding sites were. Five sites were identified, and these included: M1-Q3, Q30, L42, Q170-R172, and S183 (Figure 3.4).

```
MFQTGGLIVFYGLLAQTMAQFGGLPVPLDQTLPLNVNPALPLSPTGLAGSLTNALSNGLLSGGLLGILENLPLLDILKPG
PPP-------------------------P----------P-------------------------------------

GGTSGGLLGGLLGKVTSVIPGLNNIIDIKVTDPQLLELGLVQSPDGHRLYVTIPLGIKLQVNTPLVGASLLRLAVKLDIT
---------------------------------------------------------------------------

AEILAVRDKQERIHLVLGDCTHSPGSLQISLLDGLGPLPIQGLLDSLTGILNKVLPELVQGNVCPLVNEVLRGLDITLVH
---------PPP----------P-----------------------------------------------------

DIVNMLIHGLQFVIKV
----------------
```

Figure 3.4: Predicted protein-protein and protein-polynucleotide binding sites for hBPIFA1. hBPIFA1 protein sequence, showing predicted binding sites of hBPIFA1 indicated with letter 'P' underneath the sequence. Analysis was performed using Predict Protein Open software (https://ppopen.informatik.tu-muenchen.de/).

To obtain more detailed information about hBPIFA1, I analysed hBPIFA1 protein sequence for conserved sites and domains using ExPASy Prosite, EBI IterPro, and Motif Scan. These conserved domains and sites are represented in the Table 3.1. Analysis predicted that hBPIFA1 contains a Casein kinase II phosphorylation site and a N-myristoylation site. Randomised probability value for these sites was lower than 1, suggesting the probability of significant match. Leucine-rich region was also detected in the sequence of hBPIFA1, with the randomised probability value lower than 1. Analysis also revealed the presence of two conserved domains in the hBPIFA1 protein sequence:

1) lipid-binding serum glycoprotein, N-terminal domain, and 2) bactericidal permeability-increasing protein, alpha/beta superfamily domain. These two conserved domains are the signature domains of the BPI/LBP protein superfamily (EMBL-EBI, 2019b, EMBL-EBI, 2019a).

Table 3.1: Conserved domains and sites of human BPIFA1.

Name	Pattern (if available)	Access number	Randomised probability E-value (if available)	Region
Casein kinase II phosphorylation site	[ST]-x(2)-[DE]	PS00006	1.482e-02	190 to 193 (SLLD)
N-myristoylation site	G-{EDRKHPFYW}-x(2)-[STAGCN]-{P}	PS00008	1.397e-02	46 to 51 (GLAGSL) 49 to 54 (GSLTNA) 58 to 63 (GLLSGG) 62 to 67 (GGLLGI) 66 to 71 (GILENL) 80 to 85 (GGGTSG) 82 to 87 (GTSGGL) 85 to 90 (GGLLGG) 86 to 91 (GLLGGL) 89 to 94 (GGLLGK) 202 to 207 (GLLDSL) 233 to 238 (GLDITL)
Leucine-rich region profile/ matrix		PS50319		58 to 234 aa
Lipid-binding serum glycoprotein, N-terminal domain		IPR017942		58 to 233 aa
Bactericidal permeability-increasing protein, alpha/beta domain superfamily		IPR017943		102-245aa

3.3.1.3 Bioinformatic analysis of mouse BPIFA1 protein sequence

In this study, I also used a bioinformatic approach to analyse mBPIFA1 protein sequence and determine differences between mBPIFA1 and hBPIFA1. mBPIFA1 protein sequence was analysed through Predict Protein Open software. Results showed that mBPIFA1 can also be classified as an alpha-beta protein as it contains: α-helices > 30% and β-strands > 20%. In addition, data of predicted solvent accessibility composition of mBPIFA1 showed that 58% of mBPIFA1 residues are exposed with more than 16% of their surface. Residues C204 and C246 were defined to form a disulphide bond which is expected to be important for structure stability. The residue composition of mBPIFA1 was determined using Predict Protein open software. Data showed that leucine accounts for the highest percentage of amino acids present within the protein sequence (23.7%) and glycine (12.2%) is the second most common amino acid present in the sequence. These data showed that mBPIFA1 same as hBPIFA1 is a leucine-glycine rich protein. To understand which regions of mBPIFA1 may be involved in the binding process, the protein sequence was analysed through Predict Protein Open software to predict protein-protein and protein-polynucleotide binding sites. Four sites were identified, and these included: M1, Q46, G195, and P208 (Figure 3.5). This analysis suggests that binding sites of mBPIFA1 differ from the binding sites of hBPIFA1 (Figure 3.4).

Figure 3.5: Predicted protein-protein and protein-polynucleotide binding sites for mBPIFA1.
mBPIFA1 protein sequence, showing predicted binding sites of mBPIFA1 indicated with letter 'P' underneath the sequence. Analysis was done using Predict Protein Open software (https://ppopen.informatik.tu-muenchen.de/).

I also analysed the protein for conserved sites and domains using EBI InterPro and Motif Scan. These conserved domains and sites are listed in the Table 3.2. mBPIFA1, like hBPIFA1, contains Casein kinase II phosphorylation and N-myristoylation sites. In addition, mBPIFA1 contains N-glycosylation and Protein kinase C phosphorylation sites, which are not detected in hBPIFA1. Leucine-rich region was also detected in the mBPIFA1 protein sequence. Analysis also revealed the presence of proline-rich region in mBPIFA1, but the value of randomised probability was not significant (E-value > 1). The signature domains of BPI/LBP protein superfamily were detected in mBPIFA1.

Table 3.2: Conserved domains and sites of mouse BPIFA1.

Name	Pattern (if available)	Access number	Randomised probability E-value (if available)	Region
Casein kinase II phosphorylation site	[ST]-x(2)-[DE]	PS00006		224-227 (SFLD) 254-257 (SGLD)
N-myristoylation site	G-{EDRKHPFYW}-x(2)-[STAGCN]-{P}	PS00008		55-60 (GLPLAV) 82-87 (GGLLSG) 91-96 (GILENI) 105-110 (GGGNSN) 111-116 (GLVGGL) 161-166 (GLTLNV) 251-256 (GILSGL)
N-glycosylation site	N-{P}-[ST]-{P}	PS00001		182-185 (NITA) 228-231 (NLTG)
Protein kinase C phosphorylation site	[ST]-x-[RK]	PS00005		210-212 (SLK)
Leucine-rich region profile/ matrix		PS50319	0.0036	3-181 aa
Proline-rich region profile/ matrix		PS50099	3.1	25-68 aa
Lipid-binding serum glycoprotein, N-terminal domain		IPR017942		83-256 aa
Bactericidal permeability-increasing protein, alpha/beta domain superfamily		IPR017943		126-276 aa

3.3.1.4 Multiple sequences alignment of BPIFA1

Multiple sequences alignment confirmed that the extreme N-terminal region of BPIFA1 exhibits the highest variability among the species (Figure 3.6). The N-terminal region of mBPIFA1 contains a PLPL repeat which seems to be rodent specific as PLPL repeat region is also observed in BPIFA1 protein sequences of wood mouse and rat. This PLPL repeat is structured in rodent BPIFA1 but is missing from the sequence of hBPIFA1 and is not present in the crystal structure of hBPIFA1, suggesting that it is unstructured (Bingle and Craven, 2002, Garland et al., 2013). In addition, mBPIFA1 contains three N-glycosylation sites, which are absent from hBPIFA1. Results suggest that the glycosylation status of the protein varies between species. However, the cysteine residues forming the disulphide bond of BPIFA1 are highly conserved among all species (Figure 3.6).

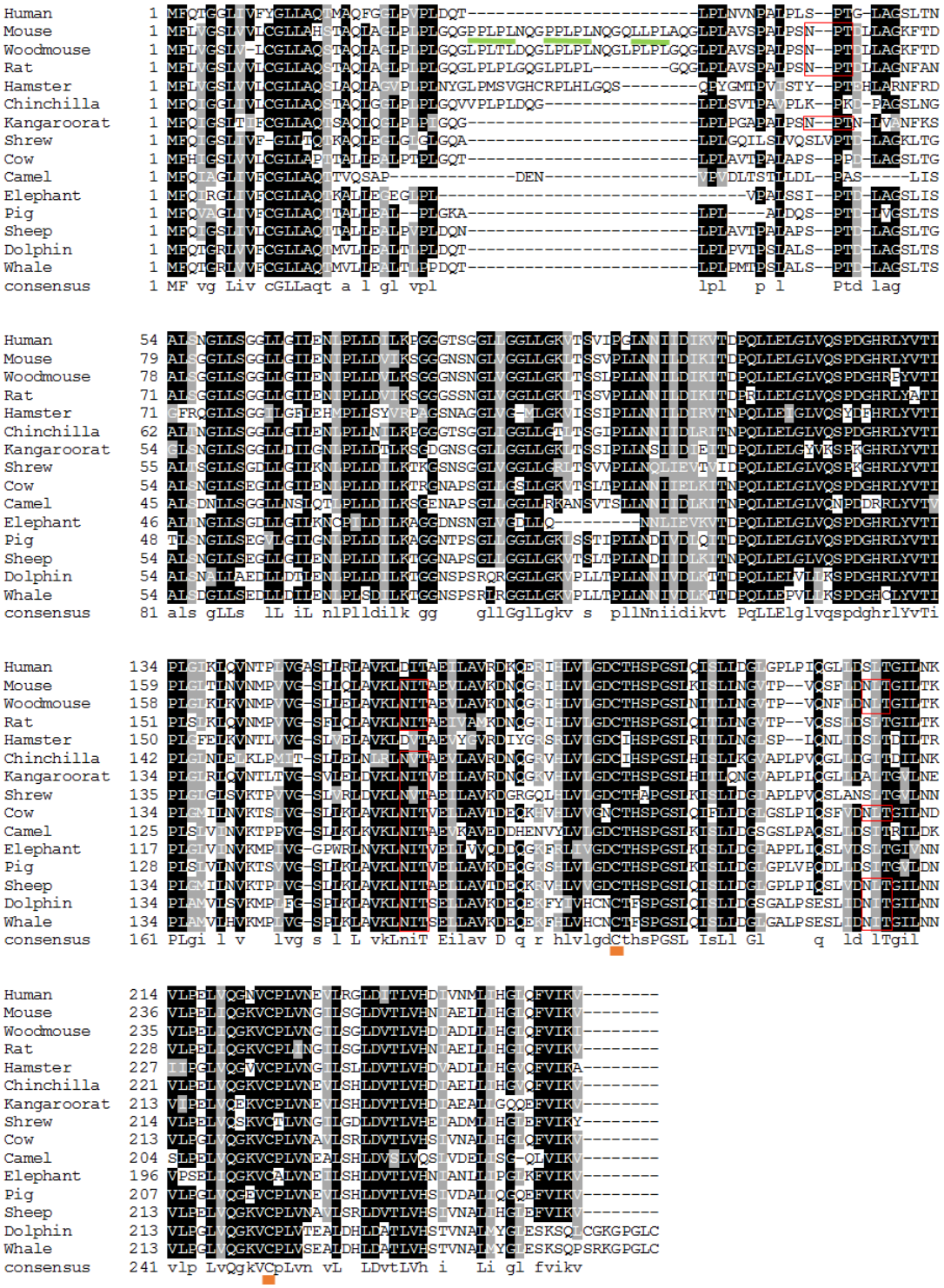

Figure 3.6: The N-terminal sequence of BPIFA1 exhibits the highest variability among the species.

PLPL repeat region of mBPIFA1 is highlighted with green line underneath. N-glycosylation sites are highlighted in red rectangles. Conserved cysteine residues are highlighted with orange line underneath. Multiple sequences alignment was produced using Kalign and BoxShade version 3.2, written by K. Hofmann and M. Baron. Capital letters mean that same amino acid appears in each sequence and lower-case letters mean that structurally similar amino acid is present in each sequence.

3.3.2 Full-length human BPIFA1 (FL-hBPIFA1) and pcDNA3.1 vector system

3.3.2.1 Establishment of a stable NCI-H292 cell line expressing GFP-tagged hBPIFA1

A human pulmonary mucoepidermoid carcinoma cell line NCI-H292 was transfected with pcDNA3.1 plasmid containing FL-hBPIFA1 cDNA (Figure 3.7 A-B) to obtain secreted BPIFA1-GFP fusion protein for functional analysis. NCI-H292 cells were chosen for these experiments due to their reported ability to express BPIFA1 (Chu et al., 2010) and previous successful usage in tranfection assays with plasmids containg BPIFA1 cDNA (Chu et al., 2007).

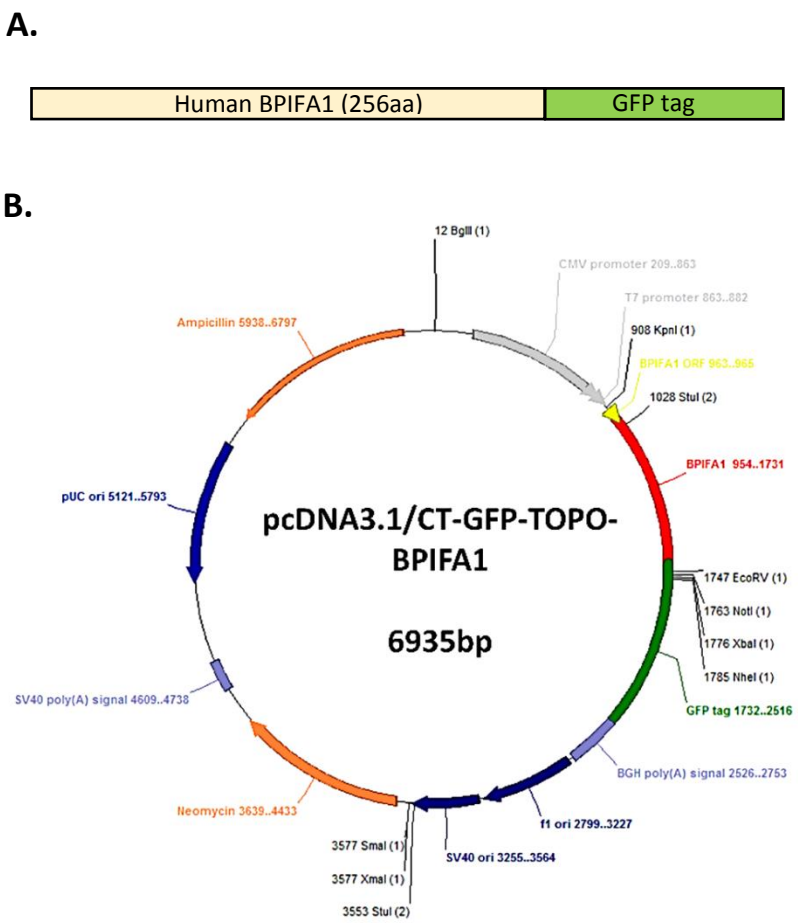

Figure 3.7: Generation of full-length hBPIFA1-GFP fusion construct.
Figure shows a schematic diagram of FL-hBPIFA1 tagged with GFP (**A**) and plasmid map of hBPIFA1-GFP fusion construct (**B**). Plasmid map was generated using a plasmid editor program ApE (Version 8.5.2.0).

Transfection of NCI-H292 cells was performed using FuGENE® HD and G418 selection was used to isolate positively transfected cells. However, G418 selection did not work efficiently and consequently, a serial dilutions method was used to isolate BPIFA1-positive single cell colonies. These single cell colonies were expanded, and some were seeded onto 8-well glass chamber slides for visualisation under a fluorescent microscope to determine the isolation efficiency of positive transfectants. This showed that only a small number of cells were FL-hBPIFA1-GFP positive (Figure 3.8 A), suggesting that the process had not achieved clonal selection of high expressing cells. However, I was able to detect FL-BPIFA1-GFP production by transfected cells (Figure 3.8 B). A band of approximately 52kDa size was detected with anti-human BPIFA1 antibody and it represented FL-hBPIFA1 tagged with GFP (BPIFA1: 25 kDa, and GFP tag: 26.9 kDa). The amount of protein produced was small and appeared to be insufficient for future assays. Therefore, I decided to remove BPIFA1 negative cells from the stable cell line to increase BPIFA1 production.

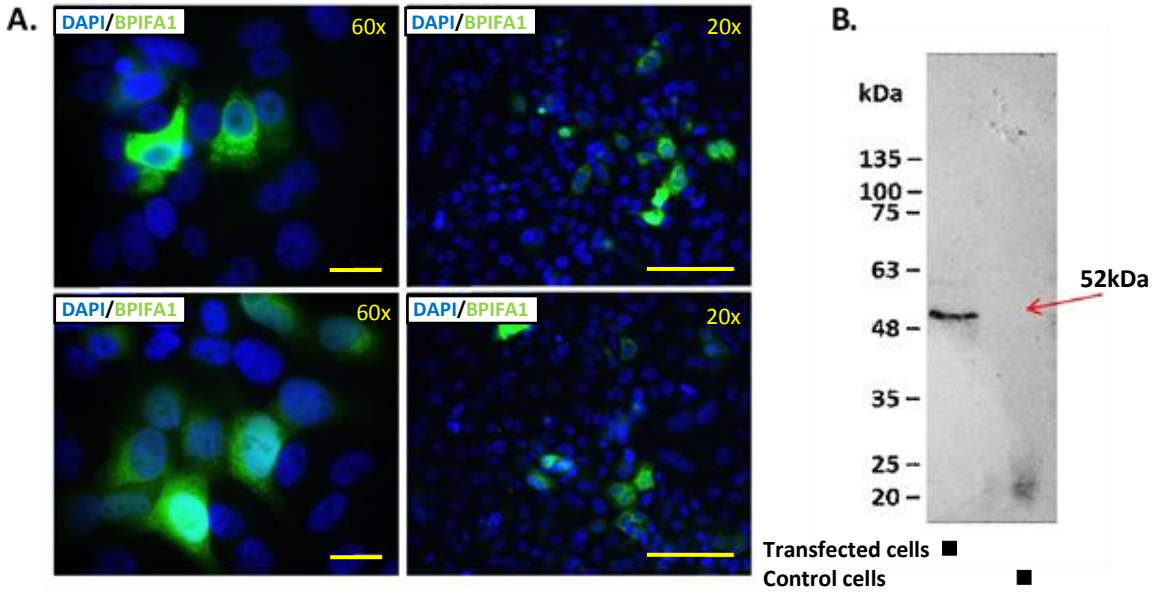

Figure 3.8: NCI-H292 cells transfected with FL-hBPIFA1/pcDNA3.1 construct.
Images taken of NCI-H292 cells indicated an unsuccessful establishment of stable cell line using G418 selection and isolation of single cell colonies. Negative cells are blue (nuclei counterstained with DAPI), whereas BPIFA1 positive cells are green (GFP fluorescence). Images were taken at 20x and 60x magnification using Olympus epifluorescence microscope (scale bar: 20x magnification - 100µm; 60x magnification - 20µm). Images were processed using ImageJ-win32 program **(A)**. Results of western blotting showed the production of FL-hBPIFA1-GFP (indicated by red arrow (~52kDa): 25 kDa BPIFA1 and 26.9kDa GFP tag) by transfected NCI-H292 cells. Production of protein was detected using anti-human BPIFA1 antibody **(B)**.

3.3.2.2 Cell sorting of FL-hBPIFA1-GFP positive cells

As isolation of positively transfected clones using G418 selection and serial dilutions methods was not efficient, I used cell sorting to enrich for hBPIFA1-GFP positive cells. A population of transfected cells was sorted into BPIFA1 positive and negative cells (Figure 3.9 A). Highly fluorescent cells were selected as BPIFA1 positive cells, accounting for approximately 20% of the cells from the cell population ($6x10^6$ cells were taken for sorting). BPIFA1-GFP positive and negative cells were seeded into different T75 flasks and grown until almost confluent. Isolation efficiency of BPIFA1-GFP positive cells was determined by fluorescence microscopy and data showed a highly efficient isolation of positive cells (Figure 3.9 B-C). Subsequently, the conditioned medium (serum containing and serum-free) samples from BPIFA1-GFP positive and negative cells were collected for protein secretion analysis. The western blotting membrane was probed with anti-human BPIFA1 antibody. The results demonstrated that a small quantity of protein was secreted by positive cells incubated in serum supplemented medium whereas no secretion of protein was observed by cells incubated in the serum-free conditions. BPIFA1-GFP was not detected in the conditioned medium samples collected from negative cells (Figure 3.9 D). On the basis of the above results, I concluded that pcDNA3.1-BPIFA1 construct was not useful for my work as using it I could not generate large amounts of secreted BPIFA1-GFP. Thus, I decided to change pcDNA3.1 vector system into of Flp-In™ System which is suggested to be highly effective in the generation of stable cell lines, constitutively expressing recombinant proteins (Invitrogen, 2010).

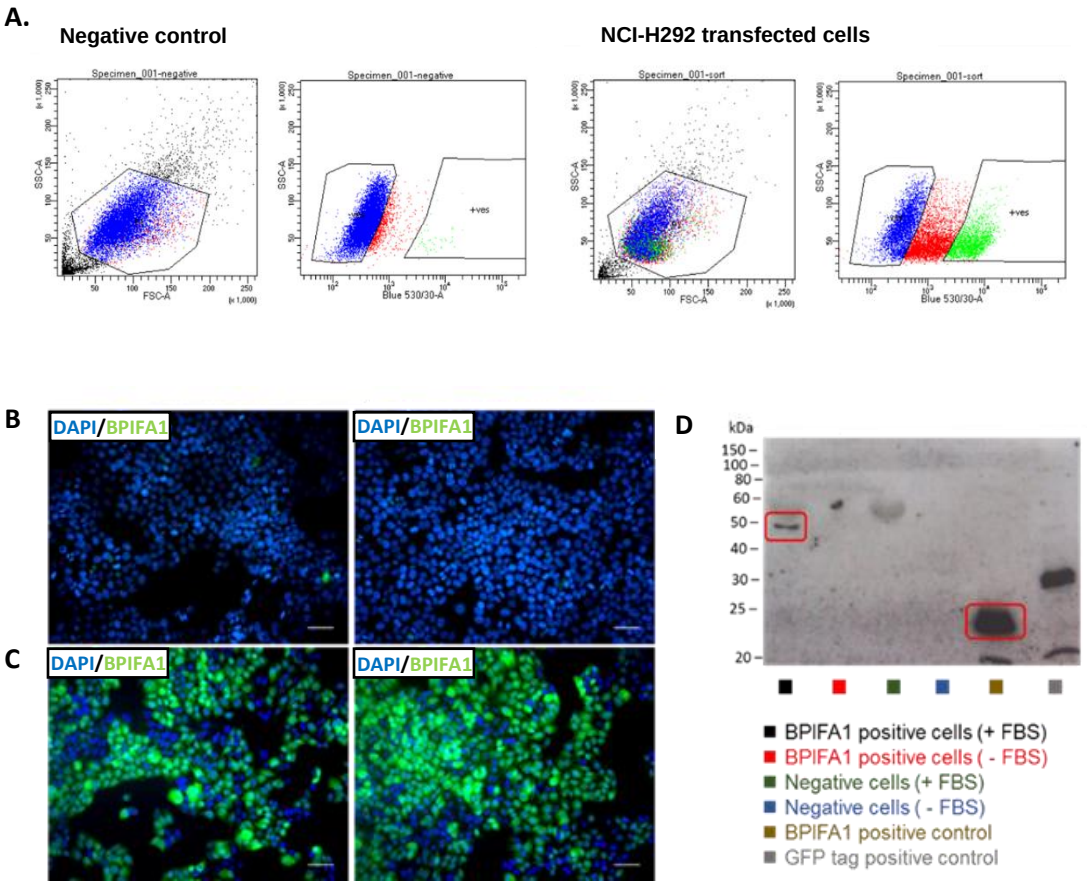

Figure 3.9: BPIFA1 expression and secretion by positively selected NCI-H292 cells.
A FL-hBPIFA1-GFP mixed cell population was sorted into BPIFA1-GFP positive and negative cells. Cells in the first field are blue and they represent negative cells. Cells in the second field are green and they are BPIFA1 positive cells. Black colour cells are debris, while red colour cells represent cell population which did not show high level of fluorescence. Approximately 1% of the negative control cells were auto-fluorescent **(A)**. BPIFA1-GFP positive cells (**B**: negative cells; **C**: BPIFA1-GFP positive cells). Images were taken at 20x magnification (scale bar: 100µm) using fluorescence microscope (Axioplan 2 Imaging, Zeiss). Images were processed using ImageJ-win32 program **(B-C)**. Secretion of FL-BPIFA1-GFP (~52 kDa size band (25kDa BPIFA1 and 26.9kDa GFP tag) – boxed in red) by positive cells incubated overnight in serum containing medium. Second band (~25kDa) circled in the red represents a positive control for BPIFA1. Other bands on the blot are a result of non-specific binding. Protein of interest was detected using anti-human BPIFA1 antibody **(D)**.

3.3.3 Human BPIFA1 and pcDNA5/FRT vector system

3.3.3.1 Generation of hBPIFA1 constructs into pcDNA5/FRT vector system

On the basis of the above data, I chose pcDNA5/FRT plasmid instead of pcDNA3.1, because it is highly effective in generation of stable cell lines expressing gene of interest. In this system a pcDNA5/FRT construct is integrated in the genome of a Flp-In™ System host cell line via an FRT site (Invitrogen, 2010). Consequently, usage of Flp-In™ System should provide effective and time efficient way for generation of stable cell lines. To generate GFP-tagged hBPIFA1-pcDNA5/FRT constructs, I subcloned full length (length: 256aa), F/R1 (length: 39aa), and F/R2 (length: 58aa) hBPIFA1-pcDNA3.1 constructs into pcDNA5/FRT vector system. All BPIFA1 constructs contain N-terminal region. F/R1 construct was designed to analyse the functional importance of the S18 region (G22-A39), whereas F/R2 construct was designed to study the importance of the leucine-glycine rich region. A schematic representation of the BPIFA1 constructs is shown in Figure 3.10 A-C.

A.

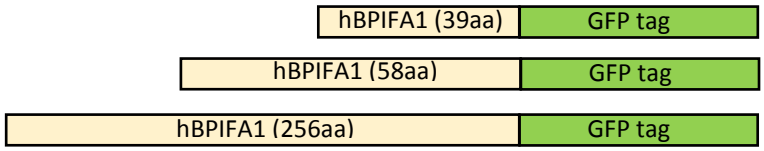

B.

```
>Human 39aa BPIFA1
MFQTGGLIVFYGLLAQTMAQFGGLPVPLDQTLPLNVNPA

>Human 58aa BPIFA1
MFQTGGLIVFYGLLAQTMAQFGGLPVPLDQTLPLNVNPALPLSPTGLAGSLTNALS
NG

>Human 256aa BPIFA1
MFQTGGLIVFYGLLAQTMAQFGGLPVPLDQTLPLNVNPALPLSPTGLAGSLTNALS
NGLLSGGLLGILENLPLLDILKPGGGTSGGLLGGLLGKVTSVIPGLNNIIDIKVTD
PQLLELGLVQSPDGHRLYVTIPLGIKLQVNTPLVGASLLRLAVKLDITAEILAVRD
KQERIHLVLGDCTHSPGSLQISLLDGLGPLPIQGLLDSLTGILNKVLPELVQGNVC
```

C.

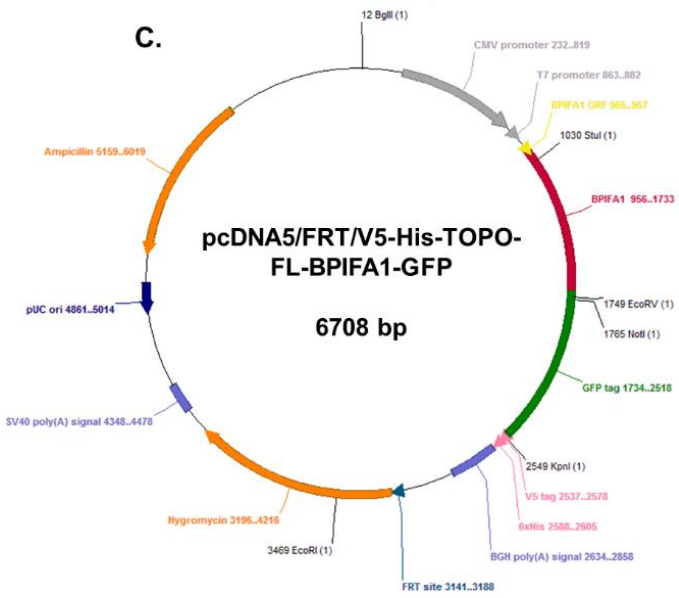

Figure 3.10: Generation of GFP-tagged hBPIFA1-pcDNA5/FRT constructs.
Figure shows a schematic diagram of series of different sizes hBPIFA1-GFP constructs (**A**). Protein sequences of hBPIFA1-GFP constructs (FL: 256aa; F/R1: 39aa; and F/R2: 58aa) are also shown in the FASTA format (**B**). Plasmid map of GFP-tagged hBPIFA1-GFP-pcDNA5/FRT construct is also represented (**C**). Plasmid map was generated using a plasmid editor program ApE (Version 8.5.2.0).

To prepare hBPIFA1 constructs for cloning into pcDNA5/FRT system, *E. coli* cells were transformed with DNA of BPIFA1-pcDNA3.1 constructs and miniprepped. Minipreps were digested with HindIII and BamHI to verify the quality of DNA products. Restriction

digest products were visualised on an agarose gel. Digestion of FL-BPIFA1 was expected to produce three fragments when cut with HindIII (207bp, 795bp and ~6kb) and BamHI (557bp, 826bp, and ~6kb), whereas the restriction digest of F/R1-BPIFA1 was expected to produce two fragments (HindIII: 355bp and ~6kb; BamHI: 736bp and ~6kb). Digestion of F/R2-BPIFA1 with HindIII and BamHI was also expected to produce two fragments (HindIII: 207bp and ~6kb; BamHI: 776bp and ~6kb). All fragments of the correct sizes were detected (Figure 3.11).

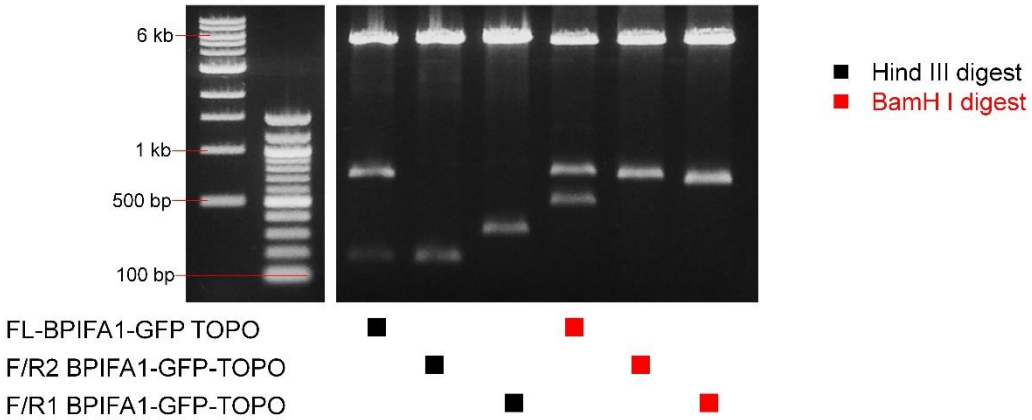

Figure 3.11: Restriction digests of GFP-tagged hBPIFA1/pcDNA3.1 constructs.
Restriction digests of all hBPIFA1-GFP-TOPO constructs suggested that human BPIFA1 was inserted in the forward orientation for the gene to be transcribed and translated into the protein as the fragments of expected sizes were observed.

Subsequently, all constructs were sent for Sanger sequencing to verify the orientation of the insert and scan for any possible mutations. The FL-hBPIFA1 construct was sequenced from forward and reverse direction (to ensure that all required sequence was read through), whereas the smaller hBPIFA1 constructs (F/R1 and F/R2) were sequenced only from forward direction. Results showed no mutations in hBPIFA1-GFP sequences and that all sequences read through into the GFP tag (Appendix II: S1-S3).

3.3.3.2 Cloning hBPIFA1-GFP constructs into pcDNA5/FRT

To prepare DNA of BPIFA1 constructs for cloning, the coding region of FL-, F/R1-, and F/R2-BPIFA1-GFP constructs was amplified using primers flanking the CT-GFP-TOPO

cloning site. This showed successful amplification of hBPIFA1-GFP constructs as fragments of approx. 1.5 kb and 1 kb sizes were observed (Figure 3.12).

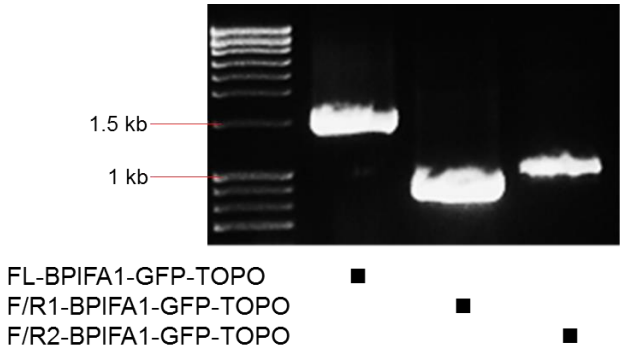

Figure 3.12: Amplification of the coding region of hBPIFA1-GFP constructs with PCR. Fragment of approx. 1.5kb size represents FL-BPIFA1 construct, whereas fragments of approx. 1kb size represents F/R1- and F/R2-BPIFA1 constructs.

Subsequently, PCR products were cloned into pcDNA5/FRT vector system to generate FL-, F/R1-, and F/R2-BPIFA1-GFP expression plasmids. Minipreps were digested with NcoI to verify the orientation of the insert. Restriction digests were expected to produce four fragments as following (if inserts were the correct way round):

FL-BPIFA1 – 4740bp, 1608bp, 938bp, and 416bp;

F/R1-BPIFA1 – 3740bp, 1608bp, 416bp, and 290bp;

F/R2-BPIFA1 – 3740bp, 1608bp, 416bp, and 347bp.

Fragments of the expected sizes were detected (Figure 3.13 A-B), suggesting the insertion of gene in the forward orientation in some minipreps and allowing it to be transcribed and translated into the protein.

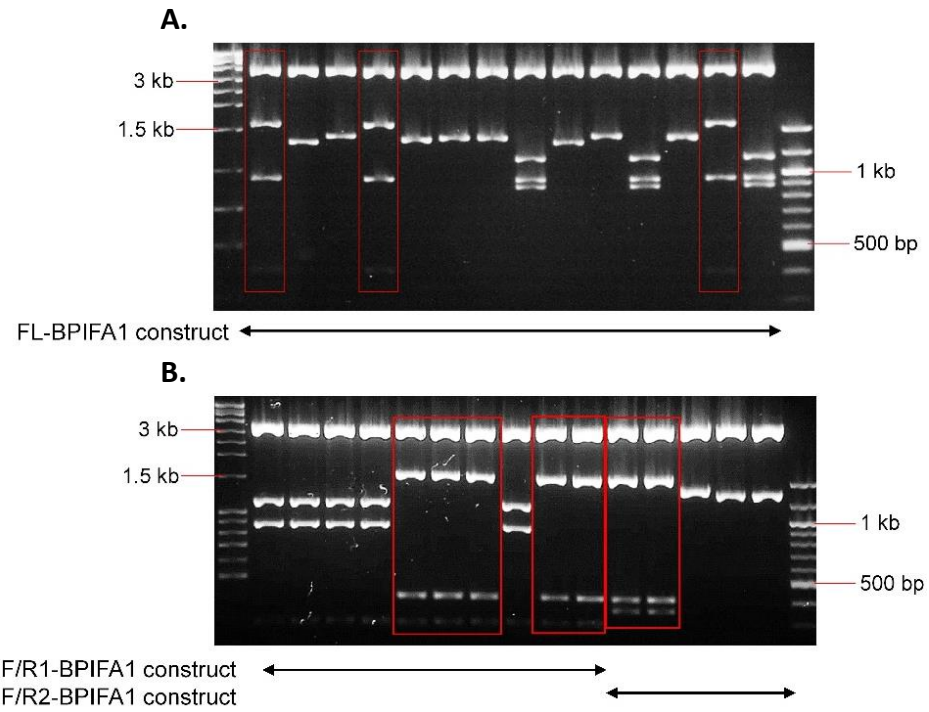

Figure 3.13: Restriction digests of GFP tagged hBPIFA1-pcDNA5/FRT constructs.
Results of GFP-tagged FL- (**A**), F/R1- (**B**), and F/R2-hBPIFA1-pcDNA5/FRT (**B**) restriction digestion. Fragments of correct sizes are highlighted in red rectangles.

All constructs were sent for sequencing to validate the orientation of insert and to scan for any possible mutations. Results showed no mutations in hBPIFA1-GFP sequences and all sequences read through into the GFP tag (Appendix: S4-S6).

3.3.3.3 Transfected Flp-In-CHO cells did not secrete hBPIFA1-GFP proteins

For transfection assays, I used Flp-In-CHO cell line which contains an integrated FRT site for establishing gene expression from a Flp-In™ System expression vector. I produced maxipreps of all hBPIFA1-pcDNA5/FRT constructs and used them in co-transfections of CHO cells with pOG44 expression plasmid (Appendix II: S7). Co-transfections were performed using Lipofectamine® and the following day medium containing hygromycin B was added to the cells to select positive transfectants. After establishment of stable cell lines, cell samples were analysed using fluorescence microscopy and data showed that selection of positive cells with hygromycin B was not successful as only a small number of BPIFA1-GFP positive cells were observed. It

meant that stable cell lines consisted of BPIFA1 positive and negative cells, and cells that expressed low levels of the GFP fusion protein (Figure 3.14).

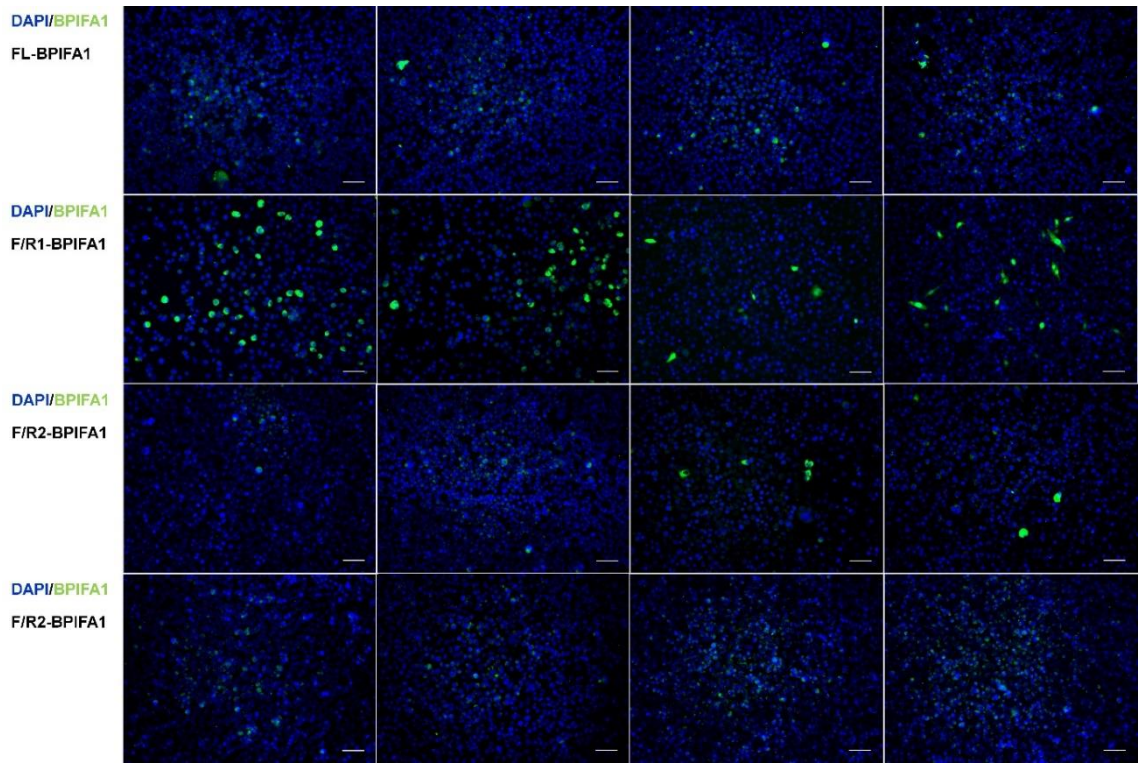

Figure 3.14: CHO cells transfected with GFP-tagged hBPIFA1-pcDNA5/FRT constructs after selection with hygromycin B.
Images showed unsuccessful establishment of stable cell-lines expressing BPIFA1 as only a small number of BPIFA1-GFP positive cells were observed. Scale bar: 100µm.

Since I could observe some GFP positive cells in the stable cell lines, I decided to find out whether integration of BPIFA1-pcDNA5/FRT DNA into the genome of the CHO cells had occurred and whether proteins were produced and secreted by the cells. Genomic DNA was amplified using PCR and the results showed that transfection of CHO cells was successful as genomic DNA of hBPIFA1-GFP constructs was detected (Figure 3.15).

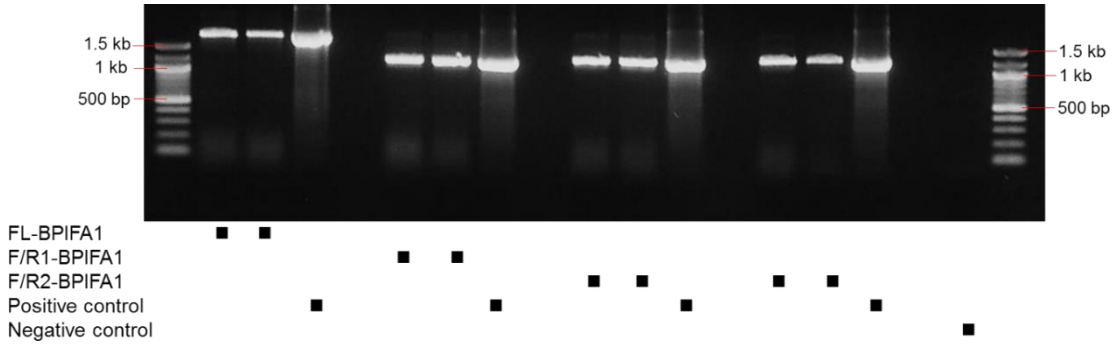

Figure 3.15: Genomic DNA analysis of CHO cells transfected with GFP-tagged hBPIFA1-pcDNA5/FRT constructs.
PCR results, showing a successful integration of GFP-tagged hBPIFA1-plasmid DNA into the genome of CHO cells. Plasmid DNA of all hBPIFA1 constructs was used as positive control. Negative control was used to verify quality of PCR reaction regarding any possible contamination.

Western blotting probed with anti-GFP tag antibody for detection of BPIFA1 proteins appeared to show that BPIFA1-GFP recombinant proteins were produced by CHO cells in small amounts but none of the proteins were secreted into the media (Figure 3.16 A-D). Full-length and F/R2-BPIFA1-GFP proteins were produced in smaller quantities compared to the production of F/R1-BPIFA1-GFP ($8x10^5$ cells were used for analysis).

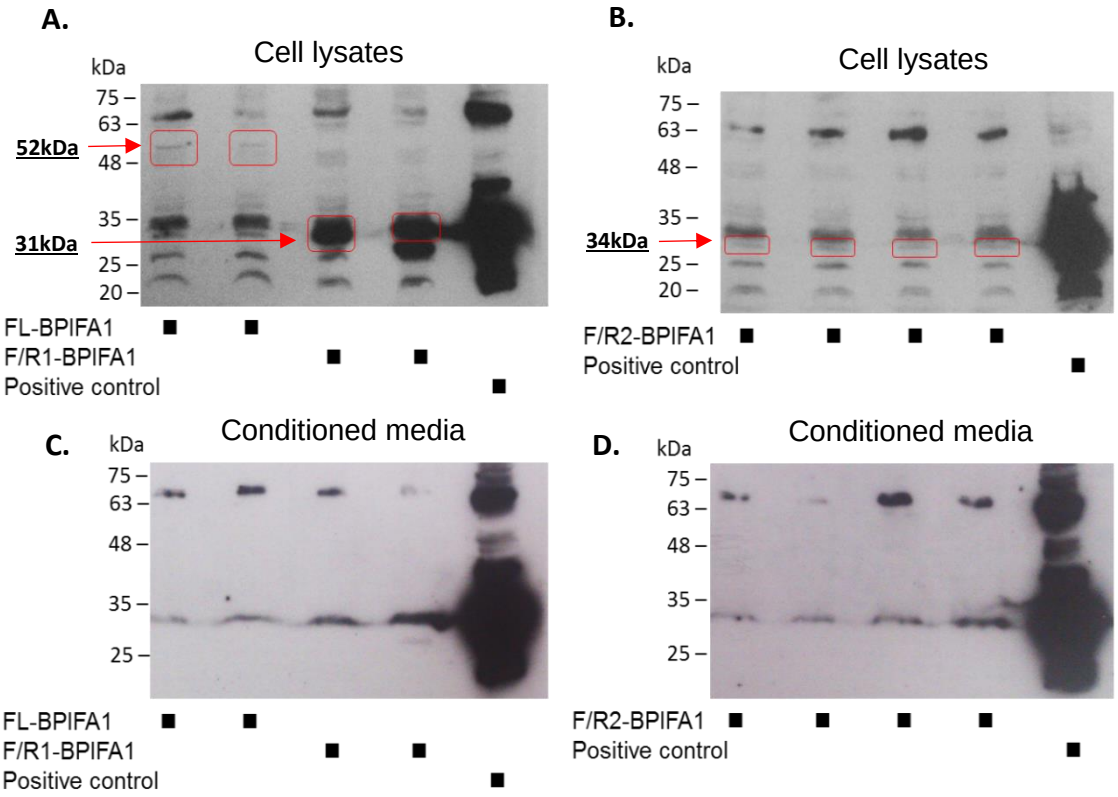

Figure 3.16: Analysis of FL-, F/R1, and F/R2-BPIFA1-GFP production and secretion. Western blotting results, showing FL-hBPIFA1-GFP (~52kDa size: FL-BPIFA1 25kDa and GFP tag 26.9kDa) (**A**) and F/R2-hBPIFA1-GFP (~34kDa size: F/R2-hBPIFA1 ~7kDa and GFP tag 26.9kDa) (**B**) production in smaller quantities compared to the production of F/R1-BPIFA1-GFP (~31kDa size: F/R1-hBPIFA1 ~4kDa and GFP tag 26.9kDa) (**A**). Secretion of hBPIFA1 proteins was not observed (**C**-**D**). Positive control (GFP tag positive sample: 26.9 kDa) was used for western blot quality verification. Western blots were probed with anti-GFP tag antibody. Production of proteins is highlighted in red boxes. Other bands on the blots are a result of non-specific binding. Data is representative of results from two independent transfection experiments (n=2).

This data suggested that this method was for some reason not suitable for my uses as stable cell lines did not secret hBPIFA1-GFP proteins. Therefore, I decided to use a different vector system and I chose the mammalian expression VR1255 plasmid for my future experiments. I also speculated that GFP tag may have caused a negative effect on BPIFA1 production and secretion, consequently I decided to change it into smaller tag (FLAG tag) to eliminate possibilities of protein misfolding and degradation.

3.3.4 BPIFA1 and VR1255 vector system

3.3.4.1 Production of VR1255 DNA for the cloning reactions

The mammalian expression vector VR1255 (Figure 3.17), was previously used for the production and secretion of recombinant proteins (Jayawardane et al., 2008). VR1255 was originally developed as a DNA vaccine delivery vector (Hartikka et al., 1996). However, it is widely used for *in vitro* experiments aiming to generate large quantities of recombinant proteins (Hartikka et al., 1996, Norman et al., 1997).

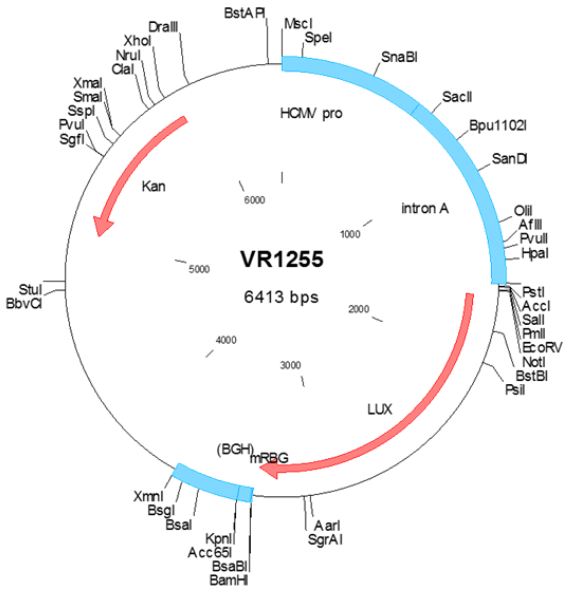

Figure 3.17: Map of mammalian VR1255 plasmid.

VR1255 DNA was transformed into *E. coli* and maxipreparation was carried out. The plasmid was digested with NotI and BamHI to generate a linear DNA for the cloning reactions. The expected 1652bp and 4761bp bands were detected (Figure 3.18 A) and the linearised VR1255 DNA fragment of 4761bp size was recovered from the gel. The quality of DNA was verified using agarose gel electrophoresis (Figure 3.18 B).

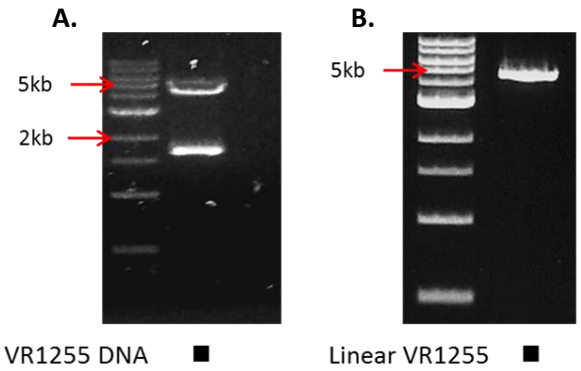

Figure 3.18: Production of VR1255 DNA for the cloning reactions.
VR1255 maxiprep was digested with NotI and BamHI and fragments of correct sizes were observed (1652bp and 4761bp) (**A**). DNA fragment of 4761bp size was recovered from the agarose gel and quality of plasmid DNA was tested using agarose gel electrophoresis (**B**).

3.3.4.2 Generation of human FLAG-tagged S18 deletion BPIFA1-VR1255

DNA sequence of the FLAG-tagged S18 deletion *Bpifa1* construct was synthesised by GeneArt™ Gene Synthesis service. S18 deletion BPIFA1 missing amino acids 22-42 of BPIFA1 with a C-terminal FLAG tag (Figure 3.19) was used to investigate the importance of S18 region for the protein's bacterial binding properties.

```
>Human full-length hBPIFA1
MFQTGGLIVFYGLLAQTMAQFGGLPVPLDQTLPLNVNPALPLSPTGLAGSLTNALSNGLLSG
GLLGILENLPLLDILKPGGGTSGGLLGGLLGKVTSVIPGLNNIIDIKVTDPQLLELGLVQSP
DGHRLYVTIPLGIKLQVNTPLVGASLLRLAVKLDITAEILAVRDKQERIHLVLGDCTHSPGS
LQISLLDGLGPLPIQGLLDSLTGILNKVLPELVQGNVCPLVNEVLRGLDITLVHDIVNMLIH
GLQFVIKV
```

Figure 3.19: Human S18 deletion BPIFA1.
The part of full-length BPIFA1 highlighted in the red indicates a region of protein which was deleted to generate S18 deletion BPIFA1.

This was transformed into *E. coli* and the DNA was purified and digested with NotI and BglII to enable recovery of the fragment (773bp) from an agarose gel (Figure 3.20 A) The quality of recovered BPIFA1 construct DNA was verified by gel electrophoresis (Figure 3.20 B).

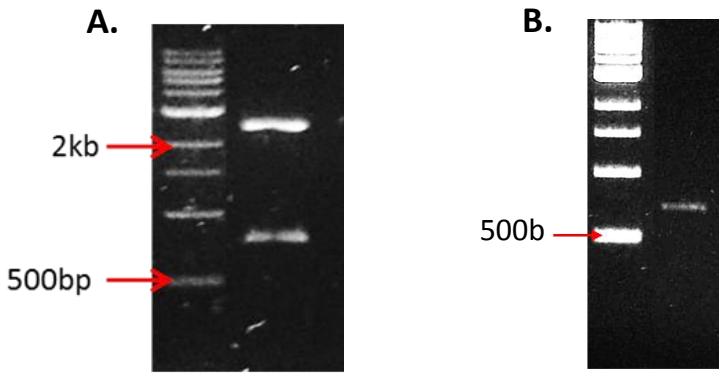

Figure 3.20: Restriction digestion of FLAG-tagged S18 deletion BPIFA1-pMA-T DNA and recovery of S18 deletion BPIFA1-FLAG DNA from agarose gel.
Miniprep of S18 deletion BPIFA1-pMA-T construct was digested with restriction endonucleases to enable a recovery of construct DNA. Fragments of correct sizes were observed (773bp and 2361bp) (**A**). DNA of interest (773bp) was recovered from agarose gel and its quality was verified (**B**).

The recovered DNA of S18 deletion BPIFA1-FLAG was used in the ligation reactions with linear VR1255 vector (digested with BamHI and NotI) to generate a S18 deletion BPIFA1-VR1255 construct. Following ligation reaction, *E. coli* cells were transformed and miniprepped. The minipreps were verified using EcoRV and KpnI, and BamHI and XbaI digestions. Results showed the expected sizes of DNA fragments (EcoRV and KpnI: 818bp and 4644bp; BamHI and XbaI: 315bp and 5147bp), suggesting that a FLAG-tagged S18 deletion BPIFA1-VR1255 construct was generated (Figure 3.21).

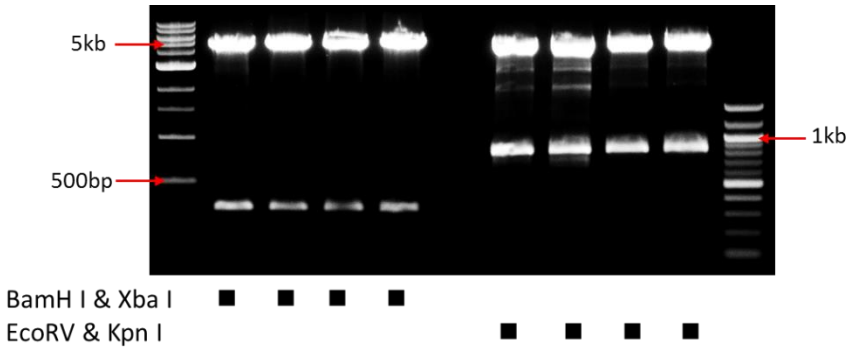

Figure 3.21: Restriction digestion of FLAG-tagged S18 deletion BPIFA1-VR1255 DNA.
Fragments of interest (BamHI and XbaI: 315bp and 5147bp; EcoRV and KpnI: 818bp and 4644bp) were observed, meaning that S18 deletion BPIFA1-FLAG DNA was successfully ligated with linear VR1255 DNA.

The DNA was sent for sequencing to verify the orientation of the insert and scan for any possible mutations. No mutations were found and the sequence read-through into the FLAG tag. Subsequently, a maxiprep was performed and digested to verify the quality of DNA: 1) BamHI; 2) KpnI and BamHI; 3) EcoRV and KpnI. Results confirmed DNA fragments of the correct sizes (BamHI: 5462bp; KpnI and BamHI: 349bp and 5113bp; EcoRV and KpnI: 818bp and 4644bp) (Figure 3.22).

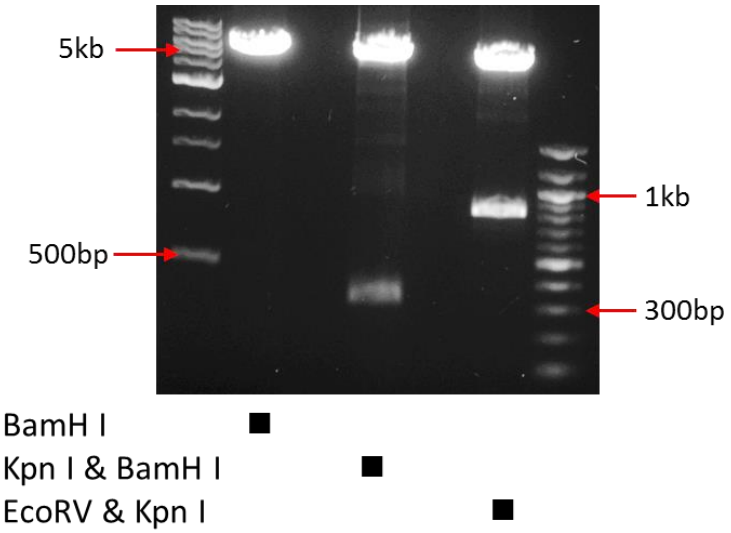

Figure 3.22: Restriction digestion of FLAG-tagged S18 deletion BPIFA1-VR1255 maxiprep. Fragments of interest (BamHI: 5462bp; KpnI and BamHI: 349bp and 5113bp; EcoRV and KpnI: 818bp and 4644bp) were observed meaning that quality of maxiprep sample was good.

3.3.4.3 Preparation of human FLAG-tagged full-length and cysteine mutant BPIFA1-VR1255 constructs for transfection assays

To examine the importance of the disulphide bond for hBPIFA1's functions, I used a cysteine mutant hBPIFA1-FLAG. This mutant BPIFA1 has cysteine 224 residue mutated into glycine, meaning that protein does not contain disulphide bond (Figure 3.23). A single base pair mutation was used to make this change in which original T nucleotide (741) was mutated into G nucleotide.

>Human cysteine mutant BPIFA1
MFQTGGLIVFYGLLAQTMAQFGGLPVPLDQTLPLNVNPALPLSPTGLAGSLTNALSNGLLSG
GLLGILENLPLLDILKPGGGTSGGLLGGLLGKVTSVIPGLNNIIDIKVTDPQLLELGLVQSP
DGHRLYVTIPLGIKLQVNTPLVGASLLRLAVKLDITAEILAVRDKQERIHLVLGDCTHSPGS
LQISLLDGLGPLPIQGLLDSLTGILNKVLPELVQGNVGPLVNEVLRGLDITLVHDIVNMLIH
GLQFVIKV

Figure 3.23: Human cysteine mutant BPIFA1.
Glycine amino acid is highlighted in the red colour and it represents a location where single nucleotide mutation was done, leading to the replacement of cysteine residue by glycine residue.

To prepare the FLAG-tagged cysteine mutant and full-length hBPIFA1-VR1255 constructs for transfection assays, I transformed *E. coli* cells with DNA of constructs and digested them with NotI and BamHI. The results showed fragments of the correct sizes (534bp and 5879bp) (Figure 3.24 A). Subsequently, both constructs were maxiprepped and these were digested with NotI and BamHI. DNA fragments of the expected sizes were detected (Figure 3.24 B).

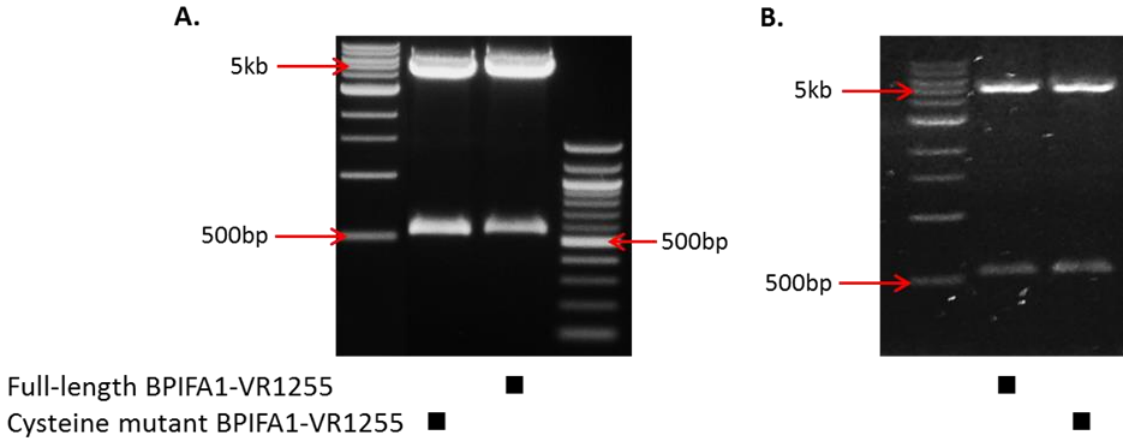

Figure 3.24: Restriction digestion of FLAG-tagged full-length and cysteine mutant hBPIFA1-VR1255 construct DNA.
Miniprep samples (**A**) and maxiprep samples (**B**) of FLAG-tagged full-length and cysteine mutant hBPIFA1-VR1255 were digested with NotI and BamHI to verify a quality of product. Restriction digests were run on agarose gel and fragments of correct sizes were observed (534bp and 5879bp).

3.3.4.4 DNA amplification of mouse BPIFA1 and cloning into pCRII-TOPO

I also generated FLAG-tagged mBPIFA1-VR1255 construct. cDNA from WT mTECs was used for amplification of mBPIFA1 DNA. The primer pair used in PCR contained BamHI and NotI restriction sites for ligation into VR1255 (digested with BamHI and NotI). The reverse primer also encoded a FLAG tag to enable generation of a FLAG-tagged

mBPIFA1 construct. After PCR amplification, the DNA fragment was visualised (Figure 3.25 A) and cloned into pCRII-TOPO. DNA was miniprepped and digested with BamHI and NotI. Five (of six) contained DNA fragments of the correct size (41, 46, 878, and 3897bp). Fragments of 41 and 46bp were impossible to observe, therefore, cloning was verified by detecting fragments of 878bp and 3897bp sizes (Figure 3.25 B).

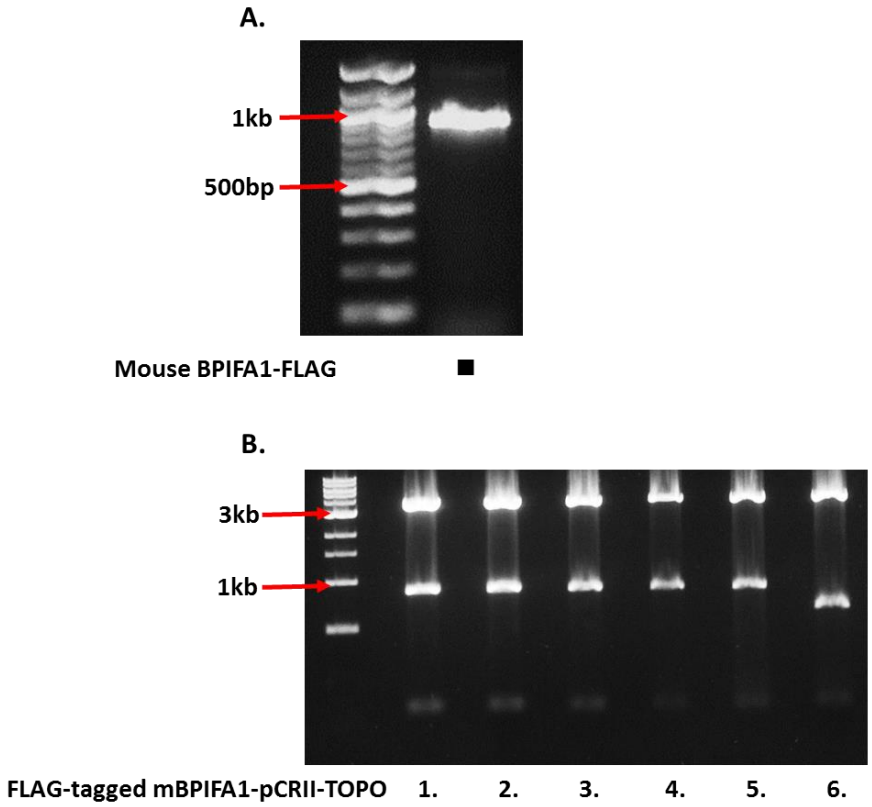

Figure 3.25: Amplification and cloning of mouse BPIFA1 into pCRII-TOPO.
Mouse BPIFA1 DNA was amplified (**A**) and cloned into pCRII-TOPO. Five (1-5) clones contained DNA fragments of correct sizes (878 and 3897bp), following digestion with BamHI and NotI (**B**).

3.3.4.5 Ligation of mBPIFA1-FLAG with VR1255

DNA fragments of mBPIFA1-FLAG (878bp) (samples 1-5; Figure 3.25) were extracted and verified using gel electrophoresis (Figure 3.26). DNA of linear VR1255 vector (digested with BamHI and NotI) was run on the same gel (Figure 3.26). This enabled determination of VR1255 and mBPIFA1 DNA concentrations which were important to define for the ligation reactions.

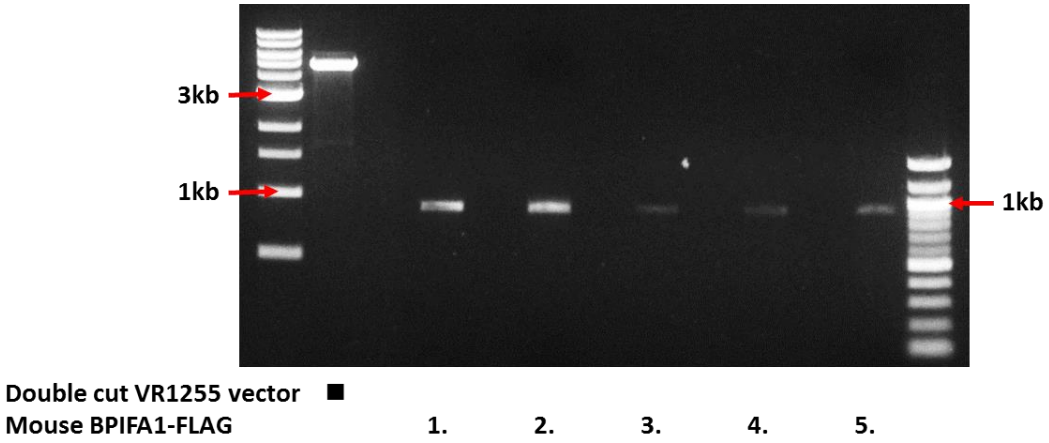

Figure 3.26: Extracted DNA of mouse BPIFA1-FLAG and double cut VR1255 vector.
Results show double cut vector DNA (BamHI and NotI digested) and mBPIFA1-FLAG DNA samples. Samples 1 and 2 were used for ligation reactions.

Ligation reactions of mBPIFA1-FLAG DNA with VR1255 vector were performed at ratios of 1:1, 1:3, and 3:1. Subsequently, DNA was extracted and digested with EcoRV and KpnI or HindIII to verify successful cloning. Detection of the correct size DNA fragments (HindIII: 2153 and 3438bp; EcoRV and KpnI: 947 and 4644bp) confirmed that mBPIFA1-FLAG was present in four samples (Figure 3.27).

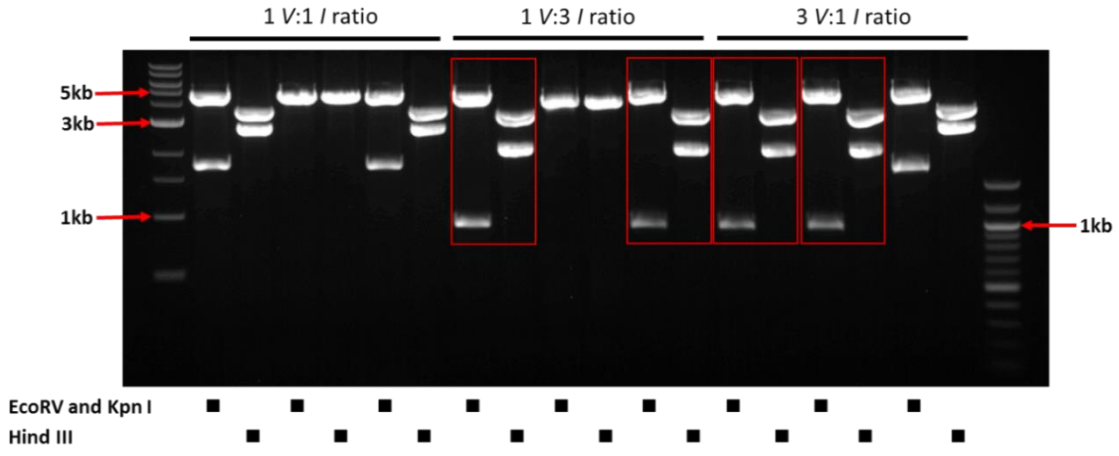

Figure 3.27: Verification of mouse BPIFA1-FLAG in VR1255.
Mouse BPIFA1-FLAG DNA was present in four samples of extracted plasmid DNA (highlighted in red rectangles), whereas other five samples of extracted plasmid did not contain DNA of interest. Abbreviations: V – vector, I – insert.

3.3.4.6 Preparation of FLAG-tagged mBPIFA1-VR1255 for transfection assays

DNA samples were sequenced to validate the orientation of insert and scan for any possible mutations. Subsequently, a validated construct was maxiprepped to produce DNA for use in transfection assays.

3.3.4.7 Production and secretion BPIFA1-FLAG recombinant proteins

Transient transfections of HEK293T cells were performed with DNA of FLAG-tagged human and mouse BPIFA1-VR1255 constructs to generate recombinant proteins. Initially, I undertook a small-scale transfection (24-well plate) of HEK293T cells with DNA of all human FLAG-tagged BPIFA1-VR1255 constructs to determine which proteins would be produced and secreted. Cell lysates and conditioned media were collected and examined by SDS-PAGE analysis. Blots were probed with anti-FLAG tag antibody for detection of proteins. All BPIFA1-FLAG recombinant proteins were produced and secreted into the serum supplemented media (Figure 3.28 A-B).

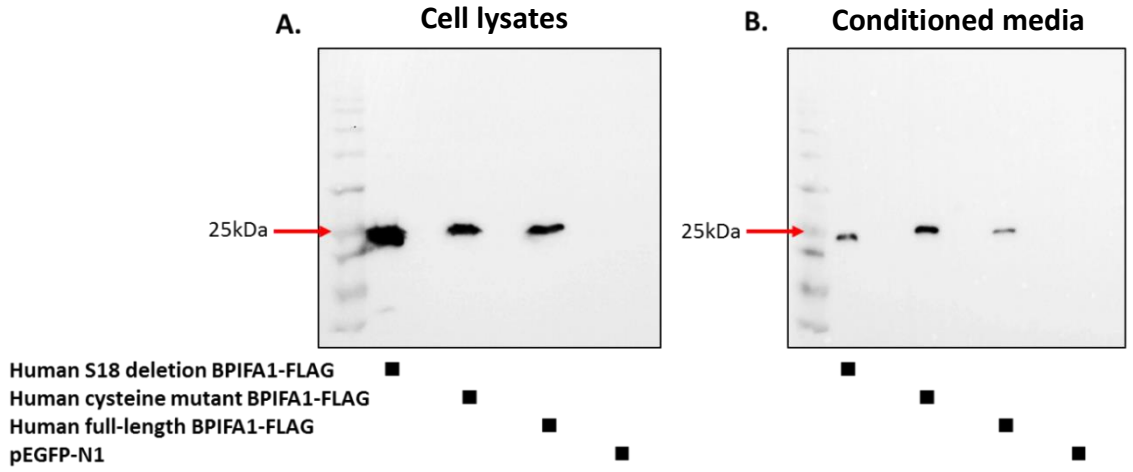

Figure 3.28: Small-scale transfection of HEK293T cells with human FLAG-tagged BPIFA1-VR1255 constructs.
Production of all BPIFA1-FLAG recombinant proteins by transfected HEK293T cells was detected (**A**) as was a secretion of proteins into the serum supplemented media (**B**). Full-length and cysteine mutant BPIFA1 proteins: approximately 25.9kDa; S18 deletion BPIFA1: approximately 23.7kDa. Cells transfected with pEGFP-N1 vector only were used as transfection efficiency control. Western blots were probed with anti-FLAG tag antibody.

Next, large-scale transfections of HEK293T cells were performed to generate large quantities of secreted BPIFA1 proteins. Cell lysate and conditioned media samples were collected and analysed by SDS-PAGE as before. Again, all BPIFA1-FLAG recombinant proteins were produced and secreted (Figure 3.29 A-D). However, the secretion of proteins was lower in serum-free cell culture conditions compared to serum supplemented cell culture conditions. The levels of proteins were also variable in samples collected on different days.

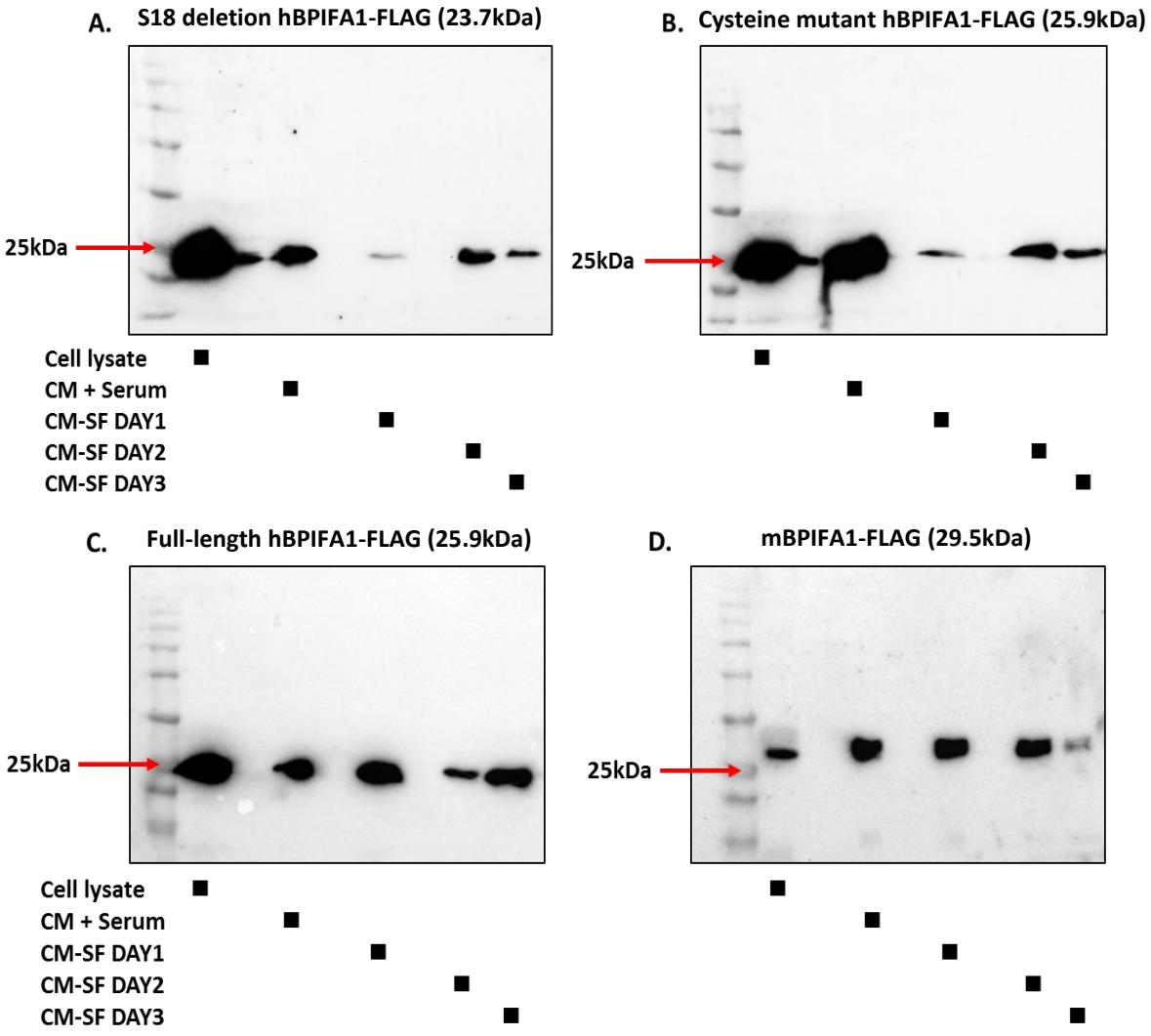

Figure 3.29: Large-scale transfections of HEK293T cells with FLAG-tagged human and mouse BPIFA1-VR1255 constructs.
Production and secretion of human S18 deletion (**A**), cysteine mutant (**B**), and full-length (**C**) BPIFA1-FLAG recombinant proteins by transfected HEK293T cells were detected as were the production and secretion of mouse BPIFA1-FLAG recombinant protein (**D**). Full-length and cysteine mutant BPIFA1-FLAG: ~25.9kDa; S18 deletion BPIFA1-FLAG: ~23.7kDa; and mouse BPIFA1-FLAG: ~29.5kDa. Abbreviations: CM – conditioned medium, and SF – serum free. Western blots were probed with anti-FLAG tag antibody.

3.3.4.8 Observation of BPIFA1-FLAG proteins in NCI-H292 cells

To visualise human and mouse BPIFA1-FLAG proteins in cells, the NCI-H292 cell line was chosen as they grow as a monolayer of cells and enable high quality imaging. NCI-H292 cells were transfected with DNA and stained for immunofluorescence imaging. Anti-FLAG tag primary antibody was used for detection of BPIFA1-FLAG proteins and detected with an Alexa Flour 488 secondary antibody, which stained proteins green. Data appear to show some difference between full-length BPIFA1 proteins and mutant BPIFA1 proteins. Some transfected cells were observed to contain highly fluorescent granules and it appeared that cells transfected with mutant hBPIFA1 contained more of such cells compared to the cells transfected with full-length BPIFA1 (Figure 3.30 A-D). This experiment was performed twice, and similar results were obtained on the both occasions (Appendix II: S8).

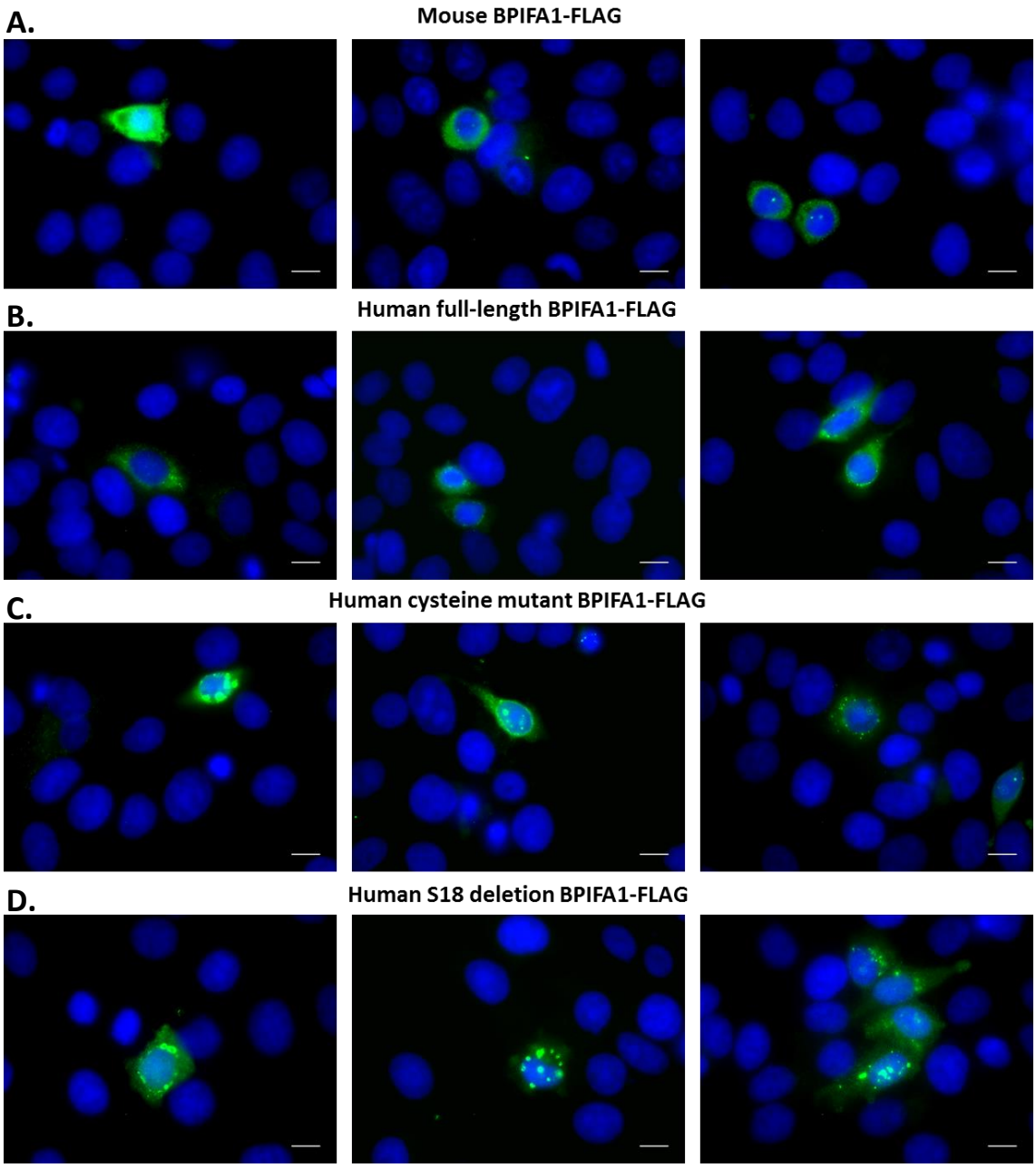

Figure 3.30: Detection of human and mouse FLAG-tagged proteins in NCI-H292 cells.
Images were taken at 100x magnification with immunofluorescence microscope (Zeiss Axioplan 2) (scale bar: 10µm). Nuclei of transfected NCI-H292 cells were stained by DAPI in blue and BPIFA1-FLAG proteins of interest (**A**: mBPIFA1-FLAG; **B**: FL-hBPIFA1-FLAG; **C**: cysteine mutant hBPIFA1-FLAG; **D**: S18 deletion hBPIFA1-FLAG) were stained in green using Alexa Flour 488. Images were processed using ImageJ-win32 program. Data is representative of results from two independent experiments (n=2).

Subsequently, more detailed analysis was performed by analysing 10 imaged fields per well of transfected cells. The total number of cells per field were counted as well as the number of transfected cells positive and negative for fluorescent granules. This analysis

suggested that cells transfected with cysteine mutant hBPIFA1-FLAG and S18 deletion hBPIFA1-FLAG contained over 5x more cells with fluorescent granules than cells transfected with full-length human and mouse BPIFA1-FLAG (Table 3.3).

Table 3.3: Percentages of transfected cells with and without fluorescent granules

NCI-H292 cells transfected with BPIFA1 construct	Average % of cells with fluorescent granules	Average % of cells without fluorescent granules	Ratio of cells with granules vs cells without granules
FL-hBPIFA1-FLAG	7.8%	4.2%	1.9 : 1
mBPIFA1-FLAG	5.4%	5.9%	0.9 : 1
Cysteine mutant hBPIFA1-FLAG	13.8%	2%	6.9 : 1
S18 deletion hBPIFA1-FLAG	19.3%	1%	19.3 : 1

3.3.4.9 Purification of FLAG-tagged BPIFA1 proteins secreted by transfected HEK293T cells

I aimed to purify BPIFA1-FLAG proteins from serum-free conditioned media for bacterial pull-down assays. Anti-FLAG® M2 affinity gel beads were used for purification of BPIFA1-FLAG proteins from serum-free conditioned media. After purification, samples of purified proteins, beads, and conditioned media were collected for SDS-PAGE analysis and membranes were probed with anti-FLAG tag antibody. All BPIFA1-FLAG proteins were isolated, but purification efficiency was low (Figure 3.31 A-D). Full-length human and mouse BPIFA1-FLAG proteins were still detected in the conditioned media after purification. Additionally, proteins were detected on the beads after elution, suggesting that elution of proteins from anti-FLAG® M2 affinity gel beads was not highly effective (Figure 3.31 A-D).

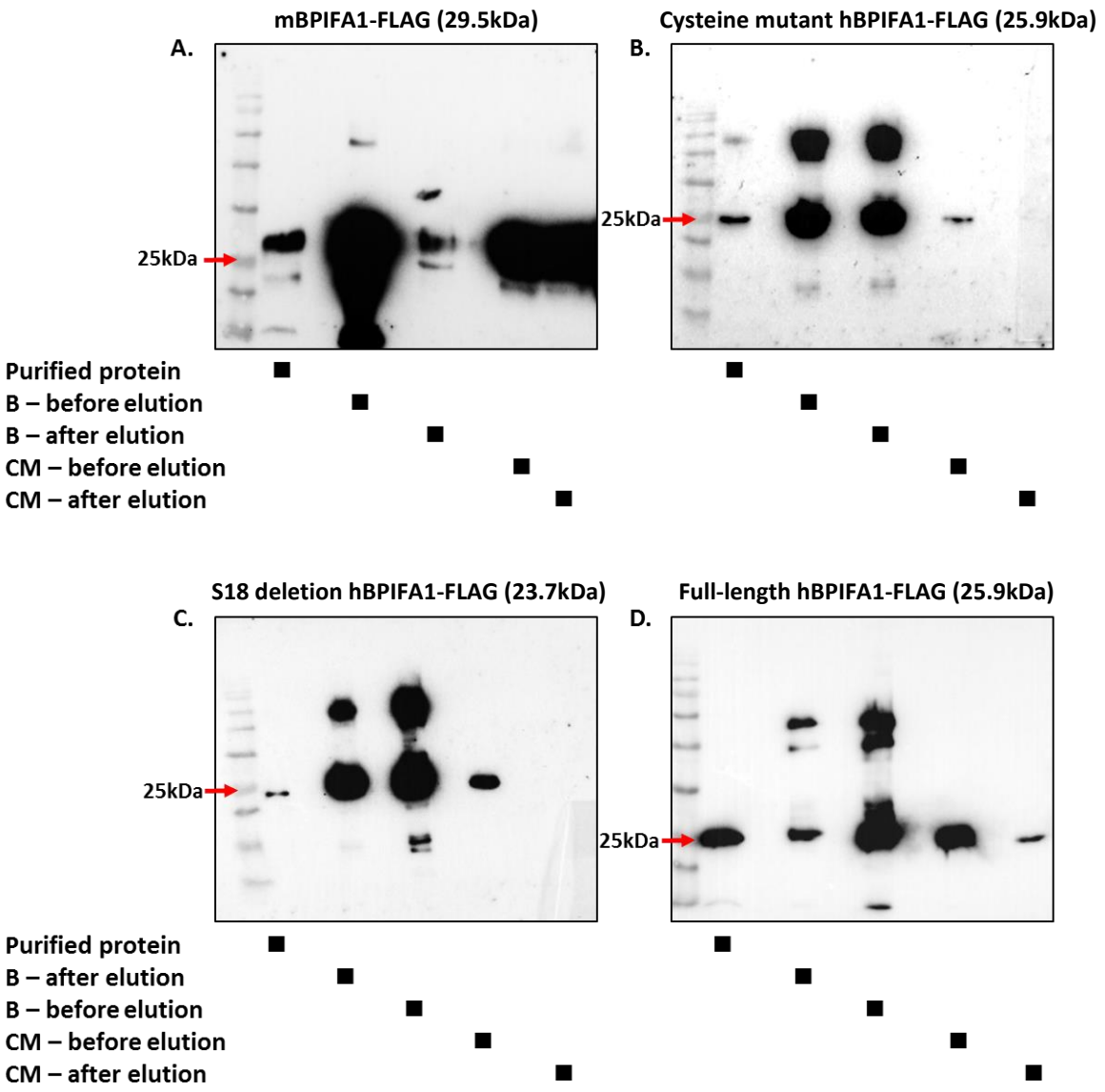

Figure 3.31: Purification of BPIFA1-FLAG from the serum-free conditioned medium samples.
Mouse (**A**), human cysteine mutant (**B**), human S18 deletion (**C**) and human full-length (**D**) BPIFA1-FLAG recombinant proteins were purified from serum-free conditioned media. All membranes were exposed for the appropriate period of time for visualisation (mouse BPIFA1-FLAG: 3 minutes; human cysteine mutant BPIFA1-FLAG: 20 minutes; human S18 deletion BPIFA1-FLAG: 20 minutes; and human full-length BPIFA1-FLAG: 30 seconds). Full-length and cysteine mutant BPIFA1-FLAG: ~25.9kDa; S18 deletion BPIFA1-FLAG: ~23.7kDa; and mouse BPIFA1-FLAG: ~29.5kDa. Western blots were probed with anti-FLAG tag antibody. Abbreviations: B – beads; CM – conditioned medium. Additional fragments observed on SDS-PAGE membranes may be associated with non-specific binding of anti-FLAG tag antibody.

Amounts of purified BPIFA1-FLAG proteins were compared using SDS-PAGE. The same volume of each purified protein was used for analysis. Results suggested that amounts of human cysteine mutant and S18 deletion BPIFA1-FLAG purified proteins

were markedly lower compared to mouse and human full-length BPIFA1-FLAG proteins (Figure 3.32).

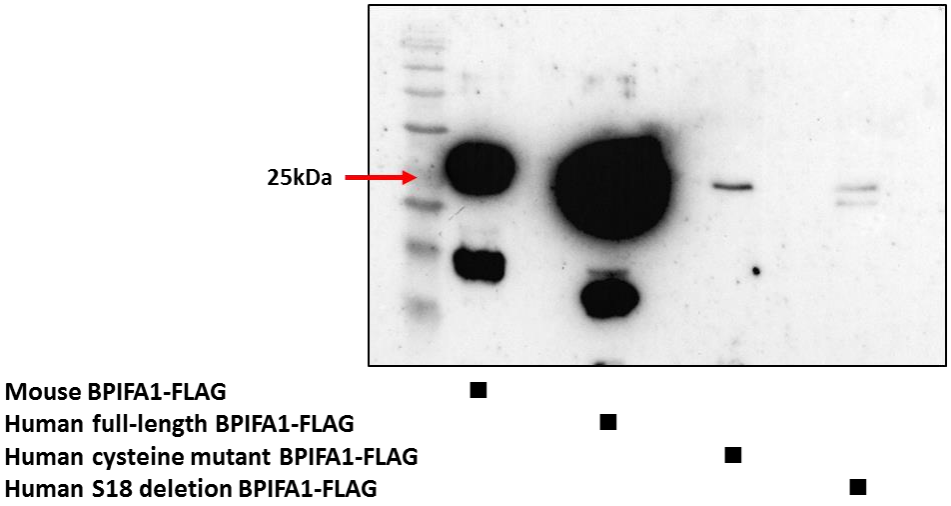

Figure 3.32: Amounts of BPIFA1-FLAG purified proteins.
Greater quantities of full-length human and mouse BPIFA1-FLAG purified proteins were obtained compared to the amounts of human mutant BPIFA1-FLAG purified proteins. Full-length and cysteine mutant BPIFA1-FLAG: ~25.9kDa; S18 deletion BPIFA1-FLAG: ~23.7kDa; and mouse BPIFA1-FLAG: ~29.5kDa. Western blots were probed with anti-FLAG tag antibody. Additional fragments present on SDS-PAGE membrane may represent degradation products of the proteins.

Therefore, I decided that mouse BPIFA1 purified protein would be used in the bacterial pull-down assays, whereas human BPIFA1 purified proteins would not be used due to significantly limited amounts available. Interactions of BPIFA1 proteins with bacterial pathogens are described in **Chapter 4**.

3.4 Discussion

3.4.1 Characteristics of human and mouse BPIFA1 proteins

Protein sequences of mouse and human BPIFA1 were analysed using bioinformatic approach to acquire information about BPIFA1. Sequence and structure similarity of human BPIFA1 protein to BPI/LBP protein superfamily members is important as it suggests the role of hBPIFA1 in the host defence.

My analysis demonstrated that the disulphide bond of hBPIFA1 and BPI is at the same position within the protein structures. I also showed that mouse BPIFA1 contains two cysteine residues (C204 and C246) which form a disulphide bond. BPIFA1 cysteine residues forming a disulphide bond are completely conserved among all species and it may be highly important for entire protein structure stability and proper folding. Furthermore, the disulphide bond of BPI was reported to be crucial for the secretion of biologically active BPI protein (Horwitz et al., 1996). It suggests that disulphide bond may also be crucial for the activity of BPIFA1.

Human and mouse BPIFA1 protein sequences were also analysed in more detail searching for conserved domains, sites and residues. Casein kinase II phosphorylation site and N-myristoylation site were detected in both human and mouse BPIFA1, whereas N-glycosylation and Protein Kinase C phosphorylation sites were detected only within mBPIFA1. The presence of Casein kinase II phosphorylation site may suggest that BPIFA1 can be phosphorylated and regulated by Casein kinase II which is an active serine/threonine protein kinase, having a broad range of physiological targets and playing a role in the variety of cellular functions (e.g. cell viability maintenance) (Litchfield, 2003). The presence of an N-myristoylation site within BPIFA1 suggests that myristate (14-carbon fatty acid) can be attached onto glycine residues of BPIFA1 via N-myristoyltransferase catalysation and may influence the localisation, structural conformation, and biological functions of BPIFA1 (Maurer-Stroh et al., 2002, Wright et al., 2010). Prediction of Protein Kinase C phosphorylation site within the mBPIFA1

suggests that mBPIFA1 can be phosphorylated by Protein Kinase C which is involved in a variety of the signalling pathways, regulating lipid hydrolysis and cellular functions (Freeley et al., 2011, Newton, 1995). This suggests that Protein Kinase C may be involved in the regulation of mBPIFA1 activity. In addition, N-glycosylation sites within mBPIFA1 were predicted, suggesting that mBPIFA1 protein can be N-glycosylated by attachment of an oligosaccharide to selected asparagine amino acid in the protein sequence. N-linked protein glycosylation may greatly affect the function of mBPIFA1 as it is known that N-glycosylation leads to post-translational modifications of protein which affect protein folding and biological activity (Aebi, 2013, Medus et al., 2017, Spiro, 2002). In contrast, no N-glycosylation sites were detected in hBPIFA1, suggesting a possible difference between the biological functions of human and mouse BPIFA1 proteins.

Bioinformatic analysis confirmed that human and mouse BPIFA1 proteins contain a leucine-rich region, which may enable both proteins to interact with a variety of substrates and this, in turn, may allow them to function in host defence. It was also reported that a single leucine-rich region may have the ability to interact with several different substrates, including lipids, nucleic acids, and hormones (Helft et al., 2011, Ng and Xavier, 2011). Proteins containing leucine-rich repeats were reported to be involved in chemokine- and cytokine-mediated signalling, immunity and host defence. For instance, TLR and NOD-like receptors contain leucine-rich repeats which enable them to recognise a structurally diverse set of microbial elements (Ng and Xavier, 2011). Therefore, the leucine-rich region of BPIFA1 may be associated with a variety of important biological functions. Analysis of this region should be of high interest as it may provide information about the activity of BPIFA1.

mBPIFA1 contains a proline-rich region which is not present in hBPIFA1. The region 25-68aa of mBPIFA1 contains eight PL repeats and thirteen proline residues, whereas hBPIFA1 contains only three PL repeats and six proline residues. In addition, the region 22-42aa of hBPIFA1 is unstructured whereas the same region in mBPIFA1 is structured (Garland et al., 2013). Hereby, these two traits of hBPIFA1 make it different from

mBPIFA1. Proline repeats were reported to be involved in the molecular conformation of proteins and peptides (Morgan and Rubenstein, 2013, Williamson, 1994). Proline is also known as a good ligand because of its large flat hydrophobic surface which enables binding to other hydrophobic surfaces. In addition, proline-rich regions were reported to enable peptides to bind rapidly to other proteins and this ability was suggested to be associated with the restricted mobility of proline amino acid (Williamson, 1994). Some proline-rich peptides were also reported to have antimicrobial activity (Casteels et al., 1989, Falla et al., 1996). Therefore, this would suggest that proline-rich repeats may influence mBPIFA1 activity and this makes it of high interest to determine their importance for the biological activity of mBPIFA1. It is also interesting that some proline residues are accompanied by leucine residues in human and mouse BPIFA1 proteins and appears as proline-leucine repeats rather than only proline-repeats, suggesting that these unique combination of amino acids may be associated with the certain biological function or functions of BPIFA1.

Potential protein-protein and protein-polynucleotide binding sites of mouse and human BPIFA1 were also predicted in this study. Prediction of residues involved in the protein binding is useful as it can provide the insights about interactions between BPIFA1 and other proteins. Understanding of such interactions is important because protein-protein interactions play a role in the variety of biological processes (Reichmann et al., 2007). For example, one of the predicted residues of hBPIFA1 involved in the binding is Q30. This residue is present in the S18 region (amino acids: G22-A39) of hBPIFA1 which specifically binds to the glycosylated β-subunit of ENaC and participates in regulation of β-ENaC processing (Garland et al., 2013, Hobbs et al., 2013). It may suggest that Q30 residue plays a role in the binding of hBPIFA1 to β-ENaC. Therefore, understanding the roles of other BPIFA1 residues involved in the binding process would be of great interest. Overall, bioinformatic analysis of BPIFA1 provided important insights into possible functions of protein and revealed differences between mouse and human BPIFA1 proteins.

3.4.2 The pcDNA3.1 system did not provide sufficient amounts of hBPIFA1

In this study, I used the pcDNA3.1 expression system as this vector contains a human cytomegalovirus immediate-early promoter/enhancer which should have enabled expression of BPIFA1 in transfected mammalian cells (Invitrogen, 2004). In addition, pcDNA3.1 should have allowed establishment of stable cell lines using G418 selection. The NCI-H292 cell line used for transfection assays is known to express *BPIFA1* but expression levels were shown to be approximately 32-fold lower than those of well-differentiated primary airway epithelial cells (Chu et al., 2010, Thaikoottathil and Chu, 2011). I transfected NCI-H292 cells with DNA of GFP-tagged hBPIFA1-pcDNA3.1 and attempted to select BPIFA1-positive cells using G418. G418 selection should kill cells which do not contain plasmid DNA (Gibco, 2015). However, my findings indicated ineffectiveness of G418 selection. This may have been caused by the usage of penicillin and streptomycin in the cell culture as it has been suggested that the use with G418 may lead to the low/no selection activity of G418 as they are competitive inhibitors of G418 (Gibco, 2015). Consequently, I decided to use a serial dilutions method for the isolation of positive cells, but the single cell colonies which were generated consisted of BPIFA1-GFP positive and negative cells. Production of BPIFA1-GFP by these cells was detected, but protein levels were very low. Subsequently, cell sorting by flow cytometry was used to sort the mixed cell population into positive and negative cells. Isolation efficiency of positive cells indicated great effectiveness of the method and secretion of BPIFA1-GFP was also detected, but again levels of protein were lower than expected. BPIFA1 should have been readily secreted into the media from the transfected cells but after cells were transferred into serum-free medium, no secretion of protein was observed. Absence of BPIFA1 secretion by cells cultured in serum-free conditions was unexpected but could be a result of cells being unhealthy or lacking nutrients which may cause impairment of cellular functions (Li et al., 2015, Rezaei et al., 2013). Due to low amounts of BPIFA1, I

decided to change the method and use pcDNA5/FRT expression system in the attempt to obtain larger quantities of BPIFA1.

3.4.3 No secretion of BPIFA1 using pcDNA5/FRT expression system

A series of different sizes of BPIFA1-GFP constructs were generated in pcDNA5/FRT expression system and used for transfections of Flp-In-CHO cells. Stable cell lines were established using hygromycin B selection. Analysis of transfected cells showed a successful integration of BPIFA1-plasmid DNA into the genome of CHO cells. However, BPIFA1-GFP proteins were produced in extremely small quantities and again no secretion of proteins was observed. Stable cell lines appeared to contain only a small proportion of BPIFA1-GFP positive cells. A number of reasons might have caused this. Firstly, co-integration of the plasmid bacterial backbone with the gene of interest into FRT recombination site may have occurred and caused infectiveness of Flp-In™ system. Negative effects of plasmid bacterial backbone elements on the expression levels of transfected genes have been reported (Chen et al., 2003, Jakobsen et al., 2010). Expression levels of transfected gene could also be affected by *lacZ-Zeocin* selection marker gene which resides in the docking site, containing recombinase recognition sequences and a stably expressed gene (Invitrogen, 2010, Jakobsen et al., 2010). Furthermore, additional transgenes, such as enhanced green fluorescent protein (eGFP), in the site of the transfected gene have also been shown to cause a negative impact on the expression levels of the gene of interest in this system (Dalle et al., 2005). All of this suggests, that host cells transfected with DNA of BPIFA1-pcDNA5/FRT construct may be negative for *BPIFA1* expression or express only low levels of *BPIFA1* but still be resistant to hygromycin B. It could of course be possible that the fusion protein itself is not optimal for secretion as the GFP may negatively influence production and secretion. I was not able to formally test this, and it was not considered to be important as it was clear that this system was not optimal for my needs.

3.4.4 Production, secretion, and purification of BPIFA1-FLAG proteins

Human and mouse FLAG-tagged BPIFA1 constructs were, therefore, generated in the mammalian VR1255 vector system. BPIFA1 proteins were fused to a FLAG tag instead of GFP, as it approximately 30 times smaller than GFP. The aim here was to avoid any risks of protein misfolding and degradation caused by GFP (Stepanenko et al., 2008, Zimmer, 2002). This change in expression technology allowed production and secretion of all human and mouse BPIFA1-FLAG recombinant proteins. However, the yield of secreted BPIFA1 recombinant proteins by transiently transfected cells was variable. This might be the result of inconsistent transfection efficiency rates (Dalton and Barton, 2014). In addition, the amounts of secreted proteins were not as high as expected and it may be because of BPIFA1 being normally secreted into the apical cell surface (Campos et al., 2004, Di et al., 2003). During this project, all cells were grown in submerged culture conditions and it may be a reason for the secretion of BPIFA1 being not as high as anticipated. Future studies aiming to achieve greater quantities of secreted BPIFA1 could try to transfect cells cultured in ALI conditions. In addition some other stable cell expression system could be used. In my study, I also observed that secretion of recombinant proteins was reduced once cells were transferred to the serum-free culture conditions. Decreased levels of recombinant proteins in the serum-free cell culture conditions have been reported (Li et al., 2015, Rezaei et al., 2013). Despite finding reduced levels of recombinant proteins in the serum-free cell culture, I decided to use secreted proteins in serum-free media because of the nature of my experiments. It is well recognised that absence of serum in the cell culture considerably simplifies purification process of proteins and eliminates any potential contamination (Sinacore et al., 2000). I also required secreted proteins in the serum-free conditioned media to investigate BPIFA1 binding to bacteria. I purified mouse and human BPIFA1-FLAG recombinant proteins from the serum-free conditioned media using anti-FLAG® M2 affinity gel. All human and mouse BPIFA1-FLAG proteins were purified from media but amounts of

purified proteins were low. Full-length mouse and human proteins were produced at highest levels, but some secreted protein was left in the media after purification. The efficiency of purification was always lower with mutant BPIFA1-FLAG proteins. In many cases the majority of the protein were not eluted from the beads, meaning that only small amounts of proteins were purified from the conditioned media. Mutations made to hBPIFA1 proteins could lead to the conformational changes of S18 deletion and cysteine mutant BPIFA1 proteins which, in turn, affected purification efficiency. In addition, the fusion of BPIFA1 proteins to FLAG tag instead of 3x FLAG tag might have caused a decrease in the purification rates. Purification of recombinant proteins from media was described to improve when 3x FLAG tag was used (Terpe, 2003). Therefore, the use of 3x FLAG tagged proteins should be considered in the future work requiring purified proteins. It is also possible that the protein *per se* has an ability to bind to the affinity resin without interaction through the FLAG domain. In this case FLAG peptide might not always elute the protein. This suggestion is supported by the fact that previous antibody affinity work in the laboratory has shown that the protein bound to affinity resin in the absence of specific antibody (unpublished).

3.4.5 Subcellular localisation of BPIFA1-FLAG recombinant proteins

The subcellular localisation of human and mouse BPIFA1-FLAG proteins appeared to be in the cell cytoplasm. However, some transfected cells were observed to contain highly fluorescent granule-shaped objects, which suggested that BPIFA1 was also localised within these granules. Quantitative analysis suggested that the number of cells containing fluorescent granules was greater in the cells transfected with mutant BPIFA1 constructs compared to full-length BPIFA1 constructs. It also appeared that cells transfected with S18 deletion BPIFA1-FLAG contained a greater number of cells with fluorescent granules compared to the cells transfected with cysteine mutant BPIFA1-FLAG. Thus, these data may suggest that mutant BPIFA1 proteins enter a different secretory pathway compared to the non-mutant BPIFA1. This change in the secretory

pathway may be associated with the masking of localisation targeting sequence and conformational change of protein (Bauer et al., 2015, Stadler et al., 2013). I speculate that the localisation targeting sequence may be present in G22-L42 region of hBPIFA1 as it would explain the increased presence of the S18 deletion BPIFA1 in the granule-shaped objects. Frequent presence of cysteine mutant BPIFA1 in the spherical-shaped objects may be a result of protein's conformational change caused by deletion of the disulphide bond. I suggest that these spherical-shaped objects were cell vesicles. There are two possible reasons for mutant protein's localisation within vesicles. Firstly, it might be a consequence of the increased load on the cell secretory system due to overexpression of *BPIFA1* and secondly, it may be associated with the destruction of misfolded mutant BPIFA1. Cellular functions strictly regulate translation of mRNA into the protein and in the case of misfolding, newly produced protein may be translocated in the vesicles by protein quality control mechanism for re-folding or degradation to the cytosol (Bauer et al., 2015, Kaganovich, 2017). This may also be the cause for low levels of these two proteins being produced in the transfected cells described above.

The correct protein localisation is crucial for the proper protein function and information on the protein localisation could provide the insights into cellular functions of protein. Therefore, in the future it will be of great interest to identify the subcellular localisation of native BPIFA1 and understand the factors that cause a change in the localisation of protein.

3.5 Key experimental conclusions

- N-terminal region of BPIFA1 exhibits the highest variability among the species.
- Bioinformatic analysis of mBPIFA1 showed that protein is leucine- and proline-rich, whereas hBPIFA1 could only be determined as leucine-rich protein. In addition, mBPIFA1 can be N-glycosylated, whereas hBPIFA1 cannot be N-glycosylated.
- NCI-H292 cells were successfully transfected with GFP-tagged hBPIFA1-pcDNA3.1 construct and cell sorting enabled the generation of hBPIFA1-GFP stable cell line. However, protein secretion was low.
- No secretion of recombinant BPIFA1-GFP proteins was achieved using pcDNA5/FRT expression system.
- Production and secretion of mouse and human BPIFA1-FLAG proteins were achieved using VR1255 plasmids and HEK293T cells.
- Purification of BPIFA1-FLAG proteins was not highly effective. Amounts of purified FL-hBPIFA1-FLAG and mutant hBPIFA1-FLAG proteins were not sufficient for the functional studies of BPIFA1.

CHAPTER 4: THE BINDING OF BPIFA1 TO BACTERIA

4.1 Introduction

Respiratory tract infections are one of the most common human infections, causing high morbidity and mortality globally. Over 17 billion incidences of upper respiratory tract infections were reported in 2015 (GBD, 2016) and over 2.7 million deaths were caused by lower respiratory tract infections in the same year (GBD, 2017). Annually pneumonia alone causes 1.8 million deaths of children under 5 years of age worldwide (WHO/UNICEF, 2009). *S. pneumoniae*, *S. aureus*, and *H. influenzae* are among the most common bacterial pathogens causing pneumonia (Siegel and Weiser, 2015). *H. influenzae* and *S. pneumoniae* are also a leading cause of otitis media (Pettigrew et al., 2008). All of these microorganisms belong to the commensal flora of the nasopharynx. However, they can spread from their normal environmental niche into sterile sites of the respiratory tract (e.g. lungs, middle ear, and sinuses) and cause local and invasive bacterial infections. In such cases these microbes become opportunistic pathogens (Bosch et al., 2013, Pettigrew et al., 2008, Siegel and Weiser, 2015). Healthy humans whose nasopharynx is colonised by *S. pneumoniae*, *H. influenzae*, and *S. aureus* serve as reservoirs for bacterial transmission to the susceptible host. In a balanced state, the epithelial layer of the respiratory tract mucosa is the first line of the host defence against bacterial and viral invaders. However, the loss of barrier function may allow pathogens to cross through mucus layer and invade epithelial cells; where they can cause infection and induce the development of infectious disease (Bosch et al., 2013, Pettigrew et al., 2008). In many cases, respiratory tract infections caused by bacteria are treated with specific antibiotics. However, the over-prescription and inappropriate use of antibiotics over decades have resulted in the emergence and spread of antibiotic-resistant bacterial strains (Fahey et al., 1998, Prat and Lacoma, 2016). Consequently, the development of new therapeutics is important for the treatment of bacterial respiratory tract infections. Potential alternative to antibiotics are natural host antimicrobial peptides and proteins secreted by airway epithelial cells which exhibit rapid action, bactericidal properties,

broad spectrum activity against bacteria, low bacterial resistance, and low immunogenicity (Bals, 2000, Czaplewski et al., 2016, Prat and Lacoma, 2016).

As outlined in the introduction, BPIFA1 is an abundantly secreted protein released by airway epithelial cells in the upper respiratory tract and pharynx (Bingle and Craven, 2002). BPIFA1 exhibits antimicrobial properties (Gally et al., 2011, Liu et al., 2013, Sayeed et al., 2013) and the S18 peptide derived from the N-terminal region of BPIFA1 can regulate the cleavage and activation of ENaC (Garcia-Caballero et al., 2009, Garland et al., 2013, Rollins et al., 2010). Consequently, the S18 peptide has attracted a lot of interest and currently Spyryx Biosciences is developing S18 peptide-based therapy for the treatment of CF (Fellner et al., 2016). BPIFA1 proteins or BPIFA1 derived peptides could potentially be used in the future for the treatment of bacterial respiratory tract infections, but, firstly, the mechanisms by which BPIFA1 performs its antimicrobial activity must be determined.

Therefore, I proposed to investigate the role of BPIFA1 in the host defence by examining BPIFA1's binding to bacterial pathogens. To fulfil this task, I used secreted endogenous and recombinant BPIFA1 proteins in bacterial pull-down assays with *S. aureus*, *S. pneumoniae*, and NTHi.

4.2 Objectives of this study

The overarching aim of this study was to investigate the binding ability of BPIFA1 to different types of bacteria. In order to perform the functional analysis of BPIFA1, the following objectives had to be accomplished:

1. To investigate human BPIFA1's binding to bacteria.
2. To determine the importance of disulphide bond and S18 region for human BPIFA1's binding to bacterial pathogens.
3. To compare the bacterial binding functions of full-length mouse BPIFA1 with full-length human BPIFA1.

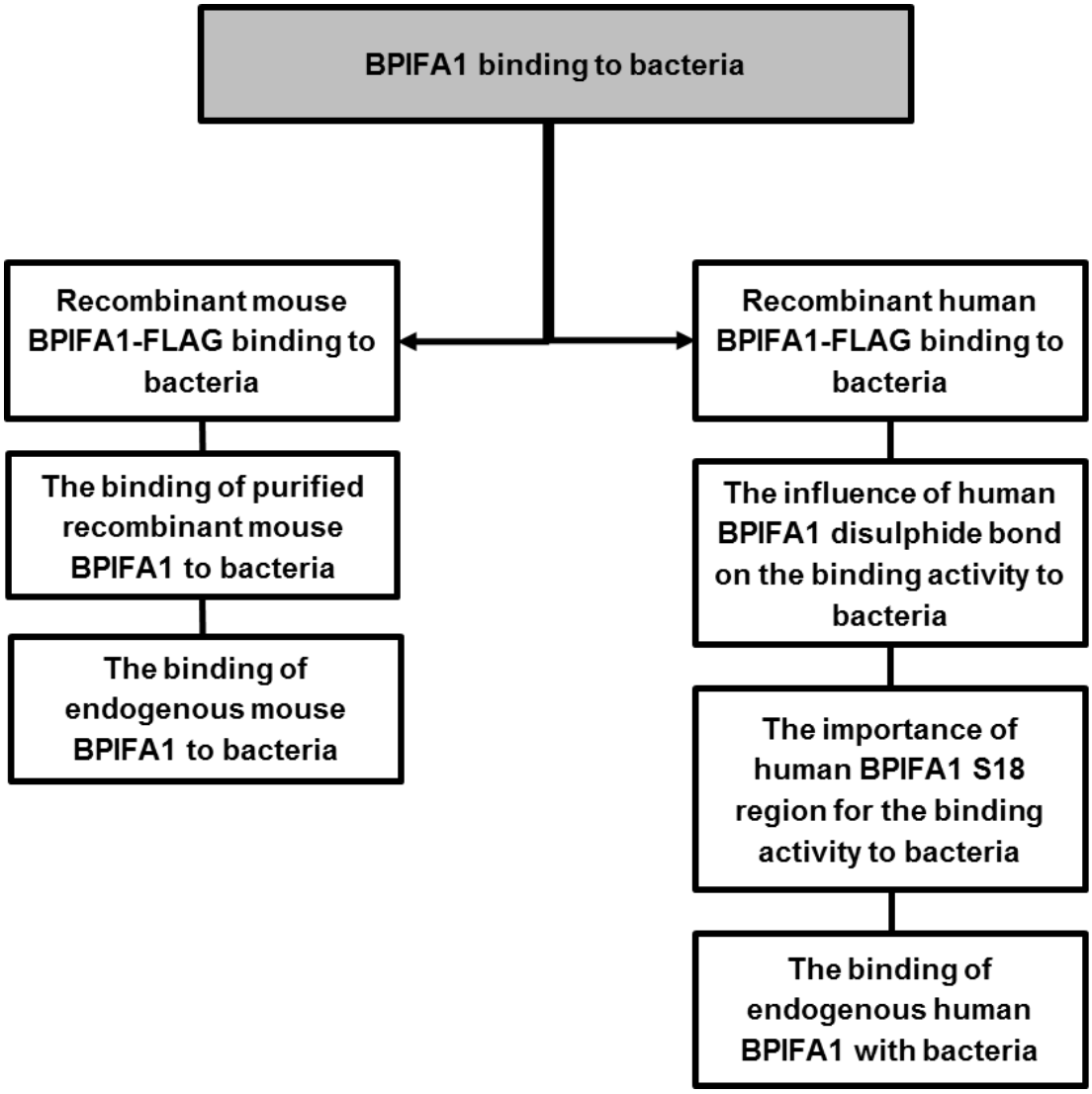

Figure 4.1: Study plan for this chapter.

4.3 Results

4.3.1 Analysis of BPIFA1 binding to bacteria

Bacterial pull-down assays were performed to investigate the ability of human and mouse BPIFA1 proteins to bind to bacteria. I also aimed to determine the importance of disulphide bond and S18 region for bacterial binding activity of human BPIFA1. Human and mouse BPIFA1 proteins were used in the bacterial pull-downs using four different incubation time periods: 0, 10, 30, and 60 minutes. The types of human and mouse BPIFA1 proteins and the amounts of each protein used in the assays are listed in Table 4.1. After the binding assays were performed, the bacterial-protein pellet and pull-down fluid samples were collected for SDS-PAGE analysis. Original protein samples and bacterial cells were used as controls. Membranes were probed with anti-human BPIFA1 antibody for detection of human BPIFA1 and with anti-mouse BPIFA1 antibody for detection of mouse BPIFA1.

Table 4.1: The list of BPIFA1 proteins used in the bacterial pull-down assays.

Protein	Amount
Mouse endogenous BPIFA1	25µl of ALI wash
Mouse recombinant BPIFA1-FLAG	50µl of serum free conditioned media
Purified mouse recombinant BPIFA1-FLAG	10µl of purified protein in TBS
Human endogenous BPIFA1	10µl of ALI wash
Human recombinant full-length BPIFA1-FLAG	50µl of serum free conditioned media
Human recombinant cysteine mutant BPIFA1-FLAG	50µl of serum free conditioned media
Human recombinant S18 deletion BPIFA1-FLAG	50µl of serum free conditioned media

4.3.2 The binding of full-length human BPIFA1-FLAG to bacteria

To determine whether recombinant hBPIFA1 could bind to bacteria, I performed bacterial pull-down assays using FLAG-tagged FL-BPIFA1 and three different types of bacteria: *S. aureus*, *S. pneumoniae*, and NTHi. The results suggested that recombinant hBPIFA1 bound to bacteria at all time points (Figure 4.2 A-C). However, the binding of hBPIFA1 to microbes appeared to be weak as the majority of protein was detected in the bacterial pull-down fluid samples, meaning that the majority of protein did not bind to bacteria.

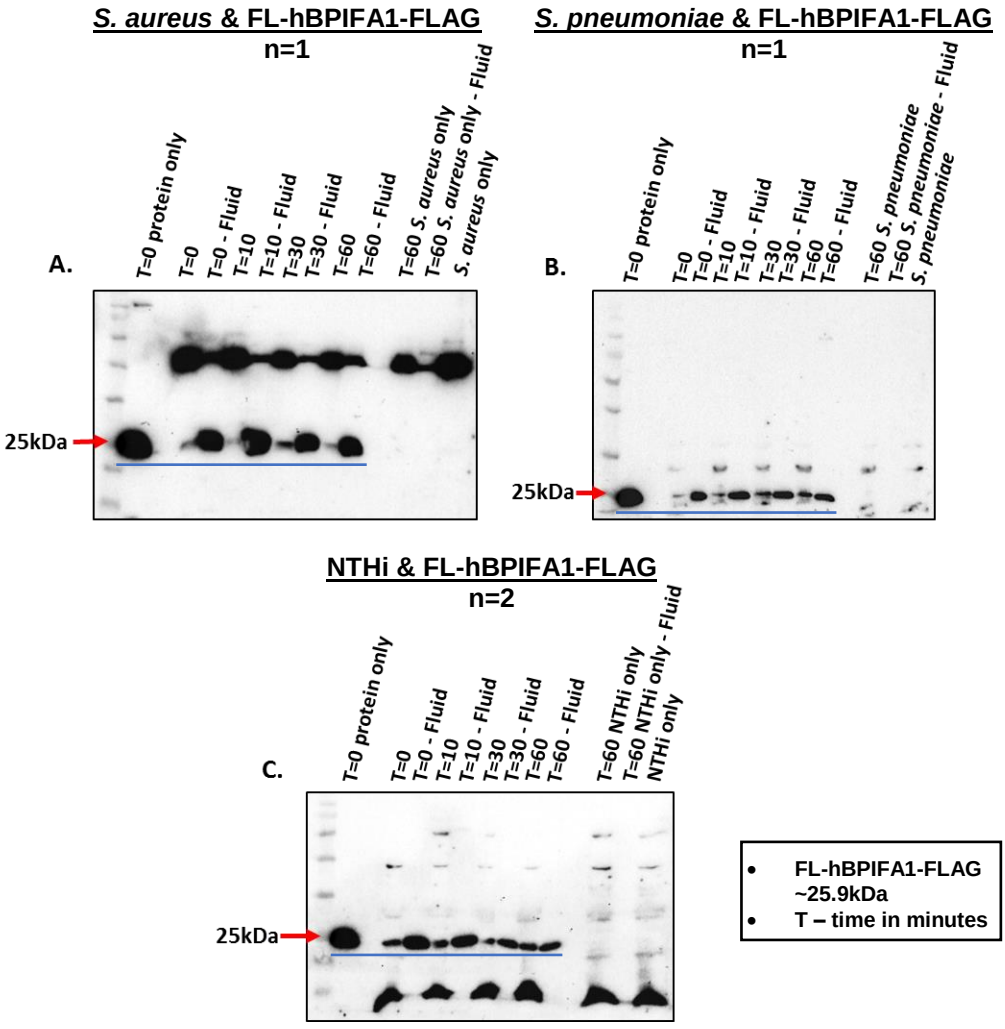

Figure 4.2: The binding of FL-hBPIFA1-FLAG to bacteria.
The binding of FLAG-tagged FL-hBPIFA1 to *S. aureus* ($2x10^8$) (**A**), *S. pneumoniae* ($8.5x10^7$) (**B**), and NTHi ($5x10^9$) (**C**). All membranes were probed with anti-human BPIFA1 antibody and exposed for 30 mins. Additional bands represent non-specific binding of antibodies to bacteria. Pull-down experiments with *S. aureus* and *S. pneumoniae* were performed once (n=1). Data of NTHi pull-down is representitive of results from two independent experiments (n=2). Full-length hBPIFA1-FLAG: ~25.9kDa (demonstrated by a blue line).

4.3.3 The binding of cysteine mutant human BPIFA1-FLAG to bacteria

To determine the importance of the disulphide bond in binding, I used the cysteine mutant BPIFA1-FLAG in the bacterial pull-down studies. The disulphide bond is completely conserved in all BPIF proteins and is assumed to be important for protein stability. The results demonstrated that hBPIFA1 lacking disulphide bond retained its ability to bind to Gram-negative and Gram-positive bacteria. Protein bound to bacteria at all incubation periods and binding activity appeared to increase over time (Figure 4.3 A-C). However, the binding ability appeared to be weak as a lot of protein was still retained in the bacterial pull-down fluid samples. Overall, the ability of cysteine mutant hBPIFA1-FLAG to bind bacteria resembled that of FL-hBPIFA1-FLAG.

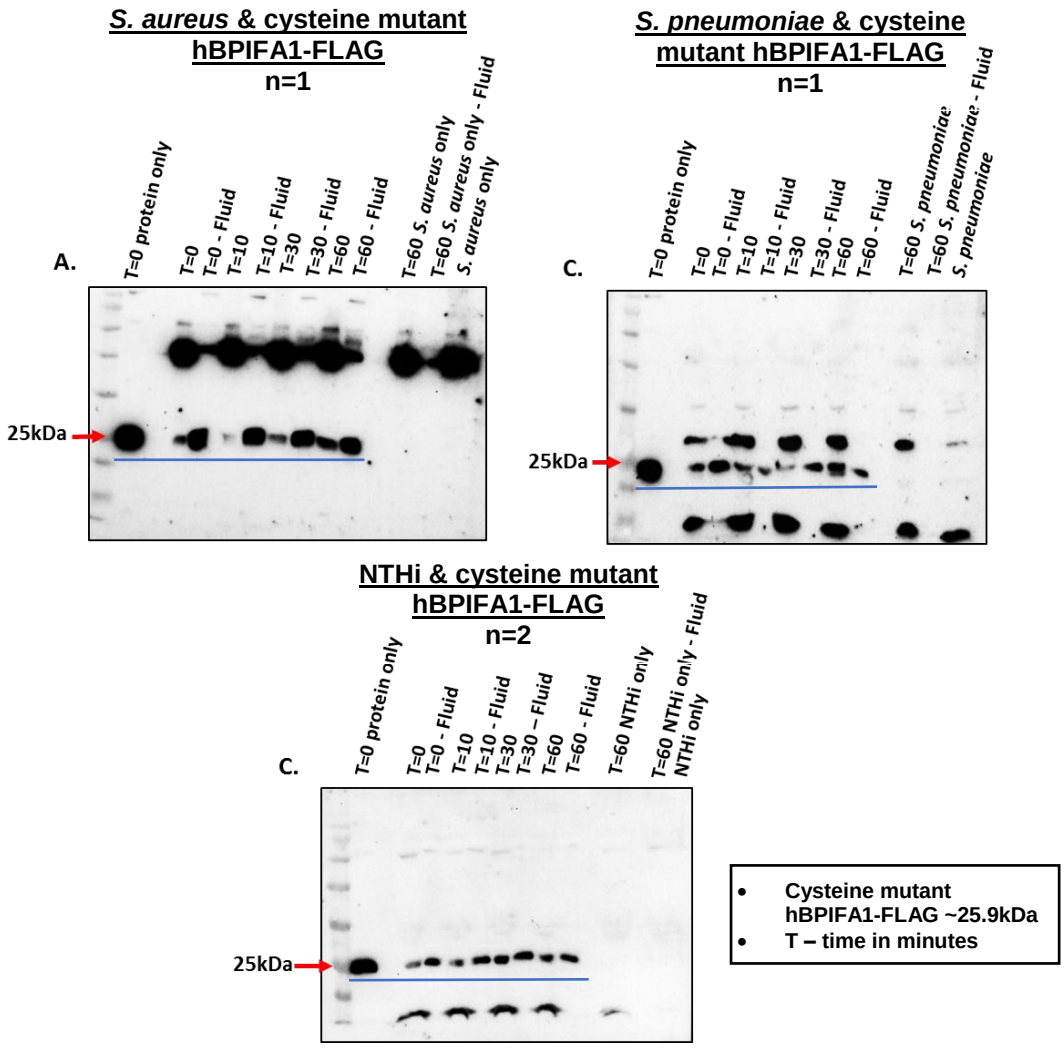

Figure 4.3: The binding of cysteine mutant hBPIFA1-FLAG to bacteria.
The binding of FLAG-tagged cysteine mutant hBPIFA1 to *S. aureus* ($2x10^8$) (**A**), *S. pneumoniae* ($8.5x10^7$) (**B**), and NTHi ($5x10^9$) (**C**). All membranes were probed with anti-human BPIFA1 antibody. Membranes **A** and **C** were exposed for 25 mins, and membrane **C** was exposed for 60 mins. Additional bands represent non-specific binding of antibodies to bacteria. Pull-down experiments with *S. aureus* and *S. pneumoniae* were performed once (n=1). Data of NTHi pull-down is representitive of results from two independent experiments (n=2). Cysteine mutant hBPIFA1-FLAG: ~25.9kDa (demonstrated by a blue line).

4.3.4 The binding of S18 deletion human BPIFA1-FLAG to bacteria

Next, I examined the significance of the S18 region for the bacterial binding function of hBPIFA1 using the S18 deletion hBPIFA1-FLAG. The data showed that hBPIFA1 lacking residues 22-42 did not bind to bacteria (Figure 4.4 A-C). These findings suggest that S18 region may be important for hBPIFA1's ability to bind to bacteria.

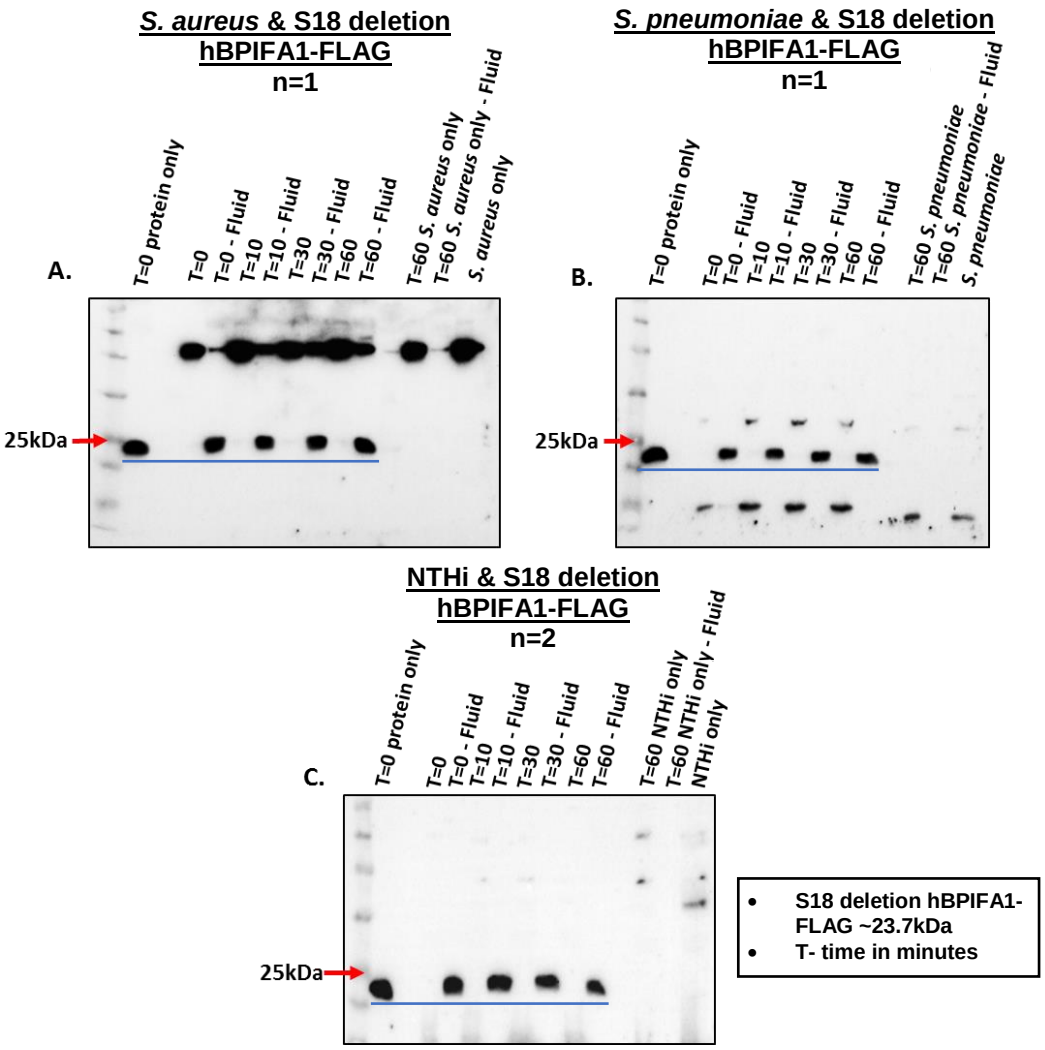

Figure 4.4: The binding of S18 deletion hBPIFA1-FLAG to bacteria.
The binding of FLAG-tagged S18 deletion hBPIFA1 to *S. aureus* ($2x10^8$) (**A**), *S. pneumoniae* ($8.5x10^7$) (**B**), and NTHi ($5x10^9$) (**C**). All membranes were probed with anti-human BPIFA1 antibody. Exposures of membranes: **A** – 8 mins; **B** – 15 mins; **C** – 10 mins. Additional bands represent non-specific binding of antibodies to bacteria. Pull-down experiments with *S. aureus* and *S. pneumoniae* were performed once (n=1). Data of NTHi pull-down is representitive of results from two independent experiments (n=2). S18 deletion hBPIFA1-FLAG: ~23.7kDa (demonstrated by a blue line).

4.3.5 The binding of endogenous human BPIFA1 to bacteria

The ability of endogenous hBPIFA1 (from HBEC ALI culture washes) to bind to respiratory pathogens was investigated to compare differences between the binding of the endogenous protein and recombinant hBPIFA1-FLAG. Results showed that endogenous hBPIFA1 bound to *S. pneumoniae* and NTHi, but no binding to *S. aureus* was detected (Figure 4.5 A-C). Some unbound protein was also detected in the pull-down fluids from the experiments performed with *S. pneumoniae* and NTHi.

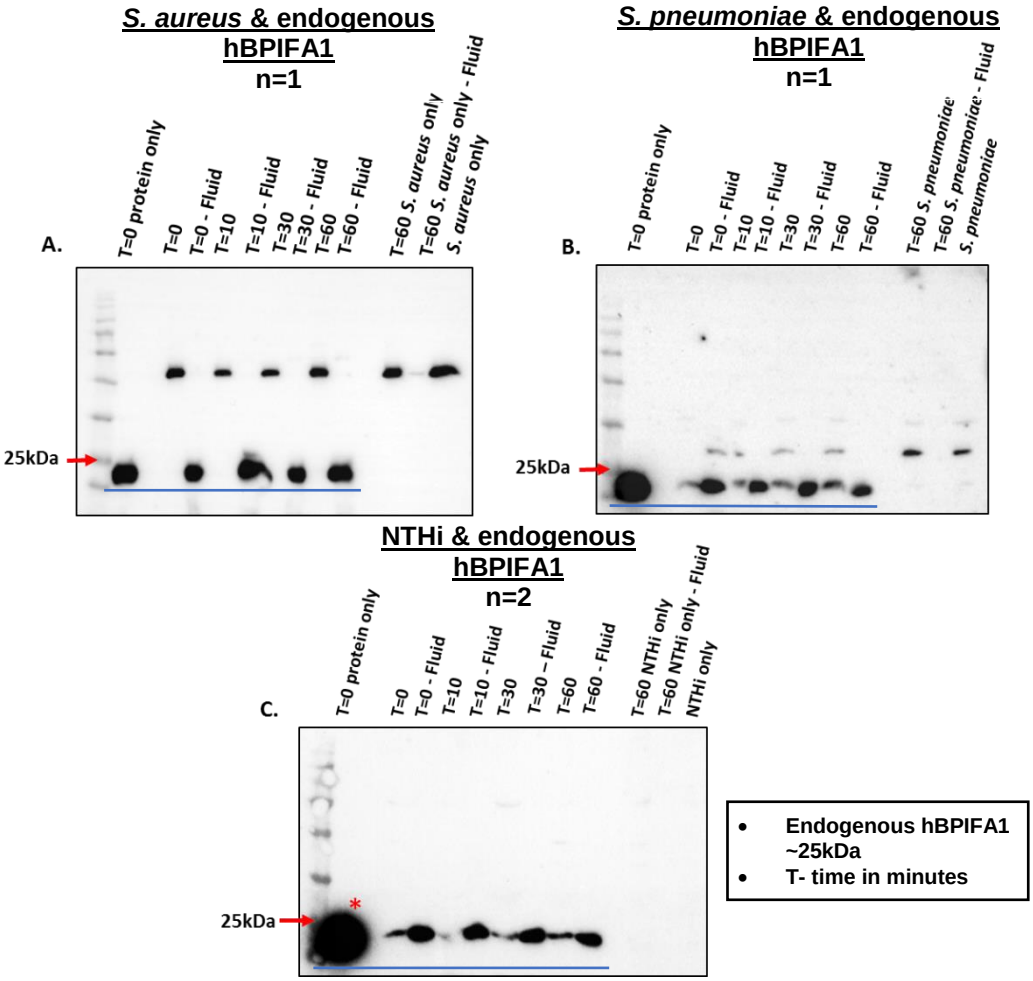

Figure 4.5: The binding of endogenous human BPIFA1 to bacteria.
The binding of endogenous hBPIFA1 to *S. aureus* ($2x10^8$) (**A**), *S. pneumoniae* ($8.5x10^7$) (**B**), and NTHi ($5x10^9$) (**C**). All membranes were probed with anti-human BPIFA1 antibody. Exposures of membranes: **A** – 2 mins; **B** – 25 mins; **C** – 15 mins. Additional bands represent non-specific binding of antibodies to bacteria. Asterisk symbol indicates that an excess of control BPIFA1 sample (T=0) was used. Pull-down experiments with *S. aureus* and *S. pneumoniae* were performed once (n=1). Data of NTHi pull-down is representitive of results from two independent experiments (n=2). Endogenous hBPIFA1: ~25kDa (demonstrated by a blue line).

4.3.6 The binding of recombinant mouse BPIFA1-FLAG to bacteria

To determine the ability of mouse BPIFA1 to bind to bacteria, I investigated the binding of unpurified recombinant mBPIFA1-FLAG to respiratory pathogens. The binding of protein to *S. aureus* appeared to not to be present or very weak (Figure 4.6 A). The findings demonstrated that recombinant mBPIFA1-FLAG bound to *S. pneumoniae* and NTHi, but that some unbound protein was detected in the pull-down fluids (Figure 4.6 B-C). Results also suggested that that the binding of mBPIFA1-FLAG to NTHi increased over the time (Figure 4.6 C).

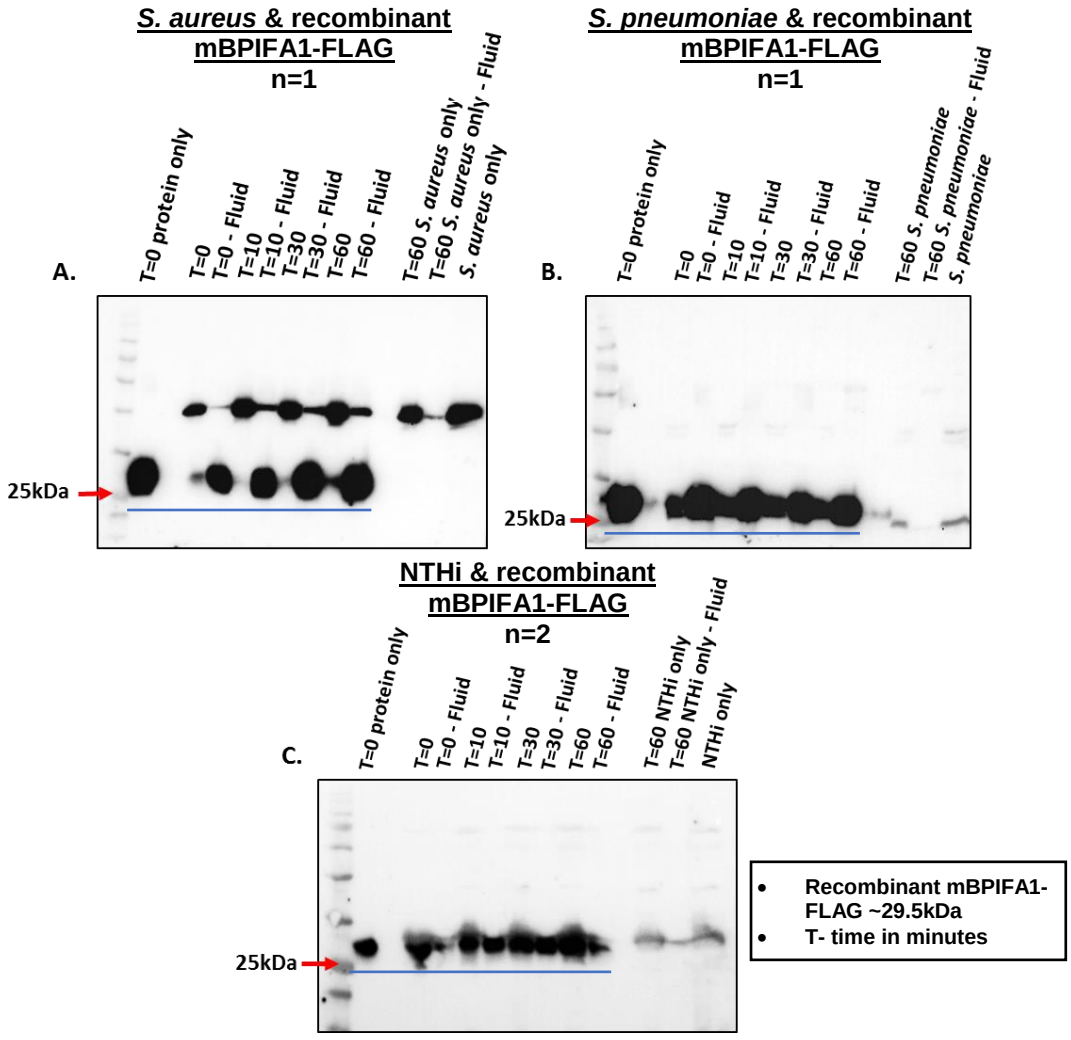

Figure 4.6: The binding of recombinant mouse BPIFA1-FLAG to bacteria.
The binding of FLAG-tagged mBPIFA1 to *S. aureus* ($2x10^8$) (**A**), *S. pneumoniae* ($8.5x10^7$) (**B**), and NTHi ($5x10^9$) (**C**). All membranes were probed with anti-mouse BPIFA1 antibody and exposed for 2 mins. Additional bands represent non-specific binding of antibodies to bacteria. Pull-down experiments with *S. aureus* and *S. pneumoniae* were performed once (n=1). Data of NTHi pull-down is representitive of results from two independent experiments (n=2). Recombinant mBPIFA1-FLAG: ~29.5kDa (demonstrated by a blue line).

4.3.7 The binding of purified recombinant mBPIFA1-FLAG to bacteria

Availability of purified mBPIFA1-FLAG enabled me to investigate the direct capability of mBPIFA1-FLAG to bind to bacteria. Using such samples meant that any other components present in the conditioned media would not influence binding of the protein to microbes as they were removed during protein purification process. Analysis of pull-down samples showed that the binding of purified mBPIFA1-FLAG to *S. aureus* appeared to be limited (Figure 4.7 A). However, results also demonstrated that mBPIFA1-FLAG bound to *S. pneumoniae* and NTHi (Figure 4.7 B-C). The binding of purified mBPIFA1-FLAG to microbes appeared to be similar at all time points examined during this study.

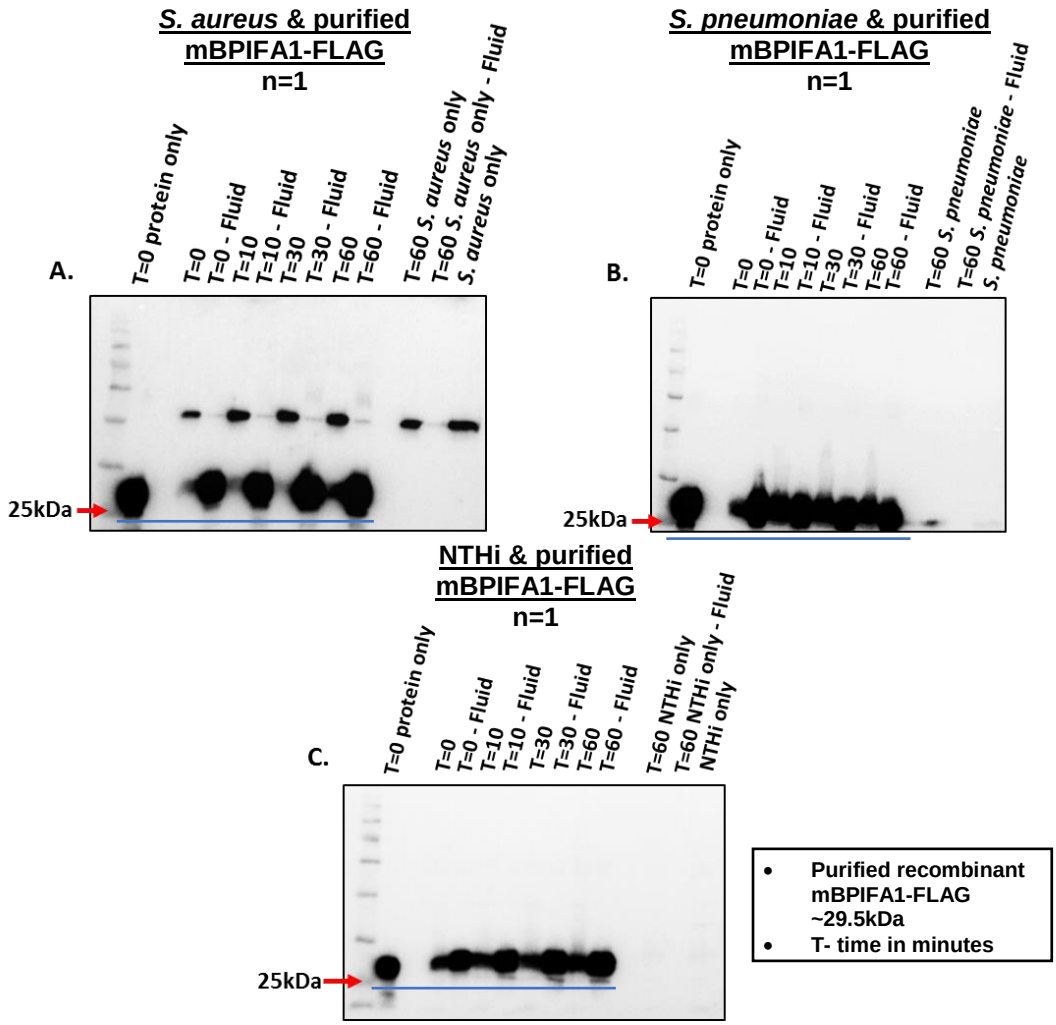

Figure 4.7: The binding of purified recombinant mouse BPIFA1-FLAG to bacteria.
The binding of purified mBPIFA1-FLAG to *S. aureus* ($2x10^8$) (**A**), *S. pneumoniae* ($8.5x10^7$) (**B**), and NTHi ($5x10^9$) (**C**). All membranes were probed with anti-mouse BPIFA1 antibody. Exposures of membranes: **A** – 20 sec; **B** – 30 sec; **C** – 10 sec. Additional bands represent non-specific binding of antibodies to bacteria. Pull-down experiments were performed once (n=1). Purified recombinant mBPIFA1-FLAG: ~29.5kDa (demonstrated by a blue line).

4.3.8 The binding of endogenous mouse BPIFA1 to bacteria

The ability of endogenous mouse BPIFA1 (from mTEC ALI washes) to bind to bacteria was investigated. The results showed that endogenous mBPIFA1 bound to *S. aureus* and NTHi, but not to *S. pneumoniae* (Figure 4.8 A-C). The binding of endogenous mBPIFA1 to *S. aureus* appeared to increase over the time (Figure 4.8 A). The ability of endogenous mBPIFA1 (Figure 4.8 A) to bind to *S. aureus* is the opposite to the situation with recombinant mBPIFA1-FLAG (Figure 4.6 A) as this protein showed very limited binding to the pathogen. Contrasting results were also observed in the pull-downs with *S. pneumoniae* as recombinant mBPIFA1-FLAG (Figure 4.6 B) was shown to bind to the pathogen whereas endogenous mBPIFA1 did not (Figure 4.8 B). The findings also suggested that endogenous mBPIFA1 bound to NTHi much more efficiently than recombinant protein as no unbound protein was detected in the pull-down fluids at any time point (Figure 4.8 C).

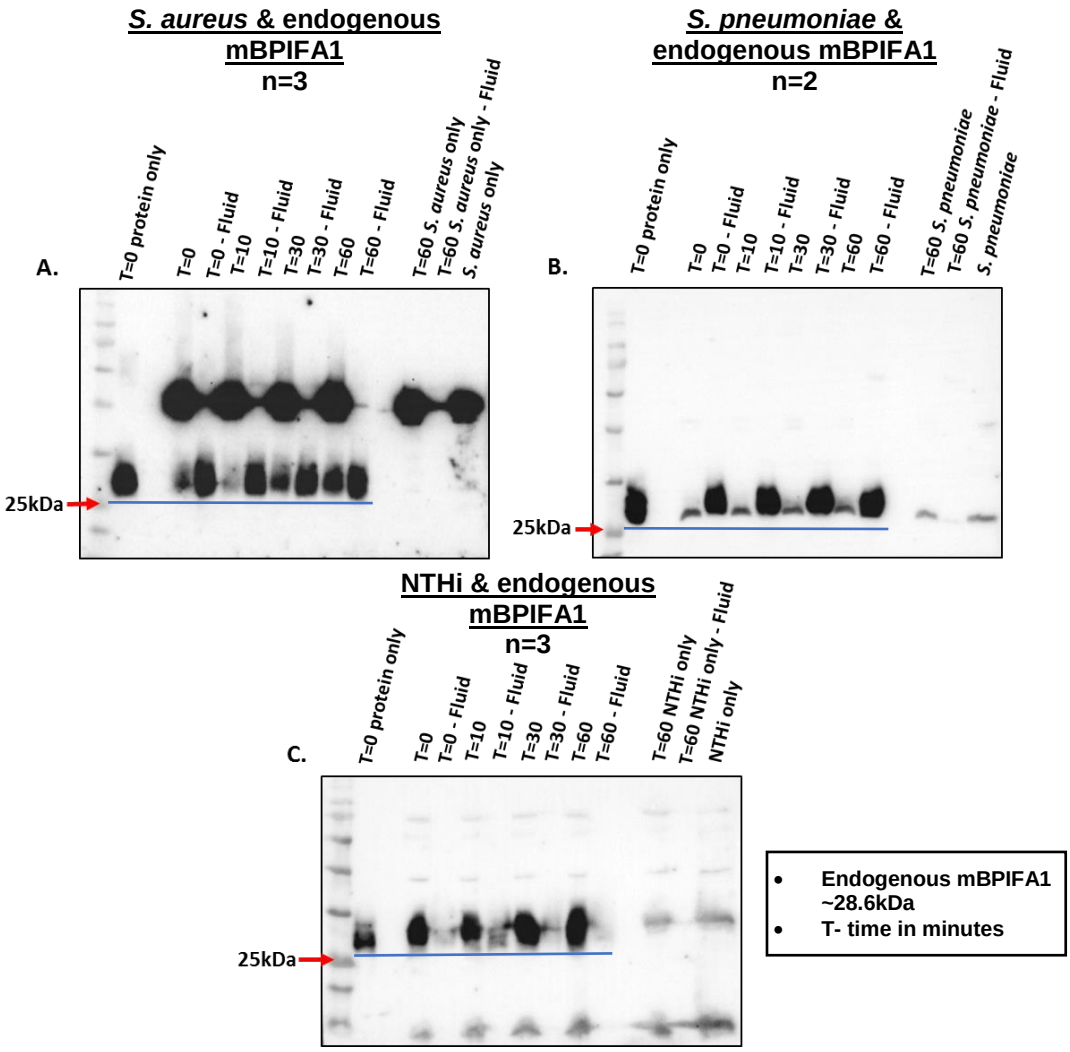

Figure 4.8: The binding of endogenous mouse BPIFA1 to bacteria.
The binding of endogenous mBPIFA1 to *S. aureus* ($2x10^8$) (**A**), *S. pneumoniae* ($8.5x10^7$) (**B**), and NTHi ($5x10^9$) (**C**). All membranes were probed with anti-mouse BPIFA1 antibody. Exposures of membranes: **A** – 10 mins; **B** – 2 mins; **C** – 2 mins. Additional bands represent non-specific binding of antibodies to bacteria. Data of *S. pneumoniae* pull-down is representative of results from two independent experiments (n=2). Data of *S. aureus* and NTHi pull-downs are representitive of results from three independent experiments (n=3). Endogenous mouse BPIFA1: ~28.6kDa (demonstrated by a blue line).

On the basis of the above data, I decided to investigate whether a reduced number of NTHi would cause a decrease in the binding of endogenous mBPIFA1 to bacteria. The same amount of protein was used for the binding assays with $5x10^9$ (Figure 4.9 A), $1x10^9$ (Figure 4.9 B), and $2x10^8$ (Figure 4.9 C) of NTHi. The results showed that the binding of endogenous mBPIFA1 gradually decreased with the lower numbers of NTHi (Figure 4.9

A-C). Results also suggested that more protein was detected in the fluids from bacterial pull-downs in which 5x (Figure 4.9 B) and 25x (Figure 4.9 C) times less of NTHi bacteria were used compared to the amounts of protein detected in the fluids obtained from binding assays with the highest number of bacteria ($5x10^9$ NTHi) (Figure 4.9 A).

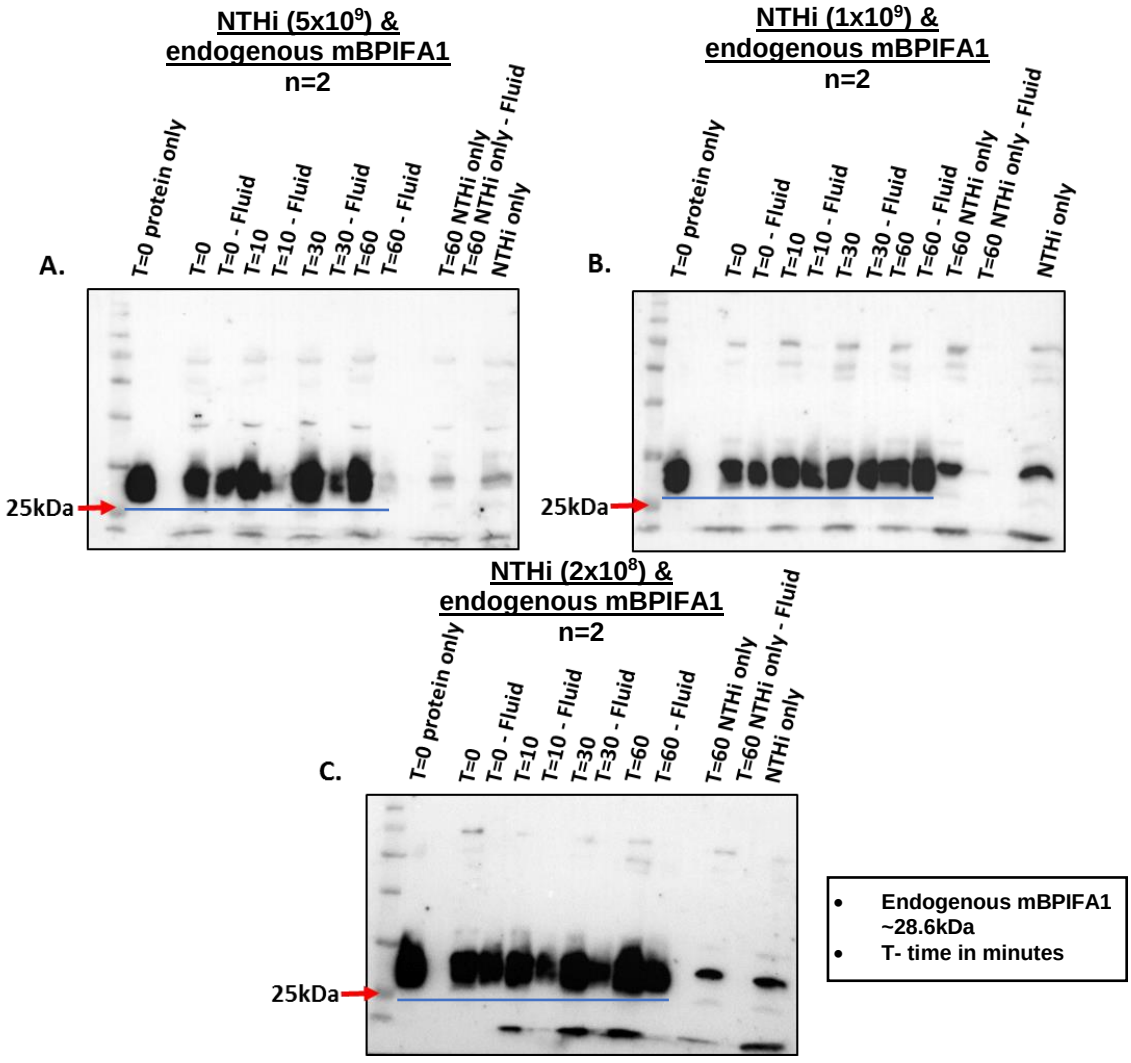

Figure 4.9: The binding of endogenous mBPIFA1 to different numbers of NTHi.
The binding of endogenous mBPIFA1 to $5x10^9$ (**A**), $1x10^9$ (**B**), and $2x10^8$ (**C**) of NTHi. All western blot membranes were probed with anti-mouse BPIFA1 antibody. Exposures of membranes: **A** – 2 mins; **B** – 3 mins; **C** – 8 mins. Additional fragments present on SDS-PAGE membranes was a result of non-specific binding of antibodies to NTHi. Data of pull-downs are representative of results from two independent experiments (n=2). Endogenous mouse BPIFA1: ~28.6kDa (demonstrated by a blue line).

Overall, the results from the pull-down experiments suggest that human BPIFA1 can bind to *S. aureus*, *S. pneumoniae*, and NTHi. Deletion of the disulphide bond appeared not to affect the binding activity of human BPIFA1. However, human BPIFA1 lacking S18 region (22-42aa) did not bind to bacteria. In addition, the binding activity of recombinant human BPIFA1 to *S. aureus* appeared to be different from endogenous human BPIFA1. The data also suggest that the binding of human BPIFA1 to the pathogens is similar to the binding of mouse BPIFA1. Mouse BPIFA1 bound to Gram-positive and Gram-negative bacteria, however different preparations of mouse BPIFA1 appeared to influence the protein's binding activity to bacteria. Ability of endogenous mouse BPIFA1 to bind to NTHi appeared to decrease with the reducing amounts of bacteria, suggesting that protein's binding may be dose-dependent. Findings from this study also showed that mouse and human BPIFA1 binding to pathogens increased over the time, suggesting that protein's bacterial binding may be influenced by the length of exposure.

4.4 Discussion

Experiments in this chapter were performed to look at the ability of BPIFA1 to bind to the commensal bacteria. Recombinant and endogenous BPIFA1 proteins were used in the bacterial pull-down assays to investigate BPIFA1's binding to bacteria, including *S. aureus* strain SH1000, NTHi-375-SR, and *S. pneumoniae* strain D39. NTHi-375-SR strain and *S. aureus* strain SH1000 were chosen for the work because of their previous use in our group investigating the role of BPIFA1 in the bacterial infections of middle ear epithelial cells (Mulay et al., 2016) and human bronchial epithelial cells (Chloe Marshall, unpublished), respectively. *S. pneumoniae* strain D39 was chosen for binding assays because of its broad use in the studies investigating mucosal and invasive bacterial infections, and its extreme virulence in murine infection models (Lanie et al., 2007, Marriott et al., 2012). Using simple bacterial pull-downs, I aimed to identify if BPIFA1 had the ability to bind to bacteria and to compare binding activity of human BPIFA1 with mouse BPIFA1. I also examined the importance of disulphide bond and S18 region for microbial binding activity of human BPIFA1. Bacterial pull-down technique was chosen for its usefulness in the identification of direct protein-protein interactions (Louche et al., 2017). The results from this work appear to show some differences in the protein's bacterial binding activity, which may be influenced by the different preparations of BPIFA1.

4.4.1 The binding ability of human BPIFA1 to bacteria

Findings from this study suggest that hBPIFA1 can bind to *S. aureus*, *S. pneumoniae*, and NTHi. However, the binding function of hBPIFA1 seemed to be affected by different preparations of protein and modifications made to the protein sequence. It was observed that recombinant full-length hBPIFA1-FLAG bound to all microbes, but endogenous hBPIFA1, secreted by HBECs, appeared to lack the ability of binding to *S. aureus*. Yet, it should be highlighted that *S. aureus* bacterial-pull down was performed only once in this study due to the limited availability of secreted endogenous hBPIFA1. It is also

interesting that some studies have shown that recombinant hBPIFA1 does not exhibit anti-growth and anti-biofilm functions against *S. aureus* (Ahmad et al., 2016, Walton et al., 2016). However, more recent study by Yu et al., showed that BPIFA1 shows antimicrobial properties against *S. aureus* (Yu et al., 2018). Based on these conflicting findings, I suggest that the activity of hBPIFA1 against *S. aureus* should be further investigated to determine the true antimicrobial functions of hBPIFA1 against this pathogen.

My data also showed that cysteine mutant hBPIFA1 can bind to bacteria, suggesting that the absence of disulphide bond does not lead to the loss of BPIFA1's bacterial binding activity. It implies that disulphide bond may not have a great influence on this biological activity of hBPIFA1. This is in contrast to data from work with BPI, as it was shown to become biologically inactive after disulphide bond removal (Horwitz et al., 1996). However, it has also been reported that exposure of BPIFA1 to the cigarette smoke triggers a disulphide bond modification which alters BPIFA1 structure. This disulphide bond modification was shown to inhibit BPIFA1's ability to bind and control ENaC activity (Moore et al., 2018). Therefore, this may imply that disulphide bond does not have impact on BPIFA1's bacterial binding activity, but it may influence other biological functions of protein. However, more detailed investigation should be performed to fully confirm that deletion of disulphide bond does not have any influence on the BPIFA1's bacterial binding function. In this study, pull-down assays were performed only with three different microbes and the number of pull-down replicates was low. In addition, the nature of pull-down experiments do not allow to determine if the strength of the protein's binding to pathogens has been affected after removal of disulphide bond. To answer this question, other types of assays (e.g. immunoprecipitation), allowing more quantitative analysis of results, should be used in the future.

BPIFA1 with deletion of S18 region was shown to lack binding ability, suggesting that the S18 region (22-42aa) of hBPIFA1 plays an important role in the protein's bacterial binding activity. However, further investigation is required to fully determine the

importance of S18 region for BPIFA1's bacterial binding activity. It is possible that deletion of S18 region may result in conformational changes of BPIFA1 which may cause the loss of bacterial binding function. Interestingly, it was recently shown that the S18 peptide (22-39aa) did not possess antimicrobial activity against Gram-negative pathogen and that BPIFA1 mutant protein lacking amino acids M1-S43 retained full antimicrobial activity (Ahmad et al., 2016). In addition, it was reported that human BPIFA1 lacking S18 region retains its ability to bind LPS from Gram-negative pathogens (Walton et al., 2016). Based on my results and the findings reported in the above studies, the importance of S18 region for biological activity of human BPIFA1 requires further investigation.

4.4.2 The binding of mouse BPIFA1 to bacteria

The binding of mouse BPIFA1 to pathogens was analysed in this study to understand the possible differences in the bacterial binding between mouse and human proteins. It was observed that mouse BPIFA1's bacterial binding activity was similar to that of human BPIFA1 as mouse BPIFA1 also bound to *S. aureus*, *S. pneumoniae*, and NTHi. Bacterial binding of mBPIFA1 differed with the different preparations of the protein. Endogenous mBPIFA1 bound to *S. aureus* and NTHi, whereas recombinant mBPIFA1-FLAG, including the purified protein, bound to *S. pneumoniae* and NTHi. This change in the bacterial binding activity of mBPIFA1 may be caused by the different preparations of the protein. The ability of endogenous mBPIFA1 to bind *S. aureus* compared to recombinant mBPIFA1-FLAG may be conferred by other naturally secreted proteins and peptides (e.g. lactoferrin, beta-defensins, mucins) found in the apical cell secretions from mTECs. In the study by Ventura et al., mouse host proteins were eluted from *S. aureus* recovered from the airways of mice 6 hours following intranasal inoculation. Direct binding ability of mBPIFA1 to *S. aureus* was detected (Ventura et al., 2008). My results are in the agreement with this study, suggesting that mBPIFA1 binds to *S. aureus*, but for this binding to happen other naturally secreted components of epithelial cell secretions may be required. However, the same proteins and peptides found in the apical cell secretions

may inhibit rather than enhance the binding of endogenous mBPIFA1 to *S. pneumoniae*. Inability of endogenous mBPIFA1 to bind to *S. pneumoniae* could also be caused by *S. pneumoniae* D39 strain itself as it is highly virulent in murine infection models (Lanie et al., 2007), meaning that it may be negatively affecting other naturally secreted mouse proteins and peptides in the apical secretions, and this, in turn, negatively alters the binding ability of endogenous mBPIFA1. Other naturally secreted mouse proteins and peptides were not present in recombinant mBPIFA1 preparation and it may be a reason for the ability of recombinant mBPIFA1 to bind to *S. pneumoniae*. This may suggest that mBPIFA1 performs its biological activity to the full extent in the presence of other natural components of the airway secretions.

The ability of mBPIFA1 to bind to NTHi appeared to be similar with the different preparations of protein, as endogenous and recombinant mBPIFA1, including the purified protein bound to NTHi. However, it should be mentioned that all-input endogenous mBPIFA1 bound to NTHi during bacterial binding assays, whereas some unbound recombinant mBPIFA1 was detected in the pull-down fluids. This may suggest that endogenous mBPIFA1 is better at binding to NTHi than recombinant mBPIFA1. The binding of endogenous mBPIFA1 may be enhanced because of other naturally secreted proteins and peptides found in the apical secretions of mTECs or it may be associated with the lack of FLAG tag. It is possible that tagging of recombinant mBPIFA1 with FLAG may cause some conformational changes of the protein which may affect the bacterial binding function.

Taking all results into consideration, I suggest that mouse and human BPIFA1 proteins exhibit bacterial binding ability and this may be one of the functions that the protein plays in host defence against bacterial infections. It appears that bacterial binding of recombinant BPIFA1 proteins differ from endogenous BPIFA1 proteins because of the presence of other naturally secreted molecules in the apical cell secretions. It may also

be suggested that the usage of endogenous BPIFA1 together with other naturally secreted components of the airway secretions may mimic better *in situ* antimicrobial functions of BPIFA1. In addition, it appeared that the binding of mouse and human BPIFA1 to bacteria was time-dependent. I was unable to quantify whether a larger amount of protein associated with bacteria over the time, because of limitations of my experimental design: 1) different amounts of different protein preparations were used in the bacterial pull-downs; 2) western blotting analysis of pull-down samples was performed without a loading control; and 3) small number of pull-down replicates. Consequently, more quantitative investigation is required to fully determine whether BPIFA1's binding activity increases with the longer exposures to bacteria.

In this study, I also showed that mouse BPIFA1 binds to NTHi and Jiang et al. reported that BPIFA1 deficiency in mice leads to the increase of bacterial burden in the murine lungs after NTHi challenge (Jiang et al., 2013b). It suggests that mouse BPIFA1 plays a role in the host defence against this pathogen. The ability of mouse BPIFA1 to bind to NTHi may be conferred by the proline-rich region which is found in the sequence of protein. It was reported that proline-rich regions enable peptides to bind to other proteins (Williamson, 1994) and that proteins, containing proline-rich region, have broad antimicrobial properties and exhibit specific activity against Gram-negative bacteria (Casteels et al., 1989, Falla et al., 1996). It is also possible that ability of mouse BPIFA1 to bind to NTHi may be associated with the fact that mouse BPIFA1 can be N-glycosylated. N-glycosylation is known to affect the biological activity of proteins and glycoproteins are well recognised to have an ability to bind to bacteria and serve as the vehicle for bacterial clearance (Kukuruzinska and Lennon, 1998, Lee et al., 2015, Lis and Sharon, 1993). I suggest that post-translational modification of mBPIFA1 with N-linked glycans may be important for its binding functions to NTHi. Based on my findings, showing the binding ability of mouse BPIFA1 to NTHi and currently existing data, demonstrating the importance of mouse BPIFA1 in the host defence, I decided to further

investigate the function of mouse BPIFA1 against NTHi using an *in vitro* infection model which is described in **Chapter 5**.

4.5 Key experimental conclusions

- Human and mouse BPIFA1 proteins bound to *S. aureus*, *S. pneumoniae*, and NTHi.
- Recombinant mouse and human BPIFA1 appeared to exhibit a different binding abilities to the microbes when compared with endogenous mouse and human BPIFA1 proteins, respectively. These findings suggest that BPIFA1's binding may be influenced or modified by the presence of other naturally secreted components of epithelial cell secretions.
- Removal of disulphide bond did not influence the binding of human BPIFA1 to bacteria, but deletion of residues 22-42 inhibited binding to the pathogens, suggesting that S18 region may influence biological activity of protein.

CHAPTER 5: INVESTIGATING THE SUSCEPTIBILITY OF WT AND *Bpifa1*$^{-/-}$ mTECs TO NTHi INFECTION

5.1 Introduction

The mouse is one of the most used animal model for the study of respiratory infections and is widely used for *in vivo* and *in vitro* studies. The respiratory tract of mice exhibits similarities to the human respiratory tract, meaning that it can be used as the laboratory model to investigate human respiratory system and diseases. However, there are also interspecies differences in the respiratory tract which should be considered when translating results from the animal study to the humans. For example, the human nasal airway and nasal turbinates are of less complex structure than they are in the mouse; the reason for this may be associated with the main functions of nasal airway (Harkema et al., 2006, Reznik, 1990). The primary function of human nasal airway is breathing whereas olfaction and breathing are the main functions of mouse nasal airway (Harkema et al., 2006, Reznik, 1990). In addition, although the distribution of nasal epithelium (i.e. squamous, respiratory, transitional, and olfactory) from nasal passages to the nasopharynx is similar in the mice and humans, the proportion of each epithelium type and cell types differ (Harkema et al., 2006, Reznik, 1990). The trachea of the mouse and human also share similarities as they both contain cartilage rings and submucosal glands, and both are lined by pseudostratified ciliated epithelium. However, there are differences between mouse and human tracheas too (Reznik, 1990, Rock et al., 2010). In humans, the cartilage rings extend for several bronchial generations, but, in mice, they are found only in the extrapulmonary airways. Submucosal glands are only present in the upper section of mouse trachea, whereas, in humans, their presence extends deeper into the lung. Furthermore, mouse trachea is lined by pseudostratified epithelium which later changes into a simple cuboidal epithelium in the mainstem bronchi, whereas, in humans, the pseudostratified epithelium is present up to the terminal bronchioles (Reznik, 1990, Rock et al., 2010). Mouse lower respiratory tract also shares similarities with human lower respiratory tract, but, generally, the structure of mouse lower airways is greatly different from human lower airways (Irvin and Bates, 2003, Miller et al., 1993,

Suarez et al., 2012). For example, mouse and human lungs contain lobes. However, right lung of mice consists of four lobes, whereas right lung of humans is divided into three lobes. Mouse left lung has only a single lobe, whereas human left lung consists of two lobes (Suarez et al., 2012). In addition, although mouse and human have lung pleura, mouse lung pleura is thin, whereas human lung pleura is thick (Irvin and Bates, 2003). Airway branching is a feature of mouse and human respiratory tract, but, in mice, airway branching follows monopodial pattern, whereas, in humans, it follows dichotomous pattern (Irvin and Bates, 2003, Miller et al., 1993). The number of airway generations also differ in mouse and human: mouse lung consists of 13-17 airway generations, whereas human lung consists of 17-21 airway generations (Irvin and Bates, 2003). Therefore, similarities and differences exist between mouse and human respiratory tract. These differences may be a reason for mouse not being a very good animal model to study human respiratory diseases such as COPD, CF, and asthma (Persson, 2002, Williams and Roman, 2016).

Despite these differences, mice are still commonly used for investigation of human respiratory tract diseases and infections due to their relatively low cost, size, and availability of good murine genetic information. In addition, mouse model allows the usage of *in vivo* experimental techniques which would not be ethically appropriate to be used in human studies. There are examples of *in vivo* studies performed using mouse models to study a variety of viral (Akram et al., 2018, Cormier et al., 2010) and bacterial (Bayes et al., 2016, Pilloux et al., 2016) infections. In recent years, techniques were developed to obtain murine epithelial cells from respiratory tract tissues for differentiation into the upper airway-like epithelium (Davidson et al., 2000, Mulay et al., 2016, You et al., 2002, You and Brody, 2013). These cells were shown to express airway epithelium specific genes, meaning that they consist of non-ciliated (e.g. secretory cells) and ciliated cells. Expression of *Zo-1* indicated that cellular tight-junctions are also formed (Davidson et al., 2000, Mulay et al., 2016, You et al., 2002, You and Brody, 2013). Development of *in vitro* mouse cell culture models, mimicking the *in vivo* host airway epithelium and its

microenvironment, provide unique possibilities to study behaviour, morphology, and immune responses of airway epithelium to bacterial and viral stimuli. In our laboratory these models were applied to investigate host-pathogen interactions in studies examining IAV infection of mouse tracheal epithelium (Akram et al., 2018) and NTHi infection of mouse middle ear epithelium (Mulay et al., 2016).

In addition, genetic approaches have been employed to generate murine targeted gene knockouts which enabled investigation of specific molecular pathways and genes involved in the host defence against bacterial and viral infections (Buer and Balling, 2003). Human BPIFA1 is produced and secreted by the upper respiratory tract epithelium and its orthologue is present in mice (Weston et al., 1999). Mouse *Bpifa1* knockouts have been generated and provide possibilities to study biological functions of BPIFA1. A role of BPIFA1 in airway host defence against microbial pathogens was investigated in the several *in vivo* and *in vitro* studies using *Bpifa1*$^{-/-}$ models (Akram et al., 2018, Jiang et al., 2013, Liu et al., 2013b, Mulay et al., 2016). Understanding the biological activity of mouse BPIFA1 in host defence against viral and bacterial infections could provide important insights in the understanding the functions of human BPIFA1.

My results in **Chapter 4** suggested that mouse BPIFA1 can bind to NTHi. Therefore, I undertook to investigate whether the loss of BPIFA1 in mTEC culture would lead to the greater susceptibility of the cells to NTHi infection. To fulfil this task, I used mTECs isolated from WT and *Bpifa1*$^{-/-}$ mice and exposed both types of mTEC cultures to NTHi. Host defence responses against this microbial pathogen were studied and compared.

5.2 Objectives of this chapter

The overarching aim of this chapter was to determine whether the loss of BPIFA1 in mTEC culture would lead to the enhanced susceptibility of the cells to NTHi infection. To examine this, the following objectives were required to be completed:

1. To isolate mTECs, from WT and *Bpifa1*$^{-/-}$ mice, and differentiate cells into the upper airway-like epithelium.
2. To assess the effect of loss of BPIFA1 on the susceptibility of mTEC culture to NTHi challenge.
3. To compare immune responses generated by WT and *Bpifa1*$^{-/-}$ mTECs to bacterial stimulus.

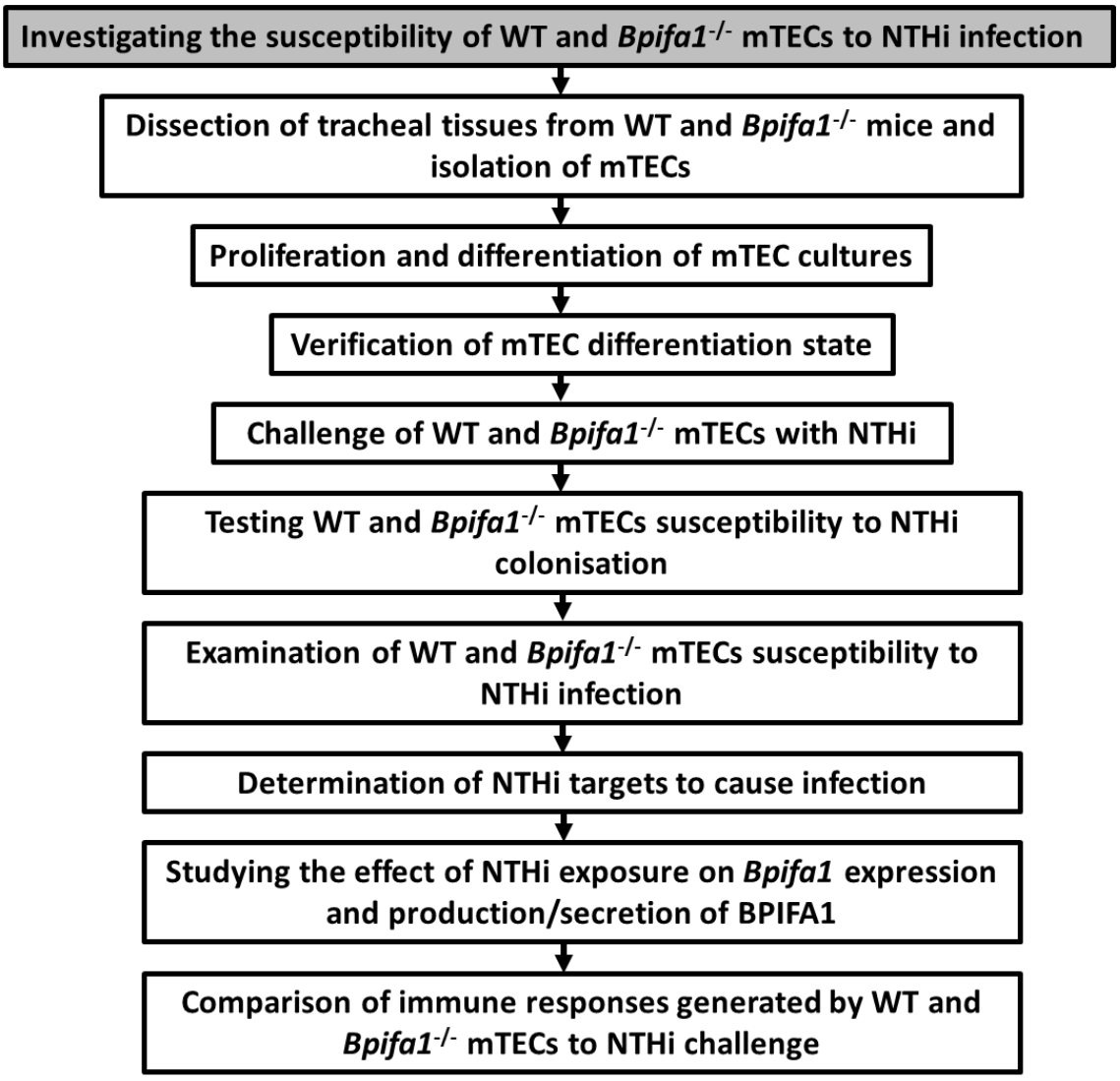

Figure 5.1: Study plan for this chapter.

5.3 Results

5.3.1 Characterisation of mTECs

Growth and morphology of mTECs were observed during submerged and ALI cultures. $3x10^5$ of cells were seeded per transwell and only a small number of cells were seen attached to the membrane three days after seeding (Figure 5.2 A-B). Epithelial cells appeared elongated, establishing a contact with nearby cells and forming epithelial cell islands. Cells proliferated in the submerged culture and formed a confluent monolayer within seven days of seeding (Figure 5.2 C-D). ALI was induced on confluence, revealing compactly arranged mTECs (Figure 5.2 E-F). After seven days of ALI culture, cells started changing morphology and movement of cilia was observed (Figure 5.2 G-H). Two major types of mTECs, flat non-ciliated cells and ciliated cells, were observed in the monolayer of cells on day fourteen of ALI culture (Figure 5.2 I-J). Morphology of non-ciliated cells was of a cobble-stone appearance which is a characteristic of upper airway epithelium. Well-defined cell boundaries were observed in differentiated mTECs by day fourteen. No apparent differences in the growth and morphology of the cells were identified in *Bpifa1*$^{-/-}$ mTECs compared to WT mTECs. Mouse tracheal fibroblasts were cultured to obtain a pure population of fibroblasts (Figure 5.2 K-L) and used as a negative control for gene expression and immunoblotting studies.

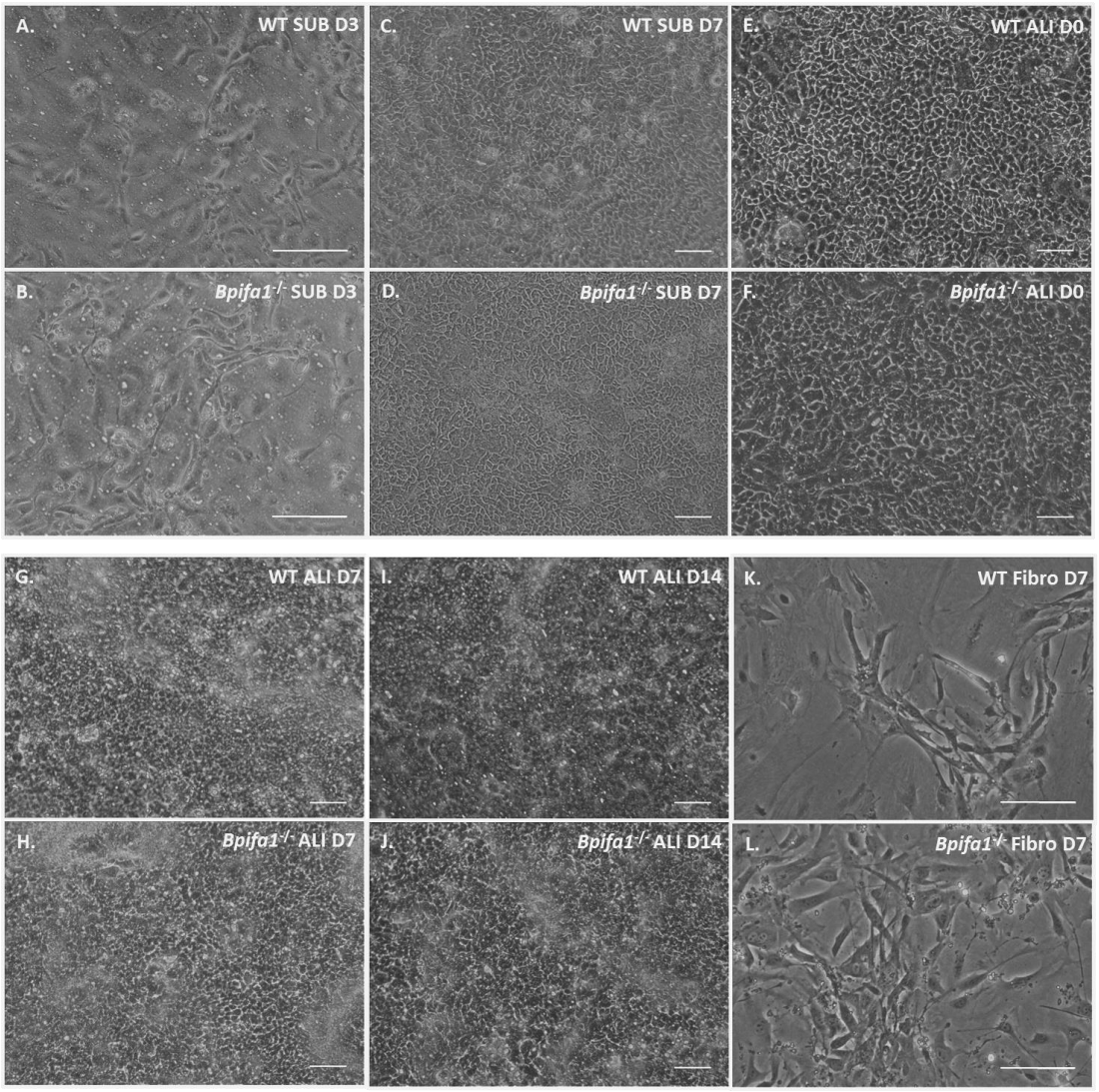

Figure 5.2: Characteristics of mTEC growth in the cell culture.

Phase contrast pictures demonstrating WT and *Bpifa1*$^{-/-}$ mTECs in the submerged and ALI culture conditions (**A-J**). mTECs in the submerged cell culture three days after seeding (**A-B**). Monolayers of WT and *Bpifa1*$^{-/-}$ cells in the submerged culture seven days after seeding (**C-D**). Cells compactly arranged after induction of ALI (**E-F**). Different types of cells observed, including ciliated cells on day 7 in ALI culture (**G-H**). WT and *Bpifa1*$^{-/-}$ mTECs in ALI culture on the day 14. No apparent differences observed (**I-J**). Growth of fibroblasts on the treated tissue culture dishes (**K-L**). Abbreviations: WT- wild-type; SUB – submerged; D – day; ALI – air liquid interface; Fibro – fibroblasts. Images were taken at 10x and 20x magnifications with light microscope (Nikon Eclipse TS100; scale bar: 100µm) and processed using ImageJ-win32.

5.3.2 Epithelial markers of mTEC cultures

The expression of cell-type specific genes was studied in the isolated mTECs and mTECs in the culture at day 0, and day 14 ALI using PCR. Isolated mouse fibroblast cDNA was used in PCR reactions as a negative control (Figure 5.3 A). The expression of *Oaz1* (ornithine decarboxylase antizyme 1), which is involved in the regulation of cell growth and proliferation in all types of tissues (Mangold, 2005), was assessed and used as a housekeeping gene in all PCR reactions. Expression of *Tekt1* (tektin 1 – ciliated cell marker) was detected in the isolated and ALI-day 14 culture differentiated WT and *Bpifa1*$^{-/-}$ mTECs, suggesting that ciliated cells were present in the cell populations. No expression of *Tekt1* was observed in ALI-day 0 cell cultures. Expression of *Bpifa1* (secretory cell marker) was strong in the isolated and ALI-day 14 culture differentiated WT mTECs compared to ALI-day 0 WT mTECs. The expression of *Ltf* (lactoferrin – secretory cell marker) was detected in the isolated mTECs and mTECs in the culture conditions at ALI-day 0, and ALI-day 14. This expression data verified that ALI-day 14 cells differentiated into the upper airway-like epithelium. In addition, western blotting showed that BPIFA1 was detected in apical secretion washes collected on ALI-day 7, 9, and 14, but not on the second day in ALI WT cell culture (Figure 5.3 B). No secreted BPIFA1 was detected in differentiated *Bpifa1*$^{-/-}$ mTECs (Figure 5.3 C).

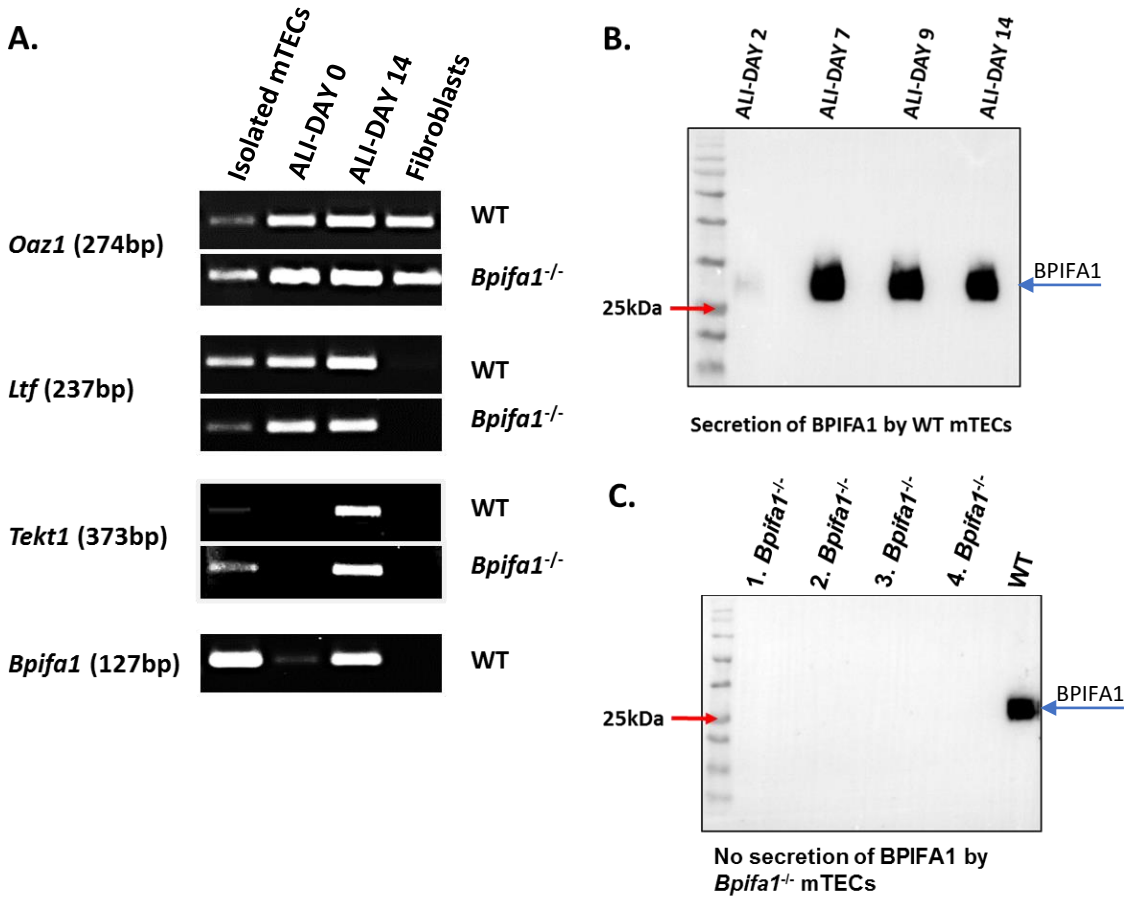

Figure 5.3: Epithelial markers of mTECs.
PCR results, showing the expression of upper airway epithelium specific genes in isolated mTECs and cultured mTECs at ALI-day 0, and ALI-day 14 (**A**). Identification of BPIFA1 secretion by differentiating WT mTECs using western blotting analysis. Data are representative of the results from two independent batches of WT mTECs (n=2) (**B**). The absence of secreted BPIFA1 in the apical secretion washes from four batches of ALI-day 14 differentiated *Bpifa1*$^{-/-}$ mTECs compared with the apical secretion wash from ALI-day 14 differentiated WT mTECs, as a positive control (**C**).

Unpublished RNA-Seq data from our laboratory showed that *Bpifa1* deletion did not cause alterations in gene profile of *Bpifa1*$^{-/-}$ mTECs compared to WT mTECs. RNA-Seq results demonstrated that *Bpifa1*$^{-/-}$ mTECs differed from WT mTECs by the expression of only four genes (excluding *Bpifa1*): *Prg4* (approx. three-fold increase), *Spp1* (approx. two-fold increase), *Wfdc18* (approx. two-fold increase), *Plekhs1* (approx. two-fold increase). *Prg4* encodes for proteoglycan 4 which has been reported to be involved in the protection of articulating joints by controlling the lubrication of the cartilage surfaces and regulating the synovial cell growth (Rhee et al., 2005). It has also been suggested

that proteoglycan 4 influences the proliferation of hematopoietic progenitor cells by controlling parathyroid hormone functions (Novince et al., 2011). *Spp1* encodes for osteopontin, which is found in all body fluids and in the proteinaceous matrix of mineralized tissues. It has been suggested that osteopontin may be important to cell-matrix interactions and immune responses (Denhardt et al., 2001, Manabe et al., 2008). Osteopontin is known as signalling molecule, having inflammatory and anti-inflammatory properties. It has been reported that osteopontin can influence the release of IL-12, IFN-γ, and IL-10 (Denhardt et al., 2001). Mouse *Wfdc18* gene codes for WAP four-disulphide core domain protein 18 and *Plekhs1* gene codes for pleckstrin homology domain-containing family S member 1 protein. Currently, both of these proteins are uncharacterised (UniProt, 2019a, UniProt, 2019b). However, the existing protein sequence analysis of WAP four-disulphide core domain protein 18 suggests that it may act as proteinase inhibitor (UniProt, 2019a).

5.3.3 Localisation of airway epithelium specific proteins in mTEC cultures

I used IFC microscopy to confirm a successful differentiation of WT mTECs into the upper airway-like epithelium. ALI-day 14 cells were processed and stained with IFC antibodies for BPIFA1 (Akram et al., 2018, Mulay et al., 2016, Musa et al., 2012), β-tubulin (Akram et al., 2018), and zonula occludens-1 (ZO-1) (Mulay et al., 2016); nuclei were counterstained with DAPI (Figure 5.4). I successfully detected BPIFA1 (marker of non-ciliated cells) (Figure 5.4 A) and β-tubulin (marker of ciliated cells; present in the cilia) (Figure 5.4 B) in WT mTEC cultures. ZO-1 staining was also positive in WT mTECs, suggesting establishment of cellular tight-junctions within the cell cultures (Figure 5.4 C). Tight-junction formation further confirmed successful differentiation of WT mTECs into the upper airway-like epithelium.

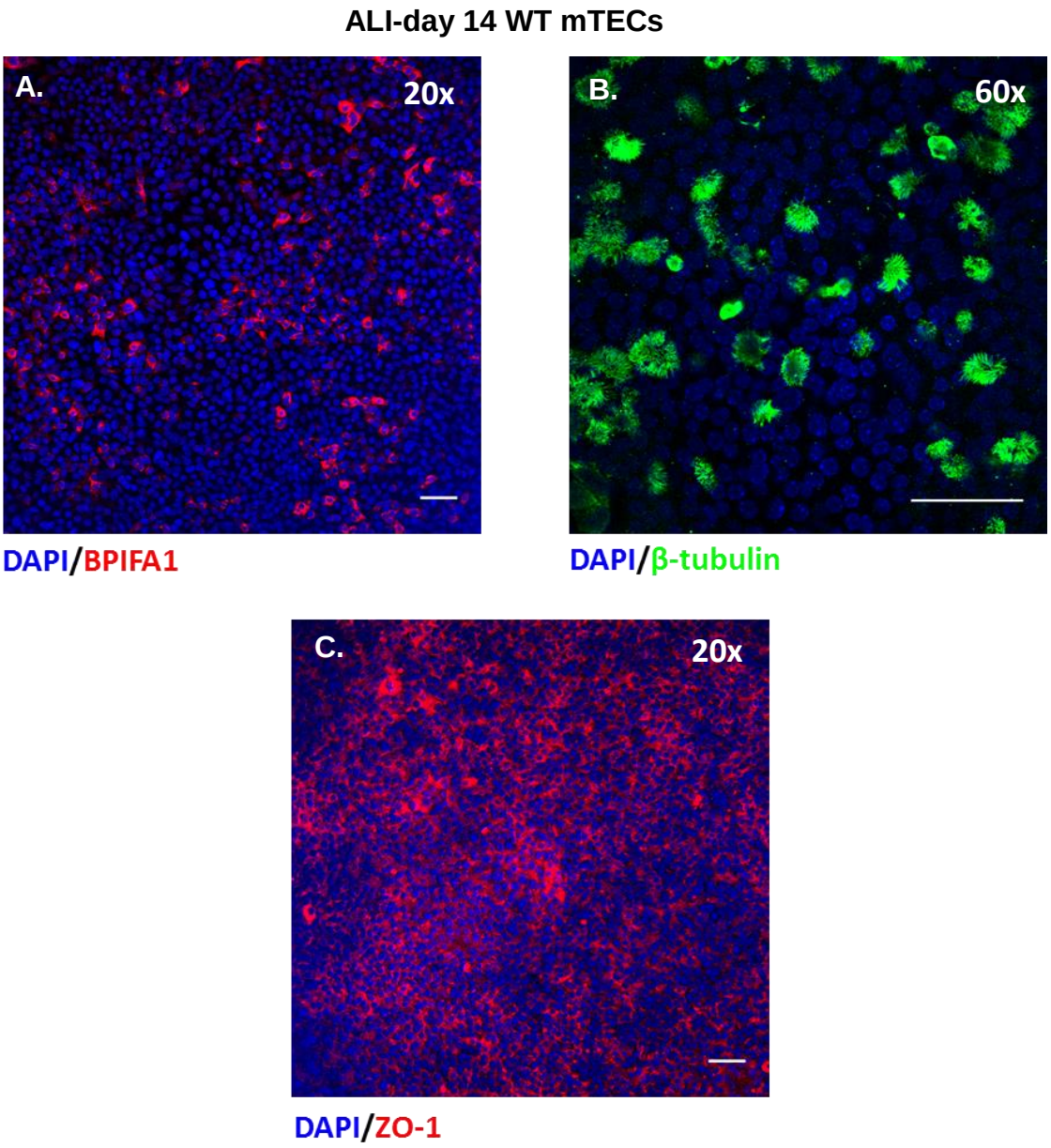

Figure 5.4: Differentiation of WT mTECs into the upper airway-like epithelium.
ALI-day 14 mTECs were processed and stained for BPIFA1 (**A**), β-tubulin (**B**), and ZO-1 (**C**). Nuclei were counterstained with DAPI. Detection of these epithelial markers confirmed a successful differentiation of mTECs. Images were processed using ImageJ-win32. Scale bar: 50µm. Data are representative of results from two independent batches of WT mTECs.

Differentiation of WT and *Bpifa1*$^{-/-}$ mTECs was previously validated in our laboratory (Figure 5.5 A-D). Data also demonstrated that BPIFA1 is not localised within ciliated cells and is present within non-ciliated cells (Akram et al., 2018) (Figure 5.5 A).

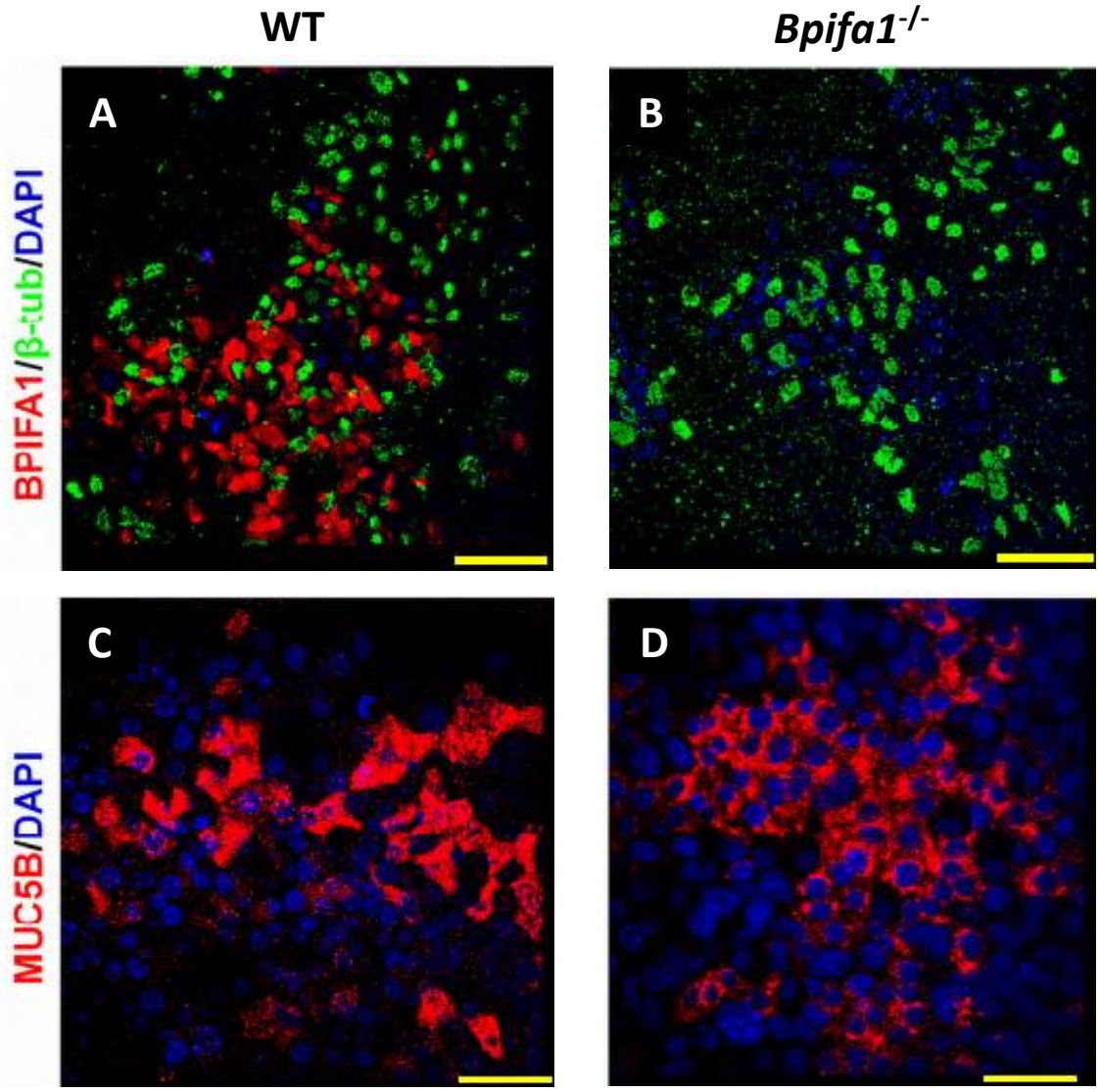

Figure 5.5: Validation of WT and *Bpifa1*$^{-/-}$ mTEC differentiation.
ALI-day 14 differentiated mTECs showed successful mTEC differentiation into the upper airway-like epithelium. Cells stained for β-tubulin, BPIFA1, and nuclei counterstained with DAPI (**A, B**). Cells stained for MUC5B and nuclei counterstained with DAPI (**C, D**). Images were re-used and modified with permission from (Akram et al., 2018), copyright 2017 Mucosal Immunology. Scale bar: 50µm.

5.3.4 NTHi colonises *Bpifa1*$^{-/-}$ mTECs more rapidly than WT mTECs

Results from bacterial pull-down assays suggested that mouse BPIFA1 bound to NTHi after short incubation periods. Consequently, I decided to expose mTECs to live NTHi to understand the effect of BPIFA1 loss on the susceptibility of mTECs to NTHi. I used live NTHi in my studies, as it has been suggested that live bacteria causes more biologically relevant immunostimulation of cells (King et al., 2008, Kirkham et al., 2013, Pizzutto et al., 2014). Differentiated mTECs isolated from WT and *Bpifa1*$^{-/-}$ mice were exposed to GFP-tagged NTHi at MOI of 200, 500, and 1000 for 1 hour and after exposure cells were incubated for 24, 48, and 72 hours. The sizes of bacterial inoculum and periods of cell exposure to NTHi were chosen based on the study by Mulay et al. (Mulay et al., 2016). Before washing of cell apical surfaces and fixation of cells, NTHi-exposed mTECs were imaged using IF microscope at 24, 48, and 72 hours post-infection (hpi) to observe the ability of NTHi to colonise mTECs. Bacterial colonisation was visible in WT (Figure 5.6 A1) and *Bpifa1*$^{-/-}$ (Figure 5.6 D1) mTEC cultures exposed to GFP-tagged NTHi at MOI-200 at 72 hpi, however the intensity of NTHi colonisation appeared to be greater in *Bpifa1*$^{-/-}$ mTECs. As expected, NTHi colonisation appeared higher in mTEC cultures exposed to NTHi at MOI-500 (Figure 5.6 B1, E1) and MOI-1000 (Figure 5.6 C1, F1) compared to mTECs exposed to NTHi at MOI-200 (Figure 5.6 A1, D1). Bacterial colonisation did not cause a substantial damaged to WT and *Bpifa1*$^{-/-}$ mTEC monolayers as no development of holes/gaps in mTEC cultures were observed even after 72 hours post-exposure (Figure 5.6 A2-F2).

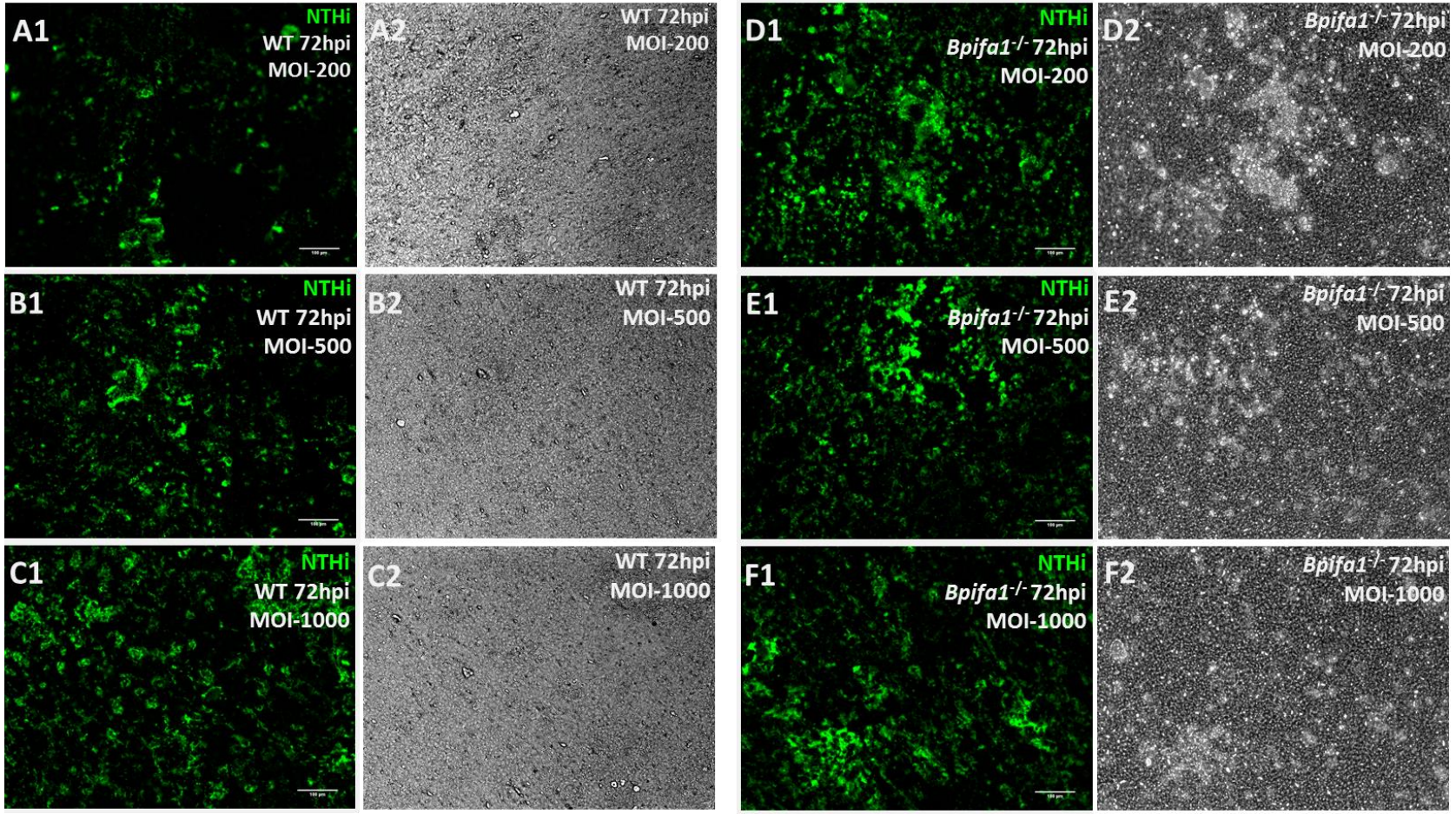

Figure 5.6: NTHi colonisation did not cause a substantial damage to the monolayer of mTECs.

IF images, showing GFP-tagged NTHi (green) colonisation at 72hpi in day-14 ALI WT (**A1**, **B1**, **C1**) and *Bpifa1*$^{-/-}$ (**D1**, **E1**, **F1**) mTECs with the corresponding phase contrast images of WT cell monolayers (**A2, B2, C2**) and *Bpifa1*$^{-/-}$ cell monolayers (**D2, E2, F2**). Scale bar: 100µm. Images were processed using ImageJ-win32. Data are representative of the results from three independent batches of mTECs (n=3).

After observing a potential difference in the bacterial colonisation intensity between WT and *Bpifa1*$^{-/-}$ mTECs cultured in ALI conditions, I investigated whether WT mTECs are more resistant to NTHi colonisation than *Bpifa1*$^{-/-}$ mTECs by measuring integrated intensity of green fluorescence in 3 batches of WT and *Bpifa1*$^{-/-}$ mTECs exposed to GFP-tagged NTHi at MOI-200, MOI-500, and MOI-1000. Intensity of green fluorescence was measured of six fields on every membrane using ImageJ-win32 program (Figure 2.4). IF images of mTECs exposed to NTHi at MOI-200 suggested that WT mTECs are more resistant to NTHi colonisation than *Bpifa1*$^{-/-}$ mTECs (Figure 5.7 A-F). The values of green fluorescence integrated intensity were measured and analysed using two-way ANOVA with Sidak multiple comparison tests. Results showed that there was no statistically significant difference in the bacterial colonisation level between WT and *Bpifa1*$^{-/-}$ mTECs at all time points (24hpi: p=0.32; 48hpi: p=0.14; 72hpi: p=0.27) (Figure 5.7 G). However, a trend towards an increased NTHi colonisation in *Bpifa1*$^{-/-}$ mTECs compared to WT mTECs was observed (Figure 5.7 G). Data showed a great variation in NTHi colonisation between individual batches of mTECs. Two-way ANOVA also indicated a clear progression in the bacterial colonisation of NTHi-exposed mTECs from 24hpi to 72hpi (p=0.005).

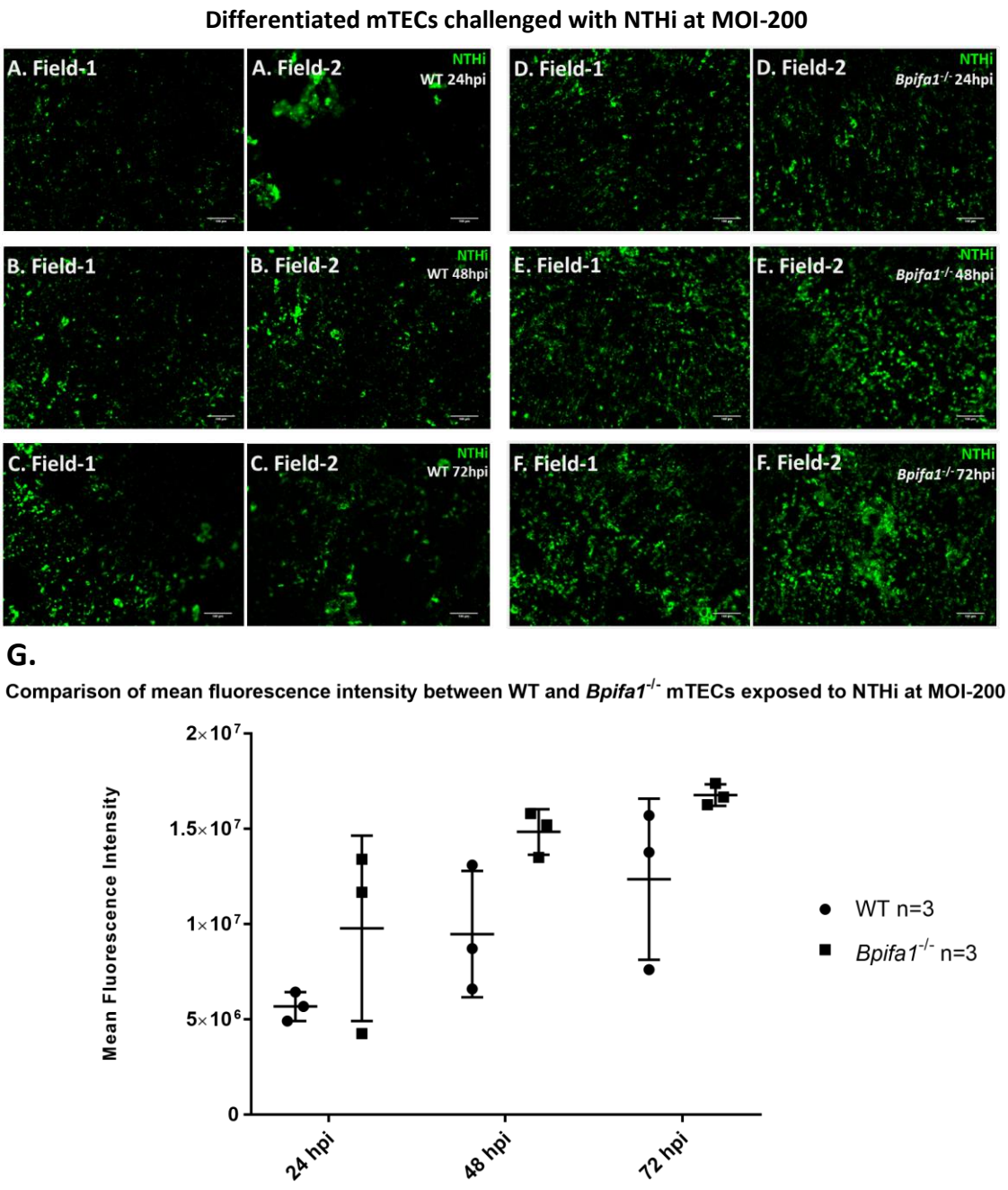

Figure 5.7: Progression of bacterial colonisation in mTECs exposed to NTHi at MOI-200.

IF images, showing the progression of NTHi (GFP-tagged, fluorescent green) colonisation in day-14 ALI WT (**A**, **B**, **C**) and *Bpifa1*$^{-/-}$ (**D**, **E**, **F**) mTEC cultures at 24hpi (**A**, **D**), 48hpi (**B**, **E**), and 72hpi (**C**, **F**). Each panel demonstrates 2 fields at 20x magnification. Scale bar: 100µm. Images were processed using ImageJ-win32. The mean green fluorescence intensity in WT and *Bpifa1*$^{-/-}$ mTEC cultures exposed to NTHi was quantified using 20x magnification IF images. The difference in the mean colonisation intensity (n=3) (measured using ImageJ-win32) between WT and *Bpifa1*$^{-/-}$ mTECs was not statistically significant. Two-way ANOVA with Sidak multiple comparison tests were used to analyse the data (**G**) mean ± SD, n=3 individual batches of mTEC culture. Each black dot and black square in the graphs represent an independent batch of mTEC culture.

Subsequently, I analysed the intensity pattern of NTHi colonisation in mTEC cultures exposed to NTHi at MOI-500. IF images of bacterial-exposed mTECs again suggested that WT mTECs are more resistant to NTHi colonisation than *Bpifa1*$^{-/-}$ mTECs (Figure 5.8 A-F). Again, no statistically significant difference in the bacterial colonisation level between WT and *Bpifa1*$^{-/-}$ mTECs were detected at any time points (24hpi: p=0.44; 48hpi: p=0.40; 72hpi: p=0.45) (Figure 5.8 G). However, a trend towards an increased NTHi colonisation in *Bpifa1*$^{-/-}$ mTECs compared to WT mTECs was again observed (Figure 5.8 G). Two-way ANOVA also indicated a clear progression in the bacterial colonisation of NTHi-exposed mTECs from 24hpi to 72hpi (p=0.003).

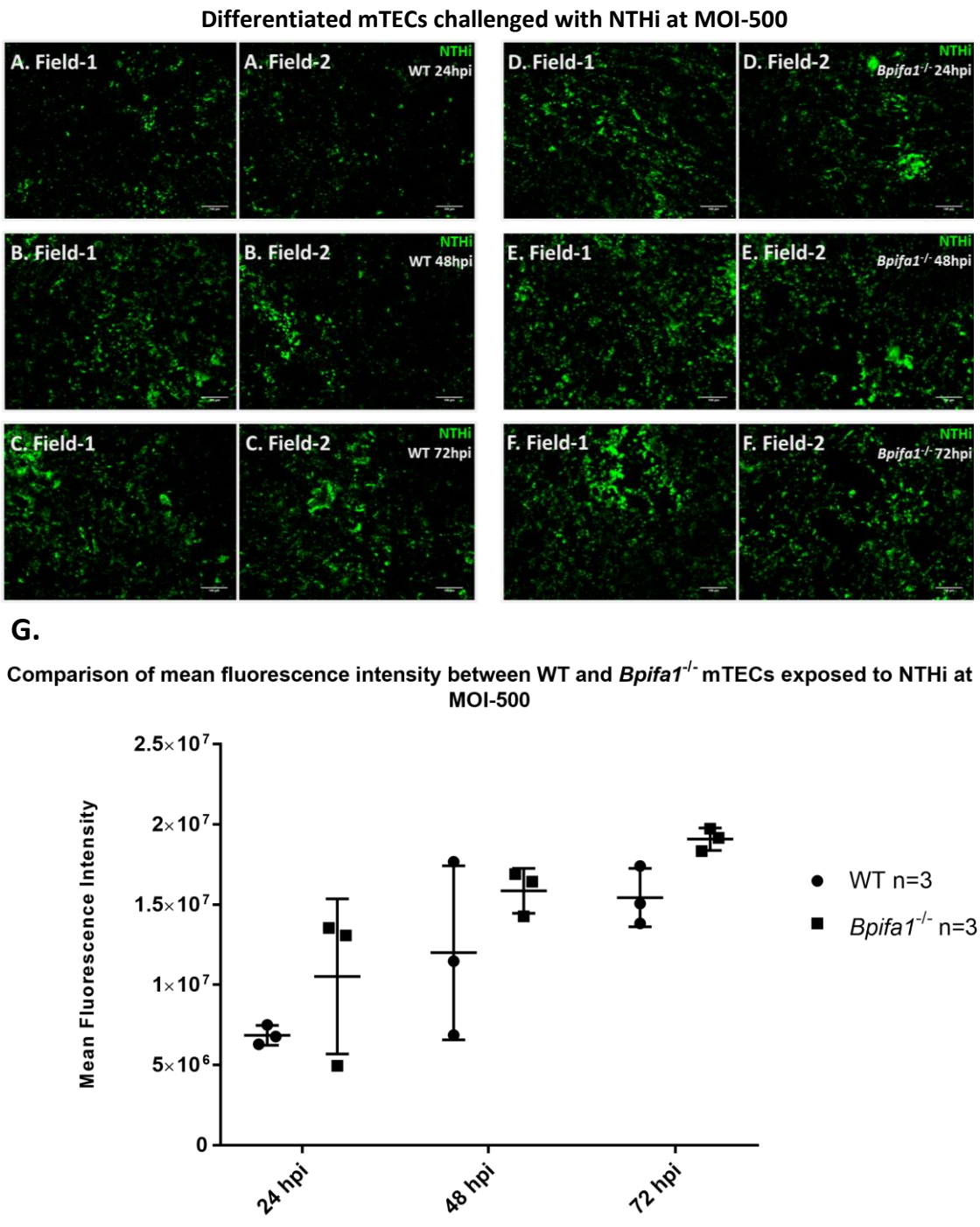

Figure 5.8: Progression of bacterial colonisation in mTECs exposed to NTHi at MOI-500.
IF images, showing the progression of NTHi (GFP-tagged, fluorescent green) colonisation in day-14 ALI WT (**A**, **B**, **C**) and *Bpifa1*$^{-/-}$ (**D**, **E**, **F**) mTEC cultures at 24hpi (**A**, **D**), 48hpi (**B**, **E**), and 72hpi (**C**, **F**). Each panel demonstrates 2 fields at 20x magnification. Scale bar: 100µm. Images were processed using ImageJ-win32. The mean green fluorescence intensity in WT and *Bpifa1*$^{-/-}$ mTEC cultures exposed to NTHi was quantified using 20x magnification IF images. The difference in the mean colonisation intensity (n=3) (measured using ImageJ-win32) between WT and *Bpifa1*$^{-/-}$ mTECs was not statistically significant. Two-way ANOVA with Sidak multiple comparison tests were used to analyse the data (**G**) mean ± SD, n=3 individual batches of mTEC culture. Each black dot and black square in the graphs represent an independent batch of mTEC culture.

Bacterial colonisation intensity of mTECs exposed to NTHi at MOI-1000 at 24hpi, 48hpi, and 72hpi was also investigated. Again, IF images of bacterial-exposed mTECs appeared to suggest that NTHi colonisation was greater in *Bpifa1*$^{-/-}$ mTECs than in WT mTECs (Figure 5.9 A-F). However, this difference between two phenotypes was not that clear as it may have been in mTECs exposed to NTHi at MOI-200 (Figure 5.7 A-F) and MOI-500 (Figure 5.8 A-F). No statistically significant difference in the bacterial colonisation level between WT and *Bpifa1*$^{-/-}$ mTECs was detected (24hpi: p=0.78; 48hpi: p=0.53; 72hpi: p=0.83) (Figure 5.9 G). However, a trend towards an increased NTHi colonisation in *Bpifa1*$^{-/-}$ mTECs compared to WT mTECs was again observed at all time points (Figure 5.9 G). Two-way ANOVA indicated a clear progression in the bacterial colonisation of NTHi-exposed mTECs from 24hpi to 72hpi (p=0.001).

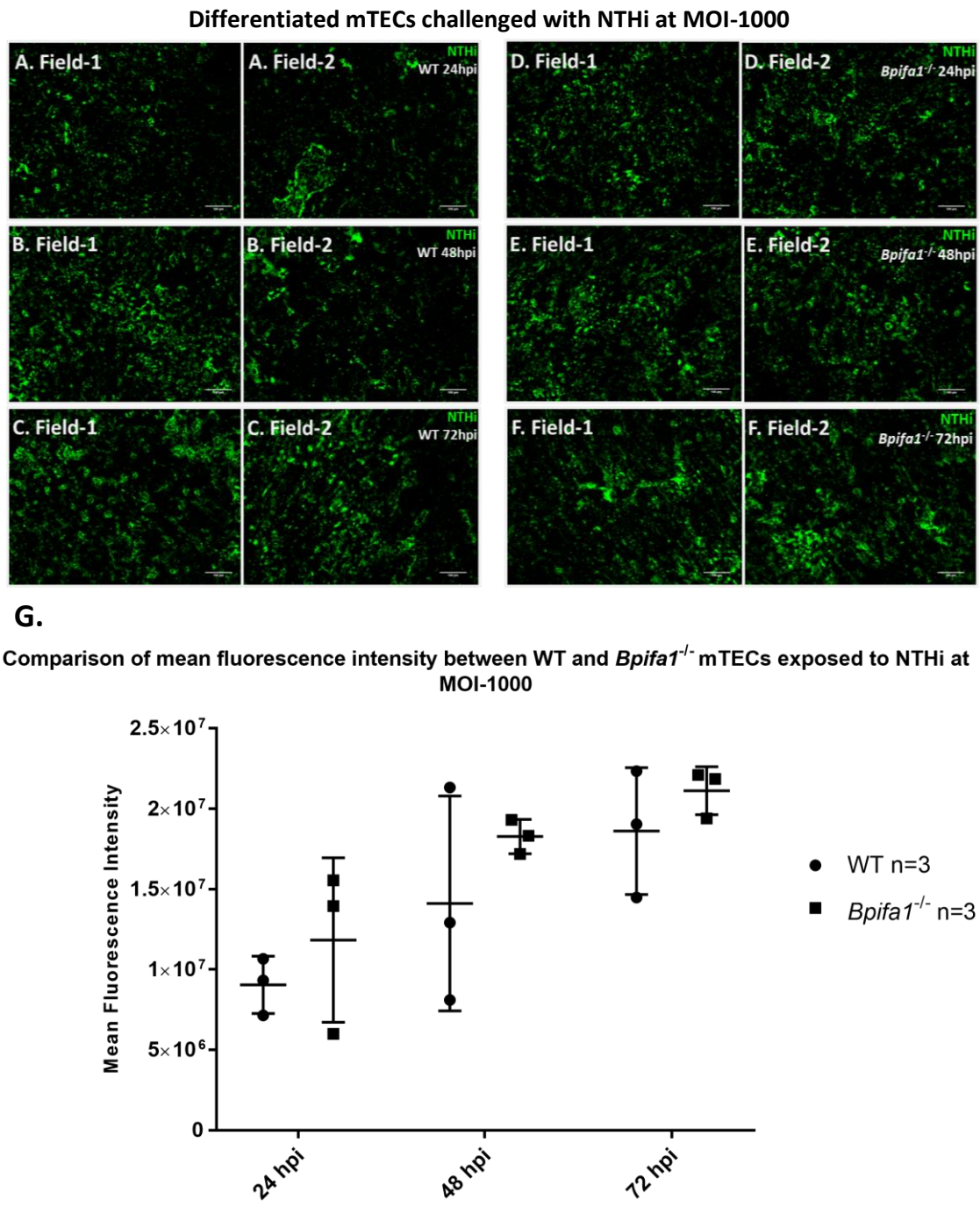

Figure 5.9: Progression of bacterial colonisation in mTECs exposed to NTHi at MOI-1000.
IF images, showing the progression of NTHi (GFP-tagged, fluorescent green) colonisation in day-14 ALI WT (**A**, **B**, **C**) and *Bpifa1*$^{-/-}$ (**D**, **E**, **F**) mTEC cultures at 24hpi (**A**, **D**), 48hpi (**B**, **E**), and 72hpi (**C**, **F**). Each panel demonstrates 2 fields at 20x magnification. Scale bar: 100µm. Images were processed using ImageJ-win32. The mean green fluorescence intensity in WT and *Bpifa1*$^{-/-}$ mTEC cultures exposed to NTHi was quantified using 20x magnification IF images. The difference in the mean colonisation intensity (n=3) (measured using ImageJ-win32) between WT and *Bpifa1*$^{-/-}$ mTECs was not statistically significant. Two-way ANOVA with Sidak multiple comparison tests were used to analyse the data (**G**); mean ± SD, n=3 individual batches of mTEC culture. Each black dot and black square in the graphs represent an independent batch of mTEC culture.

5.3.5 mTECs exhibit resistance to NTHi infection

After images of NTHi colonisation in WT and *Bpifa1*$^{-/-}$ mTECs were taken, cells were washed to remove loosely associated bacteria with the apical surface of cells and fixed for immunofluorescent staining to evaluate what I considered to be bacterial infection. Four central fields of the filter were imaged using the confocal microscope at 10x magnification at 72hrs post-exposure. No clear difference in the intensity of NTHi infection between WT and *Bpifa1*$^{-/-}$ mTECs was observed (Figure 5.10 A-F). The data also suggest that deletion of *Bpifa1* did not cause sudden NTHi infection of the cells. A seemingly inverse response of mTECs to MOI was also observed as the intensity of intracellular bacterial infection appeared to increase in the direction of MOI-1000 to MOI-200. Analysis also suggested that mTECs exhibit resistance to NTHi infection as only a small number of fields were observed to be positive for NTHi infection at 72hrs post-exposure.

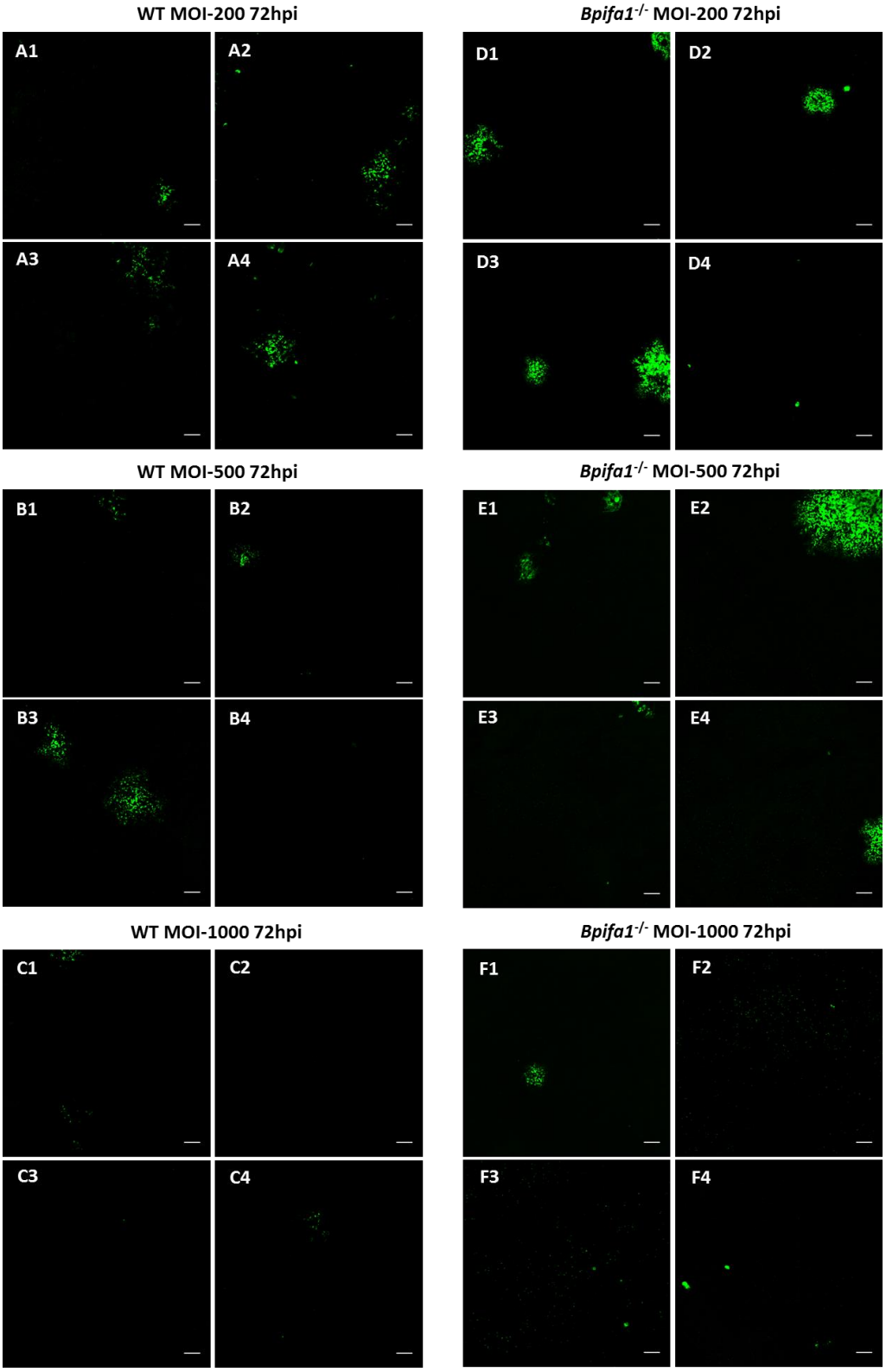

Figure 5.10: NTHi caused a patchy infection of WT and *Bpifa1*$^{-/-}$ mTECs.
IFC images, showing patchy NTHi infection in WT mTEC culture exposed to NTHi at MOI-200 (**A1-A4**), MOI-500 (**B1-B4**), and MOI-1000 (**C1-C4**). Patchy pattern of NTHi infection also demonstrated in IFC images of *Bpifa1*$^{-/-}$ mTEC culture exposed to NTHi at MOI-200 (**D1-D4**), MOI-500 (**E1-E4**), and MOI-1000 (**F1-F4**). Images of four central fields of the filter were taken at 72hpi using confocal microscope at 10x magnification. Scale bar: 100µm. Data are representative of the results from four independent batches of WT and *Bpifa1*$^{-/-}$ mTECs.

I next analysed the apical secretion washes from NTHi exposure experiments to investigate if increasing amounts of NTHi were present over time. As the NTHi used in the challenge studies was GFP tagged, I used an anti-GFP antibody as a surrogate to detect NTHi in washes. Results showed the presence of NTHi in all apical secretion washes collected at 48hpi and 72hpi (Figure 5.11). Some NTHi also appeared to be present in the washes collected from *Bpifa1*$^{-/-}$ mTECs at 24hpi but not in the washes collected from WT mTECs at 24hpi. The data also suggested that the number of NTHi increased over time as the intensity of band was greater in apical washes collected at the later time points. These results suggest that the majority of bacteria observed on the live cells were loosely associated with the surface and not causing intracellular infection of mTECs.

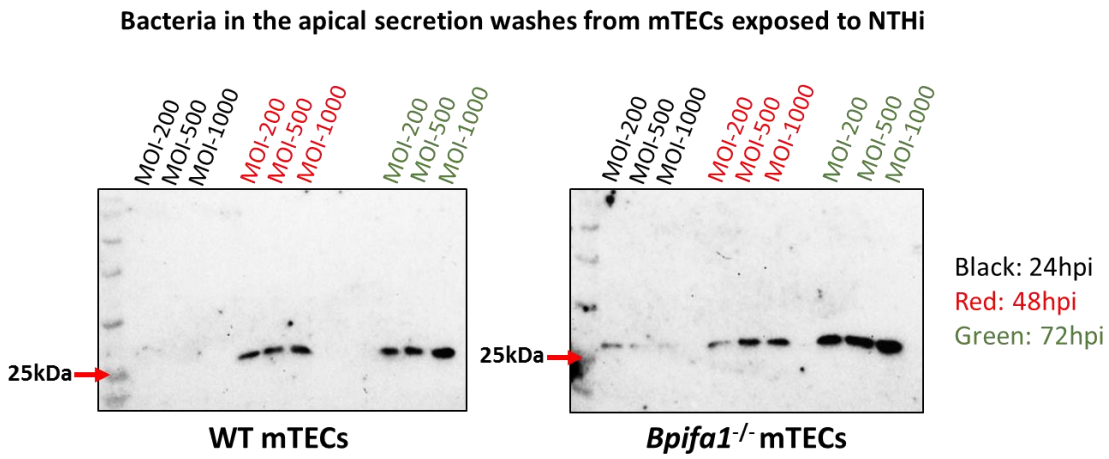

Figure 5.11: Bacteria in the apical secretion washes from mTECs exposed to NTHi.
Results of western blotting, demonstrating the presence of NTHi in the apical secretion washes from WT and *Bpifa1*$^{-/-}$ mTECs. Data are representative of four independent batches of WT and *Bpifa1*$^{-/-}$ mTEC cultures (n=4). Both membranes were exposed for the same length of time.

Subsequently, I analysed the western blotting results using densitometry and two-way ANOVA with Sidak multiple comparison tests to determine if bacterial colonisation differed between WT and *Bpifa1*$^{-/-}$ mTECs. No statistically significant difference in the bacterial colonisation between two phenotypes of mTECs were detected (Figure 5.12 A-C). However, there appeared to be a trend towards an increased amount of NTHi in the apical washes from *Bpifa1*$^{-/-}$ mTECs compared to WT mTECs, with exception of this trend being opposite at 48hpi with mTECs exposed to NTHi at MOI-500 (Figure 5.12 B) and MOI-1000 (Figure 5.12 C). In addition, two-way ANOVA indicated a clear progression in the bacterial colonisation of mTECs from 24hpi to 72hpi (MOI-200: $p<0.0001$; MOI-500: $p<0.0001$; MOI-1000: $p=0.0004$). The results from this analysis are similar to the results obtained from the analysis of IF images using ImageJ-win32 (Figure 5.7-5.9).

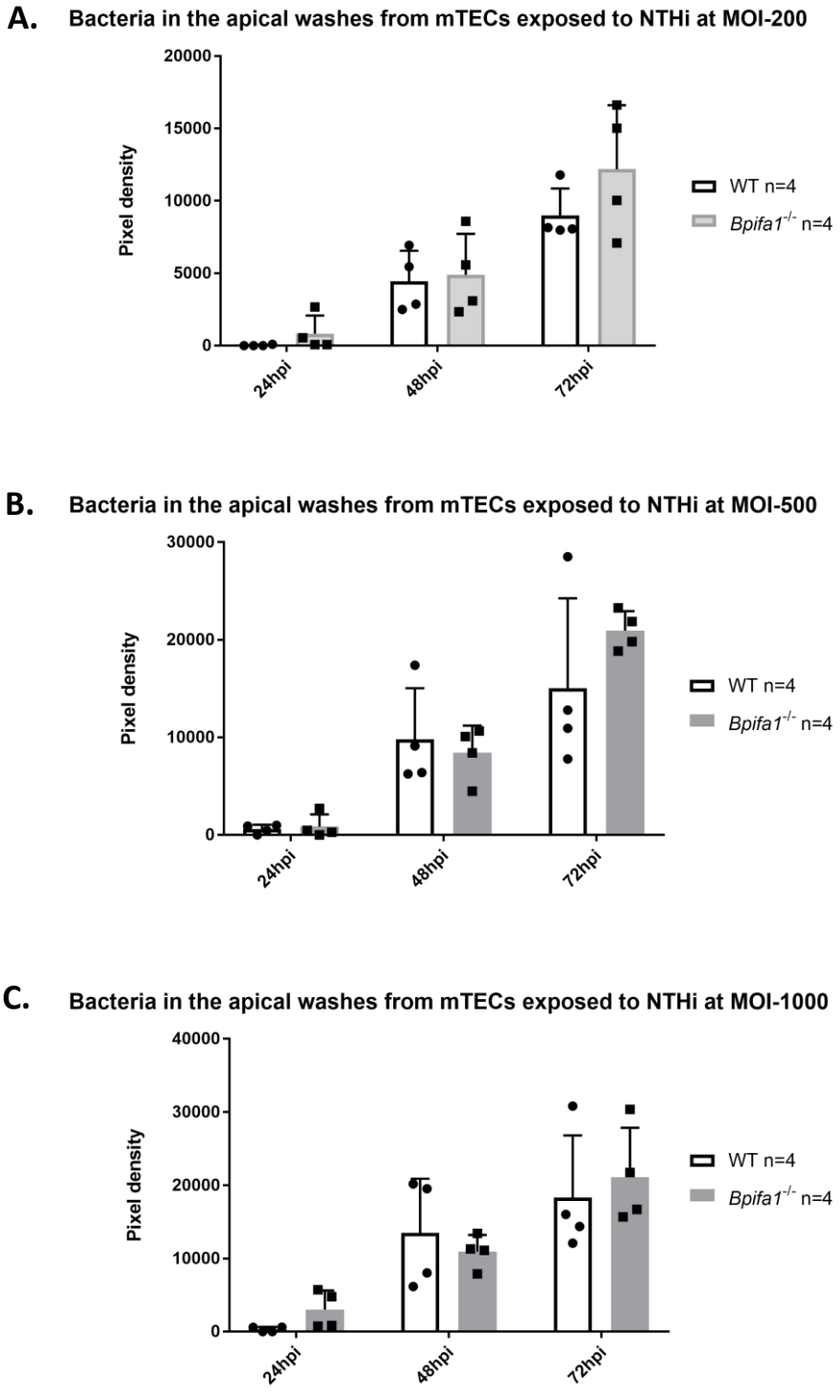

Figure 5.12: Bacteria in the apical washes from mTECs exposed to NTHi.

NTHi in the apical washes from mTECs exposed to NTHi at MOI-200 (**A**), MOI-500 (**B**), and MOI-1000 (**C**). Each black dot and black square in the graphs represent an independent batch of mTEC culture. Pixel density values obtained from densitometry analysis of western blotting membranes were analysed using two-way ANOVA with Sidak multiple comparison tests; mean ± SD, n=4 individual batches of mTEC culture.

5.3.6 NTHi associates with multiple cell types of mouse tracheal epithelium

I next imaged fields of WT and *Bpifa1*$^{-/-}$ mTECs positive for NTHi infection and analysed IFC images using ImageJ-win32 program, aiming to determine the type of cells NTHi associates with. First of all, I analysed NTHi-exposed mTECs stained for FOXJ1 and β-tubulin (markers of ciliated cells: FOXJ1 – nuclear marker of ciliated cells; β-tubulin – marker of cilia) using confocal microscopy and ImageJ-win32. Results appeared to suggest that NTHi can associate with ciliated cells as some co-localisation between GFP-tagged NTHi and ciliated cells stained for FOXJ1 (Figure 5.13 A-B) and β-tubulin (Figure 5.14 A-B) was observed. However, this association was not specific as bacteria was also associated with non-FOXJ1 expressing cells. No clear differences were observed in the ability of NTHi to associate with WT and *Bpifa1*$^{-/-}$ cells.

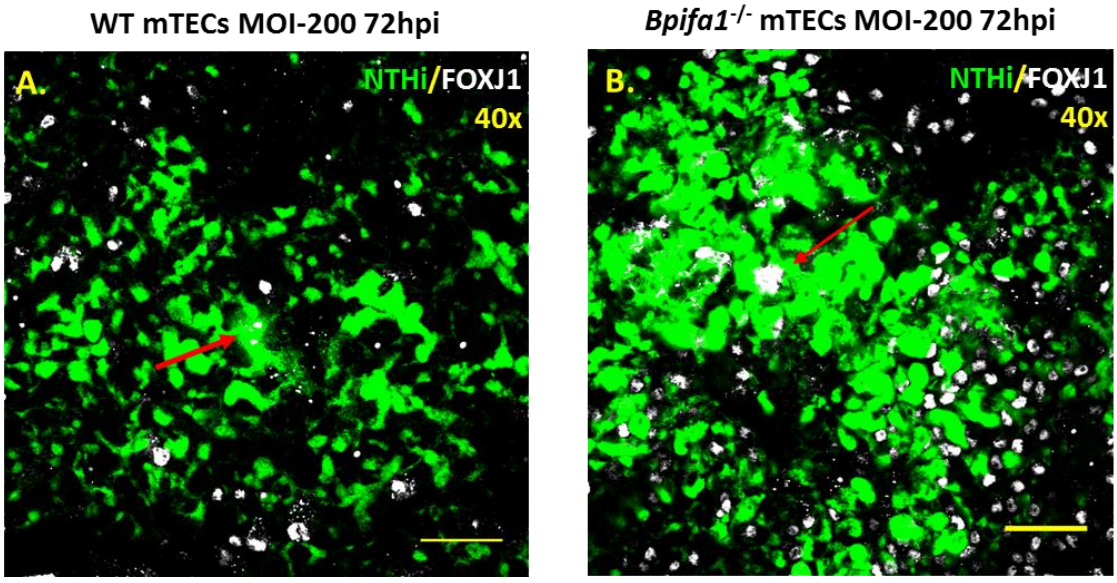

Figure 5.13: Association of GFP-tagged NTHi with ciliated cells of mTEC culture.
IFC images of WT mTECs (**A**) and *Bpifa1*$^{-/-}$ mTECs (**B**) exposed to NTHi at MOI-200, showing the ability of NTHi (GFP – green) to associate with ciliated cells (FOXJ1 – white) at 72hpi. NTHi association with ciliated cells is demonstrated with the red arrows. Scale bar: 50μm. Data are representative of two independent batches of cell culture (n=2).

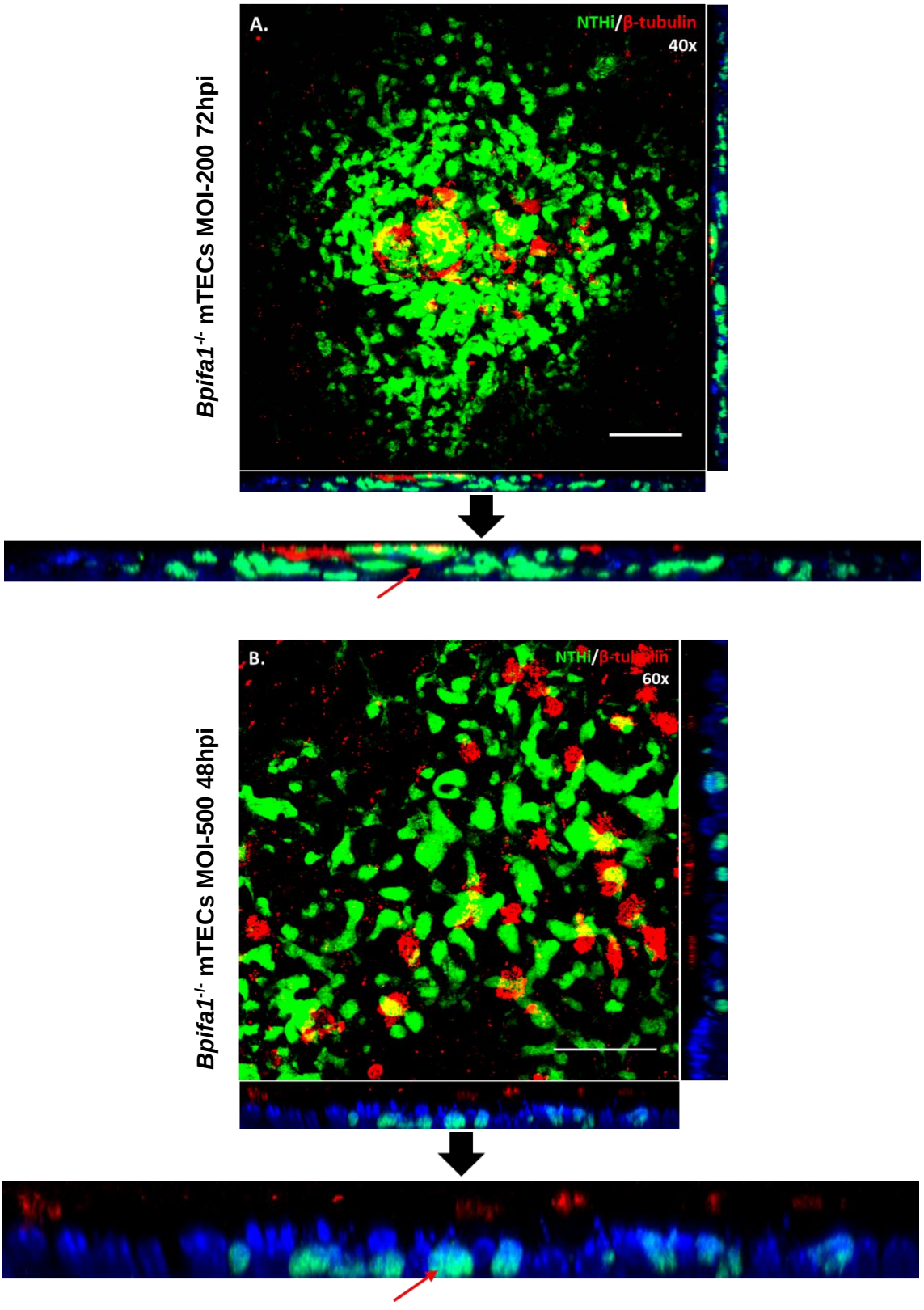

Figure 5.14: Association of GFP-tagged NTHi with ciliated cells of *Bpifa1*$^{-/-}$ mTEC culture.
IFC images of *Bpifa1*$^{-/-}$ mTECs exposed to NTHi at MOI-200 (**A**) and MOI-500 (**B**), showing the ability of NTHi (GFP – green) to associate with the cilia of ciliated cells (β-tubulin – red) at 48 and 72hpi. Z-stack images of cross sections of mTECs demonstrating the internalisation of bacteria within mouse tracheal epithelial cells. Examples of internalised bacteria are highlighted with red arrows in enlarged sections of Z-stacks. Co-localisation between NTHi and β-tubulin is seen in yellow. Data are representative of two independent batches of cell culture (n=2). Scale bar: 50µm.

Secondly, I aimed to determine whether NTHi associated with MUC5B-positive cells. I stained NTHi-exposed mTECs for MUC5B (a marker of the goblet cells) and analysed the samples using confocal microscopy and ImageJ-win32. Results suggested that NTHi can associate with goblet cells in *Bpifa1*$^{-/-}$ (Figure 5.15 A-B) and WT (Figure 5.16 A-C) cultures as some co-localisation between GFP-tagged NTHi and MUC5B-positive cells was observed. However, this association of NTHi with MUC5B-positive cells was not specific as NTHi was also associated with some non-MUC5B positive cells. No clear differences were observed in the ability of NTHi to associate with WT and *Bpifa1*$^{-/-}$ goblet cells. Having IFC images, showing a greater staining for MUC5B in NTHi-exposed *Bpifa1*$^{-/-}$ mTECs compared to NTHi-exposed WT mTECs, analysis of MUC5B staining intensity was also performed. Results showed that increased staining of MUC5B was not a specific feature of *Bpifa1*$^{-/-}$ cells but was a result of cell batch-to-batch variation (Appendix II: S9-10).

Therefore, overall analysis of IFC images suggested that NTHi was capable of associating with the multiple epithelial cell types of mouse tracheal epithelium and did not exhibit specific preference for certain type of cells.

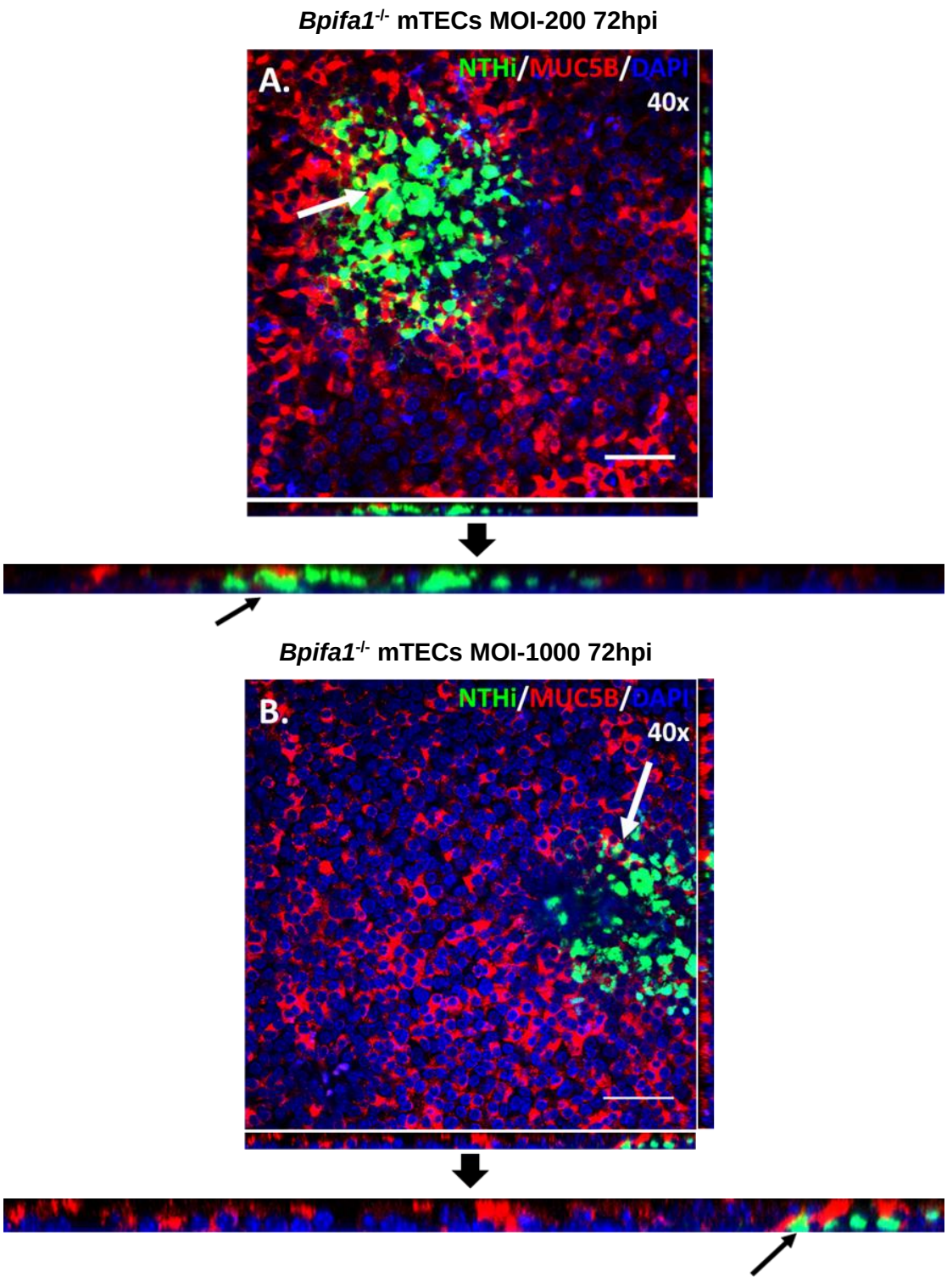

Figure 5.15: Association of GFP-tagged NTHi with *Bpifa1*$^{-/-}$ MUC5B-positive cells (goblet cells).

IFC images of *Bpifa1*$^{-/-}$ mTECs exposed to NTHi at MOI-200 (**A**) and MOI-1000 (**B**), showing the ability of GFP-tagged NTHi (GFP – green) to associate with MUC5B-positive cells (MUC5B – red) at 72hpi. Examples of NTHi association with goblet cells are demonstrated with white arrows. Z-stack images of cross sections of mTECs, suggesting NTHi internalisation within mouse tracheal epithelial cells (examples demonstrated with black arrows in enlarged sections of Z-stacks). Data are representative of two independent batches of *Bpifa1*$^{-/-}$ mTECs (n=2). Scale bar: 50µm.

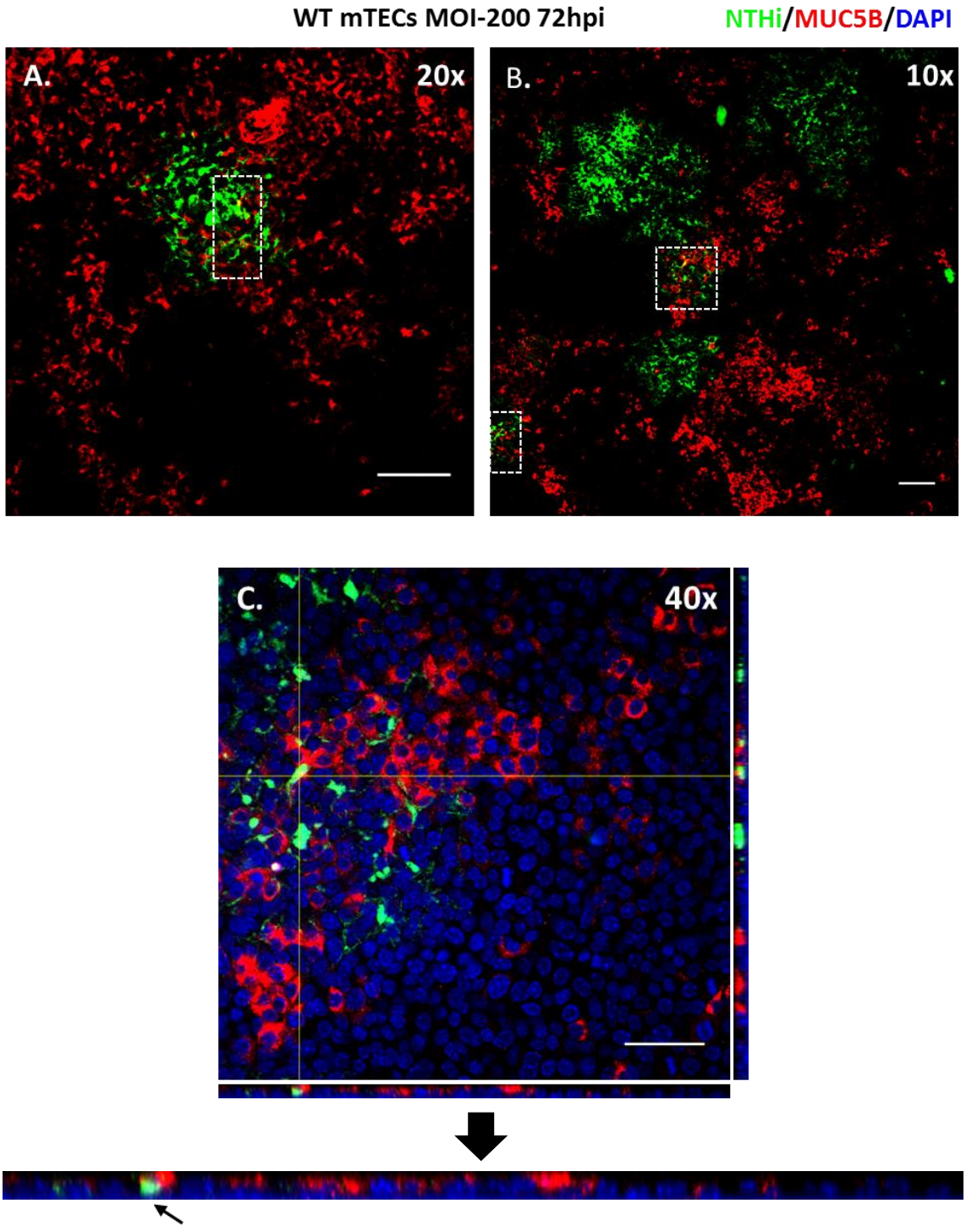

Figure 5.16: Association of GFP-tagged NTHi with WT MUC5B-positive cells (goblet cells). IFC images of WT mTECs exposed to NTHi at MOI-200 (**A-C**), showing the ability of GFP-tagged NTHi (GFP – green) to associate with MUC5B-positive cells (MUC5B – red) at 72hpi. Examples of NTHi association with MUC5B-positive cells are highlighted in white rectangles (**A-B**). Z-stack images of cross section of WT mTECs (**C**), suggesting NTHi internalisation within mouse tracheal epithelial cells (example demonstrated with black arrow in the enlarged section of Z-stack). Data are representative of two independent batches of WT mTEC cultures (n=2). Scale bar: **A-B**: 100µm; **C**: 50µm.

5.3.7 NTHi exposure of mTECs affects cellular tight-junctions

I next investigated whether NTHi was capable of associating with and disrupting cellular tight-junctions. I stained NTHi-exposed mTECs for ZO-1 (marker of cellular tight-junctions) and analysed samples using confocal microscopy and ImageJ-win32 program. No apparent specific association of NTHi with cellular tight-junctions was observed (Figure 5.17 A-D). However, analysis of IFC Z-stacks suggested that exposure of mTECs to NTHi caused a disruption of cellular tight-junctions as bacteria was observed to get into the spaces between the cells and reach the bottom layer of the cells (Figure 5.17 A-D). Damage to cellular tight-junctions caused by NTHi infection of mTECs was confirmed by analysis of IFC images using a staining for ZO-1 (Figure 5.18 A-B).

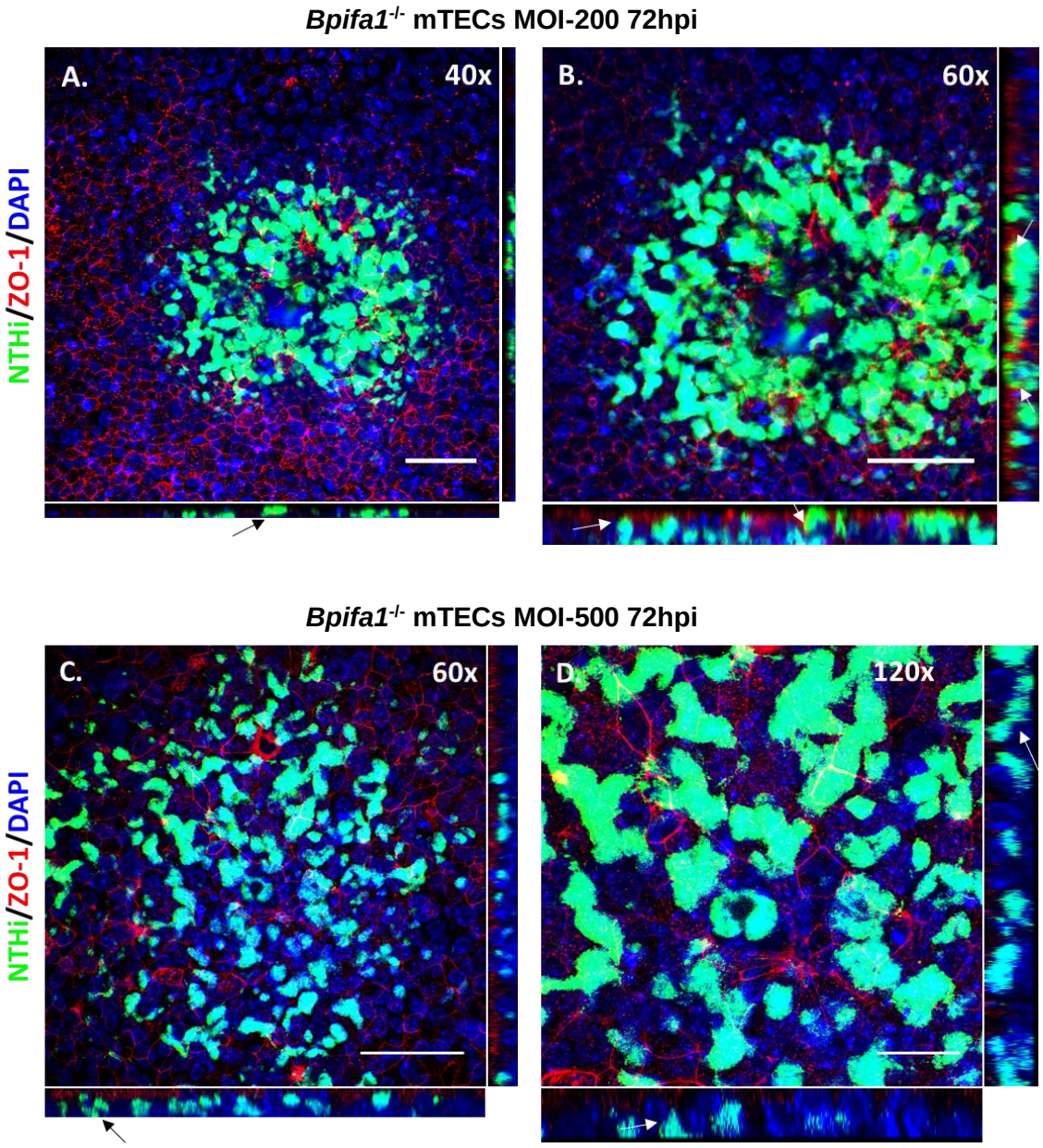

Figure 5.17: NTHi did not show association with cellular tight-junctions, stained for ZO-1. IFC images of *Bpifa1*$^{-/-}$ mTECs exposed to NTHi at MOI-200 (**A-B**) and MOI-500 (**D-E**), showing no specific association of GFP-tagged NTHi (GFP – green) with cellular tight-junctions (ZO-1 – red) at 72hpi. Z-stack images of cross sections of mTECs, demonstrating NTHi between the spaces of cells and at the bottom layer of cells. Examples of NTHi present within the gaps of cells and at the bottom layer of cells are demonstrated with black and white arrows. Data are representative of two independent batches of WT mTEC cultures (n=2). Scale bar: 50µm.

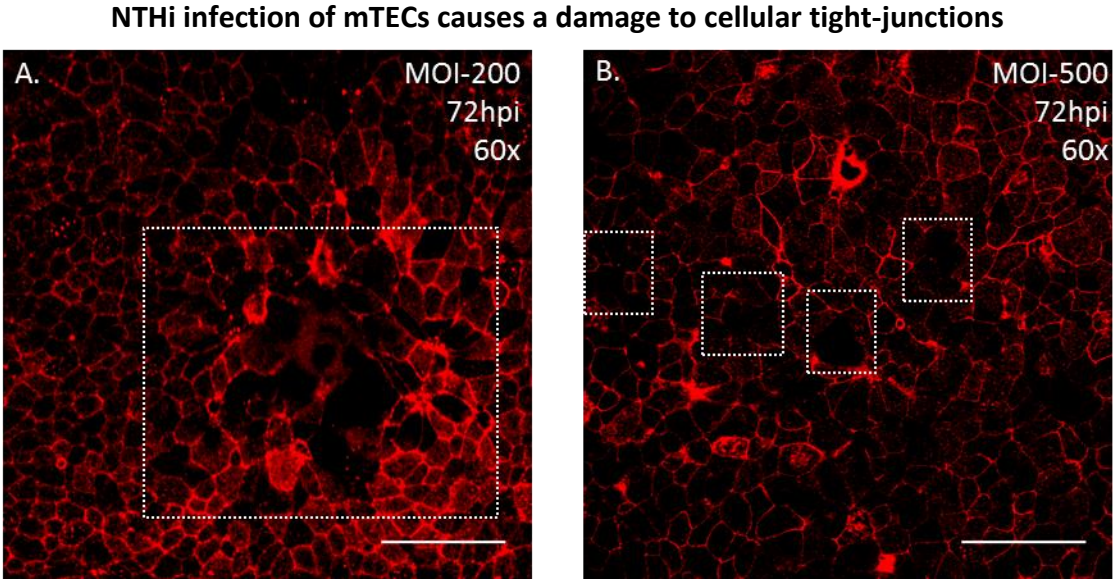

Figure 5.18: NTHi infection causes a damage to cellular tight-junctions, stained for ZO-1.
IFC images of *Bpifa1*$^{-/-}$ mTECs exposed to NTHi at MOI-200 (**A**) and MOI-500 (**B**), showing a damage of tight-junctions (ZO-1 – red) at 72hpi caused by NTHi infection. Images are representative of the fields shown in the Figure 5.17: Image A of Figure 5.18 is corresponding field of Image B of Figure 5.17; and Image B of Figure 5.18 is corresponding field of Image C of Figure 5.17. Examples of tight-junction disruption by NTHi infection are highlighted in the white rectangles. Data are representative of two independent batches of WT mTEC cultures (n=2). Scale bar: 50µm.

Subsequently, Z-stacks were taken using the confocal microscope to further investigate the ability of NTHi to cross through the layers of cells (Figure 5.19). Results showed the presence of NTHi throughout all layers of mTECs imaged (Figure 5.20). The observation of NTHi from the top to the bottom layers of cells suggested that microorganism was able to pass through layers of mTECs. Therefore, overall analysis suggested NTHi infection of mTECs damaged cellular tight-junctions and allowed the microbe to cross through the layers of cells.

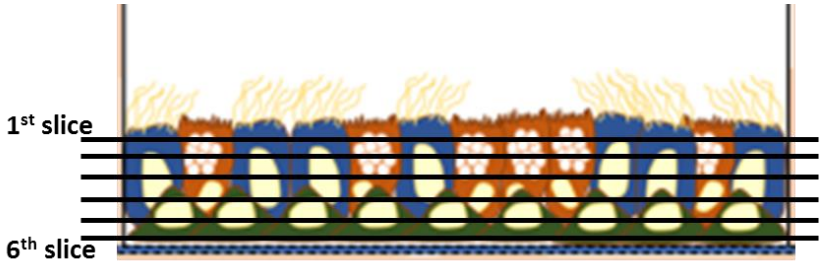

Figure 5.19: Representation of Z-stack imaging using confocal microscopy for analysis of NTHi crossing through the layers of mTECs.
Each cross-line (black) represents a section of Z-stack (1 to 6 slices).

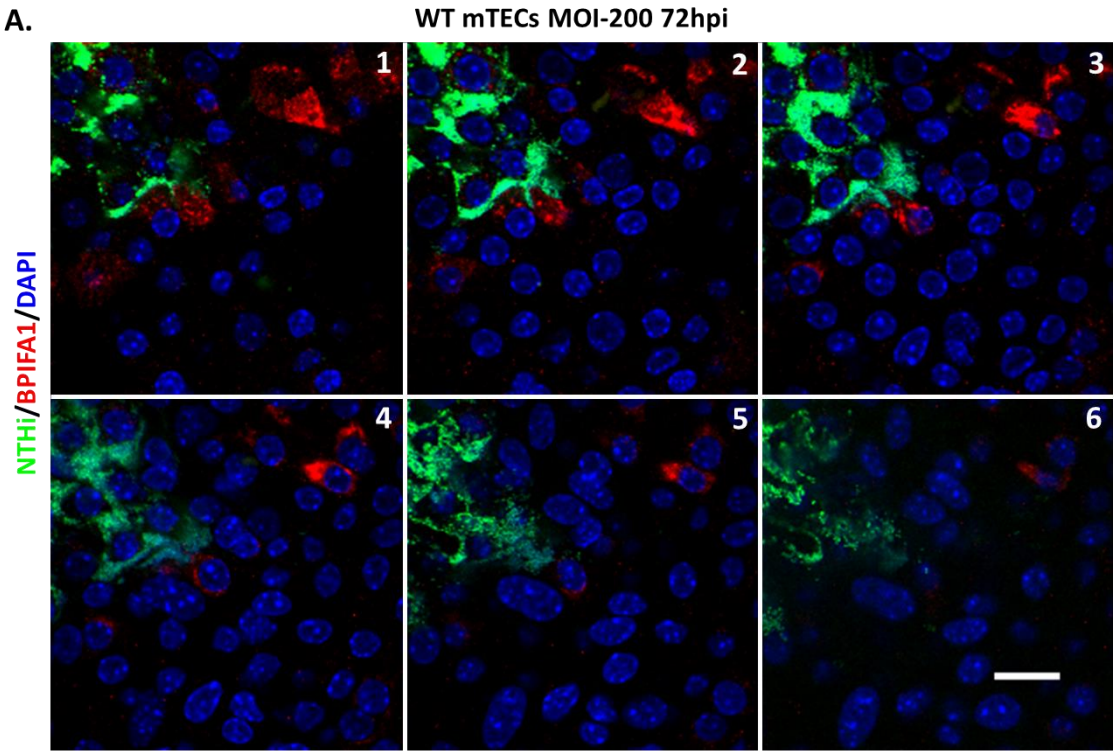

Figure 5.20: Montage view of Z-stack sections, showing NTHi crossing through the layers of WT mTECs.
Z-stack images of WT mTECs exposed to NTHi at MOI-200 (**A**), showing the presence of GFP-tagged NTHi (GFP – green) from the top to the bottom layers (left to right) of cells at 72hpi. Images were taken at 120x magnification using confocal microscope and were processed using ImageJ- win32. Data are representative of two independent batches of WT mTEC cultures (n=2). Scale bar: 20µm.

5.3.8 BPIFA1-positive cells are resistant to initial NTHi infection

WT mTECs were stained for BPIFA1 to investigate whether BPIFA1-positive cells were susceptible to NTHi infection. BPIFA1 is produced and secreted by non-ciliated epithelial cells. Analysis of IFC images suggested that BPIFA1-positive cells are resistant to initial NTHi infection as no association or internalisation of NTHi was observed with BPIFA1-positive cells (Figure 5.21).

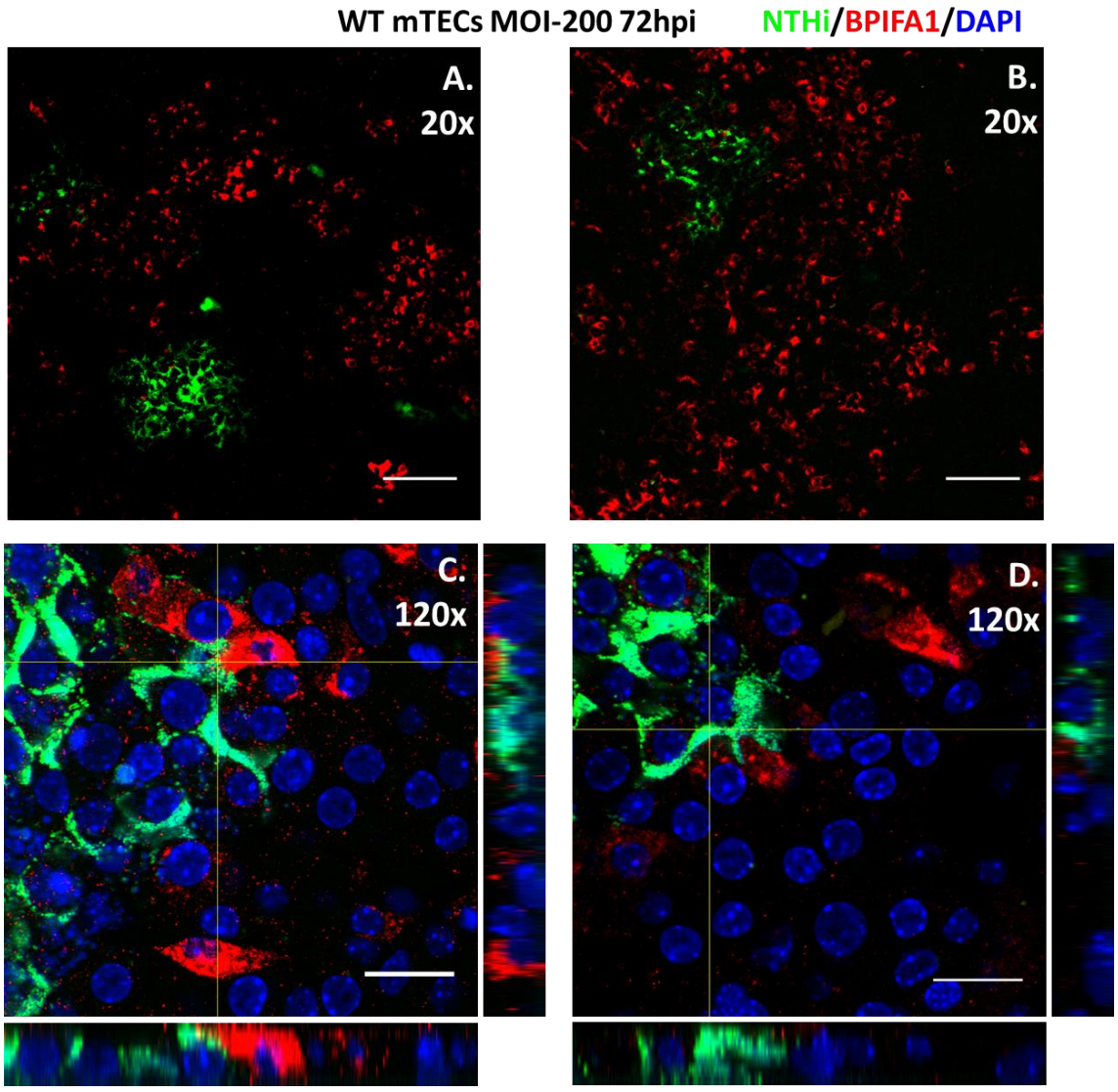

Figure 5.21: Lack of association of NTHi with BPIFA1-positive cells.
IFC images of WT mTECs exposed to NTHi at MOI-200 (**A-D**), demonstrating no association of GFP-tagged NTHi (green) with BPIFA1-positive cells (red) of WT mTECs at 72hpi. Z-stack images of cross sections of mTECs (**C, D**), showing no internalisation of NTHi within BPIFA1-positive cells. Data are representative of two independent batches of mTECs (n=2). Scale bar: **A-B**: 100µm; **C-D**: 20µm.

5.3.9 Secretion of BPIFA1 by mTECs exposed to NTHi

Analysis of IFC images suggested that BPIFA1-positive cells were resistant to initial NTHi infection. Consequently, I decided to find out whether the secretion of BPIFA1 was affected after mTEC exposure to NTHi. Apical secretions collected from MOCK-infected and NTHi-challenged WT mTECs at 24, 48, and 72 hpi were analysed for BPIFA1 secretion using dot blotting. The membrane of the dot blot was probed with anti-mouse BPIFA1 antibody. Analysis was performed using densitometry and the two-way ANOVA with Sidak multiple comparison tests were used to compare secretion of BPIFA1 by MOCK-infected and NTHi-exposed mTECs (Figure 5.22 A-C). Secretion of BPIFA1 was significantly reduced in mTEC culture exposed to NTHi at MOI-1000 at 72hpi compared to MOCK-infected mTECs ($p=0.04$). No statistically significant differences were detected at other time points, however, the trend towards the reduced secretion of BPIFA1 by mTECs exposed to NTHi was observed at all incubation time points (Figure 5.22 A-C). The figure showing dot blot results can be found in Appendix II (S11). A variability in secretion of BPIFA1 by different batches of WT mTECs was also observed (Appendix II: S11).

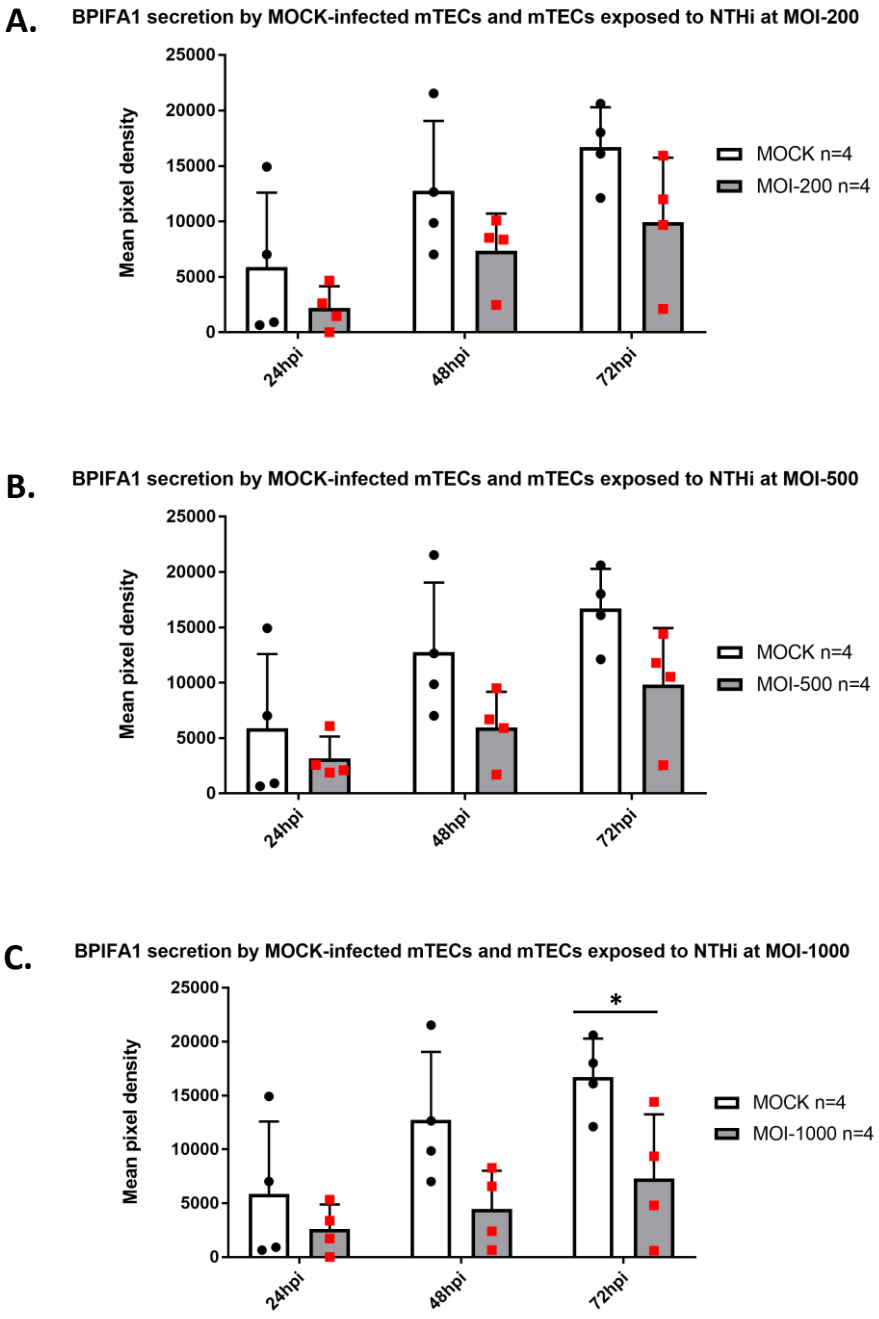

Figure 5.22: BPIFA1 secretion by NTHi-challenged WT mTECs.

Secretion of BPIFA1 by WT mTECs challenged with NTHi at MOI-200 (**A**), MOI-500 (**B**), and MOI-1000 (**C**) was compared to the secretion of protein by MOCK-infected mTECs at 24, 48, and 72hpi. The difference in the secretion of BPIFA1 by MOCK-infected mTECs at 72hpi and mTECs exposed to NTHi at MOI-1000 at 72hpi was statistically significant (p=0.04). Each black dot and red square in the graphs represent an independent batch of mTEC culture. Data was analysed using two-way ANOVA with Sidak multiple comparison tests. *p<0.05; mean ± SD, n=4 individual batches of mTEC culture.

5.3.10 NTHi exposure affects expression of *Bpifa1* and *Tekt1*

Having results, suggesting that BPIFA1-positive cells were more resistant to NTHi infection than other cells and that secretion of BPIFA1 by mTECs was reduced after NTHi exposure, I decided to investigate whether *Bpifa1* expression was also affected after NTHi challenge at 24 and 48 hours post-exposure. The PCR results suggested that NTHi slightly influenced the expression of *Bpifa1* as some down-regulation was observed in mTECs exposed to NTHi compared to MOCK-infected mTECs (Figure 5.23). However, a clear variation among the batches of WT mTECs was also detected. Expression of *Oaz1* was assessed in all batches of the cells and used as a housekeeping gene in all PCR reactions.

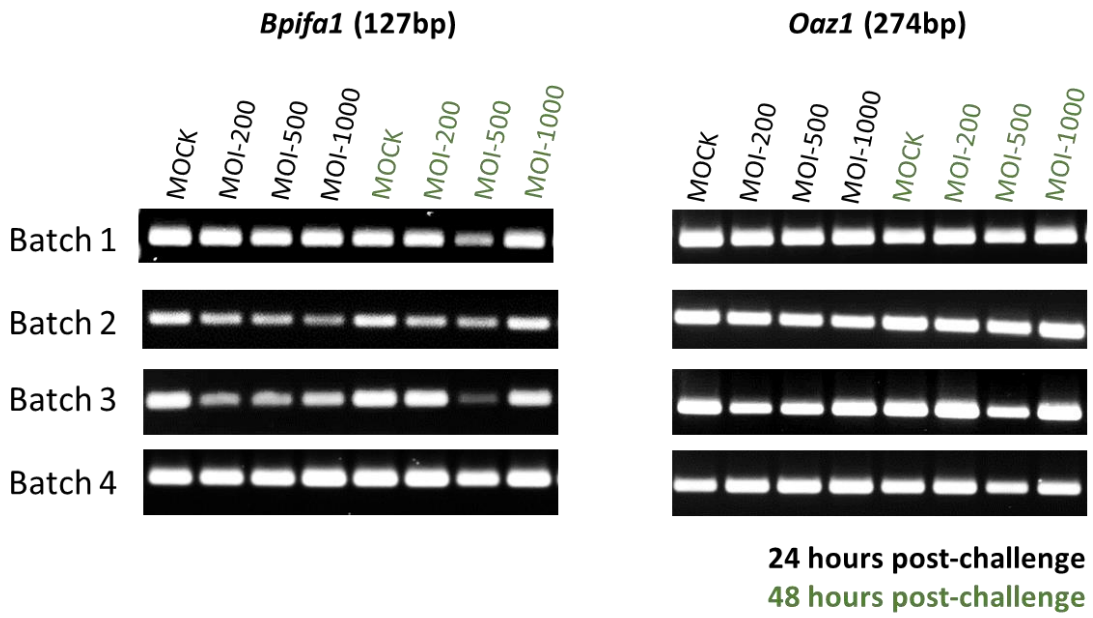

Figure 5.23: NTHi exposure appears to influence *Bpifa1* expression in WT mTECs.
PCR results, suggesting that NTHi exposure influences expression of *Bpifa1* by WT mTECs as some slight down-regulation of *Bpifa1* expression was observed. Variation among the batches of WT mTECs was also observed. Data are representative of PCR results from four independent batches of WT mTEC cultures (n=4).

I also assessed the expression of *Tekt1*, a marker for ciliated cells, to investigate if it was affected after bacterial exposure. Data showed that NTHi influenced *Tekt1* expression with down-regulation being observed at 24 hours post-exposure. However, variability among the samples was seen (Figure 5.24). I also looked at the expression of *Ltf*, which

is a component of the immune system and exhibits antimicrobial activity. NTHi caused no obvious change in the *Ltf* expression (Figure 5.24). Expression of *Oaz1* was used as a housekeeping gene in all PCR reactions.

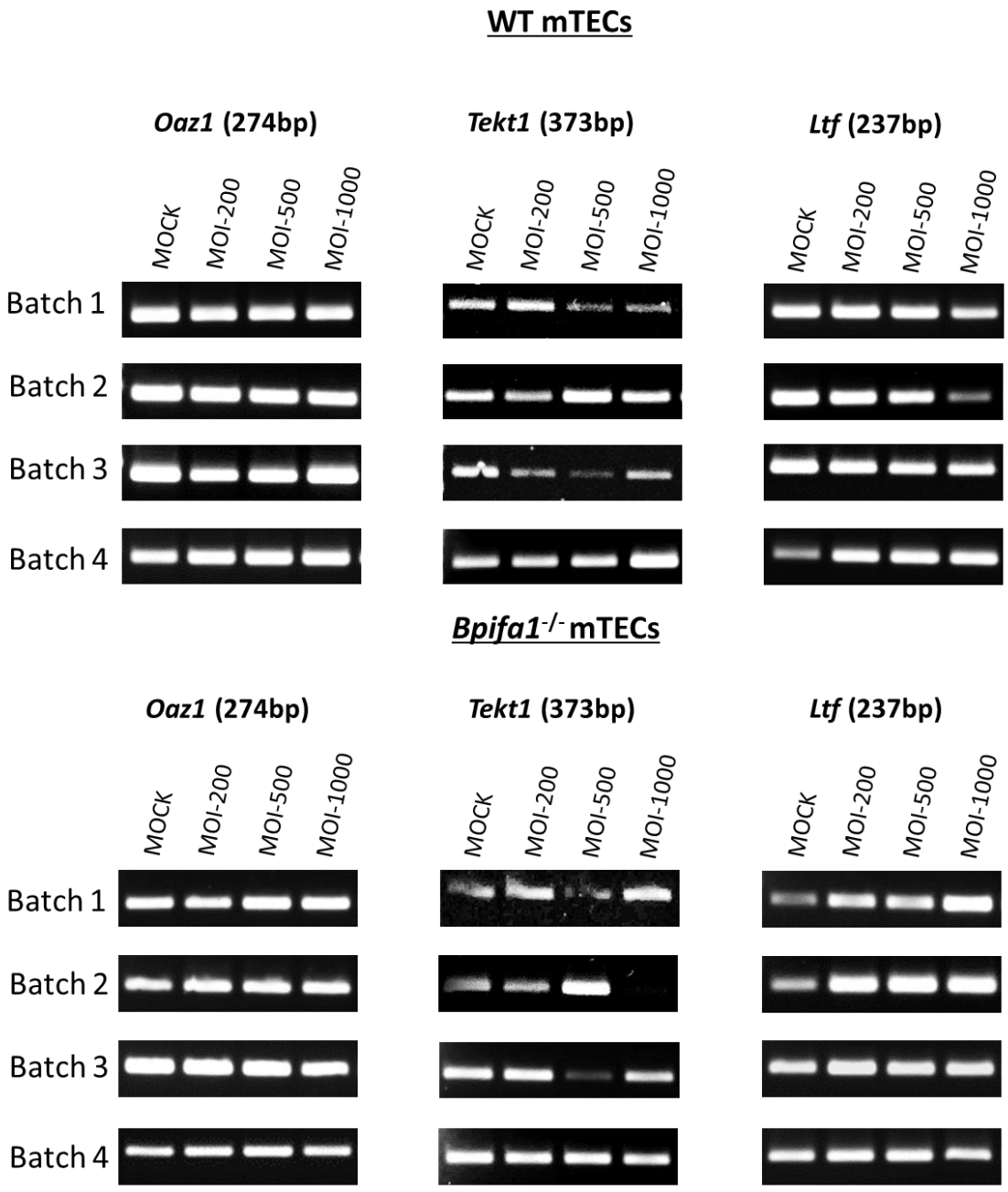

Figure 5.24: mTEC gene expression induced by NTHi at 24hpi.
Expression of the upper airway epithelium specific genes by NTHi- and MOCK-exposed WT and *Bpifa1*$^{-/-}$ mTEC cultures at 24 hours post-challenge. Data are from four independent batches of *Bpifa1*$^{-/-}$ and WT mTEC cultures (n=4).

5.3.11 Cytokine and chemokine production by NTHi exposed mTECs

Apical secretion washes collected from mTEC cultures challenged with NTHi were pooled (n=4) and analysed using Mouse Cytokine Array Panel A to determine whether the immune response to NTHi differed between WT and *Bpifa1*$^{-/-}$ mTECs. For this analysis, I decided to compare the levels of signalling molecules released 72 hours after exposure to NTHi at MOI-1000. The results show that NTHi-challenge induced a release of immune mediators from both WT (Figure 5.25) and *Bpifa1*$^{-/-}$ (Figure 5.26) mTECs. Levels of signalling molecules released by MOCK-exposed mTECs were used to establish basal levels.

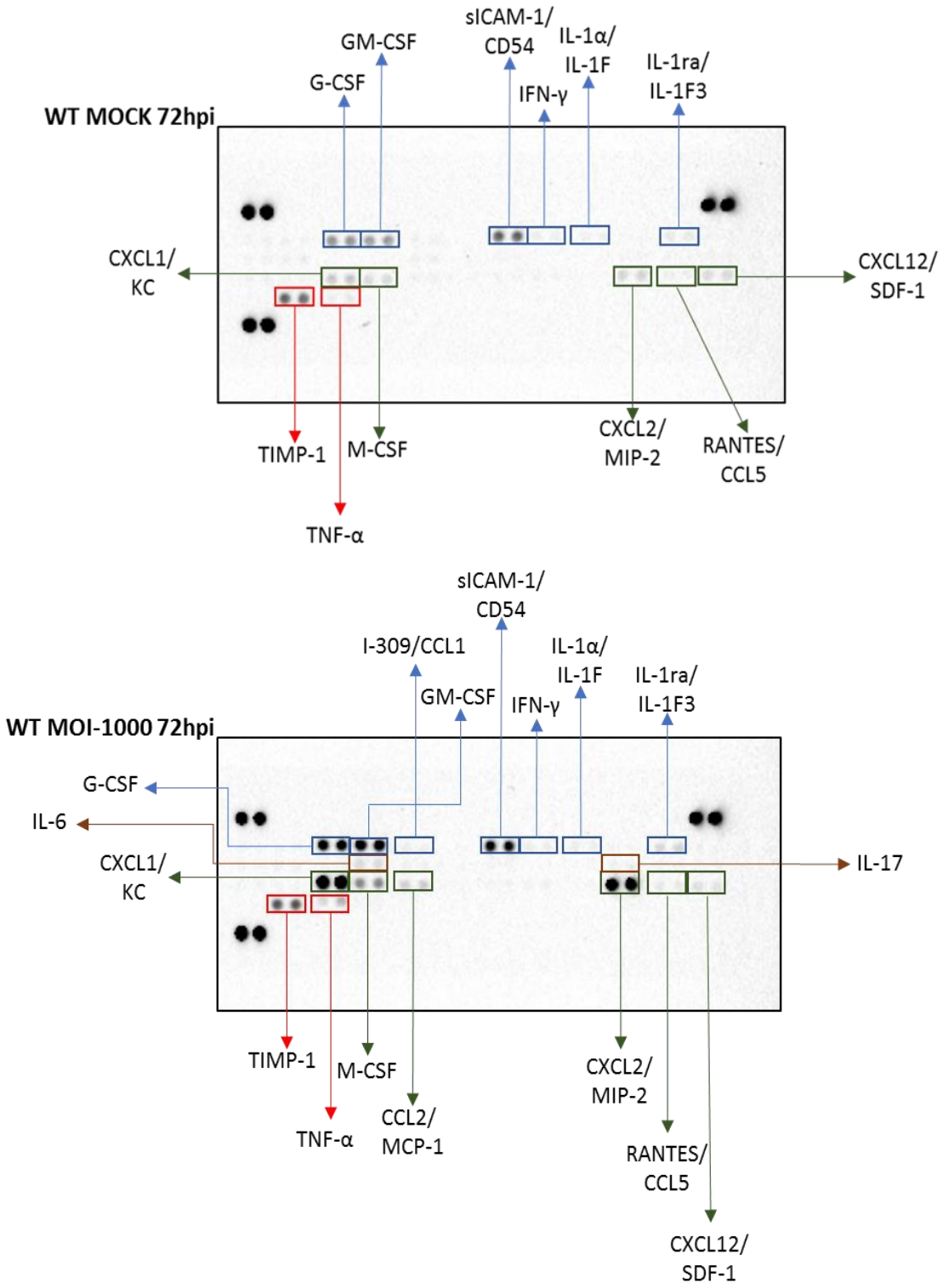

Figure 5.25: Cytokine array analysis of signalling molecules released by NTHi-exposed WT mTECs.
Apical secretion washes from four independent batches of WT mTECs were pooled and used for analysis. Immune mediators released by cells exposed to NTHi (MOI-1000) and MOCK-challenged cells at 72 hours post-challenge.

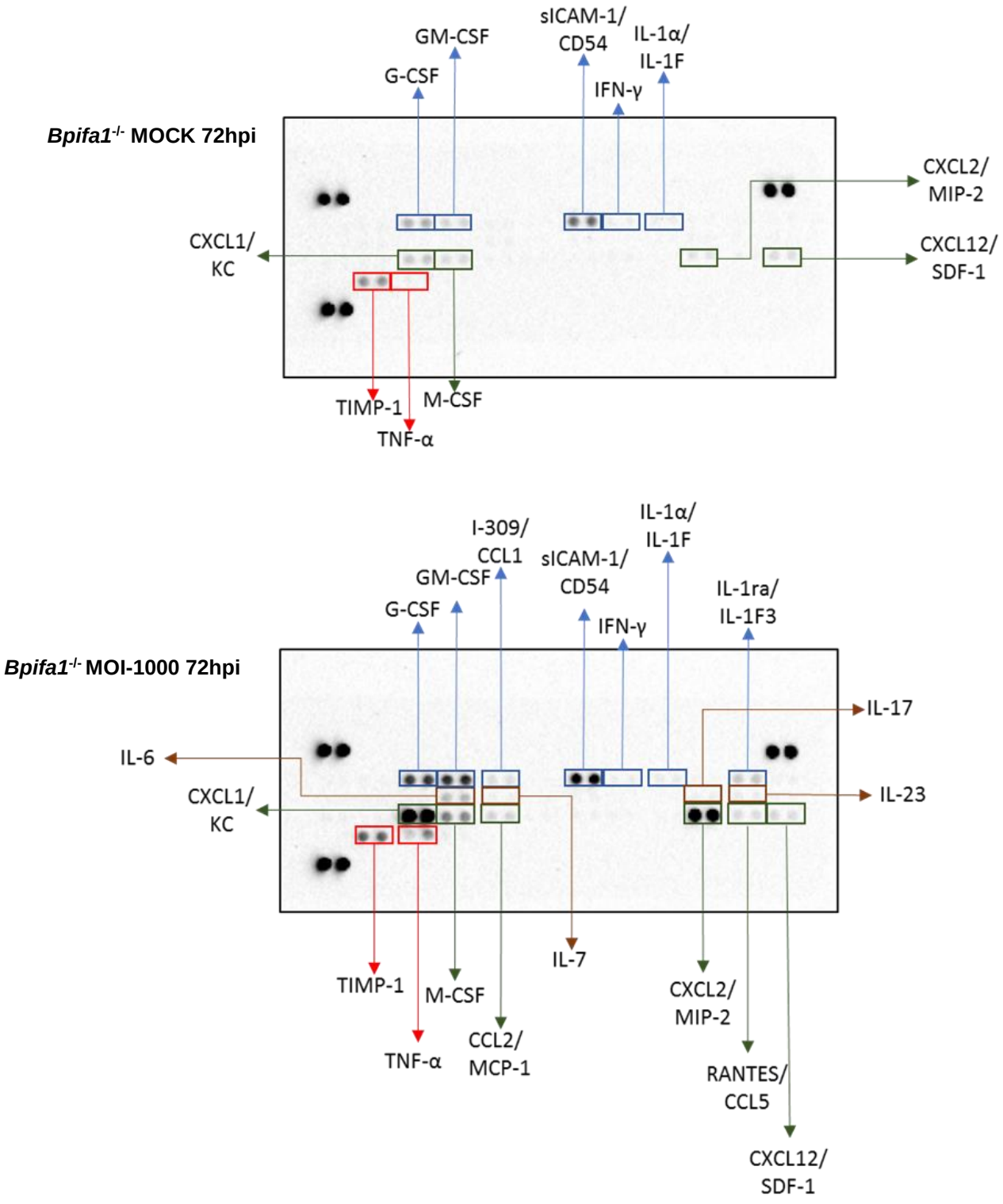

Figure 5.26: Cytokine array analysis of signalling molecules released by NTHi-exposed *Bpifa1*$^{-/-}$ mTECs.
Apical secretion washes from four independent batches of *Bpifa1*$^{-/-}$ mTECs were pooled and used for analysis. Immune mediators released by *Bpifa1*$^{-/-}$ cells exposed to NTHi (MOI-1000) and MOCK-exposed cells at 72 hours post-challenge.

The data was analysed by densitometry and graphs were plotted using GraphPad Prism. Levels of signalling molecules released by WT and *Bpifa1*$^{-/-}$ mTECs exposed to NTHi at MOI-1000 were compared after 72 hours post-challenge. Analysis of the results showed that secretion of variety of immune mediators by NTHi-exposed WT mTECs was induced (Figure 5.27 A). The same pattern was observed in *Bpifa1*$^{-/-}$ mTECs (Figure 5.27 B). Differences in the immune response generated by NTHi-exposed WT and *Bpifa1*$^{-/-}$ mTECs were assessed to determine whether the absence of BPIFA1 had an impact on the immune defences against microorganism (Figure 5.28). Analysis of results revealed no differences in the overall secretion of immune mediators by WT and *Bpifa1*$^{-/-}$ mTECs in response to NTHi challenge. Similar production of IL-7 and CXCL12 was observed by both types of mTECs. Secreted levels of IL-1α and IFN-γ cytokines by both type of cells were not high compared to the levels of other pro-inflammatory cytokines such as IL-6 and TNF-α. WT mTECs also generated slightly greater amounts of G-CSF and GM-CSF compared to NTHi-exposed *Bpifa1*$^{-/-}$ mTECs but produced levels of M-CSF were slightly lower in WT mTECs. CXCL1 and CXCL2 chemokines were produced by both types of mTECs in the greatest levels compared to the levels of all other signalling molecules released by mTECs in response to NTHi. Up-regulation in the production of CCL1, CCL2, and CCL5 was observed in both types of NTHi-exposed cells. TIMP-1 and CD54 production was also up-regulated in both types of NTHi-exposed mTECs. However, up-regulation of these immune mediators was small in NTHi-exposed WT mTECs compared to the basal levels produced in MOCK-infected WT mTECs. Overall produced levels of TIMP-1 and CD54 were slightly greater in NTHi-exposed *Bpifa1*$^{-/-}$ mTECs compared to NTHi-exposed WT mTECs.

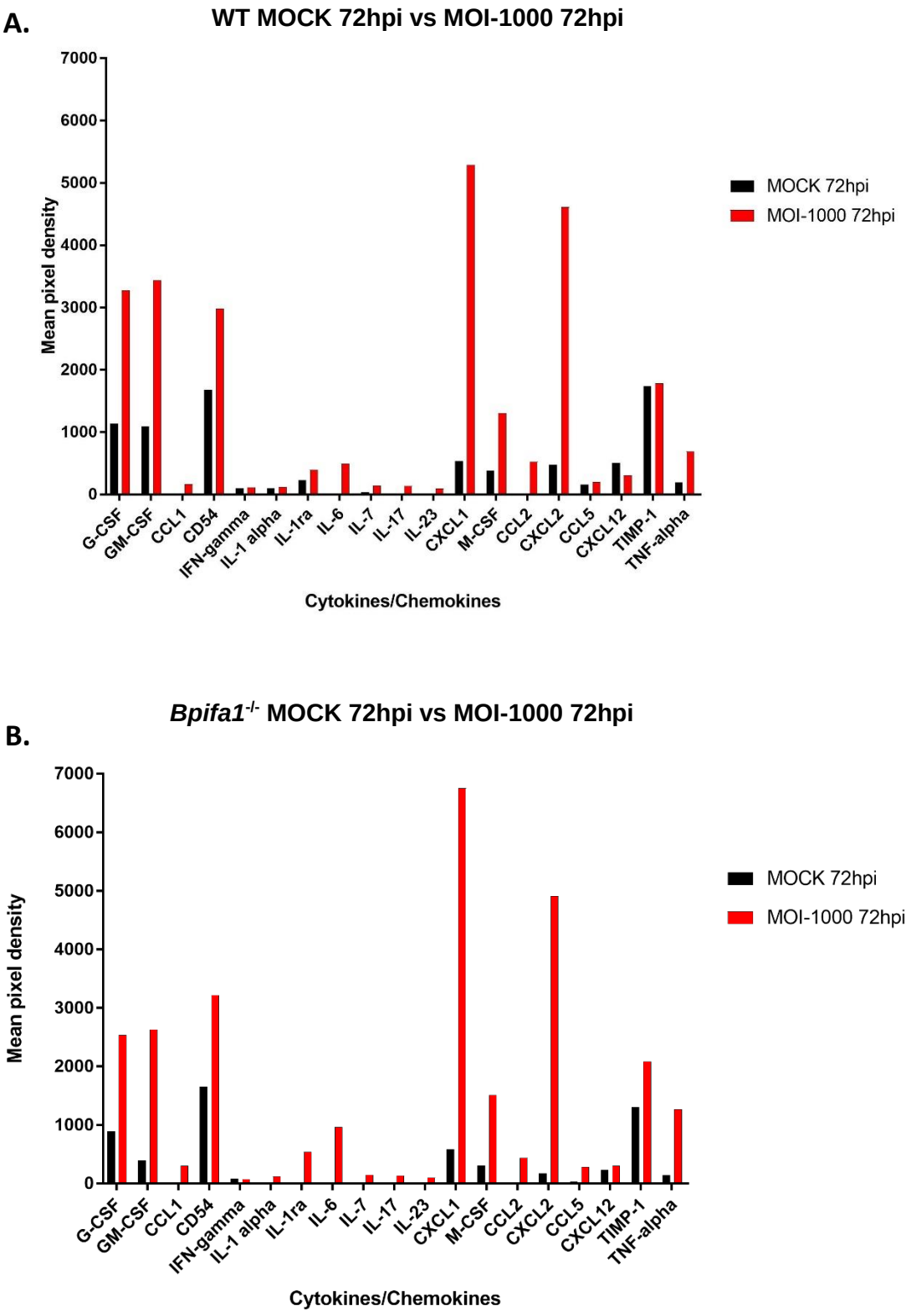

Figure 5.27: Comparison of immune mediators released by NTHi-exposed mTECs (MOI-1000).

Results of Mouse Cytokine Array Panel A, showing a generation of immune response by WT (**A**) and *Bpifa1*$^{-/-}$ (**B**) mTECs exposed to NTHi (MOI-1000) after 72 hours post-challenge. The levels of signalling molecules released by MOCK-exposed mTECs were used as the basal levels. Apical secretion washes from four individual mTEC batches were pooled. Mouse cytokine array was performed once (n=1).

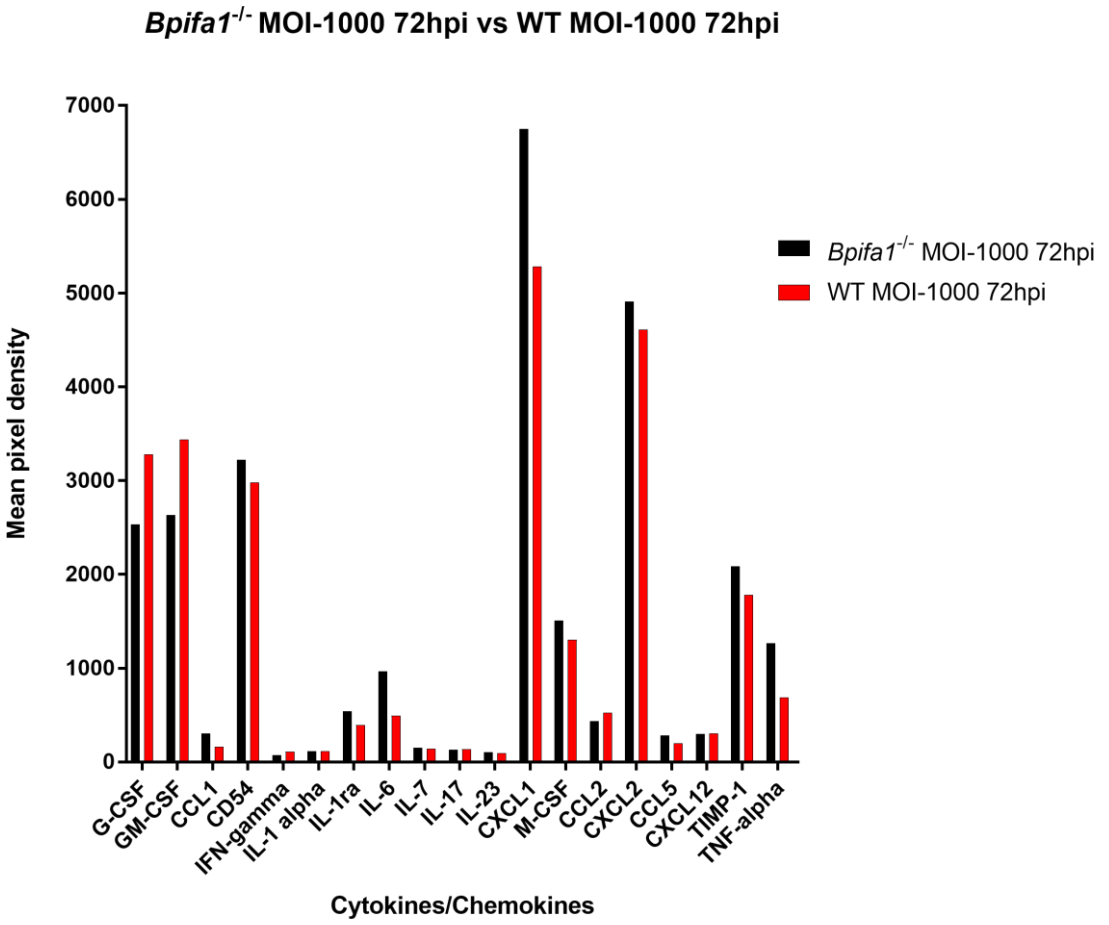

Figure 5.28: Comparison of the levels of immune mediators released by NTHi-exposed WT and *Bpifa1*$^{-/-}$ mTECs (MOI-1000) after 72 hours post-challenge.
Results of Mouse Cytokine Array, showing amounts of signalling molecules released by WT and *Bpifa1*$^{-/-}$ mTECs exposed to NTHi (MOI-1000) after 72 hours post-challenge. Apical secretion washes from four individual batches of cell cultures were pooled. Mouse cytokine array was performed once (n=1).

5.4 Discussion

5.4.1 mTEC cultures replicate an upper airway-like epithelium

For this study, I dissected tracheal tissues from WT and *Bpifa1*$^{-/-}$ mice, isolated mTECs, and differentiated these in the ALI culture for 14 days. I decided to use mTEC model in this study as it was shown to mimic *in vivo* host airway epithelium and its microenvironment. The methods for dissection of tracheas and growth of cells were adapted from the study by You et al. (You et al., 2002). These methods were previously established in our laboratory (Akram et al., 2018). I successfully applied these methods and differentiated mTECs to generate an upper airway-like epithelium. Differentiation of cells was verified using light and confocal microscopy techniques, PCR, and western blotting. The expression of airway epithelial markers such as MUC5B, FOXJ1, β-TUBULIN, BPIFA1, ZO-1 was analysed in the samples of differentiated mTEC cultures using confocal microscopy. MUC5B is known as a marker of goblet cells (Roy et al., 2014, Thai et al., 2008), whereas FOXJ1 and β-TUBULIN are the markers of ciliated cells (Eenjes et al., 2018, Jain et al., 2010, Stewart et al., 2012). BPIFA1 is characterized as marker of non-ciliated secretory cells (Musa et al., 2012), whereas ZO-1 is the marker of cellular tight-junctions (Eenjes et al., 2018, Stewart et al., 2012). Detection of the expression of all these epithelial markers in mTEC cultures confirmed the differentiation of cells in the upper airway-like epithelium. No obvious differences were observed in the expression of these epithelial markers between WT and *Bpifa1*$^{-/-}$ mTECs. In addition, secretion of BPIFA1 by differentiated WT mTECs was confirmed by western blotting as was *Bpifa1* expression by PCR. I also detected *Tekt1* (marker of ciliated cells) expression in WT and *Bpifa1*$^{-/-}$ mTEC cultures using PCR and did not observed any differences in the expression pattern between two different populations of the cells. After verification of differentiation of the WT and *Bpifa1*$^{-/-}$ mTEC cultures into the upper airway-like epithelium, I exposed both types of cells to NTHi to determine the effect of BPIFA1 loss on the susceptibility of cells to bacterium.

5.4.2 *Bpifa1*$^{-/-}$ deficiency does not cause increased NTHi colonisation

In this study, I investigated the effect of BPIFA1 loss on the susceptibility of mTECs to NTHi colonisation. My data showed a great variation in NTHi colonisation between individual batches of mTECs. As determined by GFP fluorescence, there was no statistically significant difference in the bacterial colonisation between WT cells and *Bpifa1*$^{-/-}$ cells. However, a trend towards increased NTHi colonisation in *Bpifa1*$^{-/-}$ mTECs was observed. When GFP-tagged NTHi in the apical washes was detected by western blotting, the data again showed a trend towards increased bacterial colonisation in *Bpifa1*$^{-/-}$ mTECs compared to WT mTECs. My data was variable using these two different experimental techniques. Other types of methods providing more quantitative analysis of samples or different type of the cells (e.g. non-primary cells) may be required to be used in the future studies to obtain more accurate and detailed results.

The absence of BPIFA1 may impair airway epithelial homeostasis and cause alterations in the composition of ASL leading to increased susceptibility of the cells to NTHi colonisation (Chu et al., 2007, Garland et al., 2013, Liu et al., 2013b, McGillivary and Bakaletz, 2010, Mulay et al., 2018). In previous studies, BPIFA1 was shown to be important for the mucosal homeostasis of the upper respiratory tract and its absence in airway secretions in the presence of bacterial stimulus or inflammation was reported to cause the progression of Otitis media and reduce mucociliary clearance in the ET (McGillivary and Bakaletz, 2010, Mulay et al., 2018). Detection of NTHi within the mucus layer of mTECs was expected because NTHi is a mucosal pathogen capable of binding to the mucus. Interactions of NTHi with mucus of respiratory epithelium has been reported in previous studies that showed that mucins secreted by mouse and human airway epithelium bound to NTHi (Kubiet and Ramphal, 1995, Read et al., 1991, Reddy et al., 1996, Val et al., 2015). In addition, previous studies showed that BPIFA1 is able to associate with mucins and form multimolecular complexes (Kesimer et al., 2013, Radicioni et al., 2016). On this basis, I suggest that BPIFA1 may form complexes with mucins and provide initial protection for mTECs by acting against NTHi in the mucus gel

layer. This feature of innate defence against NTHi was reduced in the cultures lacking BPIFA1. Consequently, bacterial colonisation showed a trend towards an increase in *Bpifa1*$^{-/-}$ mTECs compared to WT mTECs. It is also possible that absence of BPIFA1 altered viscoelasticity of mucus and surface tension in mTEC culture, leading to intensified NTHi colonisation in *Bpifa1*$^{-/-}$ cells. Previous studies reported that the loss of BPIFA1 was associated with increased surface tension, allowing greater bacterial biofilm formation on the apical surfaces of epithelial cells (Liu et al., 2013a, Liu et al., 2013b). It may also explain the observed trend towards an increased NTHi colonisation in *Bpifa1*$^{-/-}$ compared to WT cells. BPIFA1 deficiency may also alter viscoelasticity of mucus because the absence of BPIFA1 is associated with impaired ENaC function, causing an increase in the absorption of ASL and dehydration of mucus (Garcia-Caballero et al., 2009, Garland et al., 2013). Altered biophysical properties and viscoelasticity of mucus may be other factors contributing to the trend towards increased NTHi colonisation in *Bpifa1*$^{-/-}$ cells compared to WT cells. However, the suggestion that loss of BPIFA1 is associated with a change in viscoelasticity of mucus requires further investigation.

I also observed that secretion of BPIFA1 reduced when WT mTECs were exposed to larger bacterial inoculum. Secretion of BPIFA1 was the most reduced in WT mTECs exposed to NTHi at MOI-1000. Expression of *Bpifa1* was also affected in NTHi challenged mTECs. It seems likely that the larger bacterial inoculum generated a greater inflammatory response compared to mTECs challenged with a smaller number of bacterial cells (MOI-200). Enhanced release of inflammatory mediators into the apical secretions could down-regulate expression of *Bpifa1* (Chu et al., 2007, Wei et al., 2014) which, in turn, leads to decreased secretion of BPIFA1, meaning that mucosal homeostasis of tracheal epithelium was impaired. Impaired mucosal homeostasis within tracheal epithelium could allow NTHi to multiple and colonise a larger area of epithelial cells. These data suggest that BPIFA1 may play an initial role in the host defence against NTHi, but once mucosal homeostasis of airway epithelium is impaired, other mechanisms of the immune system are required to clear bacteria from the airways.

Reduced levels of BPIFA1 secretion in the BAL fluid of WT mice after bacterial exposure have been reported (Britto et al., 2013, Jiang et al., 2013).

Therefore, this work suggests that BPIFA1 may play a role in the innate protection against NTHi and mTECs appear to be more susceptible to NTHi colonisation in the absence of BPIFA1. NTHi colonisation is important for the initiation of tissue infection as it allows the formation of stable and persistent bacterial communities which are able to cross the mucus layer and cause infection of epithelial cells (Clementi and Murphy, 2011, Marrazzo et al., 2016).

5.4.3 NTHi causes a patchy infection of mTECs

In this study, I observed that mTECs exposed to NTHi were not readily infected and infection displayed a patchy pattern and did not depend on the bacterial inoculum size. My findings are similar to results reported in the study by Read et al., which showed that NTHi caused an infection of human nasopharyngeal mucosa organ culture, ranging from mild and patchy to severe (Read et al., 1991). However, in contrast to my work, severe epithelial disruption was also observed in this study. These differences could arise from different cell culture model, bacterial inoculum size, and type of NTHi strain used. The period of cell exposure to NTHi also could cause a great difference. I exposed mTECs to NTHi for 1 hour and non-adherent bacteria were washed off after incubation, whereas Read et al. exposed human nasopharyngeal mucosal organ cultures to NTHi for 24hrs and only after 24hrs were non-adherent bacteria washed off (Read et al., 1991). In addition, another study examining ability of NTHi to cross cell layers of 3D human airway mucosa cell culture did not report high infectivity of NTHi and only showed bacterial ability to associate with the mucus layer of cells and cross the layers of cells (Marrazzo et al., 2016). This study exposed human airway mucosal cell culture to NTHi for 2hrs and this period of bacterial exposure is similar to the bacterial exposure time used in my study. I chose the sizes of bacterial inoculum and periods of cell exposure to NTHi according to the study by Mulay et al., which challenged mouse middle ear epithelial

cells with GFP-tagged NTHi 375 strain and showed that exposure of epithelial cells to NTHi at MOI-100 resulted in the gradual progression of infection over the period from 24hrs to 72hrs post-exposure (Mulay et al., 2016). However, I was unable to see similar results and these differences may be associated with the type of cells used in my study. Mouse tracheal epithelial cells may be more resistant to NTHi strain 375 than mouse middle ear epithelial cells and different strains of NTHi should be used in the future to determine whether they could cause a greater tracheal epithelial infection.

5.4.4 BPIFA1 may contribute to the maintenance of airway mucosal homeostasis and provide an initial defence for cells against NTHi

BPIFA1 is secreted into apical secretions and its presence in the secretions of airway epithelial cells has been shown to be important for mucosal homeostasis within the airway surface microenvironment (McGillivary and Bakaletz, 2010, Mulay et al., 2018). In this study, I observed the trend towards increased bacterial colonisation in *Bpifa1*$^{-/-}$ mTEC cultures compared to WT mTEC cultures and BPIFA1-positive cells appeared to be less susceptible to NTHi invasion than other types of epithelial cells. I speculate that BPIFA1 is able to provide an initial protection for mTECs against NTHi by contributing to the maintenance of mucosal homeostasis of tracheal epithelium and directly binding to bacteria. As mentioned before, BPIFA1 can associate with mucins and form complexes (Kesimer et al., 2013, Radicioni et al., 2016), which may provide an initial protection for epithelial cells by acting against NTHi in the mucus gel layer. I suggest that bacterial cells which were able to cross the mucus layer into periciliary liquid, may be directly confronted by BPIFA1. My bacterial pull-down data has shown that mouse BPIFA1 can bind to NTHi, which may mean that BPIFA1 is able to exhibit its antimicrobial properties against the microorganism once protein is bound to it. Number of different studies reported BPIFA1's ability to exhibit antimicrobial properties against bacterial pathogens (Ahmad et al., 2016, Chu et al., 2010, Gakhar et al., 2010, Gally et al., 2011, Sayeed et al., 2013, Walton et al., 2016, Zhou et al., 2008). In this study, the mechanisms used by

mouse BPIFA1 to bind to NTHi were not directly studied, but I postulate that sialic acid residues found on postranslationally modified BPIFA1 as reported in the work by Ghafouri et al. (Ghafouri et al., 2006), may enable the binding of the protein to the bacterium. In addition, the importance of sialic acid residues in the binding to microorganisms was reported in the study by Reddy et al., which showed that sialic acid-containing oligosaccharides of mucins were responsible for the mucins ability to interact with NTHi (Reddy et al., 1996). It was demonstrated that these mucins specifically bound to several NTHi outer membrane proteins. Therefore, I suggest that mouse BPIFA1 may use the same mechanisms to interact with NTHi as mucins containing sialic acid residues. Investigation of this hypothesis should be addressed in future studies.

In this study, I also showed that epithelial cells positive for BPIFA1 appeared to be less susceptible to NTHi invasion as no association of bacterium with BPIFA1 positive cells was observed. I postulate that NTHi invasion into BPIFA1 positive cells was prevented by the protein's antimicrobial properties. BPIFA1 has been demonstrated to exhibit antimicrobial properties against multiple bacterial pathogens, including *P. aeruginosa*, *M. pneumoniae*, and *B. cepacia*. BPIFA1 has the ability to inhibit the growth of bacteria and the formation of bacterial biofilms (Ahmad et al., 2016, Chu et al., 2010, Gally et al., 2011, Gakhar et al., 2010, Liu et al., 2013b, Sayeed et al., 2013, Zhou et al., 2008). To test the hypothesis that BPIFA1 is able to prevent the initial entry of the pathogens to the cells, a stable cell line expressing BPIFA1 and control cell line negative for BPIFA1 could be exposed to the bacterial pathogen and the ability of the bacteria to cause an intracellular infection over the time could be evaluated. Data from the such type of experiment may provide some important information about BPIFA1's biological functions.

5.4.5 NTHi associates with the multiple cell types of mouse tracheal epithelium

In this study, NTHi appeared to associate with the multiple cell types of mouse tracheal epithelium. My data suggested that NTHi was capable of attaching to ciliated, goblet cells, and other unidentified type of secretory cells.

Some association of NTHi with ciliated cells was observed in both phenotypes of mTEC cultures, but no apparent differences in the ability of NTHi to adhere to WT and *Bpifa1*$^{-/-}$ ciliated cells was observed. NTHi has been reported to cause the clumping of cilia and loss of cilia in human respiratory epithelium (Ketterer et al., 1999, Read et al., 1991). In addition, heat-stable lipid A of NTHi lipooligosaccharide was shown to reduce cilia activity, cause disorganisation of cilia, and loss of cilia in the rat tracheal organ cultures (Denny, 1974, Johnson and Inzana, 1986). NTHi surface-exposed lipoprotein, known as protein D, was also reported to cause the impairment of ciliary function and the considerable loss of cilia in the organ culture of human nasopharyngeal mucosa (Janson et al., 1999). Therefore, these findings suggest that the function of cilia may be weakened by exposure to NTHi, which would eventually increase a susceptibility of ciliated cells to NTHi. The binding of NTHi to structurally damaged epithelial cells *in vitro* was reported in a study which also showed that NTHi was not able to associate with normal respiratory epithelium (Read et al., 1991). In addition, my data showed that NTHi exposure of mTECs caused a reduction in *Tekt1* expression (marker of ciliated cells). This may be caused by both NTHi and inflammatory response generated by mTECs. Therefore, it appears that different types of mechanisms can predispose ciliated cells to NTHi infection.

In this study, I also observed some association of NTHi with the patches of goblet cells (MUC5B-positive cells). This seemed not to be influenced by the absence of BPIFA1 as NTHi adherence to the goblet cells was observed in both WT and *Bpifa1*$^{-/-}$ mTEC cultures. Several studies showed NTHi invasion within human non-ciliated epithelial cells

(St Geme and Falkow, 1990, Ketterer et al., 1999, van Schilfgaarde et al., 1995). However, none of these studies identified a type of non-ciliated cells being affected by NTHi. Here, I suggest that one type of non-ciliated cell affected by NTHi was goblet cells. However, it was obvious that another type of unidentified, non-ciliated cell was also infected with NTHi and these non-ciliated cells appeared to be more susceptible to NTHi. Consequently, identification of these other types of non-ciliated epithelial cells should be determined in the future investigations. In this study, I did not analyse the mechanisms used by NTHi to enter epithelial cells, but previous studies suggested that NTHi uses micropinocytosis and microfilament-dependent processes to invade non-ciliated epithelial cells (St Geme and Falkow, 1990, Ketterer et al., 1999).

Overall, data from this study suggested that NTHi associates with the multiple cell types of mouse tracheal epithelium in order to initiate infection. My results also suggested that BPIFA1-positive non-ciliated secretory cells are more resistant to initial NTHi infection compared to the other types of mTEC cells. Based on the existing evidence, showing that internalised NTHi can survive within cells over extended period and remain intact (St Geme and Falkow, 1990, Virji et al., 1991), I suggest that NTHi invades epithelial cells to avoid host defence responses and enhance the spread of infection.

5.4.6 NTHi infection causes a disruption of cellular tight-junctions

Immunofluorescence analysis of NTHi-exposed mTECs revealed the presence of bacterial cells between *Bpifa1*$^{-/-}$ and WT mTECs, suggesting that BPIFA1 did not influence ability of bacteria to penetrate the tracheal epithelium. However, the time taken by bacteria to cross the tracheal epithelium in the presence and absence of BPIFA1 was not measured in this study and could be investigated in the future. Confocal microscopy Z-stack data showed that NTHi was able to cross through the apical layer of cells and reach the bottom layer cells. In agreement with my findings, NTHi has been shown to cross through human airway epithelium *in vitro* (Marrazzo et al., 2016, van Schilfgaarde et al., 1995). Additionally, it was demonstrated that the ability of NTHi to cross the

epithelium *in vitro* was not influenced by fimbriae or other bacterial adhesins promoting adherence, but it was dependant on bacterial protein synthesis (van Schilfgaarde et al., 1995).

The ability of NTHi to enter the spaces between mTECs should protect the bacteria from the host defence responses and facilitate bacterial spreading. I suggest that NTHi exposure of mTECs caused a dysfunction of epithelial barrier allowing bacteria to cross the apical surface of cells and reach the basolateral layer. In contrast, van Schilfgaarde et al. showed that NTHi crossed airway epithelium into basolateral compartment without causing a death of cells and disrupting integrity of epithelium (van Schilfgaarde et al., 1995). In addition, another study also demonstrated that the exposure of HBEC culture to NTHi endotoxin did not increase permeability of the cells (Khair et al., 1994). However, my data showed that NTHi exposure caused an alteration in ZO-1 staining in mTEC cultures, suggesting that cellular tight-junctions and integrity of murine tracheal epithelium were disrupted. I speculate that an inflammatory response generated by tracheal epithelium to NTHi led to this disruption of cellular tight-junctions. The presence of inflammatory mediators in the microenvironment of epithelium has previously been reported to affect epithelial barrier by increasing its permeability and altering the expression of epithelial junctional proteins (Al-Sadi et al., 2009, Capaldo and Nusrat, 2009, Georas and Rezaee, 2014, Ramezanpour et al., 2016). My data showed that NTHi exposure of mTECs induced a great release of cytokines such as: CXCL1, CXCL2, IL-6, and TNF-α. The secretion of these inflammatory mediators by mTECs to NTHi could affect epithelial barrier function. It has been reported that human IL-8/CXCL8, which is related to murine CXCL1 and CXCL2 molecules, plays a role in the regulation of epithelial barrier (Capaldo and Nusrat, 2009, Mukaida, 2003, Sorrentino et al., 2008). In the study by Sorrentino et al., it has been shown that addition of CXCL8 to epithelial cell line A549 culture caused an increased permeability of epithelial cell monolayer (Sorrentino et al., 2008). Interleukin-6 has also been found to control epithelial barrier function by causing alterations in the permeability of epithelium and reducing

transepithelial electrical resistance (Al-Sadi et al., 2009, Capaldo and Nusrat, 2009). The presence of TNF-α in the microenvironment of epithelium also causes a barrier dysfunction by reducing transepithelial resistance, impairing the function of cellular tight-junctions, and increasing epithelial tight-junction permeability (Al-Sadi et al., 2009, Brune et al., 2015, Capaldo and Nusrat, 2009, Coyne et al., 2002, Georas and Rezaee, 2014). Therefore, the inflammatory response generated by mTECs to NTHi may disrupt epithelial barrier function. I did not determine whether tracheal epithelial permeability and transepithelial electric resistance were affected by exposure to NTHi, but these two measurements could be defined in the future studies. For example, the change in the permeability of epithelium could be determined by measuring epithelial permeability to both a small solute (e.g. 10-kDa dextran) and a larger solute (e.g. 2000-kDa dextran), or to sodium and chloride ions. Localisation of other epithelial junctional proteins such as claudin, occludin, and junctional adhesion molecule could also be investigated to obtain more detailed results.

5.4.7 WT and *Bpifa1*$^{-/-}$ mTECs generated a similar inflammatory response after exposure to NTHi

Inflammatory response generated at 72 hours post-challenge by *Bpifa1*$^{-/-}$ mTECs was similar to inflammatory response induced by WT mTECs. However, I observed that *Bpifa1*$^{-/-}$ mTECs potentially released slightly greater amounts of major pro-inflammatory cytokines such as IL-6, TNF-α, CXCL1, and CXCL2. I suggest that WT mTECs may be better in controlling inflammatory response to NTHi than *Bpifa1*$^{-/-}$ mTECs. However, this requires further investigation using more quantitative methods. The release of inflammatory mediators by mTECs challenged with NTHi could be examined at the shorter bacterial exposure times. Further analysis of inflammatory response generated by mTECs to NTHi in the presence and absence of BPIFA1 would be of great interest as there is a possibility that release of inflammatory mediators would differ more at 24 and

48 hours post-exposure. This suggestion is supported by the study showing that the levels of pro-inflammatory cytokines (e.g. CXCL1, IL-6, IL-1β, CXCL2) were greater in the response to *P. aeruginosa* challenge in the absence of BPIFA1 at 6 and 24 hours post-inoculation (Liu et al., 2013b). Suggestion that BPIFA1 plays a role in regulating inflammatory response to NTHi is also supported by other studies demonstrating immunodulatory properties of BPIFA1 in *M. pneumoniae* and *P. aeruginosa* infections (Chu et al., 2007, Lukinskiene et al., 2011).

In this study, I showed that NTHi exposure activated mTECs and induced the inflammatory response. I observed an up-regulation in the release of inflammatory mediators such as CXCL1, CXCL2, IL-6, TNF-α, M-CSF, G-CSF, and GM-CSF by NTHi-exposed mTECs compared to MOCK-exposed mTECs. My observation of CXCL1, CXCL2, IL-6, and TNF-α production in response to NTHi is in accordance with other studies (Bresser et al., 1997, Clemans et al., 2000, Khair et al., 1994). Chemokines CXCL1 and CXCL2 are known as the murine homologues of human IL-8 and are mediators of neutrophil activation and chemotaxis (Hol et al., 2010, Khair et al., 1996, Turner et al., 2014). Based on this evidence, I suggest that mTECs released these chemokines to recruit neutrophils to the site of infection to aid in the fight against the spread of NTHi and eliminate bacterial cells from airway epithelium. Secretion of IL-6 and TNF-α in response to NTHi is mediated through TLR2. Previous studies showed that NTHi binds to TLR2 and this leads to activation of NF-κB signalling cascade which, in turn, mediates induction of IL-6 and TNF-α (King and Sharma, 2015, Liu et al., 2017, Lugade et al., 2011). TNF-α is an early response pro-inflammatory cytokine and plays an important role in the clearance of bacterial pathogens from the respiratory tract as it mediates recruitment of polymorphonuclear cells through regulation of CXC chemokines which stimulate migration of inflammatory cells to the site of inflammation (Strieter et al., 2002). Production of IL-6 by NTHi-exposed mTECs could also be induced by release of TNF-α. This suggestion is supported by the study showing that levels of IL-6 mRNA in HBECs increased after stimulation with TNF-α (Cromwell et al., 1992). Furthermore, it

also explains the observation of slightly higher IL-6 production by *Bpifa1*$^{-/-}$ mTECs compared to WT mTECs, because *Bpifa1*$^{-/-}$ mTECs released slightly more TNF-α than WT mTECs. IL-6 may play a multifunctional role in response to NTHi as it can function as pro-inflammatory or anti-inflammatory cytokine. IL-6 as pro-inflammatory cytokine is involved in the transition from innate immunity response to adaptive immunity response as it induces a differentiation of B-cells and T-cells and activates Natural Killer cells (Keller et al., 1996). However, IL-6 can also function as anti-inflammatory cytokine by down-regulating production of pro-inflammatory cytokines such as IFN-γ, TNF-α, CXCL2, and GM-CSF and in such manner contributes towards resolution of inflammation (Opal and DePalo, 2000).

Exposure of mTECs to NTHi led to up-regulation of GM-CSF and G-CSF pro-inflammatory cytokines which are involved in activation of polymorphonuclear cells, dendritic cells and monocytes and promote survival of these immune cells by inhibiting apoptosis (Saba et al., 2002). In addition, study by LeVine et al. demonstrated that GM-CSF plays an important role in bacterial infection as mice deficient for GM-CSF were shown to be significantly more susceptible to group B streptococcal infection compared to WT mice (LeVine et al., 1999). NTHi-challenged mTECs also up-regulated production of M-CSF compared to basal levels produced by their respective MOCK controls and this suggested that M-CSF may have an essential role in fighting against NTHi infection. My suggestion is supported by the evidence showing the importance of M-CSF in Gram-negative bacterial pneumonia as immunoneutralisation of M-CSF in mice caused increased bacterial burden, greater lung injury, and reduced survival (Bettina et al., 2016).

It is also worth to mention the up-regulation in CD54/ICAM-1 by NTHi-exposed mTECs compared to basal levels produced by MOCK-exposed mTECs. Production of CD54 increased slightly more from basal levels in NTHi-exposed *Bpifa1*$^{-/-}$ mTECs compared to WT mTECs. This may be a result of a slightly greater production of CXCL1, CXCL2, and TNF-α by NTHi-exposed *Bpifa1*$^{-/-}$ mTECs compared to NTHi-exposed WT mTECs. CD54

is an intercellular adhesion molecule produced by airway epithelial cells and plays an important role in inflammatory response as it allows adhesion of neutrophils to epithelial cells (Gómez and Prince, 2008). Importance of CD54 in NTHi infection was demonstrated in the study by Pang et al., showing that reduced levels of CD54 in mice model of COPD resulted in significantly decreased pulmonary clearance of NTHi (Pang et al., 2008).

Taking all results into consideration, I suggest that the mTEC model responds to NTHi stimulation in the manner of native respiratory tract, as secretion of TNF-α, IL-6, and IL-8 (human homologue for murine CXCL1 and CXCL2) in response to NTHi challenge correlates with previously published *in vivo* studies (Moghaddam et al., 2008, Singh et al., 2014). This makes the mTEC model valuable for studying the mechanisms of NTHi infection. Additionally, I suggest that earlier inflammatory responses generated by mTECs in response to NTHi stimulus should be studied to obtain a better insight of the effect of BPIFA1 absence on immune response to bacterial challenge.

5.4.8 Variation in the batches of mTECs

In this study, my results were influenced by mTEC batch-to-batch variation. I observed differences in the expression of epithelium-specific genes, production and secretion of proteins, and intensity of NTHi infection among the batches of mTECs. Primary cell cultures are well known to exhibit variability among different batches of cells and sometimes to provide inconsistent results. Variation in the batches of primary cell cultures can be caused by the multiple factors. One of the major factors influencing a variation in batches of cells in my study was adherence of certain type of cells after seeding. I detected that only a small portion of seeded cells was able to attach to the transwell membrane and later to proliferate and differentiate in the upper airway-like epithelium. Consequently, the composition of day-14 ALI tracheal epithelium was highly dependent on the cells which adhered to the membrane after seeding. This means that proportion of various types of cells such as goblet cells, ciliated cells and secretory cells

could be different in each batch and even well of mTECs, leading to the differences in the levels of airway epithelial markers expressed and proteins produced. Based on this, I speculate that variation in the composition of mTEC epithelium could also cause differences in the intensity of NTHi infection among the batches and wells of mTECs. A second major factor causing a variability among the batches of cells is the growth media. The media used was optimised to promote the growth and differentiation of tracheal epithelial cells (You et al., 2002) and carefully prepared every time. However, certain factors such as a lot-to-lot variation of media components (e.g. growth supporting factors) could not be controlled. Another factor which might influence variation in the batches of differentiated tracheal epithelium was caused by the sex and age of mice used in this study. However, the usage of same age and same numbers of female and male mice for preparation of mTECs was not always possible in this study.

In the future these issues can be addressed by using same age of mice, same numbers of female and male mice for each batch and increasing the number of batches and wells used for each NTHi challenge experiment. Unfortunately, I was not able to increase the number of batches used in this study due to the time required to grow and differentiate each batch of mTECs and usage of multiple wells of cells was not possible due to limited numbers of mice and wells of cells required for validation of cell differentiation.

Taking into consideration my results and existing research data, demonstrating the importance of BPIFA1 in the innate host defence, I suggest that BPIFA1 plays a role in the innate protection of tracheal epithelial cells against NTHi and the loss of this multifunctional protein increases susceptibility of mTECs to bacterial infection.

5.5 Key experimental conclusions

- WT and *Bpifa1*$^{-/-}$ mTECs differentiated into an upper airway-like epithelium.
- *Bpifa1*$^{-/-}$ mTECs showed a trend towards an increased susceptibility to NTHi colonisation compared to WT mTECs, suggesting that BPIFA1 provides an initial protection for WT mTECs against NTHi.
- mTECs exhibited resistance to NTHi infection and only patchy NTHi infection of mTECs was observed.
- NTHi was observed to associate with the multiple cell types of mouse tracheal epithelium, but not with BPIFA1-positive cells.
- NTHi infection caused a disruption of cellular tight-junctions and impairment of epithelial barrier function. This, in turn, allowed the crossing of NTHi through the layers of mTECs.
- NTHi exposure affected *Bpifa1* expression and reduced BPIFA1 secretion.
- No obvious difference was observed in the inflammatory response generated by WT and *Bpifa1*$^{-/-}$ mTECs in response to NTHi challenge at 72hpi.
- Variation in the batches of mTECs was detected.

CHAPTER 6: GENERAL DISCUSSION

BPIFA1 (SPLUNC1), the prototypic member of the wider BPI-fold containing family of putative innate defence proteins, is structurally similar to proteins with demonstrated innate immune roles (Bingle and Craven, 2002, Elsbach and Weiss, 1998, Hailman et al., 1996, Levy, 2000, Masucci-Magoulas et al., 1995). Produced mainly in the upper respiratory tract and nasopharynx, it is one of the most abundant proteins in mucosal lining fluids (Campos et al., 2004, Bingle and Bingle, 2000, Bingle et al., 2005, Britto and Cohn, 2015, Musa et al., 2012, Weston et al., 1999). Although it was originally hypothesised that the protein would be an innate immune regulator (Bingle and Craven, 2002, Chu et al., 2007, Liu et al., 2013a, Liu et al., 2013b, Lukinskiene et al., 2011, Thaikoottathil et al., 2012), the true role of the protein in protecting the mucosal surface remains to be elucidated. The mechanisms by which BPIFA1 performs its biological functions are also not fully understood and few studies have aimed to identify regions important for its activity (Ahmad et al., 2016, Walton et al., 2016, Wu et al., 2017, Zhou et al., 2006).

Data in my thesis adds support to the view that BPIFA1 plays a role in airway host defence. I showed this in a number of ways. Human and mouse BPIFA1 proteins are able to bind not only to Gram-negative bacteria (NTHi), but also to Gram-positive bacteria (*S. aureus* and *S. pneumoniae*). This suggests that BPIFA1 exhibits activity against both types of bacteria. Existing data on BPIFA1's antimicrobial activity against Gram-positive pathogens is inconclusive. Some studies suggested that human BPIFA1 does not exhibit antimicrobial activity against Gram-positive pathogens, such as *S. aureus* (Ahmad et al., 2016, Walton et al., 2016), whereas others reported that BPIFA1 shows antimicrobial properties against *S. aureus* (Yu et al., 2018). Therefore, I suggest that the biological activity of BPIFA1 against Gram-positive pathogens should be further investigated.

The ability of hBPIFA1 to bind to bacterial pathogens appeared to be influenced by the S18 region of protein, but not by the disulphide bond. In contrast to my findings, currently available data suggests that the S18 region of protein does not influence the ability of protein to bind to LPS from bacterial pathogens nor does it possess antimicrobial properties (Ahmad et al., 2016, Walton et al., 2016). It may also be possible that the S18 region of hBPIFA1 binds to a different target on the surface of bacterial cells. I suggest that further research is required to fully determine the importance of the S18 region for the biological properties of hBPIFA1.

Throughout this project, I analysed the differences of the bacterial binding between human and mouse BPIFA1 proteins. Binding of hBPIFA1 and mBPIFA1 to bacteria seemed to be generally similar and no apparent differences were observed. Both types of proteins bound to Gram-positive and Gram-negative bacteria. Ability of mBPIFA1 to bind to bacteria may be explained by the certain features of protein sequence (i.e. N-glycosylation sites and proline-rich region) as outlined in **Chapter 4** (Section 4.4). The mechanisms by which mBPIFA1 binds to bacteria were not investigated in my thesis and remain to be determined. A better understanding of the mechanisms by which mBPIFA1 performs its biological functions may also provide extra clues for the understanding biological functions of hBPIFA1.

On the basis of my findings, showing the ability of mBPIFA1 to bind to NTHi, I hypothesised that mTECs lacking BPIFA1 would exhibit an enhanced susceptibility to NTHi infection. Although statistical significance was not detected, my data showed the trend towards an increased NTHi colonisation in *Bpifa1*$^{-/-}$ compared to WT mTECs. A great variation in the bacterial colonisation between individual batches of cells was also detected. In addition, I observed that mTECs challenged with NTHi were not readily infected and infection exhibited a patchy pattern. Overall, I can say that BPIFA1 deficiency did not to lead to significantly enhanced NTHi infection in mTEC cultures. Currently, antimicrobial properties of BPIFA1 against NTHi have been analysed in two

studies (Jiang et al., 2013b, McGillivary and Bakaletz, 2010). *Bpifa1*$^{-/-}$ mice were demonstrated to have increased bacterial burden and inflammation in the lungs after NTHi exposure compared to control mice (Jiang et al., 2013b). It was also shown that chinchilla BPIFA1 exerted bactericidal activity against NTHi *in vitro* and was able to kill more than 50% of bacterial cells when used at concentration of 1.3µg/ml (McGillivary and Bakaletz, 2010). It may be possible that mBPIFA1 exhibits bactericidal activity against NTHi and this may be a reason for the lower NTHi colonisation in WT mTECs compared to *Bpifa1*$^{-/-}$ mTECs. Bacteriostatic and bactericidal properties of mBPIFA1 against NTHi were not examined in this study and remain to be determined in the future research. The true role of BPIFA1 in NTHi infection should also be determined in the future studies using a fully established NTHi infection model of mTECs.

My findings also suggested that NTHi exposure affected expression and secretion of mBPIFA1. Reduced levels of mBPIFA1 may act as a signal to initiate the activation of other immune mechanisms which are more effective for the clearance of NTHi. These findings are consistent with previous data from our laboratory showing a decrease in BPIFA1 secretion from middle ear epithelial cells challenged with NTHi (Mulay, 2016). They are also in agreement with studies which showed that exposure of WT mice to *P. aeruginosa* and *S. pneumoniae* caused a reduction in the levels of secreted BPIFA1 in the BAL fluid (Britto et al., 2013, Jiang et al., 2013). Based on these results, it could be suggested that bacterial stimulus regulates expression and secretion of BPIFA1. Fluctuations in the levels of mBPIFA1 observed after bacterial exposure may be caused not by direct effect of pathogen onto the protein but by bacterial effect on the epithelium and its microenvironment. Another reason for reduction in levels of BPIFA1 could be associated with the release of inflammatory mediators in response to the bacterium. NTHi challenge caused a considerable induction and release of inflammatory molecules in the mTEC cultures and the presence of these inflammatory molecules in the microenvironment could also have modulated levels of BPIFA1. Previous studies have

shown that expression and secretion of BPIFA1 are reduced by other immune mediators (Chu et al., 2007, Britto et al., 2013, Wei et al., 2014). Therefore, I suggest that regulation of expression and secretion of BPIFA1 may not be directly affected by the environmental insult (pathogen) but by a more general response of the airway epithelium to the organism.

Results from my study appeared to show that NTHi associates with multiple epithelial cell types but did not appear to be associated with mBPIFA1-positive cells. Perhaps mBPIFA1-positive cells are resistant to initial NTHi infection because of BPIFA1's antimicrobial properties. BPIFA1-positive cells have also been shown to exhibit resistance to IAV invasion and IAV was mainly seen to be associated with other types of epithelial cells (Akram et al., 2018). In addition, studies in our laboratory demonstrated that mouse middle ear epithelial cells positive for BPIFA1 exhibited resistance to initial NTHi infection and NTHi was observed to invade other types of epithelial cells (Mulay, 2016). All of this data suggests that BPIFA1-positive cells exhibit resistance to invading microorganism during the initial stages of infection, but that pathogens would infect BPIFA1-positive cells after mucosal homeostasis of epithelium has been impaired. I suggest that alterations in the epithelium and impaired mucosal homeostasis causes a reduction of mBPIFA1 expression and production, and that this would predispose mBPIFA1-positive cells to NTHi invasion. It is important to more fully determine the types of cells affected by NTHi as it could provide additional insights into the mechanisms used by bacterium to initiate an infection. Better understanding of the mechanisms used by NTHi to initiate infection could assist in the future development of the therapy against NTHi infections.

I was able to show that NTHi infection caused a disruption of cellular tight-junctions, suggesting that inflammatory response generated by the cells to NTHi impaired the epithelial barrier function. This, in turn, allowed the crossing of bacteria through the layers of mTECs. These activities of NTHi were not influenced by BPIFA1. These

findings are in the agreement with other studies (Marrazzo et al., 2016, van Schilfgaarde et al., 1995). Perhaps, mBPIFA1 may influence the time required by NTHi to cross through the layers of cells? It would be of great interest to determine this effect of BPIFA1 as the possibility of BPIFA1 slowing down the passage of NTHi through layers of epithelial cells would suggest that BPIFA1 may be able to delay the passage of NTHi into the circulatory system and reduce systemic infection.

My data also suggested that the presence of mBPIFA1 did not have a great impact on inflammatory response generated by NTHi-exposed mTECs, as the absence of BPIFA1 did not lead to significantly enhanced release of inflammatory molecules. Low NTHi infectivity of mTEC cultures may be a factor which influenced this. Both WT and *Bpifa1*$^{-/-}$ mTECs exhibited resistance to NTHi infection and only patchy infection was caused. This may be overcome by the usage of different NTHi strains or longer bacterial exposure times. It is also possible that NTHi growth was suboptimal, and therefore infection limited, due to the growth of the mTECs in a defined media. Variability of infection levels was also observed in mTEC cultures and may be a second factor masking the differences in the inflammatory response by WT and *Bpifa1*$^{-/-}$ mTECs. Variation in the batches of the cells may be a third factor masking differences of the inflammatory responses. I suggest that in the future studies efforts should be made to try to reduce batch-to-batch variation in culture preparations by using cell cultures grown from clonally expanded basal cells. The usage of clonally expanded basal cells may reduce variability as clonally expanded basal cells would be obtained from single batch of cells. Techniques for clonal expansion of epithelial basal cells by dual SMAD signalling inhibition has recently been achieved by using Rho Kinase inhibitor, bone morphogenetic protein (BMP), and transforming growth factor beta (TGFβ) inhibitors (Mou et al., 2016). The effect of mBPIFA1 on inflammatory response generated by the mTECs in response to pathogen may be more accurately determined if cell batch-to-batch variation could be reduced.

Summary

Data from this thesis contribute to the view that BPIFA1 plays a role in the airway defence. Here, I showed that human and mouse BPIFA1 proteins are able to bind to Gram-positive and Gram-negative bacteria. This bacterial binding of BPIFA1 may be one of the protein's functions contributing to protection of the airways against microbial invaders. The ability of human BPIFA1 to bind to bacteria appeared to be influenced by the S18 region (G22-L42) of the protein, but not the conserved disulphide bond. Further studies are required to investigate the biological importance of the S18 region for the functions of human BPIFA1. BPIFA1 may play an important role in the host defence against NTHi infection. The ability of BPIFA1 to provide initial protection for BPIFA1-positive cells against NTHi infection may imply that BPIFA1 is a mucosal defence molecule. Further research is required to directly investigate functional regions of BPIFA1 and to allow the development of systems that will permit reproducible establishment of NTHi infection of mTEC cultures.

APPENDIX I

Table I: Materials used in the sodium dodecyl sulphate polyacrylamide gel electrophoresis (SDS-PAGE).

Solution	Components	Amount
Running buffer (10x)	Tris	30.3g
	Glycine	2.9g
	20% SDS solution	50ml
	Water	Up to volume of 1000ml
Transfer buffer	Tris	2.9g
	Glycine	1.45g
	20% SDS solution	925µl
	Methanol	100ml
	Water	Up to volume of 500ml
TBS (10x)	Tris-HCl 1M pH8.0 solution	100ml
	Sodium chloride	97.3g
	Water	Up to volume of 1000ml
TBS-Tween (10x)	Tris-HCl 1M pH 8.0 solution	100ml
	Sodium chloride	97.3g
	Tween-20	5ml
	Water	Up to volume of 1000ml
2x SDS Lysis buffer	1M DTT solution	1ml
	20% SDS solution	1ml
	Glycerol	2ml
	Tris-HCl 0.5M pH6.8	1.25ml
	0.2% bromophenol blue	200 µl
	Protease Inhibitor tablet	1 tablet
	Water	4.55ml

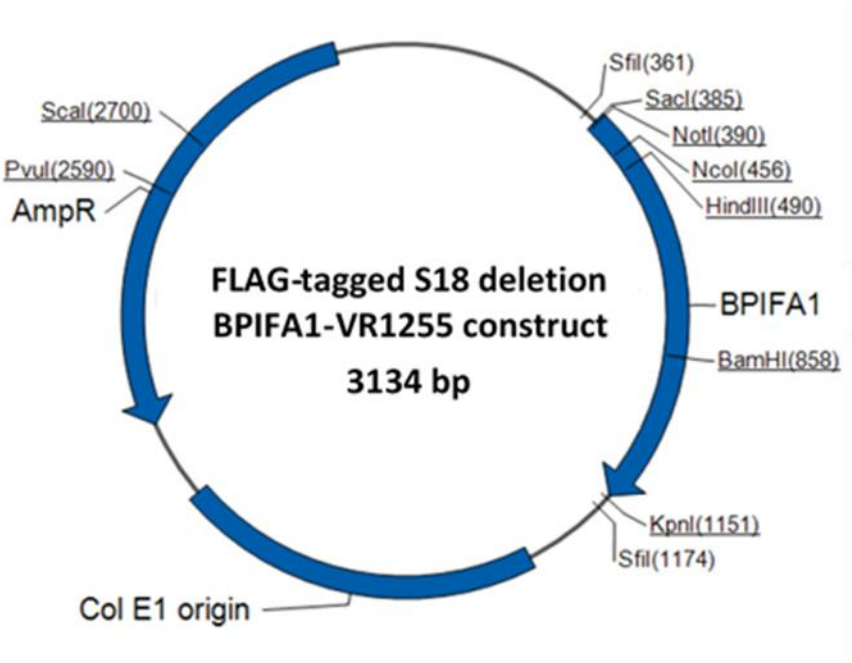

Figure I: Map of pMA-T plasmid containing FLAG-tagged S18 deletion BPIFA1 DNA.

```
1.   ATGCGGCCGCCGCCGCCACCATGTTTCAAACTGGGGGCCTCATTGTCTTCTACGGGCTGTTAGCCCAGA
70.  CCATGGCCCAGTTTAGTCCCACAGGTCTTGCAGGAAGCTTGACAAATGCCCTCAGCAATGGCCTGCTGT
139. CTGGGGGCCTGTTGGGCATTCTGGAAAACCTTCCGCTCCTGGACATCCTGAAGCCTGGAGGAGGTACTT
208. CTGGTGGCCTCCTTGGGGGACTGCTTGGAAAAGTGACGTCAGTGATTCCTGGCCTGAACAACATCATTG
277. ACATAAAGGTCACTGACCCCCAGCTGCTGGAACTTGGCCTTGTGCAGAGCCCTGATGGCCACCGTCTCT
346. ATGTCACCATCCCTCTCGGCATAAAGCTCCAAGTGAATACGCCCCTGGTCGGTGCAAGTCTGTTGAGGC
415. TGGCTGTGAAGCTGGACATCACTGCAGAAATCTTAGCTGTGAGAGATAAGCAGGAGAGGATCCACCTGG
484. TCCTTGGTGACTGCACCCATTCCCCTGGAAGCCTGCAAATTTCTCTGCTTGATGGACTTGGCCCCCTCC
553. CCATTCAAGGTCTTCTGGACAGCCTCACAGGGATCTTGAATAAAGTCCTGCCTGAGTTGGTTCAGGGCA
622. ACGTGTGCCCTCTGGTCAATGAGGTTCTCAGAGGCTTGGACATCACCCTGGTGCATGACATTGTTAACA
691. TGCTGATCCACGGACTACAGTTTGTCATCAAGGTCGACTACAAGGACGACGATGACAAGTAAAGATCTG
760. C
```

Figure II: DNA sequence of human BPIFA1-FLAG gene missing amino acids 22-42.
Start codon (ATG) and Stop codon (TAA) are highlighted in yellow. DNA sequence of FLAG tag is highlighted in orange with black underline.

Figure III: Sequencing of FLAG-tagged human S18 deletion BPIFA1-pMA-T construct. Sequencing was performed by Invitrogen GeneArt™ Gene Synthesis service. Data was analysed using FinchTV program (Version: 1.5.0). Gene sequence of interest was translated into the protein using ExPASy Translate Tool. No mutations were detected in the sequence and it was read through into FLAG tag.

Table II: Materials used in calcium phosphate transfections of HEK293T cells

Solution	Components	Amount
2x HEPES-buffered saline pH7.0 (Filter sterilised)	NaCl	8g
	HEPES	6.5g
	Na_2HPO_4-$7H_2O$	0.2g
	Distilled water	Up to volume of 500ml
2.5M $CaCl_2$ (Filter sterilised)	$CaCl_2(2H_2O)$	36.76g
	Distilled water	100ml

APPENDIX II

Figure S1: Sequencing of GFP-tagged FL-BPIFA1-pcDNA3.1 construct.
Sequencing was performed using T7 forward primer (**A**) and GFP reverse primer (**B**). Data was visualised and analysed using FinchTV program (Version: 1.5.0). Gene sequence of interest was translated into the protein sequence using ExPASy Translate Tool (**C**). No mutations were detected in the sequence and it was read through into GFP tag (black arrow indicates a beginning of GFP tag sequence).

A.

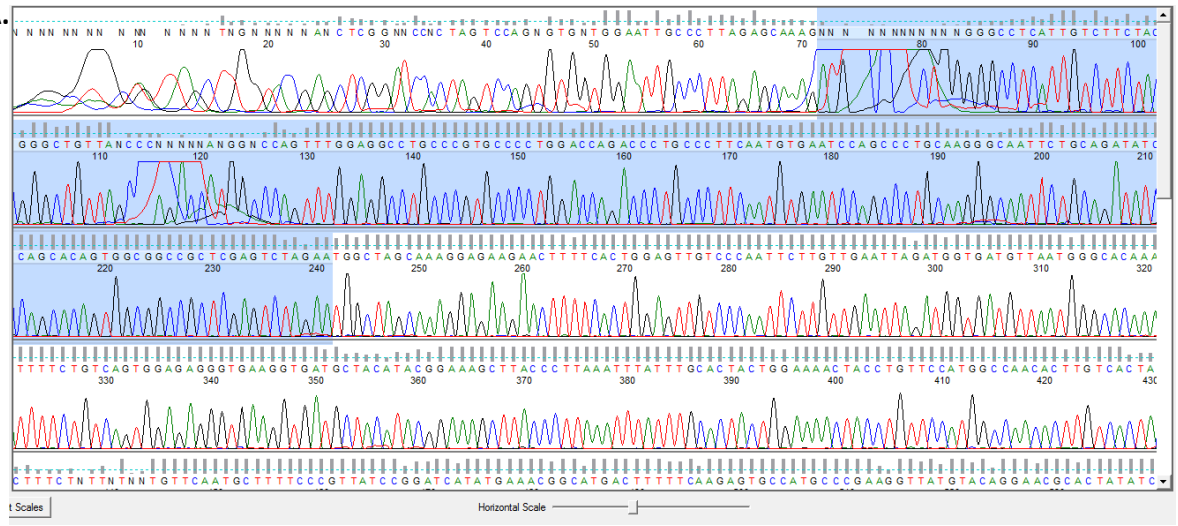

B.

Figure S2: Sequencing of GFP-tagged F/R1-BPIFA1-pcDNA3.1 construct.
Sequencing was performed using T7 forward primer (**A**). Data was visualised and analysed using FinchTV program (Version: 1.5.0). Gene sequence of interest was translated into the protein sequence using ExPASy Translate Tool (**B**). No mutations were detected in the sequence and it was read through into GFP tag (black arrow indicates a beginning of GFP tag sequence).

A.

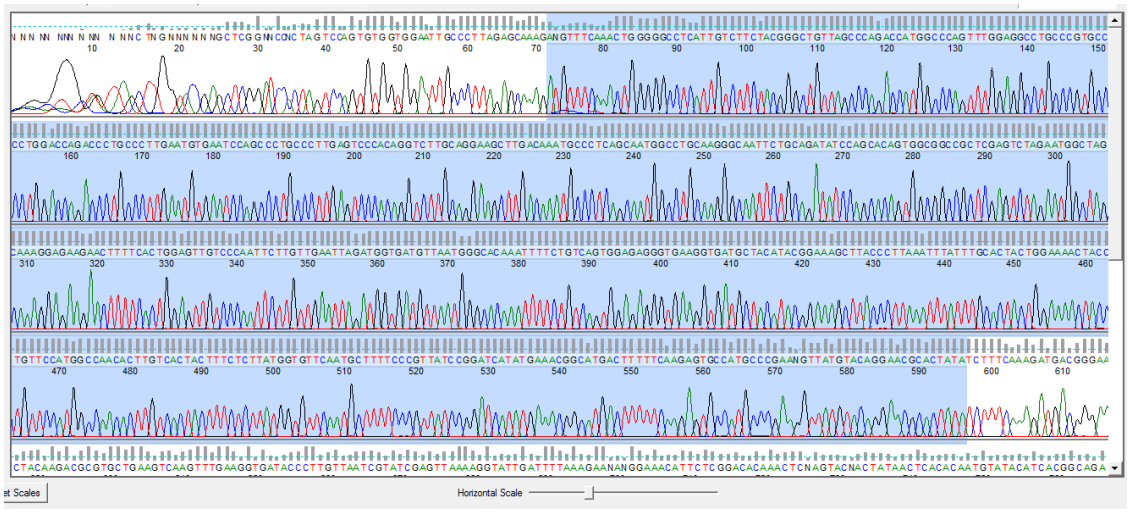

B.

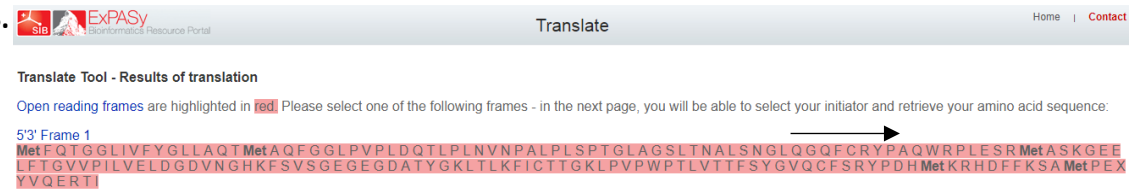

Figure S3: Sequencing of GFP-tagged F/R2-BPIFA1-pcDNA3.1 construct.
Sequencing was performed using T7 forward primer (**A**). Data was visualised and analysed using FinchTV program (Version: 1.5.0). Gene sequence of interest was translated into the protein sequence using ExPASy Translate Tool (**B**). No mutations were detected in the sequence and it was read through into GFP tag (black arrow indicates a beginning of GFP tag sequence).

Figure S4: Sequencing of GFP-tagged FL-BPIFA-pcDNA5/FRT construct.
Sequencing was performed using T7 forward primer (**A**) and BGH reverse primer (**C**). Data was visualised and analysed using FinchTV program (Version: 1.5.0). Gene sequences of interest (**B** – forward sequencing data; and **D** – reverse sequencing data) were translated into the protein sequences using ExPASy Translate Tool. No mutations were detected in the sequence and it was read through into GFP tag (black arrow indicates a beginning of GFP tag sequence).

Figure S5: Sequencing of GFP-tagged F/R1-BPIFA-pcDNA5/FRT construct.
Sequencing was performed using T7 forward primer (**A**) and BGH reverse primer (**C**). Data was visualised and analysed using FinchTV program (Version: 1.5.0). Gene sequences of interest (**B** – forward sequencing data; and **D** – reverse sequencing data) were translated into the protein sequences using ExPASy Translate Tool. No mutations were detected in the sequence and it was read through into GFP tag (black arrow indicates a beginning of GFP tag sequence).

Figure S6: Sequencing of GFP-tagged F/R2-BPIFA-pcDNA5/FRT construct.
Sequencing was performed using T7 forward primer (**A**) and BGH reverse primer (**C**). Data was visualised and analysed using FinchTV program (Version: 1.5.0). Gene sequences of interest (**B** – forward sequencing data; and **D** – reverse sequencing data) were translated into the protein sequences using ExPASy Translate Tool. No mutations were detected in the sequence and it was read through into GFP tag (black arrow indicates a beginning of GFP tag sequence).

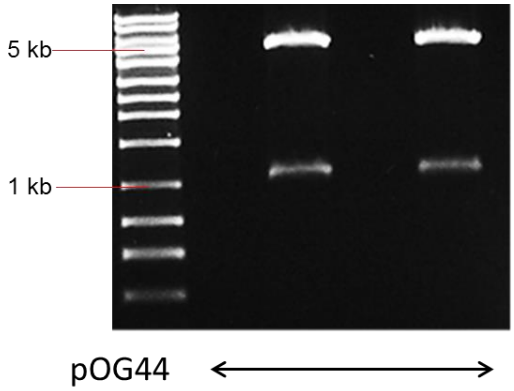

Figure S7: Verification of pOG44 expression plasmid.
E. coli cells transformed with pOG44 expression plasmid were regrown in the LB-ampicillin broth overnight to generate plasmid DNA for transfection reactions. Maxiprep samples were digested with EcoRI to verify the quality of extracted pOG44 plasmid DNA. Restriction digest on maxiprep samples was expected to produce two fragments of 1051bp and 4734bp size, indicating that maxiprep product was pOG44 plasmid DNA. Fragments of correct size were observed.

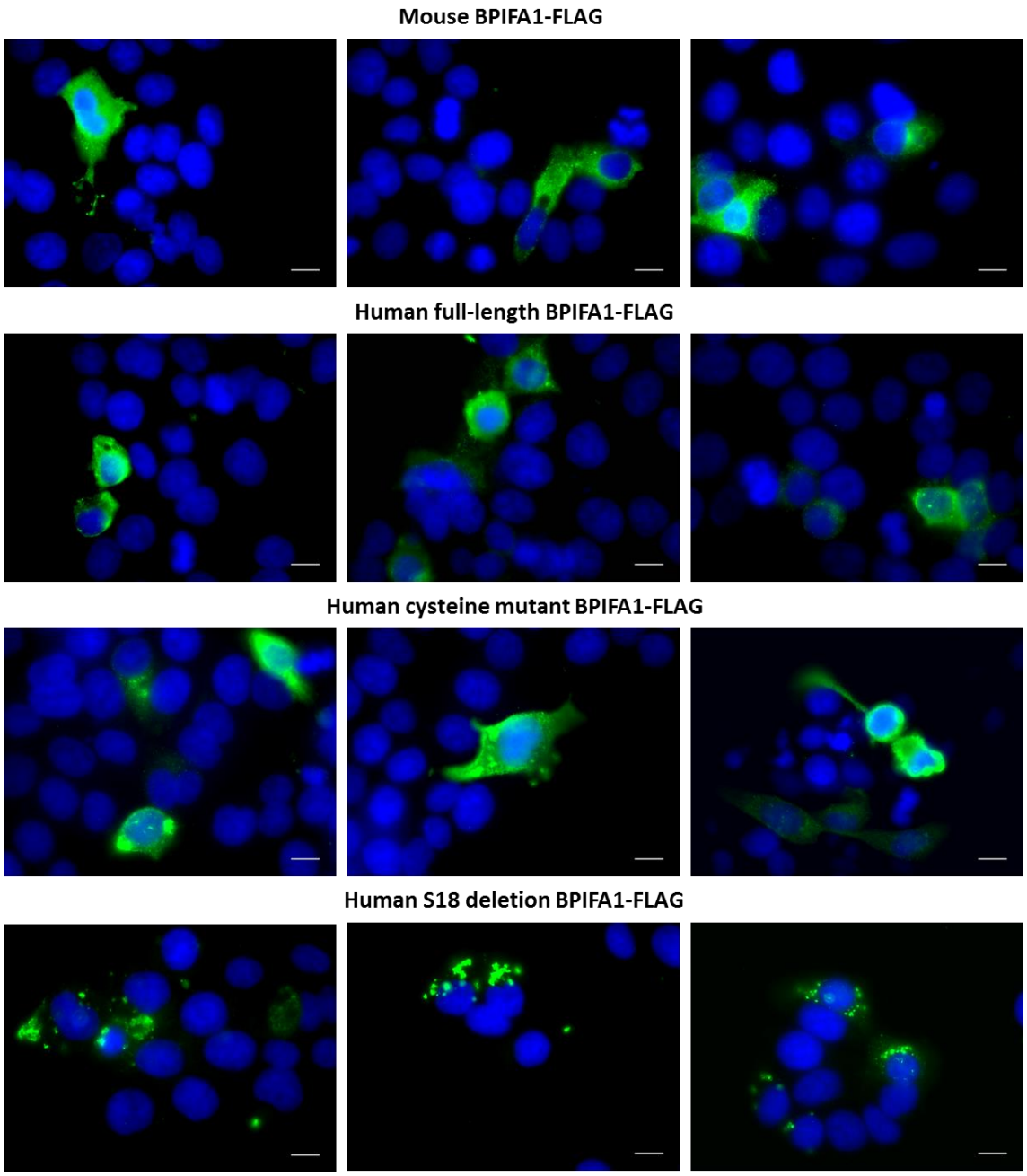

Figure S8: Detection of human and mouse FLAG-tagged proteins in NCI-H292 cells.
Images were taken at 100x magnification with immunofluorescence microscope (Zeiss Axioplan 2) (scale bar: 10µm). Nuclei of transfected NCI-H292 cells were stained by DAPI in blue and BPIFA1-FLAG proteins of interest were stained in green using Alexa Flour 488. Images were processed using ImageJ-win32 program.

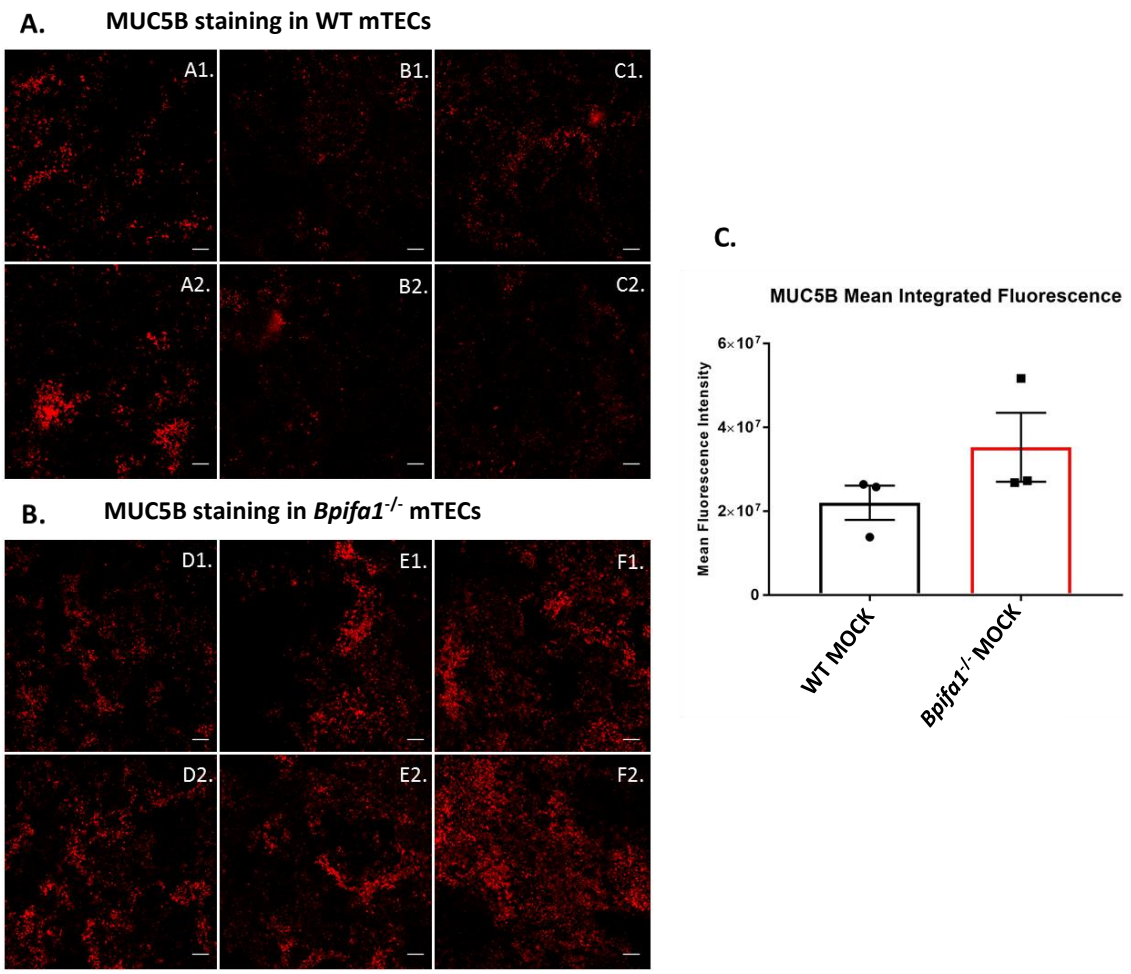

Figure S9: Staining for MUC5B is increased in *Bpifa1*$^{-/-}$ mTECs compared to WT mTECs. IFC images showing a staining for cytosolic MUC5B in MOCK-exposed WT mTECs (**A**) and MOCK-exposed *Bpifa1*$^{-/-}$ mTECs (**B**) after 72hrs post-challenge. Each panel represents 2 central fields at 10x magnification. Data are representative of 3 independent batches of WT and *Bpifa1*$^{-/-}$ mTECs. Scale bar: 100µm. Analysis of IFC images suggested an increased staining for MUC5B in MOCK-exposed *Bpifa1*$^{-/-}$ mTECs compared to MOCK-exposed WT mTECs (**C**). This increase was not statistically significant and appeared to be caused by variation in the batches of mTECs. Data was analysed using unpaired non-parametric two-tailed student's t-test and represented as mean ± SEM, n=3 individual batches of mTEC cultures.

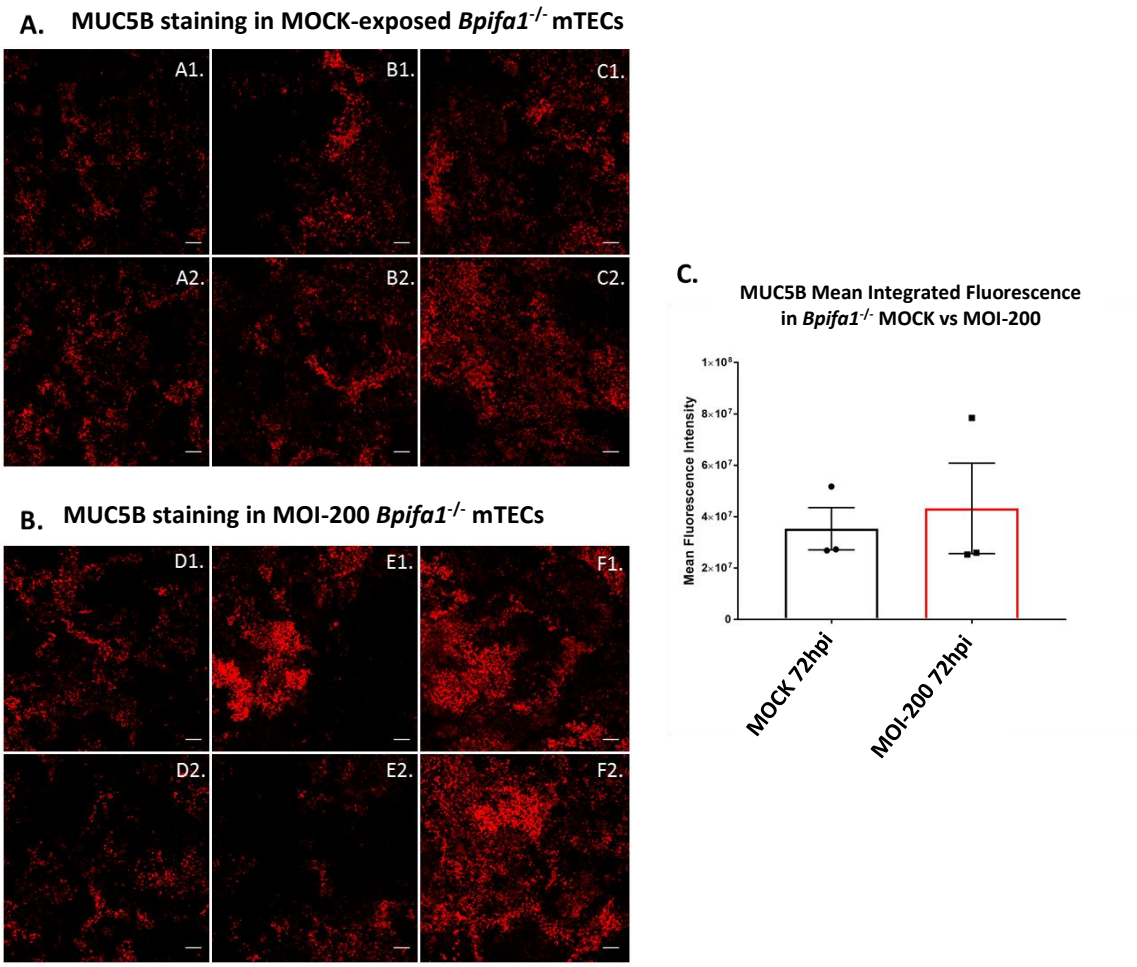

Figure S10: MUC5B staining is increased in NTHi-exposed *Bpifa1*$^{-/-}$ mTECs compared to MOCK-exposed mTECs.
IFC images showing a staining for MUC5B in MOCK-exposed *Bpifa1*$^{-/-}$ mTECs (**A**) and *Bpifa1*$^{-/-}$ mTECs exposed to NTHi at MOI-200 (**B**) after 72hrs post-challenge. Each panel represents 2 central fields at 10x magnification. Data are representative of 3 independent batches of *Bpifa1*$^{-/-}$ mTECs. Scale bar: 100µm. Analysis of IFC images suggested a slight increase in MUC5B staining in NTHi-exposed *Bpifa1*$^{-/-}$ mTECs compared to MOCK-exposed *Bpifa1*$^{-/-}$ mTECs (**C**). This increase was not statistically significant and seemed to be caused by variation in the batches of mTECs. Data was analysed using unpaired non-parametric two-tailed student's t-test and represented as mean ± SEM, n=3 individual batches of mTEC cultures.

Secretion of BPIFA1 by NTHi challenged and MOCK-infected WT mTECs

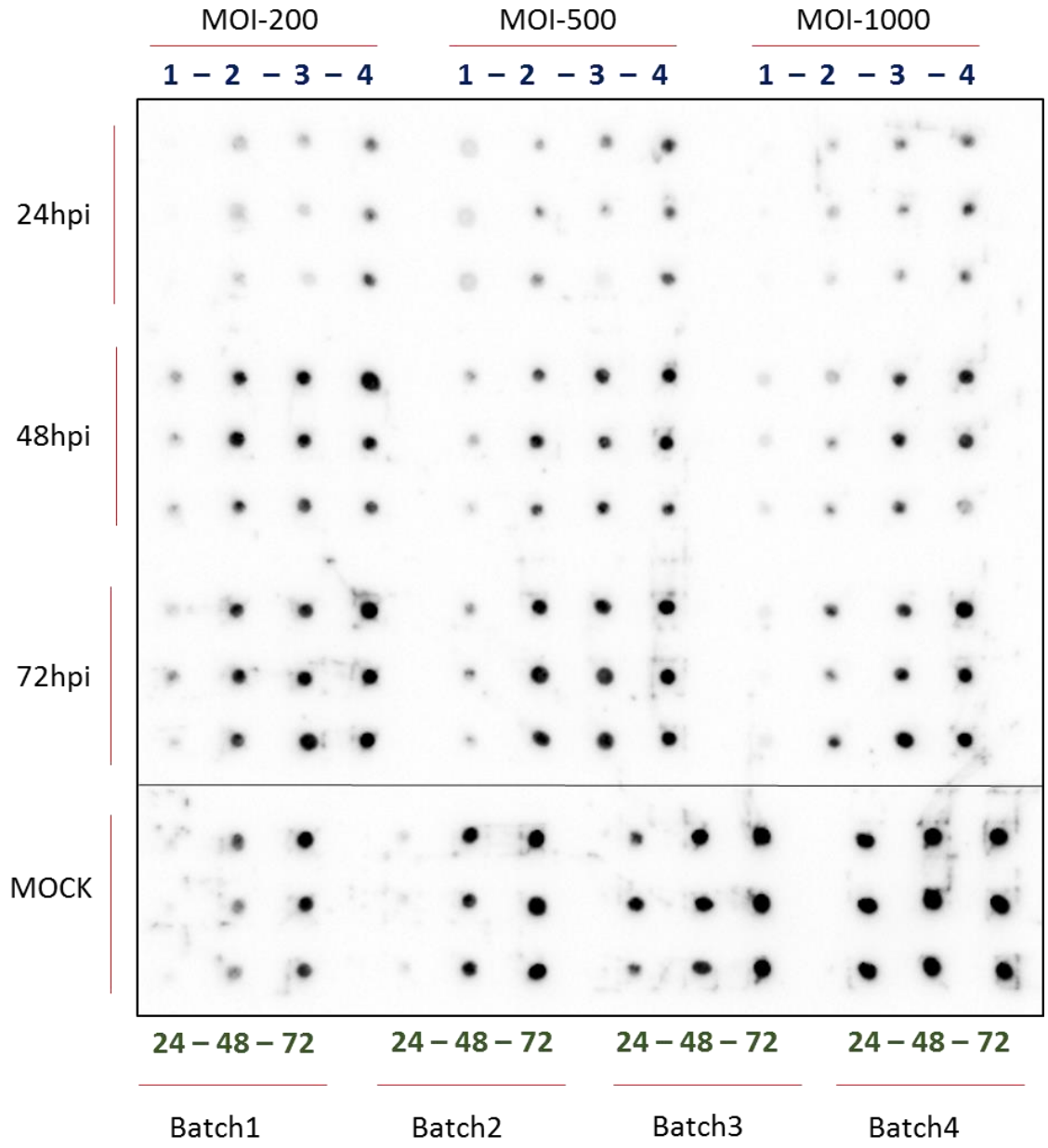

Figure S11: Secretion of BPIFA1 by NTHi- and MOCK-exposed WT mTECs.
Results of dot blotting, showing the secretion of BPIFA1 by MOCK- and NTHi-challenged (MOI-200, MOI-500, and MOI-1000) WT mTECs at 24, 48, and 72 hpi. Apical secretion washes from four independent batches of WT mTECs were analysed. Experiment was performed in the triplicates.

BIBLIOGRAPHY

ACTOR, J. K., HWANG, S. A. & KRUZEL, M. L. 2009. Lactoferrin as a natural immune modulator. *Curr Pharm Des,* 15**,** 1956-73. AEBI, M. 2013. N-linked protein glycosylation in the ER. *Biochim Biophys Acta,* 1833**,** 2430-7. ACTOR, J. K., HWANG, S. A. & KRUZEL, M. L. 2009. Lactoferrin as a natural immune modulator. *Curr Pharm Des,* 15**,** 1956-73.

AEBI, M. 2013. N-linked protein glycosylation in the ER. *Biochim Biophys Acta,* 1833**,** 2430-7. ACTOR, J. K., HWANG, S. A. & KRUZEL, M. L. 2009. Lactoferrin as a natural immune modulator. *Curr Pharm Des,* 15**,** 1956-73.

AHEARN, C. P., GALLO, M. C. & MURPHY, T. F. 2017. Insights on persistent airway infection by non-typeable Haemophilus influenzae in chronic obstructive pulmonary disease. *Pathog Dis,* 75.

AHLGREN, H. G., BENEDETTI, A., LANDRY, J. S., BERNIER, J., MATOUK, E., RADZIOCH, D., LANDS, L. C., ROUSSEAU, S. & NGUYEN, D. 2015. Clinical outcomes associated with Staphylococcus aureus and Pseudomonas aeruginosa airway infections in adult cystic fibrosis patients. *BMC Pulm Med,* 15**,** 67.

AHMAD, S., TYRRELL, J., WALTON, W. G., TRIPATHY, A., REDINBO, M. R. & TARRAN, R. 2016. Short Palate, Lung, and Nasal Epithelial Clone 1 Has Antimicrobial and Antibiofilm Activities against the Burkholderia cepacia Complex. *Antimicrob Agents Chemother,* 60**,** 6003-12.

AKIRA, S., UEMATSU, S. & TAKEUCHI, O. 2006. Pathogen recognition and innate immunity. *Cell,* 124**,** 783-801.

AKRAM, K. M., MOYO, N. A., LEEMING, G. H., BINGLE, L., JASIM, S., HUSSAIN, S., SCHORLEMMER, A., KIPAR, A., DIGARD, P., TRIPP, R. A., SHOHET, R. V., BINGLE, C. D. & STEWART, J. P. 2018. An innate defense peptide BPIFA1/SPLUNC1 restricts influenza A virus infection. *Mucosal Immunol,* 11**,** 71-81.

AL-SADI, R., BOIVIN, M. & MA, T. 2009. Mechanism of cytokine modulation of epithelial tight junction barrier. *Front Biosci (Landmark Ed),* 14**,** 2765-78.

ANDRÉ, G. O., POLITANO, W. R., MIRZA, S., CONVERSO, T. R., FERRAZ, L. F., LEITE, L. C. & DARRIEUX, M. 2015. Combined effects of lactoferrin and lysozyme on Streptococcus pneumoniae killing. *Microb Pathog,* 89**,** 7-17.

BAEK, K. T., FREES, D., RENZONI, A., BARRAS, C., RODRIGUEZ, N., MANZANO, C. & KELLEY, W. L. 2013. Genetic variation in the Staphylococcus aureus 8325 strain lineage revealed by whole-genome sequencing. *PLoS One,* 8**,** e77122.

BALS, R. 2000. Epithelial antimicrobial peptides in host defense against infection. *Respir Res,* 1**,** 141-50.

BALS, R. & HIEMSTRA, P. S. 2004. Innate immunity in the lung: how epithelial cells fight against respiratory pathogens. *Eur Respir J,* 23**,** 327-33.

BARLOW, P. G., SVOBODA, P., MACKELLAR, A., NASH, A. A., YORK, I. A., POHL, J., DAVIDSON, D. J. & DONIS, R. O. 2011. Antiviral activity and increased host defense against influenza infection elicited by the human cathelicidin LL-37. *PLoS One,* 6**,** e25333.

BASBAUM, C. B., JANY, B. & FINKBEINER, W. E. 1990. The serous cell. *Annu Rev Physiol,* 52**,** 97-113.

BAUER, N. C., DOETSCH, P. W. & CORBETT, A. H. 2015. Mechanisms Regulating Protein Localization. *Traffic,* 16**,** 1039-61.

BAYES, H. K., RITCHIE, N., IRVINE, S. & EVANS, T. J. 2016. A murine model of early Pseudomonas aeruginosa lung disease with transition to chronic infection. *Sci Rep,* 6**,** 35838.

BETTINA, A., ZHANG, Z., MICHELS, K., CAGNINA, R. E., VINCENT, I. S., BURDICK, M. D., KADL, A. & MEHRAD, B. 2016. M-CSF Mediates Host Defense during Bacterial Pneumonia by

Promoting the Survival of Lung and Liver Mononuclear Phagocytes. *J Immunol,* 196**,** 5047-55.

BINGLE, C. D., ARAUJO, B., WALLACE, W. A., HIRANI, N. & BINGLE, L. 2013. What is top of the charts? BPIFB1/LPLUNC1 localises to the bronchiolised epithelium in the honeycomb cysts in UIP. *Thorax,* 68**,** 1167-8.

BINGLE, C. D. & BINGLE, L. 2000. Characterisation of the human plunc gene, a gene product with an upper airways and nasopharyngeal restricted expression pattern. *Biochim Biophys Acta,* 1493**,** 363-7.

BINGLE, C. D., BINGLE, L. & CRAVEN, C. J. 2011a. Distant cousins: genomic and sequence diversity within the BPI fold-containing (BPIF)/PLUNC protein family. *Biochem Soc Trans,* 39**,** 961-5.

BINGLE, C. D. & CRAVEN, C. J. 2002. PLUNC: a novel family of candidate host defence proteins expressed in the upper airways and nasopharynx. *Hum Mol Genet,* 11**,** 937-43.

BINGLE, C. D., LECLAIR, E. E., HAVARD, S., BINGLE, L., GILLINGHAM, P. & CRAVEN, C. J. 2004. Phylogenetic and evolutionary analysis of the PLUNC gene family. *Protein Sci,* 13**,** 422-30.

BINGLE, C. D., SEAL, R. L. & CRAVEN, C. J. 2011b. Systematic nomenclature for the PLUNC/PSP/BSP30/SMGB proteins as a subfamily of the BPI fold-containing superfamily. *Biochem Soc Trans,* 39**,** 977-83.

BINGLE, L., BARNES, F. A., CROSS, S. S., RASSL, D., WALLACE, W. A., CAMPOS, M. A. & BINGLE, C. D. 2007. Differential epithelial expression of the putative innate immune molecule SPLUNC1 in cystic fibrosis. *Respir Res,* 8**,** 79.

BINGLE, L., CROSS, S. S., HIGH, A. S., WALLACE, W. A., DEVINE, D. A., HAVARD, S., CAMPOS, M. A. & BINGLE, C. D. 2005. SPLUNC1 (PLUNC) is expressed in glandular tissues of the respiratory tract and in lung tumours with a glandular phenotype. *J Pathol,* 205**,** 491-7.

BINGLE, L., WILSON, K., MUSA, M., ARAUJO, B., RASSL, D., WALLACE, W. A., LECLAIR, E. E., MAUAD, T., ZHOU, Z., MALL, M. A. & BINGLE, C. D. 2012. BPIFB1 (LPLUNC1) is upregulated in cystic fibrosis lung disease. *Histochem Cell Biol,* 138**,** 749-58.

BOGAERT, D., DE GROOT, R. & HERMANS, P. W. 2004. Streptococcus pneumoniae colonisation: the key to pneumococcal disease. *Lancet Infect Dis,* 4**,** 144-54.

BOON, K., BAILEY, N. W., YANG, J., STEEL, M. P., GROSHONG, S., KERVITSKY, D., BROWN, K. K., SCHWARZ, M. I. & SCHWARTZ, D. A. 2009. Molecular phenotypes distinguish patients with relatively stable from progressive idiopathic pulmonary fibrosis (IPF). *PLoS One,* 4**,** e5134.

BOSCH, A. A., BIESBROEK, G., TRZCINSKI, K., SANDERS, E. A. & BOGAERT, D. 2013. Viral and bacterial interactions in the upper respiratory tract. *PLoS Pathog,* 9**,** e1003057.

BRESSER, P., VAN ALPHEN, L., HABETS, F. J., HART, A. A., DANKERT, J., JANSEN, H. M. & LUTTER, R. 1997. Persisting Haemophilus influenzae strains induce lower levels of interleukin-6 and interleukin-8 in H292 lung epithelial cells than nonpersisting strains. *Eur Respir J,* 10**,** 2319-26.

BRITTO, C. J. & COHN, L. 2015. Bactericidal/Permeability-increasing protein fold-containing family member A1 in airway host protection and respiratory disease. *Am J Respir Cell Mol Biol,* 52**,** 525-34.

BRITTO, C. J., LIU, Q., CURRAN, D. R., PATHAM, B., DELA CRUZ, C. S. & COHN, L. 2013. Short palate, lung, and nasal epithelial clone-1 is a tightly regulated airway sensor in innate and adaptive immunity. *Am J Respir Cell Mol Biol,* 48**,** 717-24.

BRUNE, K., FRANK, J., SCHWINGSHACKL, A., FINIGAN, J. & SIDHAYE, V. K. 2015. Pulmonary epithelial barrier function: some new players and mechanisms. *Am J Physiol Lung Cell Mol Physiol,* 308**,** L731-45.

BUER, J. & BALLING, R. 2003. Mice, microbes and models of infection. *Nat Rev Genet,* 4**,** 195-205.

BUIST, A. S. 2003. Similarities and differences between asthma and chronic obstructive pulmonary disease: treatment and early outcomes. *Eur Respir J Suppl,* 39**,** 30s-35s.

CAMPOS, M. A., ABREU, A. R., NLEND, M. C., COBAS, M. A., CONNER, G. E. & WHITNEY, P. L. 2004. Purification and characterization of PLUNC from human tracheobronchial secretions. *Am J Respir Cell Mol Biol,* 30**,** 184-92.

CAPALDO, C. T. & NUSRAT, A. 2009. Cytokine regulation of tight junctions. *Biochim Biophys Acta,* 1788**,** 864-71.

CASTEELS, P., AMPE, C., JACOBS, F., VAECK, M. & TEMPST, P. 1989. Apidaecins: antibacterial peptides from honeybees. *Embo j,* 8**,** 2387-91.

CHEN, Z. Y., HE, C. Y., EHRHARDT, A. & KAY, M. A. 2003. Minicircle DNA vectors devoid of bacterial DNA result in persistent and high-level transgene expression in vivo. *Mol Ther,* 8**,** 495-500.

CHMIEL, J. F., AKSAMIT, T. R., CHOTIRMALL, S. H., DASENBROOK, E. C., ELBORN, J. S., LIPUMA, J. J., RANGANATHAN, S. C., WATERS, V. J. & RATJEN, F. A. 2014. Antibiotic management of lung infections in cystic fibrosis. I. The microbiome, methicillin-resistant Staphylococcus aureus, gram-negative bacteria, and multiple infections. *Ann Am Thorac Soc,* 11**,** 1120-9.

CHU, H. W., GALLY, F., THAIKOOTTATHIL, J., JANSSEN-HEININGER, Y. M., WU, Q., ZHANG, G., REISDORPH, N., CASE, S., MINOR, M., SMITH, S., JIANG, D., MICHELS, N., SIMON, G. & MARTIN, R. J. 2010. SPLUNC1 regulation in airway epithelial cells: role of Toll-like receptor 2 signaling. *Respir Res,* 11**,** 155.

CHU, H. W., THAIKOOTTATHIL, J., RINO, J. G., ZHANG, G., WU, Q., MOSS, T., REFAELI, Y., BOWLER, R., WENZEL, S. E., CHEN, Z., ZDUNEK, J., BREED, R., YOUNG, R., ALLAIRE, E. & MARTIN, R. J. 2007. Function and regulation of SPLUNC1 protein in Mycoplasma infection and allergic inflammation. *J Immunol,* 179**,** 3995-4002.

CIOFU, O., HANSEN, C. R. & HØIBY, N. 2013. Respiratory bacterial infections in cystic fibrosis. *Curr Opin Pulm Med,* 19**,** 251-8.

CLEMANS, D. L., BAUER, R. J., HANSON, J. A., HOBBS, M. V., ST GEME, J. W., 3RD, MARRS, C. F. & GILSDORF, J. R. 2000. Induction of proinflammatory cytokines from human respiratory epithelial cells after stimulation by nontypeable Haemophilus influenzae. *Infect Immun,* 68**,** 4430-40.

CLEMENTI, C. F. & MURPHY, T. F. 2011. Non-typeable Haemophilus influenzae invasion and persistence in the human respiratory tract. *Front Cell Infect Microbiol,* 1**,** 1.

CODY, A. J., FIELD, D., FEIL, E. J., STRINGER, S., DEADMAN, M. E., TSOLAKI, A. G., GRATZ, B., BOUCHET, V., GOLDSTEIN, R., HOOD, D. W. & MOXON, E. R. 2003. High rates of recombination in otitis media isolates of non-typeable Haemophilus influenzae. *Infect Genet Evol,* 3**,** 57-66.

CORMIER, S. A., YOU, D. & HONNEGOWDA, S. 2010. The use of a neonatal mouse model to study respiratory syncytial virus infections. *Expert Rev Anti Infect Ther,* 8**,** 1371-80.

COYNE, C. B., VANHOOK, M. K., GAMBLING, T. M., CARSON, J. L., BOUCHER, R. C. & JOHNSON, L. G. 2002. Regulation of airway tight junctions by proinflammatory cytokines. *Mol Biol Cell,* 13**,** 3218-34.

CROMWELL, O., HAMID, Q., CORRIGAN, C. J., BARKANS, J., MENG, Q., COLLINS, P. D. & KAY, A. B. 1992. Expression and generation of interleukin-8, IL-6 and granulocyte-macrophage colony-stimulating factor by bronchial epithelial cells and enhancement by IL-1 beta and tumour necrosis factor-alpha. *Immunology,* 77**,** 330-7.

CRYSTAL, R. G., RANDELL, S. H., ENGELHARDT, J. F., VOYNOW, J. & SUNDAY, M. E. 2008. Airway epithelial cells: current concepts and challenges. *Proc Am Thorac Soc,* 5**,** 772-7.

CZAPLEWSKI, L., BAX, R., CLOKIE, M., DAWSON, M., FAIRHEAD, H., FISCHETTI, V. A., FOSTER, S., GILMORE, B. F., HANCOCK, R. E., HARPER, D., HENDERSON, I. R., HILPERT, K., JONES, B. V., KADIOGLU, A., KNOWLES, D., OLAFSDOTTIR, S., PAYNE, D., PROJAN, S., SHAUNAK, S., SILVERMAN, J., THOMAS, C. M., TRUST, T. J., WARN, P. & REX, J. H. 2016. Alternatives to antibiotics-a pipeline portfolio review. *Lancet Infect Dis,* 16**,** 239-51.

DAJANI, R., ZHANG, Y., TAFT, P. J., TRAVIS, S. M., STARNER, T. D., OLSEN, A., ZABNER, J., WELSH, M. J. & ENGELHARDT, J. F. 2005. Lysozyme secretion by submucosal glands protects the airway from bacterial infection. *Am J Respir Cell Mol Biol,* 32**,** 548-52.

DALLE, B., RUBIN, J. E., ALKAN, O., SUKONNIK, T., PASCERI, P., YAO, S., PAWLIUK, R., LEBOULCH, P. & ELLIS, J. 2005. eGFP reporter genes silence LCRbeta-globin transgene expression via CpG dinucleotides. *Mol Ther,* 11**,** 591-9.

DALTON, A. C. & BARTON, W. A. 2014. Over-expression of secreted proteins from mammalian cell lines. *Protein Sci,* 23**,** 517-25.

DAVIDSON, D. J., KILANOWSKI, F. M., RANDELL, S. H., SHEPPARD, D. N. & DORIN, J. R. 2000. A primary culture model of differentiated murine tracheal epithelium. *Am J Physiol Lung Cell Mol Physiol,* 279**,** L766-78.

DE SMET, E. G., SEYS, L. J., VERHAMME, F. M., VANAUDENAERDE, B. M., BRUSSELLE, G. G., BINGLE, C. D. & BRACKE, K. R. 2018. Association of innate defense proteins BPIFA1 and BPIFB1 with disease severity in COPD. *Int J Chron Obstruct Pulmon Dis,* 13**,** 11-27.

DE STEENHUIJSEN PITERS, W. A., SANDERS, E. A. & BOGAERT, D. 2015. The role of the local microbial ecosystem in respiratory health and disease. *Philos Trans R Soc Lond B Biol Sci,* 370.

DENHARDT, D. T., GIACHELLI, C. M. & RITTLING, S. R. 2001. Role of osteopontin in cellular signaling and toxicant injury. *Annu Rev Pharmacol Toxicol,* 41**,** 723-49.

DENNY, F. W. 1974. Effect of a toxin produced by Haemophilus influenzae on ciliated respiratory epithelium. *J Infect Dis,* 129**,** 93-100.

DI, Y. P., HARPER, R., ZHAO, Y., PAHLAVAN, N., FINKBEINER, W. & WU, R. 2003. Molecular cloning and characterization of spurt, a human novel gene that is retinoic acid-inducible and encodes a secretory protein specific in upper respiratory tracts. *J Biol Chem,* 278**,** 1165-73.

DI, Y. P., TKACH, A. V., YANAMALA, N., STANLEY, S., GAO, S., SHURIN, M. R., KISIN, E. R., KAGAN, V. E. & SHVEDOVA, A. 2013. Dual acute proinflammatory and antifibrotic pulmonary effects of short palate, lung, and nasal epithelium clone-1 after exposure to carbon nanotubes. *Am J Respir Cell Mol Biol,* 49**,** 759-67.

EENJES, E., MERTENS, T. C. J., BUSCOP-VAN KEMPEN, M. J., VAN WIJCK, Y., TAUBE, C., ROTTIER, R. J. & HIEMSTRA, P. S. 2018. A novel method for expansion and differentiation of mouse tracheal epithelial cells in culture. *Sci Rep,* 8**,** 7349.

ELLISON, R. T., GIEHL, T. J. & LAFORCE, F. M. 1988. Damage of the outer membrane of enteric gram-negative bacteria by lactoferrin and transferrin. *Infect Immun,* 56**,** 2774-81.

ELSBACH, P. & WEISS, J. 1998. Role of the bactericidal/permeability-increasing protein in host defence. *Curr Opin Immunol,* 10**,** 45-9.

EMBL-EBI. 2018. *Kalign: Multiple Sequence Alignment* [Online]. Available: http://www.ebi.ac.uk/Tools/msa/kalign/ [Accessed 2018].

EMBL-EBI. 2019a. *InterPro: Bactericidal permeability-increasing protein, alpha/beta domain superfamily (IPR017943)* [Online]. Available: http://www.ebi.ac.uk/interpro/entry/IPR017943 [Accessed 10th February 2019].

EMBL-EBI. 2019b. *InterPro: Lipid-binding serum glycoprotein, N-terminal (IPR017942)* [Online]. Available: https://www.ebi.ac.uk/interpro/entry/IPR017942 [Accessed 10th February 2019].

FAHEY, T., STOCKS, N. & THOMAS, T. 1998. Systematic review of the treatment of upper respiratory tract infection. *Arch Dis Child,* 79**,** 225-30.

FALLA, T. J., KARUNARATNE, D. N. & HANCOCK, R. E. 1996. Mode of action of the antimicrobial peptide indolicidin. *J Biol Chem,* 271**,** 19298-303.

FANG, F., PAN, J., LI, Y., FENG, X. & WANG, J. 2017. Identification of potential transcriptomic markers in developing asthma: An integrative analysis of gene expression profiles. *Mol Immunol,* 92**,** 38-44.

FELLNER, R. C., TERRYAH, S. T. & TARRAN, R. 2016. Inhaled protein/peptide-based therapies for respiratory disease. *Mol Cell Pediatr,* 3**,** 16.

FENG, Y., CHEN, C. J., SU, L. H., HU, S., YU, J. & CHIU, C. H. 2008. Evolution and pathogenesis of Staphylococcus aureus: lessons learned from genotyping and comparative genomics. *FEMS Microbiol Rev,* 32**,** 23-37.

FINEGOLD, S. M. & JOHNSON, C. C. 1985. Lower respiratory tract infection. *Am J Med,* 79**,** 73-7.

FINN, R. D., ATTWOOD, T. K., BABBITT, P. C., BATEMAN, A., BORK, P., BRIDGE, A. J., CHANG, H. Y., DOSZTANYI, Z., EL-GEBALI, S., FRASER, M., GOUGH, J., HAFT, D., HOLLIDAY, G. L., HUANG, H., HUANG, X., LETUNIC, I., LOPEZ, R., LU, S., MARCHLER-BAUER, A., MI, H., MISTRY, J., NATALE, D. A., NECCI, M., NUKA, G., ORENGO, C. A., PARK, Y., PESSEAT, S., PIOVESAN, D., POTTER, S. C., RAWLINGS, N. D., REDASCHI, N., RICHARDSON, L., RIVOIRE, C., SANGRADOR-VEGAS, A., SIGRIST, C., SILLITOE, I., SMITHERS, B., SQUIZZATO, S., SUTTON, G., THANKI, N., THOMAS, P. D., TOSATTO, S. C., WU, C. H., XENARIOS, I., YEH, L. S., YOUNG, S. Y. & MITCHELL, A. L. 2017. InterPro in 2017-beyond protein family and domain annotations. *Nucleic Acids Res,* 45**,** D190-d199.

FOLLETTIE, M. T., ELLIS, D. K., DONALDSON, D. D., HILL, A. A., DIESL, V., DECLERCQ, C., SYPEK, J. P., DORNER, A. J. & WILLS-KARP, M. 2006. Gene expression analysis in a murine model of allergic asthma reveals overlapping disease and therapy dependent pathways in the lung. *Pharmacogenomics J,* 6**,** 141-52.

FORNANDER, L., GHAFOURI, B., KIHLSTRÖM, E., AKERLIND, B., SCHÖN, T., TAGESSON, C. & LINDAHL, M. 2011. Innate immunity proteins and a new truncated form of SPLUNC1 in nasopharyngeal aspirates from infants with respiratory syncytial virus infection. *Proteomics Clin Appl,* 5**,** 513-22.

FOSTER, T. J. 2017. Antibiotic resistance in Staphylococcus aureus. Current status and future prospects. *FEMS Microbiol Rev,* 41**,** 430-449.

FOXWELL, A. R., KYD, J. M. & CRIPPS, A. W. 1998. Nontypeable Haemophilus influenzae: pathogenesis and prevention. *Microbiol Mol Biol Rev,* 62**,** 294-308.

FREELEY, M., KELLEHER, D. & LONG, A. 2011. Regulation of Protein Kinase C function by phosphorylation on conserved and non-conserved sites. *Cell Signal,* 23**,** 753-62.

FUJIMOTO, H., KOBAYASHI, T. & AZUMA, A. 2015. Idiopathic Pulmonary Fibrosis: Treatment and Prognosis. *Clin Med Insights Circ Respir Pulm Med,* 9**,** 179-185.

GAILLARD, E. A., KOTA, P., GENTZSCH, M., DOKHOLYAN, N. V., STUTTS, M. J. & TARRAN, R. 2010. Regulation of the epithelial Na+ channel and airway surface liquid volume by serine proteases. *Pflugers Arch,* 460**,** 1-17.

GAKHAR, L., BARTLETT, J. A., PENTERMAN, J., MIZRACHI, D., SINGH, P. K., MALLAMPALLI, R. K., RAMASWAMY, S. & MCCRAY, P. B., JR. 2010. PLUNC is a novel airway surfactant protein with anti-biofilm activity. *PLoS One,* 5**,** e9098.

GALLY, F., DI, Y. P., SMITH, S. K., MINOR, M. N., LIU, Y., BRATTON, D. L., FRASCH, S. C., MICHELS, N. M., CASE, S. R. & CHU, H. W. 2011. SPLUNC1 promotes lung innate defense against Mycoplasma pneumoniae infection in mice. *Am J Pathol,* 178**,** 2159-67.

GANESAN, S., COMSTOCK, A. T. & SAJJAN, U. S. 2013. Barrier function of airway tract epithelium. *Tissue Barriers,* 1**,** e24997.

GARCIA-CABALLERO, A., RASMUSSEN, J. E., GAILLARD, E., WATSON, M. J., OLSEN, J. C., DONALDSON, S. H., STUTTS, M. J. & TARRAN, R. 2009. SPLUNC1 regulates airway surface liquid volume by protecting ENaC from proteolytic cleavage. *Proc Natl Acad Sci U S A,* 106**,** 11412-7.

GARLAND, A. L., WALTON, W. G., COAKLEY, R. D., TAN, C. D., GILMORE, R. C., HOBBS, C. A., TRIPATHY, A., CLUNES, L. A., BENCHARIT, S., STUTTS, M. J., BETTS, L., REDINBO, M. R. & TARRAN, R. 2013. Molecular basis for pH-dependent mucosal dehydration in cystic fibrosis airways. *Proc Natl Acad Sci U S A,* 110**,** 15973-8.

GBD 2016. Global, regional, and national incidence, prevalence, and years lived with disability for 310 diseases and injuries, 1990-2015: a systematic analysis for the Global Burden of Disease Study 2015. *Lancet,* 388**,** 1545-1602.

GBD 2017. Estimates of the global, regional, and national morbidity, mortality, and aetiologies of lower respiratory tract infections in 195 countries: a systematic analysis for the Global Burden of Disease Study 2015. *Lancet Infect Dis,* 17**,** 1133-1161.

GEORAS, S. N. & REZAEE, F. 2014. Epithelial barrier function: at the front line of asthma immunology and allergic airway inflammation. *J Allergy Clin Immunol,* 134**,** 509-20.

GHAFOURI, B., IRANDER, K., LINDBOM, J., TAGESSON, C. & LINDAHL, M. 2006. Comparative proteomics of nasal fluid in seasonal allergic rhinitis. *J Proteome Res,* 5**,** 330-8.

GHAFOURI, B., KIHLSTRÖM, E., TAGESSON, C. & LINDAHL, M. 2004. PLUNC in human nasal lavage fluid: multiple isoforms that bind to lipopolysaccharide. *Biochim Biophys Acta,* 1699**,** 57-63.

GHAFOURI, B., STÅHLBOM, B., TAGESSON, C. & LINDAHL, M. 2002. Newly identified proteins in human nasal lavage fluid from non-smokers and smokers using two-dimensional gel electrophoresis and peptide mass fingerprinting. *Proteomics,* 2**,** 112-20.

GIBCO. 2015. *Geneticin (G-418 Sulfate)* [Online]. Available: https://assets.thermofisher.com/TFS-Assets/LSG/manuals/Geneticin_UG.pdf [Accessed 2018].

GOEMINNE, P. C., NAWROT, T. S., RUTTENS, D., SEYS, S. & DUPONT, L. J. 2014. Mortality in non-cystic fibrosis bronchiectasis: a prospective cohort analysis. *Respir Med,* 108**,** 287-96.

GOSS, C. H. & MUHLEBACH, M. S. 2011. Review: Staphylococcus aureus and MRSA in cystic fibrosis. *J Cyst Fibros,* 10**,** 298-306.

GUANÍ-GUERRA, E., SANTOS-MENDOZA, T., LUGO-REYES, S. O. & TERÁN, L. M. 2010. Antimicrobial peptides: general overview and clinical implications in human health and disease. *Clin Immunol,* 135**,** 1-11.

GUERRA, F. E., BORGOGNA, T. R., PATEL, D. M., SWARD, E. W. & VOYICH, J. M. 2017. Epic Immune Battles of History: Neutrophils vs. *Front Cell Infect Microbiol,* 7**,** 286.

GÓMEZ, M. I. & PRINCE, A. 2008. Airway epithelial cell signaling in response to bacterial pathogens. *Pediatr Pulmonol,* 43**,** 11-9.

HADZHIEV, Y., YORDANOV, S., POPOVA, D. & KACHAKOVA, D. 2017. BPIFA1 Gene Expression in the Human Middle Ear Mucosa. *J Int Adv Otol,* 13**,** 340-344.

HAILMAN, E., ALBERS, J. J., WOLFBAUER, G., TU, A. Y. & WRIGHT, S. D. 1996. Neutralization and transfer of lipopolysaccharide by phospholipid transfer protein. *J Biol Chem,* 271**,** 12172-8.

HANCOCK, R. E. & LEHRER, R. 1998. Cationic peptides: a new source of antibiotics. *Trends Biotechnol,* 16**,** 82-8.

HARDER, J., MEYER-HOFFERT, U., TERAN, L. M., SCHWICHTENBERG, L., BARTELS, J., MAUNE, S. & SCHRÖDER, J. M. 2000. Mucoid Pseudomonas aeruginosa, TNF-alpha, and IL-1beta, but not IL-6, induce human beta-defensin-2 in respiratory epithelia. *Am J Respir Cell Mol Biol,* 22**,** 714-21.

HARKEMA, J. R., CAREY, S. A. & WAGNER, J. G. 2006. The nose revisited: a brief review of the comparative structure, function, and toxicologic pathology of the nasal epithelium. *Toxicol Pathol,* 34**,** 252-69.

HARTIKKA, J., SAWDEY, M., CORNEFERT-JENSEN, F., MARGALITH, M., BARNHART, K., NOLASCO, M., VAHLSING, H. L., MEEK, J., MARQUET, M., HOBART, P., NORMAN, J. & MANTHORPE, M. 1996. An improved plasmid DNA expression vector for direct injection into skeletal muscle. *Hum Gene Ther,* 7**,** 1205-17.

HELFT, L., REDDY, V., CHEN, X., KOLLER, T., FEDERICI, L., FERNANDEZ-RECIO, J., GUPTA, R. & BENT, A. 2011. LRR conservation mapping to predict functional sites within protein leucine-rich repeat domains. *PLoS One,* 6**,** e21614.

HENRIQUES-NORMARK, B. & TUOMANEN, E. I. 2013. The pneumococcus: epidemiology, microbiology, and pathogenesis. *Cold Spring Harb Perspect Med,* 3.

HIELPOS, M. S., FERRERO, M. C., FERNÁNDEZ, A. G., BONETTO, J., GIAMBARTOLOMEI, G. H., FOSSATI, C. A. & BALDI, P. C. 2015. CCL20 and Beta-Defensin 2 Production by Human Lung Epithelial Cells and Macrophages in Response to Brucella abortus Infection. *PLoS One,* 10**,** e0140408.

HOBBS, C. A., BLANCHARD, M. G., ALIJEVIC, O., TAN, C. D., KELLENBERGER, S., BENCHARIT, S., CAO, R., KESIMER, M., WALTON, W. G., HENDERSON, A. G., REDINBO, M. R., STUTTS, M. J. & TARRAN, R. 2013. Identification of the SPLUNC1 ENaC-inhibitory domain yields novel strategies to treat sodium hyperabsorption in cystic fibrosis airway epithelial cultures. *Am J Physiol Lung Cell Mol Physiol,* 305**,** L990-L1001.

HOFMANN, K. & BARON, M. 2018. *ExPASy: BoxShade (version 3.21)* [Online]. Available: http://www.ch.embnet.org/software/BOX_form.html [Accessed 2018].

HOL, J., WILHELMSEN, L. & HARALDSEN, G. 2010. The murine IL-8 homologues KC, MIP-2, and LIX are found in endothelial cytoplasmic granules but not in Weibel-Palade bodies. *J Leukoc Biol,* 87**,** 501-8.

HORWITZ, A. H., LEIGH, S. D., ABRAHAMSON, S., GAZZANO-SANTORO, H., LIU, P. S., WILLIAMS, R. E., CARROLL, S. F. & THEOFAN, G. 1996. Expression and characterization of cysteine-modified variants of an amino-terminal fragment of bactericidal/permeability-increasing protein. *Protein Expr Purif,* 8**,** 28-40.

HUNG, M. C. & LINK, W. 2011. Protein localization in disease and therapy. *J Cell Sci,* 124**,** 3381-92.

INVITROGEN. 2004. *GFP Fusion TOPO TA Expression Kits* [Online]. Available: https://tools.thermofisher.com/content/sfs/manuals/gfptopo_man.pdf [Accessed 2018].

INVITROGEN. 2010. *Flp-In System* [Online]. Available: http://tools.lifetechnologies.com/content/sfs/manuals/flpinsystem_man.pdf [Accessed 2018].

IRVIN, C. G. & BATES, J. H. 2003. Measuring the lung function in the mouse: the challenge of size. *Respir Res,* 4**,** 4.

JAIN, N., LODHA, R. & KABRA, S. K. 2001. Upper respiratory tract infections. *Indian J Pediatr,* 68**,** 1135-8.

JAIN, R., PAN, J., DRISCOLL, J. A., WISNER, J. W., HUANG, T., GUNSTEN, S. P., YOU, Y. & BRODY, S. L. 2010. Temporal relationship between primary and motile ciliogenesis in airway epithelial cells. *Am J Respir Cell Mol Biol,* 43**,** 731-9.

JAKOBSEN, J., MIKKELSEN, J. & NIELSEN, A. 2010. Elimination of the plasmid bacterial backbone in site-directed transgenesis. *Biotechniques,* 48**,** 313-6.

JANSON, H., CARL N, B., CERVIN, A., FORSGREN, A., MAGNUSDOTTIR, A. B., LINDBERG, S. & RUNER, T. 1999. Effects on the ciliated epithelium of protein D-producing and -nonproducing nontypeable Haemophilus influenzae in nasopharyngeal tissue cultures. *J Infect Dis,* 180**,** 737-46.

JAYAWARDANE, G., RUSSELL, G. C., THOMSON, J., DEANE, D., COX, H., GATHERER, D., ACKERMANN, M., HAIG, D. M. & STEWART, J. P. 2008. A captured viral interleukin 10 gene with cellular exon structure. *J Gen Virol,* 89**,** 2447-55.

JIANG, D., PERSINGER, R., WU, Q., GROSS, A. & CHU, H. W. 2013a. alpha1-Antitrypsin promotes SPLUNC1-mediated lung defense against Pseudomonas aeruginosa infection in mice. *Respir Res,* 14**,** 122.

JIANG, D., WENZEL, S. E., WU, Q., BOWLER, R. P., SCHNELL, C. & CHU, H. W. 2013b. Human neutrophil elastase degrades SPLUNC1 and impairs airway epithelial defense against bacteria. *PLoS One,* 8**,** e64689.

JOHNSON, A. P. & INZANA, T. J. 1986. Loss of ciliary activity in organ cultures of rat trachea treated with lipo-oligosaccharide from Haemophilus influenzae. *J Med Microbiol,* 22**,** 265-8.

JOO, N. S., LEE, D. J., WINGES, K. M., RUSTAGI, A. & WINE, J. J. 2004. Regulation of antiprotease and antimicrobial protein secretion by airway submucosal gland serous cells. *J Biol Chem,* 279**,** 38854-60.

KADIOGLU, A., TAYLOR, S., IANNELLI, F., POZZI, G., MITCHELL, T. J. & ANDREW, P. W. 2002. Upper and lower respiratory tract infection by Streptococcus pneumoniae is affected by pneumolysin deficiency and differences in capsule type. *Infect Immun,* 70**,** 2886-90.

KAGANOVICH, D. 2017. There Is an Inclusion for That: Material Properties of Protein Granules Provide a Platform for Building Diverse Cellular Functions. *Trends Biochem Sci,* 42**,** 765-776.

KAHLENBERG, J. M. & KAPLAN, M. J. 2013. Little peptide, big effects: the role of LL-37 in inflammation and autoimmune disease. *J Immunol,* 191**,** 4895-901.

KATO, A. & SCHLEIMER, R. P. 2007. Beyond inflammation: airway epithelial cells are at the interface of innate and adaptive immunity. *Curr Opin Immunol,* 19**,** 711-20.

KELLER, E. T., WANAGAT, J. & ERSHLER, W. B. 1996. Molecular and cellular biology of interleukin-6 and its receptor. *Front Biosci,* 1**,** d340-57.

KELLEY, L. A., MEZULIS, S., YATES, C. M., WASS, M. N. & STERNBERG, M. J. E. 2015. The Phyre2 web portal for protein modeling, prediction and analysis. *Nature Protocols,* 10**,** 845.

KEMPNER, E. S. 1993. Movable lobes and flexible loops in proteins. Structural deformations that control biochemical activity. *FEBS Lett,* 326**,** 4-10.

KESIMER, M., EHRE, C., BURNS, K. A., DAVIS, C. W., SHEEHAN, J. K. & PICKLES, R. J. 2013. Molecular organization of the mucins and glycocalyx underlying mucus transport over mucosal surfaces of the airways. *Mucosal Immunol,* 6**,** 379-92.

KETTERER, M. R., SHAO, J. Q., HORNICK, D. B., BUSCHER, B., BANDI, V. K. & APICELLA, M. A. 1999. Infection of primary human bronchial epithelial cells by Haemophilus influenzae: macropinocytosis as a mechanism of airway epithelial cell entry. *Infect Immun,* 67**,** 4161-70.

KHAIR, O. A., DAVIES, R. J. & DEVALIA, J. L. 1996. Bacterial-induced release of inflammatory mediators by bronchial epithelial cells. *Eur Respir J,* 9**,** 1913-22.

KHAIR, O. A., DEVALIA, J. L., ABDELAZIZ, M. M., SAPSFORD, R. J., TARRAF, H. & DAVIES, R. J. 1994. Effect of Haemophilus influenzae endotoxin on the synthesis of IL-6, IL-8, TNF-alpha and expression of ICAM-1 in cultured human bronchial epithelial cells. *Eur Respir J,* 7**,** 2109-16.

KIM, C. S., AHMAD, S., WU, T., WALTON, W. G., REDINBO, M. R. & TARRAN, R. 2018. SPLUNC1 is an allosteric modulator of the epithelial sodium channel. *FASEB J,* 32**,** 2478-2491.

KING, P. 2012. Haemophilus influenzae and the lung (Haemophilus and the lung). *Clin Transl Med,* 1**,** 10.

KING, P. T. & SHARMA, R. 2015. The Lung Immune Response to Nontypeable Haemophilus influenzae (Lung Immunity to NTHi). *J Immunol Res,* 2015**,** 706376.

KING, P. T., NGUI, J., FARMER, M. W., HUTCHINSON, P., HOLMES, P. W. & HOLDSWORTH, S. R. 2008. Cytotoxic T lymphocyte and natural killer cell responses to non-typeable Haemophilus influenzae. *Clin Exp Immunol,* 152**,** 542-51.

KIRKHAM, L. A., CORSCADDEN, K. J., WIERTSEMA, S. P., CURRIE, A. J. & RICHMOND, P. C. 2013. A practical method for preparation of pneumococcal and nontypeable Haemophilus influenzae inocula that preserves viability and immunostimulatory activity. *BMC Res Notes,* 6**,** 522.

KNIGHT, D. A. & HOLGATE, S. T. 2003. The airway epithelium: structural and functional properties in health and disease. *Respirology,* 8**,** 432-46.

KUBIET, M. & RAMPHAL, R. 1995. Adhesion of nontypeable Haemophilus influenzae from blood and sputum to human tracheobronchial mucins and lactoferrin. *Infect Immun,* 63**,** 899-902.

KUKURUZINSKA, M. A. & LENNON, K. 1998. Protein N-glycosylation: molecular genetics and functional significance. *Crit Rev Oral Biol Med,* 9**,** 415-48.

LANIE, J. A., NG, W. L., KAZMIERCZAK, K. M., ANDRZEJEWSKI, T. M., DAVIDSEN, T. M., WAYNE, K. J., TETTELIN, H., GLASS, J. I. & WINKLER, M. E. 2007. Genome sequence of Avery's virulent serotype 2 strain D39 of Streptococcus pneumoniae and comparison with that of unencapsulated laboratory strain R6. *J Bacteriol,* 189**,** 38-51.

LEE, H. S., QI, Y. & IM, W. 2015. Effects of N-glycosylation on protein conformation and dynamics: Protein Data Bank analysis and molecular dynamics simulation study. *Sci Rep,* 5**,** 8926.

LEE, J. M., JANG, Y. S., JIN, B. R., KIM, S. J., KIM, H. J., KWON, B. E., KO, H. J., YOON, S. I., LEE, G. S., KIM, W. S., SEO, G. Y. & KIM, P. H. 2016. Retinoic acid enhances lactoferrin-induced IgA responses by increasing betaglycan expression. *Cell Mol Immunol,* 13**,** 862-870.

LEEMING, G. H., KIPAR, A., HUGHES, D. J., BINGLE, L., BENNETT, E., MOYO, N. A., TRIPP, R. A., BIGLEY, A. L., BINGLE, C. D., SAMPLE, J. T. & STEWART, J. P. 2015. Gammaherpesvirus infection modulates the temporal and spatial expression of SCGB1A1 (CCSP) and BPIFA1 (SPLUNC1) in the respiratory tract. *Lab Invest,* 95**,** 610-24.

LEMESSURIER, K. S., LIN, Y., MCCULLERS, J. A. & SAMARASINGHE, A. E. 2016. Antimicrobial peptides alter early immune response to influenza A virus infection in C57BL/6 mice. *Antiviral Res,* 133**,** 208-17.

LEVINE, A. M., REED, J. A., KURAK, K. E., CIANCIOLO, E. & WHITSETT, J. A. 1999. GM-CSF-deficient mice are susceptible to pulmonary group B streptococcal infection. *J Clin Invest,* 103**,** 563-9.

LEVY, O. 2000. A neutrophil-derived anti-infective molecule: bactericidal/permeability-increasing protein. *Antimicrob Agents Chemother,* 44**,** 2925-31.

LI, J., LEE, Y., JOHANSSON, H. J., MAGER, I., VADER, P., NORDIN, J. Z., WIKLANDER, O. P., LEHTIO, J., WOOD, M. J. & ANDALOUSSI, S. E. 2015. Serum-free culture alters the quantity and protein composition of neuroblastoma-derived extracellular vesicles. *J Extracell Vesicles,* 4**,** 26883.

LIN, Y. C. & PETERSON, M. L. 2010. New insights into the prevention of staphylococcal infections and toxic shock syndrome. *Expert Rev Clin Pharmacol,* 3**,** 753-767.

LIS, H. & SHARON, N. 1993. Protein glycosylation. Structural and functional aspects. *Eur J Biochem,* 218**,** 1-27.

LITCHFIELD, D. W. 2003. Protein kinase CK2: structure, regulation and role in cellular decisions of life and death. *Biochem J,* 369**,** 1-15.

LITTLE, M. S. & REDINBO, M. R. 2018. Crystal structure of the mouse innate immunity factor bacterial permeability-increasing family member A1. *Acta Crystallogr F Struct Biol Commun,* 74**,** 268-276.

LIU, G. Y. 2009. Molecular pathogenesis of Staphylococcus aureus infection. *Pediatr Res,* 65**,** 71R-77R.

LIU, T., ZHANG, L., JOO, D. & SUN, S. C. 2017. NF-κB signaling in inflammation. *Signal Transduct Target Ther,* 2.

LIU, Y., BARTLETT, J. A., DI, M. E., BOMBERGER, J. M., CHAN, Y. R., GAKHAR, L., MALLAMPALLI, R. K., MCCRAY, P. B. & DI, Y. P. 2013a. SPLUNC1/BPIFA1 contributes to pulmonary host defense against Klebsiella pneumoniae respiratory infection. *Am J Pathol,* 182**,** 1519-31.

LIU, Y., DI, M. E., CHU, H. W., LIU, X., WANG, L., WENZEL, S. & DI, Y. P. 2013b. Increased susceptibility to pulmonary Pseudomonas infection in Splunc1 knockout mice. *J Immunol,* 191**,** 4259-68.

LIU, Z., GARCÍA-DÍAZ, B., CATACCHIO, B., CHIANCONE, E. & VOGEL, H. J. 2015. Protecting Gram-negative bacterial cell envelopes from human lysozyme: Interactions with Ivy inhibitor proteins from Escherichia coli and Pseudomonas aeruginosa. *Biochim Biophys Acta,* 1848**,** 3032-46.

LIVRAGHI, A. & RANDELL, S. H. 2007. Cystic fibrosis and other respiratory diseases of impaired mucus clearance. *Toxicol Pathol,* 35**,** 116-29.

LOUCHE, A., SALCEDO, S. P. & BIGOT, S. 2017. Protein–Protein Interactions: Pull-Down Assays. *In:* JOURNET, L. & CASCALES, E. (eds.) *Bacterial Protein Secretion Systems. Methods in Molecular Biology.* New York: Humana Press.

LUGADE, A. A., BOGNER, P. N., MURPHY, T. F. & THANAVALA, Y. 2011. The role of TLR2 and bacterial lipoprotein in enhancing airway inflammation and immunity. *Front Immunol,* 2**,** 10.

LUKINSKIENE, L., LIU, Y., REYNOLDS, S. D., STEELE, C., STRIPP, B. R., LEIKAUF, G. D., KOLLS, J. K. & DI, Y. P. 2011. Antimicrobial activity of PLUNC protects against Pseudomonas aeruginosa infection. *J Immunol,* 187**,** 382-90.

LYCZAK, J. B., CANNON, C. L. & PIER, G. B. 2002. Lung infections associated with cystic fibrosis. *Clin Microbiol Rev,* 15**,** 194-222.

MANABE, R., TSUTSUI, K., YAMADA, T., KIMURA, M., NAKANO, I., SHIMONO, C., SANZEN, N., FURUTANI, Y., FUKUDA, T., OGURI, Y., SHIMAMOTO, K., KIYOZUMI, D., SATO, Y., SADO, Y., SENOO, H., YAMASHINA, S., FUKUDA, S., KAWAI, J., SUGIURA, N., KIMATA, K., HAYASHIZAKI, Y. & SEKIGUCHI, K. 2008. Transcriptome-based systematic identification of extracellular matrix proteins. *Proc Natl Acad Sci U S A,* 105**,** 12849-54.

MANGOLD, U. 2005. The antizyme family: polyamines and beyond. *IUBMB Life,* 57**,** 671-6.

MARRAZZO, P., MACCARI, S., TADDEI, A., BEVAN, L., TELFORD, J., SORIANI, M. & PEZZICOLI, A. 2016. 3D Reconstruction of the Human Airway Mucosa In Vitro as an Experimental Model to Study NTHi Infections. *PLoS One,* 11**,** e0153985.

MARRIOTT, H. M., GASCOYNE, K. A., GOWDA, R., GEARY, I., NICKLIN, M. J., IANNELLI, F., POZZI, G., MITCHELL, T. J., WHYTE, M. K., SABROE, I. & DOCKRELL, D. H. 2012. Interleukin-1β regulates CXCL8 release and influences disease outcome in response to Streptococcus pneumoniae, defining intercellular cooperation between pulmonary epithelial cells and macrophages. *Infect Immun,* 80**,** 1140-9.

MARTINEZ, R. J. & CARROLL, S. F. 1980. Sequential metabolic expressions of the lethal process in human serum-treated Escherichia coli: role of lysozyme. *Infect Immun,* 28**,** 735-45.

MASUCCI-MAGOULAS, L., MOULIN, P., JIANG, X. C., RICHARDSON, H., WALSH, A., BRESLOW, J. L. & TALL, A. 1995. Decreased cholesteryl ester transfer protein (CETP) mRNA and protein and increased high density lipoprotein following lipopolysaccharide administration in human CETP transgenic mice. *J Clin Invest,* 95**,** 1587-94.

MAURER-STROH, S., EISENHABER, B. & EISENHABER, F. 2002. N-terminal N-myristoylation of proteins: refinement of the sequence motif and its taxon-specific differences. *J Mol Biol,* 317**,** 523-40.

MCDONALD, R. E., FLEMING, R. I., BEELEY, J. G., BOVELL, D. L., LU, J. R., ZHAO, X., COOPER, A. & KENNEDY, M. W. 2009. Latherin: a surfactant protein of horse sweat and saliva. *PLoS One,* 4**,** e5726.

MCGILLIVARY, G. & BAKALETZ, L. O. 2010. The multifunctional host defense peptide SPLUNC1 is critical for homeostasis of the mammalian upper airway. *PLoS One,* 5**,** e13224.

MCILWAINE, M., BRADLEY, J., ELBORN, J. S. & MORAN, F. 2017. Personalising airway clearance in chronic lung disease. *Eur Respir Rev,* 26.

MEDUS, M. L., GOMEZ, G. E., ZACCHI, L. F., COUTO, P. M., LABRIOLA, C. A., LABANDA, M. S., BIELSA, R. C., CLERICO, E. M., SCHULZ, B. L. & CARAMELO, J. J. 2017. N-glycosylation Triggers a Dual Selection Pressure in Eukaryotic Secretory Proteins. *Sci Rep,* 7**,** 8788.

MELIO, F. R. & BERGE, L. R. 2014. Upper respiratory tract infections. *In:* MARX, J. A., HOCKBERGER, R. S. & WALLS, R. M. (eds.) *Rosen's Emergency Medicine - Concepts and Clinical Practice.* Philadelphia: Elsevier Saunders.

MILLER, F. J., MERCER, R. R. & CRAPO, J. D. 1993. Lower Respiratory Tract Structure of Laboratory Animals and Humans: Dosimetry Implications. *Aerosol Science and Technology,* 18**,** 257-271.

MOGHADDAM, S. J., CLEMENT, C. G., DE LA GARZA, M. M., ZOU, X., TRAVIS, E. L., YOUNG, H. W., EVANS, C. M., TUVIM, M. J. & DICKEY, B. F. 2008. Haemophilus influenzae lysate induces aspects of the chronic obstructive pulmonary disease phenotype. *Am J Respir Cell Mol Biol,* 38**,** 629-38.

MOORE, P. J., REIDEL, B., GHOSH, A., SESMA, J., KESIMER, M. & TARRAN, R. 2018. Cigarette smoke modifies and inactivates SPLUNC1, leading to airway dehydration. *FASEB J***,** fj201800345R.

MORGAN, A. A. & RUBENSTEIN, E. 2013. Proline: the distribution, frequency, positioning, and common functional roles of proline and polyproline sequences in the human proteome. *PLoS One,* 8**,** e53785.

MOU, H., VINARSKY, V., TATA, P. R., BRAZAUSKAS, K., CHOI, S. H., CROOKE, A. K., ZHANG, B., SOLOMON, G. M., TURNER, B., BIHLER, H., HARRINGTON, J., LAPEY, A., CHANNICK, C., KEYES, C., FREUND, A., ARTANDI, S., MENSE, M., ROWE, S., ENGELHARDT, J. F., HSU, Y. C. & RAJAGOPAL, J. 2016. Dual SMAD Signaling Inhibition Enables Long-Term Expansion of Diverse Epithelial Basal Cells. *Cell Stem Cell,* 19**,** 217-231.

MUKAIDA, N. 2003. Pathophysiological roles of interleukin-8/CXCL8 in pulmonary diseases. *Am J Physiol Lung Cell Mol Physiol,* 284**,** L566-77.

MULAY, A. 2016. *The Role of BPIFA1 in Otitis Media.* PhD, University of Sheffield.

MULAY, A., AKRAM, K. M., WILLIAMS, D., ARMES, H., RUSSELL, C., HOOD, D., ARMSTRONG, S., STEWART, J. P., BROWN, S. D., BINGLE, L. & BINGLE, C. D. 2016. An in vitro model of murine middle ear epithelium. *Dis Model Mech,* 9**,** 1405-1417.

MULAY, A., HOOD, D. W., WILLIAMS, D., RUSSELL, C., BROWN, S. D. M., BINGLE, L., CHEESEMAN, M. & BINGLE, C. D. 2018. Loss of the homeostatic protein BPIFA1, leads to exacerbation of otitis media severity in the Junbo mouse model. *Sci Rep,* 8**,** 3128.

MUSA, M., WILSON, K., SUN, L., MULAY, A., BINGLE, L., MARRIOTT, H. M., LECLAIR, E. E. & BINGLE, C. D. 2012. Differential localisation of BPIFA1 (SPLUNC1) and BPIFB1 (LPLUNC1) in the nasal and oral cavities of mice. *Cell Tissue Res,* 350**,** 455-64.

NCBI 2017. Database Resources of the National Center for Biotechnology Information. *Nucleic Acids Res,* 45**,** D12-d17.

NEWTON, A. C. 1995. Protein kinase C: structure, function, and regulation. *J Biol Chem,* 270**,** 28495-8.

NG, A. & XAVIER, R. J. 2011. Leucine-rich repeat (LRR) proteins: integrators of pattern recognition and signaling in immunity. *Autophagy,* 7**,** 1082-4.

NICHOLS, D. P., JIANG, D., HAPPOLDT, C., BERMAN, R. & CHU, H. W. 2015. Therapeutic Effects of α1-Antitrypsin on Psedumonas aeruginosa Infection in ENaC Transgenic Mice. *PLoS One,* 10**,** e0141232.

NING, F., WANG, C., BERRY, K. Z., KANDASAMY, P., LIU, H., MURPHY, R. C., VOELKER, D. R., NHO, C. W., PAN, C. H., DAI, S., NIU, L., CHU, H. W. & ZHANG, G. 2014. Structural characterization of the pulmonary innate immune protein SPLUNC1 and identification of lipid ligands. *FASEB J,* 28**,** 5349-60.

NORMAN, J. A., HOBART, P., MANTHORPE, M., FELGNER, P. & WHEELER, C. 1997. Development of improved vectors for DNA-based immunization and other gene therapy applications. *Vaccine,* 15**,** 801-3.

NOVINCE, C. M., KOH, A. J., MICHALSKI, M. N., MARCHESAN, J. T., WANG, J., JUNG, Y., BERRY, J. E., EBER, M. R., ROSOL, T. J., TAICHMAN, R. S. & MCCAULEY, L. K. 2011. Proteoglycan 4, a

novel immunomodulatory factor, regulates parathyroid hormone actions on hematopoietic cells. *Am J Pathol,* 179**,** 2431-42.
O'NEILL, A. J. 2010. Staphylococcus aureus SH1000 and 8325-4: comparative genome sequences of key laboratory strains in staphylococcal research. *Lett Appl Microbiol,* 51**,** 358-61.
OPAL, S. M. & DEPALO, V. A. 2000. Anti-inflammatory cytokines. *Chest,* 117**,** 1162-72.
ORSI, N. 2004. The antimicrobial activity of lactoferrin: current status and perspectives. *Biometals,* 17**,** 189-96.
PAGNI, M., IOANNIDIS, V., CERUTTI, L., ZAHN-ZABAL, M., JONGENEEL, C. V. & FALQUET, L. 2004. MyHits: a new interactive resource for protein annotation and domain identification. *Nucleic Acids Res,* 32**,** W332-5.
PANG, B., HONG, W., WEST-BARNETTE, S. L., KOCK, N. D. & SWORDS, W. E. 2008. Diminished ICAM-1 expression and impaired pulmonary clearance of nontypeable Haemophilus influenzae in a mouse model of chronic obstructive pulmonary disease/emphysema. *Infect Immun,* 76**,** 4959-67.
PARKER, D. & PRINCE, A. 2011. Innate immunity in the respiratory epithelium. *Am J Respir Cell Mol Biol,* 45**,** 189-201.
PARKER, D. & PRINCE, A. 2012. Immunopathogenesis of Staphylococcus aureus pulmonary infection. *Semin Immunopathol,* 34**,** 281-97.
PERSSON, C. G. 2002. Con: mice are not a good model of human airway disease. *Am J Respir Crit Care Med,* 166**,** 6-7; discussion 8.
PETTIGREW, M. M., GENT, J. F., REVAI, K., PATEL, J. A. & CHONMAITREE, T. 2008. Microbial interactions during upper respiratory tract infections. *Emerg Infect Dis,* 14**,** 1584-91.
PILLOUX, L., LEROY, D., BRUNEL, C., ROGER, T. & GREUB, G. 2016. Mouse Model of Respiratory Tract Infection Induced by Waddlia chondrophila. *PLoS One,* 11**,** e0150909.
PIZZUTTO, S. J., YERKOVICH, S. T., UPHAM, J. W., HALES, B. J., THOMAS, W. R. & CHANG, A. B. 2014. Children with chronic suppurative lung disease have a reduced capacity to synthesize interferon-gamma in vitro in response to non-typeable Haemophilus influenzae. *PLoS One,* 9**,** e104236.
PRAT, C. & LACOMA, A. 2016. Bacteria in the respiratory tract-how to treat? Or do not treat? *Int J Infect Dis,* 51**,** 113-122.
PRIFTIS, K. N., LITT, D., MANGLANI, S., ANTHRACOPOULOS, M. B., THICKETT, K., TZANAKAKI, G., FENTON, P., SYROGIANNOPOULOS, G. A., VOGIATZI, A., DOUROS, K., SLACK, M. & EVERARD, M. L. 2013. Bacterial bronchitis caused by Streptococcus pneumoniae and nontypable Haemophilus influenzae in children: the impact of vaccination. *Chest,* 143**,** 152-157.
QURESHI, H., SHARAFKHANEH, A. & HANANIA, N. A. 2014. Chronic obstructive pulmonary disease exacerbations: latest evidence and clinical implications. *Ther Adv Chronic Dis,* 5**,** 212-27.
RACKLEY, C. R. & STRIPP, B. R. 2012. Building and maintaining the epithelium of the lung. *J Clin Invest,* 122**,** 2724-30.
RADICIONI, G., CAO, R., CARPENTER, J., FORD, A. A., WANG, T., LI, L. & KESIMER, M. 2016. The innate immune properties of airway mucosal surfaces are regulated by dynamic interactions between mucins and interacting proteins: the mucin interactome. *Mucosal Immunol,* 9**,** 1442-1454.
RAGLAND, S. A. & CRISS, A. K. 2017. From bacterial killing to immune modulation: Recent insights into the functions of lysozyme. *PLoS Pathog,* 13**,** e1006512.
RAGLAND, S. A., HUMBERT, M. V., CHRISTODOULIDES, M. & CRISS, A. K. 2018. Neisseria gonorrhoeae employs two protein inhibitors to evade killing by human lysozyme. *PLoS Pathog,* 14**,** e1007080.

RAMEZANPOUR, M., MORAITIS, S., SMITH, J. L., WORMALD, P. J. & VREUGDE, S. 2016. Th17 Cytokines Disrupt the Airway Mucosal Barrier in Chronic Rhinosinusitis. *Mediators Inflamm,* 2016**,** 9798206.

READ, R. C., WILSON, R., RUTMAN, A., LUND, V., TODD, H. C., BRAIN, A. P., JEFFERY, P. K. & COLE, P. J. 1991. Interaction of nontypable Haemophilus influenzae with human respiratory mucosa in vitro. *J Infect Dis,* 163**,** 549-58.

REDDY, M. S., BERNSTEIN, J. M., MURPHY, T. F. & FADEN, H. S. 1996. Binding between outer membrane proteins of nontypeable Haemophilus influenzae and human nasopharyngeal mucin. *Infect Immun,* 64**,** 1477-9.

REICHMANN, D., RAHAT, O., COHEN, M., NEUVIRTH, H. & SCHREIBER, G. 2007. The molecular architecture of protein-protein binding sites. *Curr Opin Struct Biol,* 17**,** 67-76.

REZAEI, M., ZARKESH-ESFAHANI, S. H. & GHARAGOZLOO, M. 2013. The effect of different media composition and temperatures on the production of recombinant human growth hormone by CHO cells. *Res Pharm Sci,* 8**,** 211-7.

REZNIK, G. K. 1990. Comparative anatomy, physiology, and function of the upper respiratory tract. *Environ Health Perspect,* 85**,** 171-6.

RHEE, D. K., MARCELINO, J., BAKER, M., GONG, Y., SMITS, P., LEFEBVRE, V., JAY, G. D., STEWART, M., WANG, H., WARMAN, M. L. & CARPTEN, J. D. 2005. The secreted glycoprotein lubricin protects cartilage surfaces and inhibits synovial cell overgrowth. *J Clin Invest,* 115**,** 622-31.

RICHELDI, L., COLLARD, H. R. & JONES, M. G. 2017. Idiopathic pulmonary fibrosis. *Lancet,* 389**,** 1941-1952.

ROCK, J. R., RANDELL, S. H. & HOGAN, B. L. 2010. Airway basal stem cells: a perspective on their roles in epithelial homeostasis and remodeling. *Dis Model Mech,* 3**,** 545-56.

ROLLINS, B. M., GARCIA-CABALLERO, A., STUTTS, M. J. & TARRAN, R. 2010. SPLUNC1 expression reduces surface levels of the epithelial sodium channel (ENaC) in Xenopus laevis oocytes. *Channels (Austin),* 4**,** 255-9.

ROXO-ROSA, M., DA COSTA, G., LUIDER, T. M., SCHOLTE, B. J., COELHO, A. V., AMARAL, M. D. & PENQUE, D. 2006. Proteomic analysis of nasal cells from cystic fibrosis patients and non-cystic fibrosis control individuals: search for novel biomarkers of cystic fibrosis lung disease. *Proteomics,* 6**,** 2314-25.

ROY, M. G., LIVRAGHI-BUTRICO, A., FLETCHER, A. A., MCELWEE, M. M., EVANS, S. E., BOERNER, R. M., ALEXANDER, S. N., BELLINGHAUSEN, L. K., SONG, A. S., PETROVA, Y. M., TUVIM, M. J., ADACHI, R., ROMO, I., BORDT, A. S., BOWDEN, M. G., SISSON, J. H., WOODRUFF, P. G., THORNTON, D. J., ROUSSEAU, K., DE LA GARZA, M. M., MOGHADDAM, S. J., KARMOUTY-QUINTANA, H., BLACKBURN, M. R., DROUIN, S. M., DAVIS, C. W., TERRELL, K. A., GRUBB, B. R., O'NEAL, W. K., FLORES, S. C., COTA-GOMEZ, A., LOZUPONE, C. A., DONNELLY, J. M., WATSON, A. M., HENNESSY, C. E., KEITH, R. C., YANG, I. V., BARTHEL, L., HENSON, P. M., JANSSEN, W. J., SCHWARTZ, D. A., BOUCHER, R. C., DICKEY, B. F. & EVANS, C. M. 2014. Muc5b is required for airway defence. *Nature,* 505**,** 412-6.

SABA, S., SOONG, G., GREENBERG, S. & PRINCE, A. 2002. Bacterial stimulation of epithelial G-CSF and GM-CSF expression promotes PMN survival in CF airways. *Am J Respir Cell Mol Biol,* 27**,** 561-7.

SAETTA, M. & TURATO, G. 2001. Airway pathology in asthma. *Eur Respir J Suppl,* 34**,** 18s-23s.

SAFERALI, A., OBEIDAT, M., BÉRUBÉ, J. C., LAMONTAGNE, M., BOSSÉ, Y., LAVIOLETTE, M., HAO, K., NICKLE, D. C., TIMENS, W., SIN, D. D., POSTMA, D. S., STRUG, L. J., GALLINS, P. J., PARÉ, P. D., BINGLE, C. D. & SANDFORD, A. J. 2015. Polymorphisms associated with expression of BPIFA1/BPIFB1 and lung disease severity in cystic fibrosis. *Am J Respir Cell Mol Biol,* 53**,** 607-14.

SANDERS, D. B., BITTNER, R. C., ROSENFELD, M., HOFFMAN, L. R., REDDING, G. J. & GOSS, C. H. 2010. Failure to recover to baseline pulmonary function after cystic fibrosis pulmonary exacerbation. *Am J Respir Crit Care Med,* 182**,** 627-32.

SAYEED, S., NISTICO, L., ST CROIX, C. & DI, Y. P. 2013. Multifunctional role of human SPLUNC1 in Pseudomonas aeruginosa infection. *Infect Immun,* 81**,** 285-91.

SCHEETZ, T. E., ZABNER, J., WELSH, M. J., COCO, J., EYESTONE, M. E. F., BONALDO, M., KUCABA, T., CASAVANT, T. L., SOARES, M. B. & MCCRAY, P. B. 2004. Large-scale gene discovery in human airway epithelia reveals novel transcripts. *Physiol Genomics,* 17**,** 69-77.

SCHRODINGER, L. 2015. The PyMOL Molecular Graphics System, Version 2.0 Schrödinger, LLC.

SETHI, S. 2010. Infection as a comorbidity of COPD. *Eur Respir J,* 35**,** 1209-15.

SIEGEL, S. J. & WEISER, J. N. 2015. Mechanisms of Bacterial Colonization of the Respiratory Tract. *Annu Rev Microbiol,* 69**,** 425-44.

SIGRIST, C. J., DE CASTRO, E., CERUTTI, L., CUCHE, B. A., HULO, N., BRIDGE, A., BOUGUELERET, L. & XENARIOS, I. 2013. New and continuing developments at PROSITE. *Nucleic Acids Res,* 41**,** D344-7.

SINACORE, M. S., DRAPEAU, D. & ADAMSON, S. R. 2000. Adaptation of mammalian cells to growth in serum-free media. *Mol Biotechnol,* 15**,** 249-57.

SINGH, P. K., JIA, H. P., WILES, K., HESSELBERTH, J., LIU, L., CONWAY, B. A., GREENBERG, E. P., VALORE, E. V., WELSH, M. J., GANZ, T., TACK, B. F. & MCCRAY, P. B. 1998. Production of beta-defensins by human airway epithelia. *Proc Natl Acad Sci U S A,* 95**,** 14961-6.

SINGH, P. K., TACK, B. F., MCCRAY, P. B. & WELSH, M. J. 2000. Synergistic and additive killing by antimicrobial factors found in human airway surface liquid. *Am J Physiol Lung Cell Mol Physiol,* 279**,** L799-805.

SINGH, R., MACKAY, A. J., PATEL, A. R., GARCHA, D. S., KOWLESSAR, B. S., BRILL, S. E., DONNELLY, L. E., BARNES, P. J., DONALDSON, G. C. & WEDZICHA, J. A. 2014. Inflammatory thresholds and the species-specific effects of colonising bacteria in stable chronic obstructive pulmonary disease. *Respir Res,* 15**,** 114.

SOLEAS, J. P., PAZ, A., MARCUS, P., MCGUIGAN, A. & WADDELL, T. K. 2012. Engineering airway epithelium. *J Biomed Biotechnol,* 2012**,** 982971.

SORRENTINO, R., DE SOUZA, P. M., SRISKANDAN, S., DUFFIN, C., PAUL-CLARK, M. J. & MITCHELL, J. A. 2008. Pattern recognition receptors and interleukin-8 mediate effects of Gram-positive and Gram-negative bacteria on lung epithelial cell function. *Br J Pharmacol,* 154**,** 864-71.

SPIRO, R. G. 2002. Protein glycosylation: nature, distribution, enzymatic formation, and disease implications of glycopeptide bonds. *Glycobiology,* 12**,** 43r-56r.

ST GEME, J. W., 3RD & FALKOW, S. 1990. Haemophilus influenzae adheres to and enters cultured human epithelial cells. *Infect Immun,* 58**,** 4036-44.

STADLER, C., REXHEPAJ, E., SINGAN, V. R., MURPHY, R. F., PEPPERKOK, R., UHLEN, M., SIMPSON, J. C. & LUNDBERG, E. 2013. Immunofluorescence and fluorescent-protein tagging show high correlation for protein localization in mammalian cells. *Nat Methods,* 10**,** 315-23.

STARNER, T. D., BARKER, C. K., JIA, H. P., KANG, Y. & MCCRAY, P. B. 2003. CCL20 is an inducible product of human airway epithelia with innate immune properties. *Am J Respir Cell Mol Biol,* 29**,** 627-33.

STEILING, K., KADAR, A. Y., BERGERAT, A., FLANIGON, J., SRIDHAR, S., SHAH, V., AHMAD, Q. R., BRODY, J. S., LENBURG, M. E., STEFFEN, M. & SPIRA, A. 2009. Comparison of proteomic and transcriptomic profiles in the bronchial airway epithelium of current and never smokers. *PLoS One,* 4**,** e5043.

STEINSTRAESSER, L., KRANEBURG, U., JACOBSEN, F. & AL-BENNA, S. 2011. Host defense peptides and their antimicrobial-immunomodulatory duality. *Immunobiology,* 216**,** 322-33.

STEPANENKO, O. V., VERKHUSHA, V. V., KUZNETSOVA, I. M., UVERSKY, V. N. & TUROVEROV, K. K. 2008. Fluorescent proteins as biomarkers and biosensors: throwing color lights on molecular and cellular processes. *Curr Protein Pept Sci,* 9**,** 338-69.

STEWART, C. E., TORR, E. E., MOHD JAMILI, N. H., BOSQUILLON, C. & SAYERS, I. 2012. Evaluation of differentiated human bronchial epithelial cell culture systems for asthma research. *J Allergy (Cairo),* 2012**,** 943982.

STRIETER, R. M., BELPERIO, J. A. & KEANE, M. P. 2002. Cytokines in innate host defense in the lung. *J Clin Invest,* 109**,** 699-705.

SU, A. I., WILTSHIRE, T., BATALOV, S., LAPP, H., CHING, K. A., BLOCK, D., ZHANG, J., SODEN, R., HAYAKAWA, M., KREIMAN, G., COOKE, M. P., WALKER, J. R. & HOGENESCH, J. B. 2004. A gene atlas of the mouse and human protein-encoding transcriptomes. *Proc Natl Acad Sci U S A,* 101**,** 6062-7.

SUAREZ, C. J., DINTZIS, S. M. & FREVERT, C. W. 2012. 9 - Respiratory. *In:* TREUTING, P. M. & DINTZIS, S. M. (eds.) *Comparative Anatomy and Histology.* San Diego: Academic Press.

TAM, A., WADSWORTH, S., DORSCHEID, D., MAN, S. F. & SIN, D. D. 2011. The airway epithelium: more than just a structural barrier. *Ther Adv Respir Dis,* 5**,** 255-73.

TARRAN, R. 2004. Regulation of airway surface liquid volume and mucus transport by active ion transport. *Proc Am Thorac Soc,* 1**,** 42-6.

TERPE, K. 2003. Overview of tag protein fusions: from molecular and biochemical fundamentals to commercial systems. *Appl Microbiol Biotechnol,* 60**,** 523-33.

THAI, P., LOUKOIANOV, A., WACHI, S. & WU, R. 2008. Regulation of airway mucin gene expression. *Annu Rev Physiol,* 70**,** 405-29.

THAIKOOTTATHIL, J. & CHU, H. W. 2011. MAPK/AP-1 activation mediates TLR2 agonist-induced SPLUNC1 expression in human lung epithelial cells. *Mol Immunol,* 49**,** 415-22.

THAIKOOTTATHIL, J. V., MARTIN, R. J., DI, P. Y., MINOR, M., CASE, S., ZHANG, B., ZHANG, G., HUANG, H. & CHU, H. W. 2012. SPLUNC1 deficiency enhances airway eosinophilic inflammation in mice. *Am J Respir Cell Mol Biol,* 47**,** 253-60.

TOBIAS, P. S., SOLDAU, K., IOVINE, N. M., ELSBACH, P. & WEISS, J. 1997. Lipopolysaccharide (LPS)-binding proteins BPI and LBP form different types of complexes with LPS. *J Biol Chem,* 272**,** 18682-5.

TOEWS, G. B. 2005. Impact of bacterial infections on airway diseases. 14**,** 62-68.

TURATO, G., ZUIN, R. & SAETTA, M. 2001. Pathogenesis and pathology of COPD. *Respiration,* 68**,** 117-28.

TURNER, M. D., NEDJAI, B., HURST, T. & PENNINGTON, D. J. 2014. Cytokines and chemokines: At the crossroads of cell signalling and inflammatory disease. *Biochim Biophys Acta,* 1843**,** 2563-2582.

UNIPROT. 2019a. *UniProtKB - P62810 (WFD18_MOUSE)* [Online]. Available: https://www.uniprot.org/uniprot/P62810 [Accessed 6th March 2019].

UNIPROT. 2019b. *UniProtKB - Q8BW88 (PKHS1_MOUSE)* [Online]. Available: https://www.uniprot.org/uniprot/Q8BW88 [Accessed 6th March 2019].

VAL, S., KWON, H. J., ROSE, M. C. & PRECIADO, D. 2015. Middle Ear Response of Muc5ac and Muc5b Mucins to Nontypeable Haemophilus influenzae. *JAMA Otolaryngol Head Neck Surg,* 141**,** 997-1005.

VAN ELDERE, J., SLACK, M. P., LADHANI, S. & CRIPPS, A. W. 2014. Non-typeable Haemophilus influenzae, an under-recognised pathogen. *Lancet Infect Dis,* 14**,** 1281-92.

VAN SCHILFGAARDE, M., VAN ALPHEN, L., EIJK, P., EVERTS, V. & DANKERT, J. 1995. Paracytosis of Haemophilus influenzae through cell layers of NCI-H292 lung epithelial cells. *Infect Immun,* 63**,** 4729-37.

VAREILLE, M., KIENINGER, E., EDWARDS, M. R. & REGAMEY, N. 2011. The airway epithelium: soldier in the fight against respiratory viruses. *Clin Microbiol Rev,* 24**,** 210-29.

VARGAS, P. A., SPEIGHT, P. M., BINGLE, C. D., BARRETT, A. W. & BINGLE, L. 2008. Expression of PLUNC family members in benign and malignant salivary gland tumours. *Oral Dis,* 14**,** 613-9.

VENTURA, C. L., HIGDON, R., KOLKER, E., SKERRETT, S. J. & RUBENS, C. E. 2008. Host airway proteins interact with Staphylococcus aureus during early pneumonia. *Infect Immun,* 76**,** 888-98.

VIRJI, M., KAYHTY, H., FERGUSON, D. J., ALEXANDRESCU, C. & MOXON, E. R. 1991. Interactions of Haemophilus influenzae with cultured human endothelial cells. *Microb Pathog,* 10**,** 231-45.

WADSTRÖM, T. & HISATSUNE, K. 1970. Bacteriolytic enzymes from Staphylococcus aureus. Specificity of ction of endo-beta-N-acetylglucosaminidase. *Biochem J,* 120**,** 735-44.

WALTON, W. G., AHMAD, S., LITTLE, M. S., KIM, C. S., TYRRELL, J., LIN, Q., DI, Y. P., TARRAN, R. & REDINBO, M. R. 2016. Structural Features Essential to the Antimicrobial Functions of Human SPLUNC1. *Biochemistry,* 55**,** 2979-91.

WANESS, A. 2010. Revisiting Methicillin-Resistant Staphylococcus aureus Infections. *J Glob Infect Dis,* 2**,** 49-56.

WEI, Y., XIA, W., YE, X., FAN, Y., SHI, J., WEN, W., YANG, P., LI, H. & NASAL HEALTH GROUP, C. I. N. 2014. The antimicrobial protein short palate, lung, and nasal epithelium clone 1 (SPLUNC1) is differentially modulated in eosinophilic and noneosinophilic chronic rhinosinusitis with nasal polyps. *J Allergy Clin Immunol,* 133**,** 420-8.

WESTON, W. M., LECLAIR, E. E., TRZYNA, W., MCHUGH, K. M., NUGENT, P., LAFFERTY, C. M., MA, L., TUAN, R. S. & GREENE, R. M. 1999. Differential display identification of plunc, a novel gene expressed in embryonic palate, nasal epithelium, and adult lung. *J Biol Chem,* 274**,** 13698-703.

WHITTERS, D. & STOCKLEY, R. 2012. Immunity and bacterial colonisation in bronchiectasis. *Thorax,* 67**,** 1006-13.

WHO/UNICEF. 2009. *Global action plan for prevention and control of pneumonia (GAPP)* [Online]. Available: http://apps.who.int/iris/bitstream/10665/70101/1/WHO_FCH_CAH_NCH_09.04_eng.pdf [Accessed 2018].

WIDDICOMBE, J. H. & WINE, J. J. 2015. Airway Gland Structure and Function. *Physiol Rev,* 95**,** 1241-319.

WILLIAMS, K. & ROMAN, J. 2016. Studying human respiratory disease in animals--role of induced and naturally occurring models. *J Pathol,* 238**,** 220-32.

WILLIAMSON, M. P. 1994. The structure and function of proline-rich regions in proteins. *Biochem J,* 297 (Pt 2)**,** 249-60.

WORRALL, G. 2008. Acute bronchitis. *Can Fam Physician,* 54**,** 238-9.

WRIGHT, M. H., HEAL, W. P., MANN, D. J. & TATE, E. W. 2010. Protein myristoylation in health and disease. *J Chem Biol,* 3**,** 19-35.

WU, Q., JIANG, D., MINOR, M. & CHU, H. W. 2014. Electronic cigarette liquid increases inflammation and virus infection in primary human airway epithelial cells. *PLoS One,* 9**,** e108342.

WU, T., HUANG, J., MOORE, P. J., LITTLE, M. S., WALTON, W. G., FELLNER, R. C., ALEXIS, N. E., PETER DI, Y., REDINBO, M. R., TILLEY, S. L. & TARRAN, R. 2017. Identification of BPIFA1/SPLUNC1 as an epithelium-derived smooth muscle relaxing factor. *Nat Commun,* 8**,** 14118.

YACHDAV, G., KLOPPMANN, E., KAJAN, L., HECHT, M., GOLDBERG, T., HAMP, T., HONIGSCHMID, P., SCHAFFERHANS, A., ROOS, M., BERNHOFER, M., RICHTER, L., ASHKENAZY, H., PUNTA, M., SCHLESSINGER, A., BROMBERG, Y., SCHNEIDER, R., VRIEND, G., SANDER, C., BEN-TAL, N. & ROST, B. 2014. PredictProtein--an open resource for online prediction of protein structural and functional features. *Nucleic Acids Res,* 42**,** W337-43.

YOU, Y. & BRODY, S. L. 2013. Culture and differentiation of mouse tracheal epithelial cells. *Methods Mol Biol,* 945**,** 123-43.

YOU, Y., RICHER, E. J., HUANG, T. & BRODY, S. L. 2002. Growth and differentiation of mouse tracheal epithelial cells: selection of a proliferative population. *Am J Physiol Lung Cell Mol Physiol,* 283**,** L1315-21.

YU, Z., DESLOUCHES, B., WALTON, W. G., REDINBO, M. R. & DI, Y. P. 2018. Enhanced biofilm prevention activity of a SPLUNC1-derived antimicrobial peptide against Staphylococcus aureus. *PLoS One,* 13**,** e0203621.

ZHOU, H. D., LI, G. Y., YANG, Y. X., LI, X. L., SHENG, S. R., ZHANG, W. L. & ZHAO, J. 2006. Intracellular co-localization of SPLUNC1 protein with nanobacteria in nasopharyngeal carcinoma epithelia HNE1 cells depended on the bactericidal permeability increasing protein domain. *Mol Immunol,* 43**,** 1864-71.

ZHOU, H. D., LI, X. L., LI, G. Y., ZHOU, M., LIU, H. Y., YANG, Y. X., DENG, T., MA, J. & SHENG, S. R. 2008. Effect of SPLUNC1 protein on the Pseudomonas aeruginosa and Epstein-Barr virus. *Mol Cell Biochem,* 309**,** 191-7.

ZIMMER, M. 2002. Green fluorescent protein (GFP): applications, structure, and related photophysical behavior. *Chem Rev,* 102**,** 759-81.

ZYSK, G., BEJO, L., SCHNEIDER-WALD, B. K., NAU, R. & HEINZ, H. 2000. Induction of necrosis and apoptosis of neutrophil granulocytes by Streptococcus pneumoniae. *Clin Exp Immunol,* 122**,** 61-6.